Summary of the
Bulletin of the
International Seismological Centre

2017

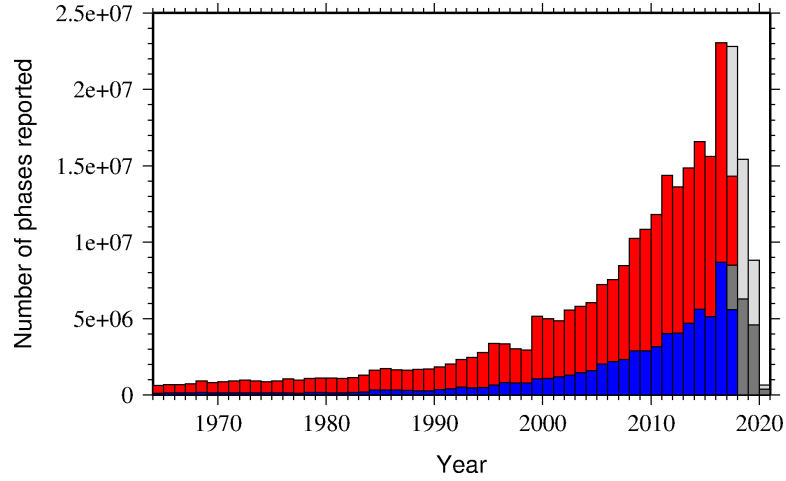### January – June

Volume 54 Issue I
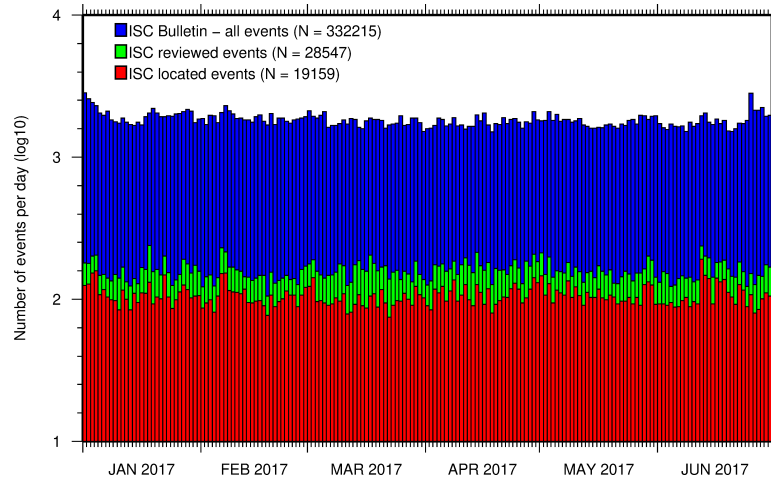
The number of phases (red) and number of amplitudes (blue) collected by the ISC for events each year since 1964. The data in grey covers the current period where data are still being collected before the ISC review takes place and are accurate at the time of publication. See Section 8.3.

The number of events within the Bulletin for the current summary period. The vertical scale is logarithmic. See Section 9.1.
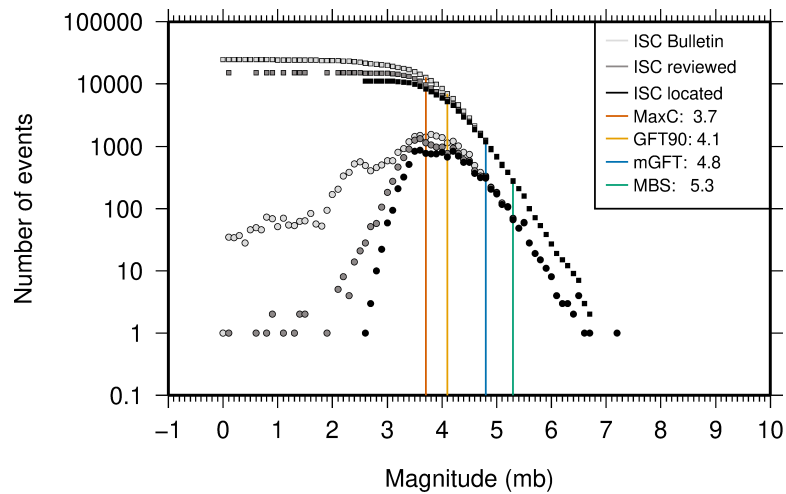
Frequency and cumulative frequency magnitude distribution for all events in the ISC Bulletin, ISC reviewed events and events located by the ISC. The magnitude of completeness (M_C) is shown for the ISC Bulletin. Note: only events with values of m_b are represented in the figure. See Section 9.4.

Summary of the
Bulletin of the
International Seismological Centre

2017

January - June

Volume 54 Issue I

Produced and edited by:
Kathrin Lieser, James Harris and Dmitry Storchak

ISC Data Products
http://www.isc.ac.uk/products/

ISC Bulletin:

> http://www.isc.ac.uk/iscbulletin/search

ISC Bulletin and Catalogue monthly files, to the last reviewed month in FFB or ISF1 format:

> ftp://www.isc.ac.uk/pub/[isf|ffb]/bulletin/*yyyy*/*yyyymm*.gz
>
> ftp://www.isc.ac.uk/pub/[isf|ffb]/catalogue/*yyyy*/*yyyymm*.gz

Datafiles for the ISC data before the Rebuild project:

> ftp://www.isc.ac.uk/pub/prerebuild/[isf|ffb]/bulletin/*yyyy*/*yyyymm*.gz
>
> ftp://www.isc.ac.uk/pub/prerebuild/[isf|ffb]/catalogue/*yyyy*/*yyyymm*.gz

ISC-EHB Bulletin:

> http://www.isc.ac.uk/isc-ehb/search/

IASPEI Reference Event List (GT bulletin):

> http://www.isc.ac.uk/gtevents/search/

ISC-GEM Global Instrumental Earthquake Catalogue:

> http://http://www.isc.ac.uk/iscgem/download.php

ISC Event Bibliography:

> http://www.isc.ac.uk/event_bibliography/bibsearch.php

International Seismograph Station Registry:

> http://www.isc.ac.uk/registries/search/

Seismological Contacts:

> http://www.isc.ac.uk/projects/seismocontacts/

Contents

1

Preface

Dear Colleague,

This is the first 2017 issue of the Summary of the ISC Bulletin, which remains the most fundamental reason for continued operations at the ISC. This issue covers earthquakes and other seismic events that occurred during the period from January to June 2017. Users can search the ISC Bulletin on the ISC website. The monthly Bulletin files are available from the ISC ftp site. For instructions, please see the www.isc.ac.uk/iscbulletin/.

This publication contains information on the ISC, its staff, Members, Sponsors and Data providers. It offers analysis of the data contributed to the ISC by many seismological agencies worldwide as well as analysis of the data in the ISC Bulletin itself. This issue also includes seismological standards and procedures used by the ISC in its operations.

Notably, this issue contains brief information on the recently released last portion of the Rebuilt ISC Bulletin for the period 1991-2010 that replaced the original ISC Bulletin data. From now on, all ISC hypocenter solutions (1964-present) are based on the ak135 velocity model and all ISC magnitudes (1964-present) are based on the latest robust procedures.

We continue publishing invited articles describing the history, current status and operational procedures at those networks that contribute data to the ISC. This time it is the turn for the seismic networks run by the Department of Geophysics of the Aristotle University of Thessaloniki in Greece and Latvian Environment, Geology and Meteorology Center.

We hope that you find this publication useful in your work. If your home-institution or company is unable, for one reason or another, to support the long-term international operations of the ISC in full by becoming a Member or a Sponsor, then, please, consider subscribing to this publication by contacting us at admin@isc.ac.uk.

With kind regards to our Data Contributors, Members, Sponsors and users,

Dr Dmitry A. Storchak
Director
International Seismological Centre (ISC)

2

The International Seismological Centre

2.1   The ISC Mandate

The International Seismological Centre (ISC) was set up in 1964 with the assistance of UNESCO as a successor to the International Seismological Summary (ISS) to carry forward the pioneering work of Prof. John Milne, Sir Harold Jeffreys and other British scientists in collecting, archiving and processing seismic station and network bulletins and preparing and distributing the definitive summary of world seismicity.

Under the umbrella of the International Association of Seismology and Physics of the Earth Interior (IASPEI/IUGG), the ISC has played an important role in setting international standards such as the International Seismic Bulletin Format (ISF), the IASPEI Standard Seismic Phase List (SSPL) and both the old and New IASPEI Manual of the Seismological Observatory Practice (NMSOP-2) (www.iaspei.org/projects/NMSOP.html).

The ISC has contributed to scientific research and prominent scientists such as John Hodgson, Eugine Herrin, Hal Thirlaway, Jack Oliver, Anton Hales, Ola Dahlman, Shigeji Suehiro, Nadia Kondorskaya, Vit Karnik, Stephan Müller, David Denham, Bob Engdahl, Adam Dziewonski, John Woodhouse and Guy Masters all considered it an important duty to serve on the ISC Executive Committee and the Governing Council.

The current mission of the ISC is to maintain:

- the ISC **Bulletin** – the longest continuous definitive summary of World seismicity (collaborating with 130 seismic networks and data centres around the world). (www.isc.ac.uk/iscbulletin/)

- the International Seismographic Station Registry (**IR**, jointly with the World Data Center for Seismology, Denver). (www.isc.ac.uk/registries/)

- the IASPEI Reference Event List (Ground Truth, **GT**, jointly with IASPEI). (www.isc.ac.uk/gtevents/)

These are fundamentally important tasks. Bulletin data produced, archived and distributed by the ISC for almost 50 years are the definitive source of such information and are used by thousands of seismologists worldwide for seismic hazard estimation, for tectonic studies and for regional and global imaging of the Earth's structure. Key information in global tomographic imaging is derived from the analysis of ISC data. The ISC Bulletin served as a major source of data for such well known products as the ak135 global 1-D velocity model and the EHB (*Engdahl et al.*, 1998) and Centennial (*Engdahl and Villaseñor*, 2002) catalogues. It presents an important quality-control benchmark for the Comprehensive Nuclear-Test-Ban Treaty Organization (CTBTO). Hypocentre parameters from the ISC Bulletin are used

by the Data Management Center of the Incorporated Research Institutions for Seismology (IRIS DMC) to serve event-oriented user-requests for waveform data. The ISC-GEM Bulletin is a cornerstone of the ISC-GEM Global Instrumental Reference Earthquake Catalogue for Global Earthquake risk Model (GEM).

The ISC Bulletin contains almost 9 million seismic events: earthquakes, chemical and nuclear explosions, mine blasts and mining induced events. Almost 2 million of them are regional and teleseismically recorded events that have been reviewed by the ISC analysts. The ISC Bulletin contains approximately 300 million individual seismic station readings of arrival times, amplitudes, periods, SNR, slowness and azimuth, reported by approximately 23,000 seismic stations currently registered in the IR. Over 9,000 stations have contributed to the ISC Bulletin in recent years. This number includes the numerous sites of the USArray. The IASPEI GT List currently contains 10583 events for which latitude, longitude and depth of origin are known with high confidence (to 5 km or better) and seismic signals were recorded at regional and/or teleseismic distances.

2.2   Brief History of the ISC

Figure 2.1: *The steel globe bearing positions of early seismic stations was used for locating positions of earthquakes for the International Seismological Summaries.*

Earthquake effects have been noted and documented from the earliest times, but it is only since the development of earthquake recording instruments in the latter half of the 19th century that a proper study of their occurrence has been possible. After the first teleseismic observation of an earthquake in 1889, the need for international exchange of readings was recognised in 1895 by Prof. John Milne and by Ernst von Rebeur Paschwitz together with Georg Gerland, resulting in the publication of the first international seismic bulletins. Milne's "Shide Circulars" were issued under the auspices of the Seismological Committee of the British Association for the Advancement of Science (BAAS), while co-workers of Gerland at the Central Bureau of the International Association of Seismology worked independently in Strasbourg (BCIS).

Following Milne's death in 1913, Seismological Bulletins of the BAAS were continued under Prof. H.H. Turner, later based at Oxford University. Upon formal post-war dissolution of the International Association of Seismology in 1922 the newly founded Seismological Section of the International Union of Geodesy and Geophysics (IUGG) set up the International Seismological Summary (ISS) to continue at Oxford under Turner, to produce the definitive global catalogues from the 1918 data-year onwards, under the auspices of IUGG and with the support of the BAAS.

ISS production, led by several professors at Oxford University, and Sir Harold Jeffreys at Cambridge

University, continued until it was superseded by the ISC Bulletin, after the ISC was formed in Edinburgh in 1964 with Dr P.L. Willmore as its first director.

During the period 1964 to 1970, with the help of UNESCO and other international scientific bodies, the ISC was reconstituted as an international non-governmental body, funded by interested institutions from various countries. Initially there were supporting members from seven countries, now there are almost 60, and member institutions include national academies, research foundations, government departments and research institutes, national observatories and universities. Each member, contributing a minimum unit of subscription or more, appoints a representative to the ISC's Governing Council, which meets every two years to decide the ISC's policy and operational programme. Representatives from the International Association of Seismology and Physics of the Earth's Interior also attend these meetings. The Governing Council appoints the Director and a small Executive Committee to oversee the ISC's operations.

Figure 2.2: ISC building in Thatcham, Berkshire, UK.

In 1975, the ISC moved to Newbury in southern England to make use of better computing facilities there. The ISC subsequently acquired its own computer and in 1986 moved to its own building at Pipers Lane, Thatcham, near Newbury. The internal layout of the new premises was designed for the ISC and includes not only office space but provision for the storage of extensive stocks of ISS and ISC publications and a library of seismological observatory bulletins, journals and books collected over many tens of years.

In 1997 the first set of the ISC Bulletin CD-ROMs was produced (not counting an earlier effort at USGS). The first ISC website appeared in 1998 and the first ISC database was put in day-to-day operations from 2001.

Throughout 2009-2011 a major internal reconstruction of the ISC building was undertaken to allow for more members of staff working in mainstream ISC operations as well as major development projects such as the CTBTO Link, ISC-GEM Catalogue and the ISC Bulletin Rebuild.

Several new ISC products have been released during 2012-2019 period, such as the ISC-EHB dataset, ISC Event Bibliography, International Seismological Contacts and ISC Seismological Dataset Repository.

2.3   Former Directors of the ISC and its U.K. Predecessors

John Milne
Publisher of the Shide Cicular Reports on Earthquakes
1899-1913

Herbert Hall Turner

Seismological Bulletins of the BAAS

1913-1922
Director of the ISS
1922-1930

Harry Hemley Plaskett
Director of the ISS
1931-1946
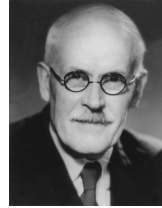
Harold Jeffreys
Director of the ISS
1946-1957

Robert Stoneley
Director of the ISS
1957-1963

P.L. (Pat) Willmore
Director of the ISS
1963-1970
Director of the ISC
1964-1970

Edouard P. Arnold
Director of the ISC
1970-1977

Anthony A. Hughes
Director of the ISC
1977-1997

Raymond J. Willemann
Director of the ISC
1998-2003

Avi Shapira
Director of the ISC
2004-2007

2.4   Member Institutions of the ISC

Article IV(a-b) of the ISC Working Statutes stipulates that any national academy, agency, scientific institution or other non-profit organisation may become a Member of the ISC on payment to the ISC of a sum equal to at least one unit of subscription and the nomination of a voting representative to serve on the ISC's governing body. Membership shall be effective for one year from the date of receipt at the ISC of the annual contribution of the Member and is thereafter renewable for periods of one year.

The ISC is currently supported with funding from its 72 Member Institutions and NSF Award EAR-1811737 from the US National Science Foundation.

Figures 2.3 and 2.4 show major sectors to which the ISC Member Institutions belong and proportional

financial contributions that each of these sectors make towards the ISC's annual budget.
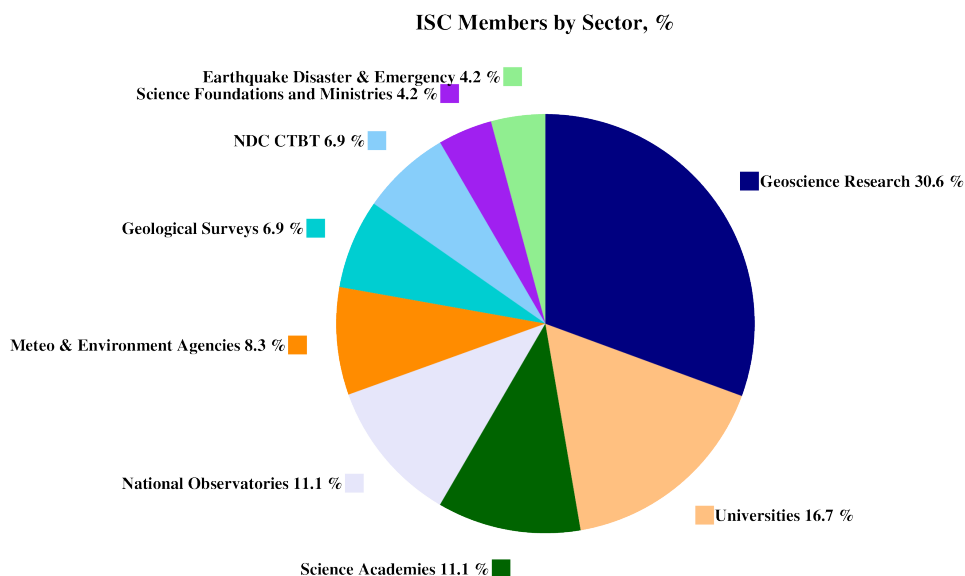
Figure 2.3: *Distribution of the ISC Member Institutions by sector in year 2013 as a percentage of total number of Members.*
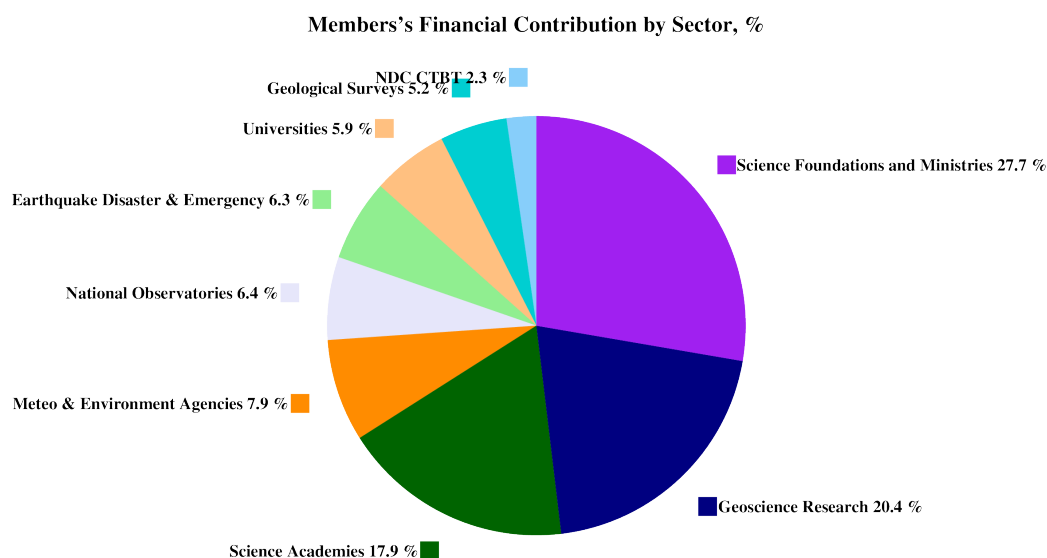
Figure 2.4: *Distribution of Member's financial contributions to the ISC by sector in year 2013 as a percentage of total annual Member contributions.*

There follows a list of all current Member Institutions with a category (1 through 9) assigned according to the ISC Working Statutes. Each category relates to the number of membership units contributed.

Centre de Recherche en Astronomie, Astrophysique et Géophysique (CRAAG) Algeria www.craag.dz Category: 1

Geoscience Australia Australia www.ga.gov.au Category: 4

Bundesministerium für Wissenschaft, Forschung und Wirtschaft (BMWFW) Austria www.bmbwk.gv.at Category: 2

Centre of Geophysical Monitoring (CGM) of the National Academy of Sciences of Belarus
Belarus
www.cgm.org.by
Category: 1

Belgian Science Policy Office (BELSPO)
Belgium

Category: 1

Observatorio Nacional
Brazil
www.on.br
Category: 1

Seismological Observatory, Institute of Geosciences, University of Brasilia
Brazil
www.obsis.unb.br
Category: 1

Universidade de São Paulo, Centro de Sismologia
Brazil
www.sismo.iag.usp.br
Category: 1

National Institute of Geophysics, Geodesy and Geography (NIGGG), Bulgarian Academy of Sciences
Bulgaria
www.niggg.bas.bg
Category: 1

The Geological Survey of Canada
Canada
gsc.nrcan.gc.ca
Category: 4

Centro Sismologico Nacional, Universidad de Chile
Chile

Category: 1

China Earthquake Administration
China
www.cea.gov.cn
Category: 4

Institute of Earth Sciences, Academia Sinica
Chinese Taipei
www.earth.sinica.edu.tw
Category: 1

Geological Survey Department
Cyprus
www.moa.gov.cy
Category: 1

Insitute of Geophysics, Academy of Sciences of the Czech Republic
Czech Republic
www.avcr.cz
Category: 1
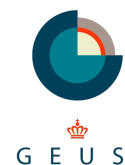
Geological Survey of Denmark and Greenland (GEUS)
Denmark
www.geus.dk
Category: 2

National Research Institute for Astronomy and Geophysics (NRIAG), Cairo
Egypt
www.nriag.sci.eg
Category: 1

The University of Helsinki
Finland
www.helsinki.fi
Category: 2

Laboratoire de Détection et de Géophysique/CEA
France
www-dase.cea.fr
Category: 2

Institute National des Sciences de l'Univers
France
www.insu.cnrs.fr
Category: 4

Institute of Radiological and Nuclear Safety (IRSN), joint authority of the Ministries of Defense, the Environment, Industry, Research, and Health
France

Category: 1

GeoForschungsZentrum Potsdam
Germany
www.gfz-potsdam.de
Category: 2

Bundesanstalt für Geowissenschaften und Rohstoffe
Germany
www.bgr.bund.de
Category: 4

The Seismological Institute, National Observatory of Athens
Greece
www.noa.gr
Category: 1

The Hungarian Academy of Sciences
Hungary
www.mta.hu
Category: 1

The Icelandic Meteorological Office
Iceland
www.vedur.is
Category: 1

National Geophysical Research Institute (NGRI), Council of Scientific and Industrial Research (CSIR)
India

Category: 2
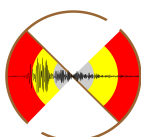
National Centre for Seismology, Ministry of Earth Sciences of India
India
www.moes.gov.in
Category: 4

Iraqi Meteorological Organization and Seismology
Iraq
www.imos-tm.com
Category: 1

Dublin Institute for Advanced Studies
Ireland
www.dias.ie
Category: 1

The Geophysical Institute of Israel
Israel
www.gii.co.il
Category: 1

Soreq Nuclear Research Centre (SNRC)
Israel
www.soreq.gov.il
Category: 1

Istituto Nazionale di Geofisica e Vulcanologia
Italy
www.ingv.it
Category: 3

Istituto Nazionale di Oceanografia e di Geofisica Sperimentale
Italy
www.ogs.trieste.it
Category: 1

University of the West Indies at Mona
Jamaica
www.mona.uwi.edu
Category: 1

Japan Agency for Marine-Earth Science and Technology (JAMSTEC)
Japan
www.jamstec.go.jp
Category: 2
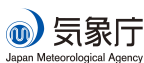
The Japan Meteorological Agency (JMA)
Japan
www.jma.go.jp
Category: 5

Earthquake Research Institute, University of Tokyo
Japan
www.eri.u-tokyo.ac.jp
Category: 3

National Institute of Polar Research (NIPR)
Japan
www.nipr.ac.jp
Category: 1

Royal Scientific Society
Jordan
www.rss.jo
Category: 1

Institute of Geophysics, National University of Mexico
Mexico
www.igeofcu.unam.mx
Category: 1

Centro de Investigación Científica y de Educación Superior de Ensenada (CICESE)
Mexico
resnom.cicese.mx
Category: 1
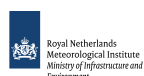
The Royal Netherlands Meteorological Institute (KNMI)
Netherlands
www.knmi.nl
Category: 2

GNS Science
New Zealand
www.gns.cri.nz
Category: 3

The University of Bergen
Norway
www.uib.no
Category: 2

Stiftelsen NORSAR
Norway
www.norsar.no
Category: 2

Institute of Geophysics, Polish Academy of Sciences
Poland
www.igf.edu.pl
Category: 1

Instituto Português do Mar e da Atmosfera
Portugal
www.ipma.pt
Category: 2

Red Sísmica de Puerto Rico
Puerto Rico
redsismica.uprm.edu
Category: 1

Korean Meterological Administration
Republic of Korea
www.kma.go.kr
Category: 1

National Institute for Earth Physics
Romania
www.infp.ro
Category: 1

Russian Academy of Sciences
Russia
www.ras.ru
Category: 5

Earth Observatory of Singapore (EOS), an autonomous Institute of Nanyang Technological University
Singapore
www.earthobservatory.sg
Category: 1

Environmental Agency of Slovenia
Slovenia
www.arso.gov.si
Category: 1

Council for Geoscience
South Africa
www.geoscience.org.za
Category: 1

Institute of Earth Sciences Jaume Almera
Spain
www.ictja.csic.es
Category: 1

Institut Cartogràfic i Geològic de Catalunya (ICGC)
Spain
www.icgc.cat
Category: 1

Uppsala Universitet Sweden www.uu.se Category: 2	National Defence Research Establishment (FOI) Sweden www.foi.se Category: 1	The Swiss Academy of Sciences Switzerland www.scnat.ch Category: 2	
The Seismic Research Centre, University of the West Indies at St. Augustine Trinidad and Tobago www.uwiseismic.com Category: 1	Kandilli Observatory and Earthquake Research Institute Turkey www.koeri.boun.edu.tr Category: 1	Disaster and Emergency Management Authority (AFAD) Turkey www.deprem.gov.tr Category: 2	
AWE Blacknest United Kingdom www.blacknest.gov.uk Category: 1	British Geological Survey United Kingdom www.bgs.ac.uk Category: 2	The Royal Society United Kingdom www.royalsociety.org Category: 6	
Incorporated Research Institutions for Seismology U.S.A. www.iris.edu Category: 1	National Earthquake Information Center, U.S. Geological Survey U.S.A. www.neic.usgs.gov Category: 1	The National Science Foundation of the United States. (Grant No. EAR-1811737) U.S.A. www.nsf.gov Category: 9	
University of Utah Seismograph Stations (UUSS) U.S.A. Category: 1	Alaska Earthquake Center (AEC), University of Alaska Fairbanks U.S.A. Category: 1	Texas Seismological Network (TexNet), Bureau of Economic Geology, J.A. & K.G. Jackson School of Geosciences, University of Texas at Austin U.S.A. www.beg.utexas.edu Category: 1	

In addition the ISC is currently in receipt of grants from the International Data Centre (IDC) of the Preparatory Commission of the Comprehensive Nuclear-Test-Ban Treaty Organization (CTBTO), FM Global, Lighthill risk Network, USGS (Award G18AP00035) and BGR.

2.5 Sponsoring Organisations

Article IV(c) of the ISC Working Statutes stipulates any commercial organisation with an interest in the objectives and/or output of the ISC may become an Associate Member of the ISC on payment of an

Associate membership fee, but without entitlement to representation with a vote on the ISC's governing body.

REF TEK www.reftek.com

REF TEK designs and manufactures application specific, high-performance, battery-operated, field-portable geophysical data acquisition devices for the global market. With over 35 years of experience, REF TEK provides customers with complete turnkey solutions that include high resolution recorders, broadband sensors, state-of-the-art communications (V-SAT, GPRS, etc), installation, training, and continued customer support. Over 7,000 REF TEK instruments are currently being used globally for multiple applications. From portable earthquake monitoring to telemetry earthquake monitoring, earthquake aftershock recording to structural monitoring and more, REF TEK equipment is suitable for a wide variety of application needs.

GeoSIG *swiss made to measure* http://www.geosig.com/
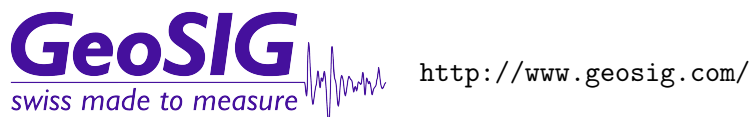
GeoSIG provides earthquake, seismic, structural, dynamic and static monitoring and measuring solutions As an ISO Certified company, GeoSIG is a world leader in design and manufacture of a diverse range of high quality, precision instruments for vibration and earthquake monitoring. GeoSIG instruments are at work today in more than 100 countries around the world with well-known projects such as the NetQuakes installation with USGS and Oresund Bridge in Denmark. GeoSIG offers off-the-shelf solutions as well as highly customised solutions to fulfil the challenging requirements in many vertical markets including the following:

- Earthquake Early Warning and Rapid Response (EEWRR)
- Seismic and Earthquake Monitoring and Measuring
- Industrial Facility Seismic Monitoring and Shutdown
- Structural Analysis and Ambient Vibration Testing
- Induced Vibration Monitoring
- Research and Scientific Applications

泰德 TAIDE http://www.tai-de.com/en/

Zhuhai Taide Enterprise Co., Ltd. (Taide), a China based seismograph manufacturer, was set up in 1992. It is located in the city of Zhuhai, Guangdong Province, south-east China. The main products of

Taide include data loggers, digitizers, all-band seismometers and accelerometers, intensity meters, magnetometers, strain meters, and software for earthquake related analysis. Over 80 professional engineers are employed at Taide, responsible for R&D, assembling and updating the hardware and software, and a team of 10 are engaged in stringent quality control and marketing.

In 2016, in collaboration with the Institute of Geophysics (China Earthquake Administration), Taide set up an Engineering Research Center for Earthquake Monitoring Techniques, aiming to improve the quality of earthquake observations. Taide-made instruments have been widely adapted by earthquake observation and monitoring networks, early warning systems, marine geophysical observation projects and deep borehole projects in China, as well as by seismograph networks in Indonesia, Nepal, Cuba, Pakistan and Kenya.

http://www.guralp.com/

Güralp has been developing revolutionary force-feedback broadband seismic instrumentation for more than thirty years. Our sensors record seismic signals of all kinds, from teleseismic events occurring on the other side of the planet, to microseisms induced by unconventional hydrocarbon extraction. Our sophisticated digitisers record these signals with the highest resolution and accurate timing.

We supply individual instruments or complete seismic systems. Our services include field support such as installation and maintenance, to complete network and data management.

We design our instruments to meet increasingly complex requirements for deployment in the most challenging circumstances. As a result, you will find Güralp instruments gathering seismic data in the harshest of environments, from the Antarctic ice sheet; to boreholes 100s of metres deep; to the world's most active volcanoes and deepest ocean trenches.

http://src.com.au/

The Seismology Research Centre is an Australian earthquake observatory that began developing their own seismic recorders and data processing software in the late 1970s when digital recorders were uncommon. The Gecko is the SRC's 7th generation of seismic recorder, now available with a variety of integrated sensors to meet every monitoring requirement, including:

- Strong Motion Accelerographs
- 2Hz and 4.5Hz Blast Vibration Monitors
- Short Period 1Hz Seismographs
- Broadband 200s-1500Hz Optical Seismographs

Visit src.com.au/downloads/waves to grab a free copy of the SRC's MiniSEED waveform viewing and analysis software application, Waves.

2.6   Data Contributing Agencies

In addition to its Members and Sponsors, the ISC owes its existence and successful long-term operations to its 147 seismic bulletin data contributors. These include government agencies responsible for national seismic networks, geoscience research institutions, geological surveys, meteorological agencies, universities, national data centres for monitoring the CTBT and individual observatories. There would be no ISC Bulletin available without the regular stream of data that are unselfishly and generously contributed to the ISC on a free basis.

The Institute of Seismology, Academy of Sciences of Albania
Albania
TIR

Centre de Recherche en Astronomie, Astrophysique et Géophysique
Algeria
CRAAG

Instituto Nacional de Prevención Sísmica
Argentina
SJA

Universidad Nacional de La Plata
Argentina
LPA

National Survey of Seismic Protection
Armenia
NSSP

Curtin University
Australia
CUPWA

Geoscience Australia
Australia
AUST

Primary Industries and Resources SA
Australia
ADE

International Data Centre, CTBTO
Austria
IDC

Zentralanstalt für Meteorologie und Geodynamik (ZAMG)
Austria
VIE

Republican Seismic Survey Center of Azerbaijan National Academy of Sciences
Azerbaijan
AZER

Royal Observatory of Belgium
Belgium
UCC

Observatorio San Calixto
Bolivia
SCB

Republic Hydrometeorological Service, Seismological Observatory, Banja Luka
Bosnia and Herzegovina
RHSSO

Instituto Astronomico e Geofísico
Brazil
VAO

National Institute of Geophysics, Geology and Geography, Bulgarian Academy of Sciences
Bulgaria
SOF

Seismological Observatory of Mount Cameroon
Cameroon
SOMC

Canadian Hazards Information Service, Natural Resources Canada
Canada
OTT

Centro Sismológico Nacional, Universidad de Chile
Chile
GUC

China Earthquake Networks Center
China
BJI

Institute of Earth Sciences, Academia Sinica
Chinese Taipei
ASIES

Central Weather Bureau (CWB)
Chinese Taipei
TAP

Red Sismológica Nacional de Colombia
Colombia
RSNC

Sección de Sismología, Vulcanología y Exploración Geofísica
Costa Rica
UCR

Seismological Survey of the Republic of Croatia
Croatia
ZAG

Servicio Sismológico Nacional Cubano
Cuba
SSNC

Cyprus Geological Survey Department
Cyprus
NIC

Institute of Geophysics, Czech Academy of Sciences
Czech Republic
WBNET

Geophysical Institute, Academy of Sciences of the Czech Republic
Czech Republic
PRU

The Institute of Physics of the Earth (IPEC)
Czech Republic
IPEC

Korea Earthquake Administration
Democratic People's Republic of Korea
KEA

Geological Survey of Denmark and Greenland
Denmark
DNK

Universidad Autonoma de Santo Domingo
Dominican Republic
SDD

Observatorio Sismologico Politecnico Loyola
Dominican Republic
OSPL

Servicio Nacional de Sismología y Vulcanología
Ecuador
IGQ

National Research Institute of Astronomy and Geophysics
Egypt
HLW

Servicio Nacional de Estudios Territoriales
El Salvador
SNET

University of Addis Ababa
Ethiopia
AAE

Seismological Observatory Skopje
FYR Macedonia
SKO

Institute of Seismology, University of Helsinki
Finland
HEL

Laboratoire de Détection et de Géophysique/CEA
France
LDG

EOST / RéNaSS
France
STR

Laboratoire de Géophysique/CEA
French Polynesia
PPT

Institute of Earth Sciences/ National Seismic Monitoring Center
Georgia
TIF

Seismological Observatory Berggießhübel, TU Bergakademie Freiberg
Germany
BRG
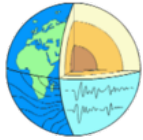
Geophysikalisches Observatorium Collm
Germany
CLL

Bundesanstalt für Geowissenschaften und Rohstoffe
Germany
BGR

Alfred Wegener Institute for Polar and Marine Research
Germany
AWI

Department of Geophysics, Aristotle University of Thessaloniki
Greece
THE

University of Patras, Department of Geology
Greece
UPSL

National Observatory of Athens
Greece
ATH

INSIVUMEH
Guatemala
GCG

Hong Kong Observatory
Hong Kong
HKC

Geodetic and Geophysical Reasearch Institute, Hungarian Academy of Sciences
Hungary
KRSZO

Icelandic Meteorological Office
Iceland
REY
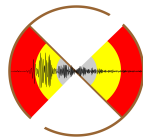
National Centre for Seismology of the Ministry of Earth Sciences of India
India
NDI

National Geophysical Research Institute
India
HYB

Badan Meteorologi, Klimatologi dan Geofisika
Indonesia
DJA

International Institute of Earthquake Engineering and Seismology (IIEES)
Iran
THR

Tehran University
Iran
TEH

Iraqi Meteorological and Seismology Organisation
Iraq
ISN

The Geophysical Institute of Israel
Israel
GII

Dipartimento per lo Studio del Territorio e delle sue Risorse (RSNI)
Italy
GEN

Istituto Nazionale di Geofisica e Vulcanologia
Italy
ROM

Laboratory of Research on Experimental and Computational Seimology
Italy
RISSC

Istituto Nazionale di Oceanografia e di Geofisica Sperimentale (OGS)
Italy
TRI

MedNet Regional Centroid - Moment Tensors
Italy
MED_RCMT

Station Géophysique de Lamto
Ivory Coast
LIC

Jamaica Seismic Network
Jamaica
JSN

National Research Institute for Earth Science and Disaster Prevention
Japan
NIED
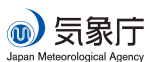
Japan Meteorological Agency
Japan
JMA

National Institute of Polar Research
Japan
SYO

Jordan Seismological Observatory
Jordan
JSO

National Nuclear Center
Kazakhstan
NNC

Seismological Experimental Methodological Expedition
Kazakhstan
SOME

Kyrgyz Seismic Network
Kyrgyzstan
KNET

Institute of Seismology, Academy of Sciences of Kyrgyz Republic
Kyrgyzstan
KRNET

Latvian Seismic Network
Latvia
LVSN

National Council for Scientific Research
Lebanon
GRAL

Geological Survey of Lithuania
Lithuania
LIT

Macao Meteorological and Geophysical Bureau
Macao, China
MCO

Antananarivo
Madagascar
TAN

Geological Survey Department Malawi
Malawi
GSDM

Malaysian Meteorological Service
Malaysia
KLM

Centro de Investigación Científica y de Educación Superior de Ensenada
Mexico
ECX

Instituto de Geofísica de la UNAM
Mexico
MEX

Institute of Geophysics and Geology
Moldova
MOLD

Seismological Institute of Montenegro
Montenegro
PDG

Centre National de Recherche
Morocco
CNRM

The Geological Survey of Namibia
Namibia
NAM

National Seismological Centre, Nepal
Nepal
DMN

IRD Centre de Nouméa
New Caledonia
NOU

Institute of Geological and Nuclear Sciences
New Zealand
WEL

Instituto Nicaraguense de Estudios Territoriales - INETER Nicaragua INET	University of Bergen Norway BER	Stiftelsen NORSAR Norway NAO
Sultan Qaboos University Oman OMAN	Micro Seismic Studies Programme, PIN-STECH Pakistan MSSP	Universidad de Panama Panama UPA
Philippine Institute of Volcanology and Seismology Philippines MAN	Institute of Geophysics, Polish Academy of Sciences Poland WAR	Instituto Dom Luiz, University of Lisbon Portugal IGIL
Instituto Português do Mar e da Atmosfera, I.P. Portugal INMG	Sistema de Vigilância Sismológica dos Açores Portugal SVSA	Centre of Geophysical Monitoring of the National Academy of Sciences of Belarus Republic of Belarus BELR
Inst. of Seismology and Geodynamics, V.I. Vernadsky Crimean Federal University Republic of Crimea CFUSG	Korea Meteorological Administration Republic of Korea KMA	National Institute for Earth Physics Romania BUC
Yakutiya Regional Seismological Center, GS SB RAS Russia YARS	Kamchatkan Experimental and Methodical Seismological Department, GS RAS Russia KRSC	Kola Regional Seismic Centre, GS RAS Russia KOLA
Altai-Sayan Seismological Centre, GS SB RAS Russia ASRS	Mining Institute of the Ural Branch of the Russian Academy of Sciences Russia MIRAS	Sakhalin Experimental and Methodological Seismological Expedition, GS RAS Russia SKHL
Geophysical Survey of Russian Academy of Sciences Russia MOS	Institute of Environmental Problems of the North, Russian Academy of Sciences Russia IEPN	Baykal Regional Seismological Centre, GS SB RAS Russia BYKL
North Eastern Regional Seismological Centre, GS RAS Russia NERS	Saudi Geological Survey Saudi Arabia SGS	Seismological Survey of Serbia Serbia BEO
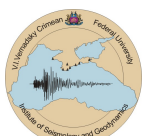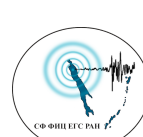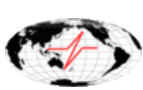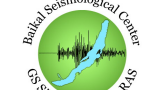
Geophysical Institute, Slovak Academy of Sciences
Slovakia
BRA

Slovenian Environment Agency
Slovenia
LJU

Council for Geoscience
South Africa
PRE

Real Instituto y Observatorio de la Armada
Spain
SFS

Instituto Geográfico Nacional
Spain
MDD

Institut Cartogràfic i Geològic de Catalunya
Spain
MRB

Sudan Seismic Network
Sudan
SSN

University of Uppsala
Sweden
UPP

Swiss Seismological Service (SED)
Switzerland
ZUR

The Seismic Research Centre
Trinidad and Tobago
TRN

Institut National de la Météorologie
Tunisia
TUN

Kandilli Observatory and Research Institute
Turkey
ISK

Disaster and Emergency Management Presidency
Turkey
DDA

National Earthquake Information Center
U.S.A.
NEIC

Red Sísmica de Puerto Rico
U.S.A.
RSPR

The Global CMT Project
U.S.A.
GCMT

IRIS Data Management Center
U.S.A.
IRIS

Pacific Northwest Seismic Network
U.S.A.
PNSN

Subbotin Institute of Geophysics, National Academy of Sciences
Ukraine
SIGU

Main Centre for Special Monitoring
Ukraine
MCSM

Dubai Seismic Network
United Arab Emirates
DSN

British Geological Survey
United Kingdom
BGS

Institute of Seismology, Academy of Sciences, Republic of Uzbekistan
Uzbekistan
ISU

Fundación Venezolana de Investigaciones Sismológicas
Venezuela
FUNV

Institute of Geophysics, Viet Nam Academy of Science and Technology
Viet Nam
PLV

Geological Survey Department of Zambia
Zambia
LSZ

Goetz Observatory
Zimbabwe
BUL

2.7 ISC Staff

Listed below are the staff (and their country of origin) who were employed at the ISC at the time of this
ISC Bulletin Summary.

- Dmitry Storchak
- Director
- Russia / United Kingdom

- Lynn Elms
- Administration Officer
- United Kingdom

- James Harris
- Senior System and
  Database Administrator
- United Kingdom

- Alfie James Barber
- System Administrator
- United Kingdom

- Oliver Rea
- System Administrator
- United Kingdom

- John Eve
- Data Collection Officer
- United Kingdom

- Domenico Di Giacomo
- Senior Seismologist
- Italy/UK

- Konstantinos Lentas
- Seismologist / Senior Developer
- Greece

- Rosemary Hulin
- Analyst
- United Kingdom

- Blessing Shumba
- Seismologist / Senior Analyst
- Zimbabwe

- Rebecca Verney
- Analyst
- United Kingdom

- Elizabeth Ayres
- Analyst / Historical Data Officer
- United Kingdom

- Kathrin Lieser
- Analyst Administrator / Summary Editor / Seismologist
- Germany

- Lonn Brown
- Seismologist / Analyst Administrator
- Canada

- Charikleia Gkarlaouni
- Seismologist / Analyst
- Greece
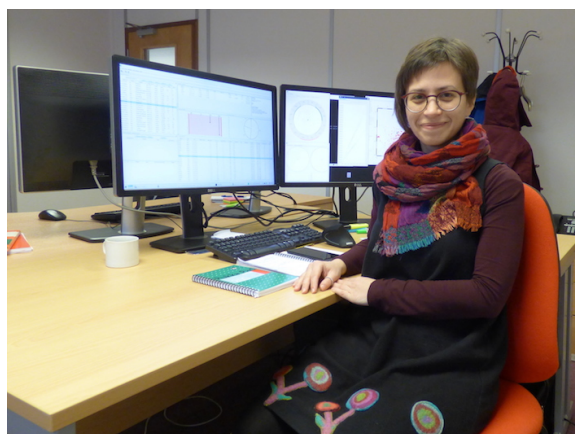
- Peter Franek
- Seismologist / Analyst
- Slovakia

- Angeliki Adamaki
- Seismologist / Analyst
- Greece

- Burak Sakarya
- Seismologist / Analyst
- Turkey
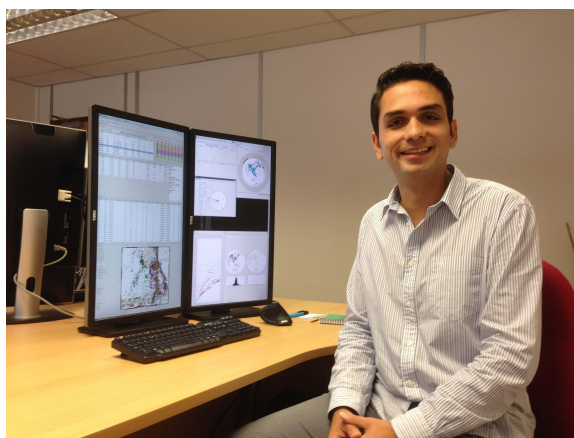
- Daniela Olaru
- Historical and
  Bibliographical Data Officer
- Romania/UK

- Tom Garth

- Seismologist, PDRA, jointly with Department of Earth Sciences at University of Oxford

- United Kingdom

3

Availability of the ISC Bulletin

The ISC Bulletin is available from the following sources:

- Web searches

  The entire ISC Bulletin is available directly from the ISC website via tailored searches.
  (www.isc.ac.uk/iscbulletin/search)
  (isc-mirror.iris.washington.edu/iscbulletin/search)

  - Bulletin search - provides the most verbose output of the ISC Bulletin in ISF or QuakeML.

  - Event catalogue - only outputs the prime hypocentre for each event, producing a simple list of events, locations and magnitudes.

  - Arrivals - search for arrivals in the ISC Bulletin. Users can search for specific phases for selected stations and events.

- CD-ROMs/DVD-ROMs

  CDs/DVDs can be ordered from the ISC for any published volume (one per year), or for all back issues of the Bulletin (not including the latest volume). The data discs contain the Bulletin as a PDF, in IASPEI Seismic Format (ISF), and in Fixed Format Bulletin (FFB) format. An event catalogue is also included, together with the International Registry of seismic station codes.

- FTP site

  The ISC Bulletin is also available to download from the ISC ftp site, which contains the Bulletin in PDF, ISF and FFB formats. (ftp://www.isc.ac.uk)
  (ftp://isc-mirror.iris.washington.edu)

Mirror service

A mirror of the ISC database, website and ftp site is available at IRIS DMC (isc-mirror.iris.washington.edu), which benefits from their high-speed internet connection, providing an alternative method of accessing the ISC Bulletin.

4

Citing the International Seismological Centre

Data from the ISC should always be cited. This includes use by academic or commercial organisations, as well as individuals. A citation should show how the data were retrieved and may be in one of these suggested forms:

4.1 The ISC Bulletin

International Seismological Centre (2020), On-line Bulletin, `https://doi.org/10.31905/D808B830`

The procedures used for producing the ISC Bulletin have been described in a number of scientific articles. Depending on the use of the Bulletin, users are encouraged to follow the citation suggestions below:

a) For current ISC location procedure:

Bondár, I. and D.A. Storchak (2011). Improved location procedures at the International Seismological Centre, *Geophys. J. Int.*, *186*, 1220-1244, `https://doi.org/10.1111/j.1365-246X.2011.05107.x`

b) For Rebuilt ISC Bulletin (currently: 1964-1990):

Storchak, D.A., Harris, J., Brown, L., Lieser, K., Shumba, B., Verney, R., Di Giacomo, D., Korger, E. I. M. (2017). Rebuild of the Bulletin of the International Seismological Centre (ISC), part 1: 1964–1979. *Geosci. Lett.* (2017) 4: 32. `https://doi.org/10.1186/s40562-017-0098-z`

c) For principles of the ISC data collection process:

R J Willemann, D A Storchak (2001). Data Collection at the International Seismological Centre, *Seis. Res. Lett.*, *72*, 440-453, `https://doi.org/10.1785/gssrl.72.4.440`

d) For interpretation of magnitudes:

Di Giacomo, D., and D.A. Storchak (2016). A scheme to set preferred magnitudes in the ISC Bulletin, *J. Seism.*, *20(2)*, 555-567, `https://doi.org/10.1007/s10950-015-9543-7`

e) For use of source mechanisms:

Lentas, K., Di Giacomo, D., Harris, J., and Storchak, D. A. (2020). The ISC Bulletin as a comprehensive source of earthquake source mechanisms, *Earth Syst. Sci. Data*, *11*, 565-578,`https://doi.org/10.5194/essd-11-565-2020`

Lentas, K. (2018). Towards routine determination of focal mechanisms obtained from first motion P-wave arrivals, *Geophys. J. Int.*, *212(3)*, 1665–1686.`https://doi.org/10.1093/gji/ggx503`

f) For use of the original (pre-Rebuild) ISC Bulletin as a historical perspective:

Adams, R.D., Hughes, A.A., and McGregor, D.M. (1982). Analysis procedures at the International Seismological Centre. *Phys. Earth Planet. Inter. 30:* 85-93,`https://doi.org/10.1016/0031-9201(82)90093-0`

4.2   The Summary of the Bulletin of the ISC

International Seismological Centre (2020), Summary of the Bulletin of the International Seismological Centre, July - December 2016, *53(II)*,`https://doi.org/10.31905/V1QQWEBC`

4.3   The historical printed ISC Bulletin (1964-2009)

International Seismological Centre, Bull. Internatl. Seismol. Cent., 46(9-12), Thatcham, United Kingdom, 2009.

4.4   The IASPEI Reference Event List

International Seismological Centre (2020), IASPEI Reference Event (GT) List, `https://doi.org/10.31905/32NSJF7V`

Bondár, I. and K.L. McLaughlin (2009). A New Ground Truth Data Set For Seismic Studies, *Seismol. Res. Lett.*, *80*, 465-472, `https://doi.org/10.1785/gssrl.80.3.465`

Bondár, E. Engdahl, X. Yang, H. Ghalib, A. Hofstetter, V. Kirichenko, R. Wagner, I. Gupta, G. Ekström, E. Bergman, H. Israelsson, and K. McLaughlin (2004). Collection of a reference event set for regional and teleseismic location calibration, *Bull. Seismol. Soc. Am.*, *94*, 1528-1545, `https://doi.org/10.1785/012003128`

Bondár, E. Bergman, E. Engdahl, B. Kohl, Y.-L. Kung, and K. McLaughlin (2008). A hybrid multiple event location technique to obtain ground truth event locations, *Geophys. J. Int.*, *175*, `https://doi.org/10.1111/j.1365-246X.2011.05011.x`

4.5   The ISC-GEM Catalogue

International Seismological Centre (2020), ISC-GEM Earthquake Catalogue, `https://doi.org/10.31905/d808b825`, 2020.

Depending on the use of the Catalogue, to quote the appropriate scientific articles, as suggested below.

a) For a general use of the catalogue, please quote the following three papers (Storchak et al., 2013; 2015; Di Giacomo et al., 2018):

Storchak, D.A., D. Di Giacomo, I. Bondár, E.R. Engdahl, J. Harris, W.H.K. Lee, A. Villaseñor and P. Bormann (2013). Public Release of the ISC-GEM Global Instrumental Earthquake Catalogue (1900-2009). *Seism. Res. Lett.*, *84*, 5, 810-815, `https://doi.org/10.1785/0220130034`

Storchak, D.A., D. Di Giacomo, E.R. Engdahl, J. Harris, I. Bondár, W.H.K. Lee, P. Bormann and A. Villaseñor (2015). The ISC-GEM Global Instrumental Earthquake Catalogue (1900-2009): Introduction, *Phys. Earth Planet. Int.*, *239*, 48-63, `https://doi.org/10.1016/j.pepi.2014.06.009`

Di Giacomo, D., E.R. Engdahl and D.A. Storchak (2018). The ISC-GEM Earthquake Catalogue (1904–2014): status after the Extension Project, *Earth Syst. Sci. Data*, *10*, 1877-1899, `https://doi.org/10.5194/essd-10-1877-2018`

b) For use of location parameters, please quote (Bondár et al., 2015):

Bondár, I., E.R. Engdahl, A. Villaseñor, J. Harris and D.A. Storchak, 2015. ISC-GEM: Global Instrumental Earthquake Catalogue (1900-2009): II. Location and seismicity patterns, *Phys. Earth Planet. Int.*, *239*, 2-13, `https://doi.org/10.1016/j.pepi.2014.06.002`

c) For use of magnitude parameters, please quote (Di Giacomo et al., 2015a; 2018):

Di Giacomo, D., I. Bondár, D.A. Storchak, E.R. Engdahl, P. Bormann and J. Harris (2015a). ISC-GEM: Global Instrumental Earthquake Catalogue (1900-2009): III. Re-computed MS and mb, proxy MW, final magnitude composition and completeness assessment, *Phys. Earth Planet. Int.*, *239*, 33-47, `https://doi.org/10.1016/j.pepi.2014.06.005`

Di Giacomo, D., E.R. Engdahl and D.A. Storchak (2018). The ISC-GEM Earthquake Catalogue (1904–2014): status after the Extension Project, *Earth Syst. Sci. Data*, *10*, 1877-1899, `https://doi.org/10.5194/essd-10-1877-2018`

d) For use of station data from historical bulletins, please quote (Di Giacomo et al., 2015b; 2018):

Di Giacomo, D., J. Harris, A. Villaseñor, D.A. Storchak, E.R. Engdahl, W.H.K. Lee and the Data Entry Team (2015b). ISC-GEM: Global Instrumental Earthquake Catalogue (1900-2009), I. Data collection from early instrumental seismological bulletins, *Phys. Earth Planet. Int.*, *239*, 14-24, `https://doi.org/10.1016/j.pepi.2014.06.005`

Di Giacomo, D., E.R. Engdahl and D.A. Storchak (2018). The ISC-GEM Earthquake Catalogue (1904–2014): status after the Extension Project, *Earth Syst. Sci. Data*, *10*, 1877-1899, `https://doi.org/10.5194/essd-10-1877-2018`

e) For use of direct values of M0 from the literature, please quote (Lee and Engdahl, 2015):

Lee, W.H.K. and E.R. Engdahl (2015). Bibliographical search for reliable seismic moments of large earthquakes during 1900-1979 to compute MW in the ISC-GEM Global Instrumental Reference Earthquake Catalogue (1900-2009), *Phys. Earth Planet. Int.*, *239*, 25-32, `https://doi.org/10.1016/j.pepi.2014.06.004`

4.6 The ISC-EHB Dataset

International Seismological Centre (2020), ISC-EHB Dataset, `https://doi.org/10.31905/PY08W6S3`

Engdahl, E.R., R. van der Hilst, and R. Buland (1998). Global teleseismic earthquake relocation with improved travel times and procedures for depth determination, *Bull. Seism. Soc. Am.*, *88*, 3, 722-743.

`http://www.bssaonline.org/content/88/3/722.abstract`

Weston, J., Engdahl, E.R., Harris, J., Di Giacomo, D. and Storchack, D.A. (2018). ISC-EHB: Reconstruction of a robust earthquake dataset, *Geophys. J. Int.*, *214*, 1, 474-484, `https://doi.org/10.1093/gji/ggy155`

4.7 The ISC Event Bibliography

International Seismological Centre (2020), On-line Event Bibliography, `https://doi.org/10.31905/EJ3B5LV6`

Also, please reference the following SRL article that describes the details of this service:

Di Giacomo, D., Storchak, D.A., Safronova, N., Ozgo, P., Harris, J., Verney, R. and Bondár, I., 2014. A New ISC Service: The Bibliography of Seismic Events, *Seismol. Res. Lett.*, *85*, 2, 354-360, `https://doi.org/10.1785/0220130143`

4.8 International Registry of Seismograph Stations

International Seismological Centre (2020), International Seismograph Station Registry (IR), `https://doi.org/10.31905/EL3FQQ40`

4.9 Seismological Dataset Repository

International Seismological Centre (2020), Seismological Dataset Repository, `https://doi.org/10.31905/6TJZECEY`

4.10 Data transcribed from ISC CD-ROMs/DVD-ROMs

International Seismological Centre, Bulletin Disks 1-27 [CD-ROM], Internatl. Seismol. Cent., Thatcham, United Kingdom, 2020.

The ISC is named as a valid data centre for citations within American Geophysical Union (AGU) publications. As such, please follow the AGU guidelines when referencing ISC data in one of their journals. The ISC may be cited as both the institutional author of the Bulletin and the source from which the data were retrieved.

5

The ISC Bulletin Rebuild Project Completed

The ISC has completed work on the last portion of the Bulletin Rebuild project, covering the period from 1991 – 2010. The rebuilt bulletin has been uploaded to the live account and is now available for use by all interested parties.

From now on, all ISC hypocentre solutions (1964-present) are based on the ak135 velocity model and all ISC magnitudes (1964-present) are based on the latest robust procedures.

The broad aims of the Rebuild project were to update, extend and homogenize the ISC Bulletin using the same velocity model, modern methods and consistent quality criteria, as well as adding additional previously unavailable data. For a more in-depth description please see the Summary from January – June 2015 (*International Seismological Centre*, 2018) and the paper published on the data years 1964 – 1979 (*Storchak et al.* (2017)). Figure 5.1 compares the ISC locations before and after the Rebuild project for the entirety of the released rebuilt ISC Bulletin from 1964 to 2010. In 2020, we are planning to submit the second scientific article describing the results of the Rebuild project.

To clarify, if you search for events on our website, you are now viewing the rebuilt ISC Bulletin. We welcome any feedback.

References

International Seismological Centre (2018), January – June 2015, *Summ. Bull. Internatl. Seismol. Cent.*, *52*(I), https://doi.org/10.31905/JSWEM8MG.

Storchak, D.A., J. Harris, L. Brown, K. Lieser, B. Shumba, R. Verney, D. Di Giacomo and E. Korger (2017), Rebuild of the Bulletin of the Internati onal Seismological Centre (ISC), part 1: 1964-1979, *Geoscience Letters*, *4*(32), https://doi.org/10.1186/s40562-017-0098-z.
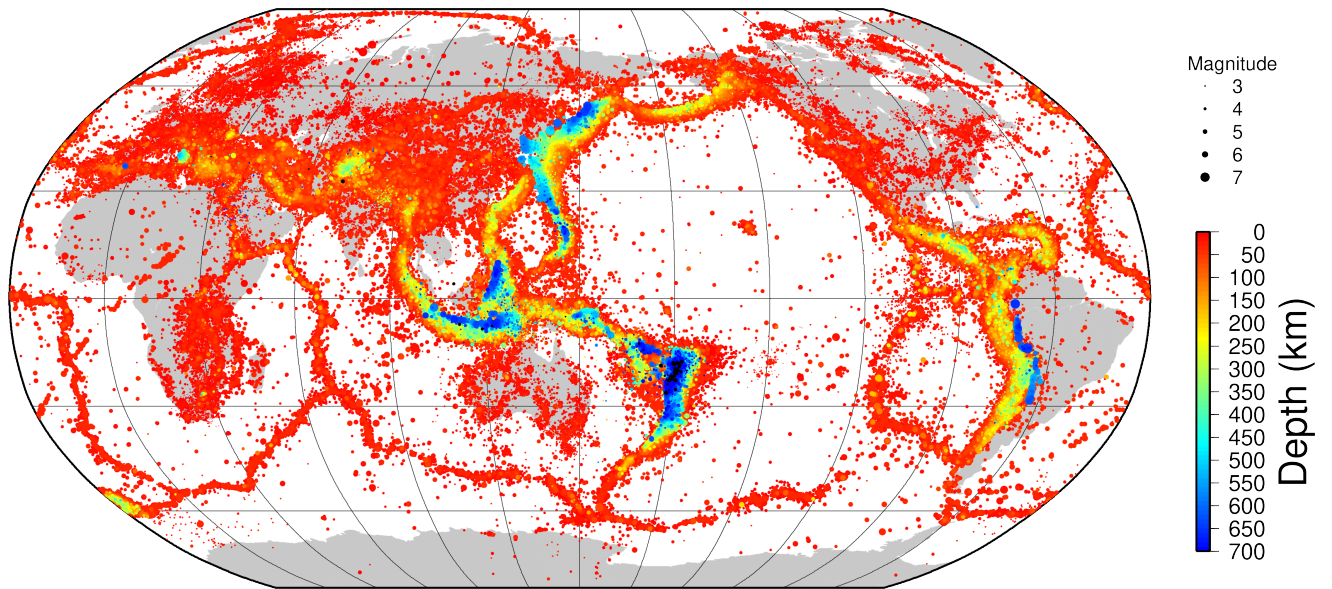
(a) Original ISC Bulletin
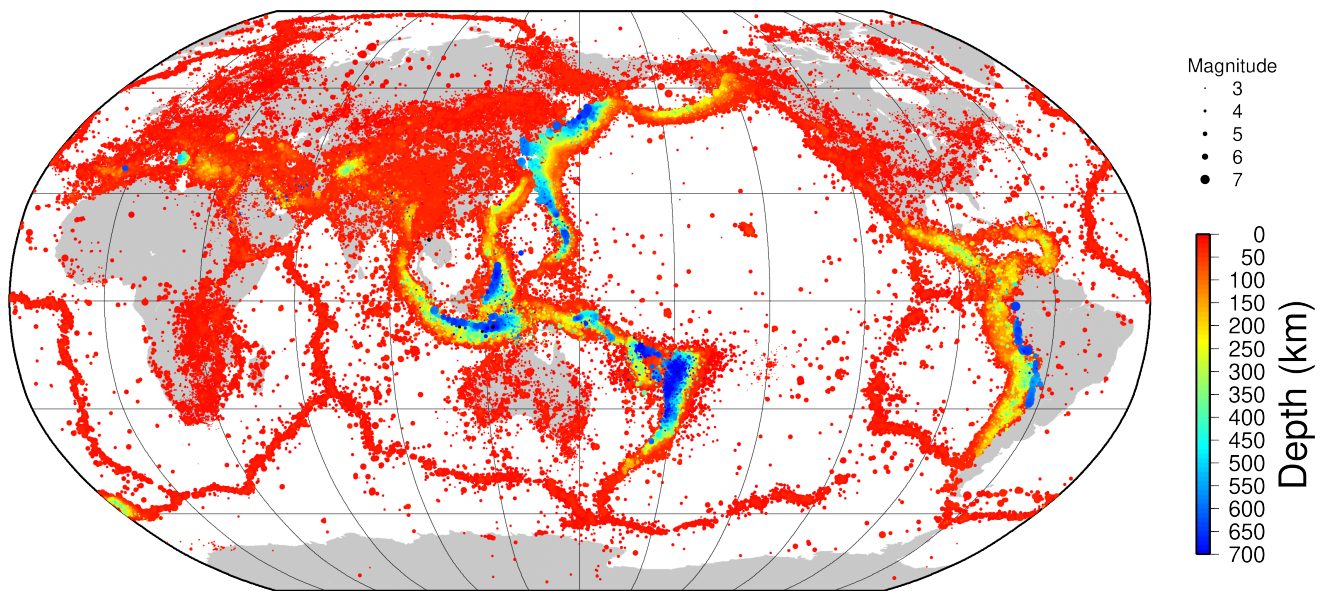
(b) Rebuilt ISC Bulletin

Figure 5.1: *Locations, depths and magnitudes of ISC relocated events, comparing the original ISC Bulletin (a) and the rebuilt ISC Bulletin (b). Data shown covers the period of 1964–2010.*

6

Operational Procedures of Contributing Agencies

6.1 The Seismological Network of Aristotle University of Thessaloniki, Greece (AUTHnet)

D.A. Vamvakaris and E.M. Scordilis

Department of Geophysics, Aristotle University, GR-54124, Thessaloniki, Greece

D.A. Vamvakaris   E.M. Scordilis

The seismological network of Aristotle University of Thessaloniki, Greece (AUTHnet), is a permanent telemetric digital network of state-of-the-art seismological instruments, offering 24/7 seismic monitoring of Greece and its surroundings. It is maintained by the personnel of the Geophysical Laboratory of AUTH (GeoLab) to detect and record local, regional and global earthquake activity (Fig. 6.1). Following the strong ($M_w = 6.5$) earthquake of 1978 in Northern Greece, the GeoLab established its first seismological stations in Thessaloniki and neighbouring areas. After several phases of upgrades, today (October 2019) AUTHnet counts 51 seismic stations spread around the country, which are in real-time communication with the Central Seismological Station in Thessaloniki (THE-SS). The network records almost every event of magnitude M>2.0 in the broader area of Greece while a seismologist on duty analyses, statistically, about 25 regional earthquakes per day. The seismic signals are recorded, digitized, transmitted and managed using appropriate hardware and software packages.

Moreover, three local networks, connected to the main network, were developed in the last 15 years in order to monitor local seismic activity in areas of special interest (Santorini, Nisyros and Cephalonia-Lefkada islands).

AUTHnet is also a founding member of the Hellenic Unified Seismic Network (HUSN), which was formed in 2007 aiming to unify all the seismological networks of Greek Institutions and act as a wide national network.

In addition to the valuable data of AUTHnet, provided by the THE-SS to the scientific community, and the research that is carried out by its scientists, THE-SS maintains strong interaction with society
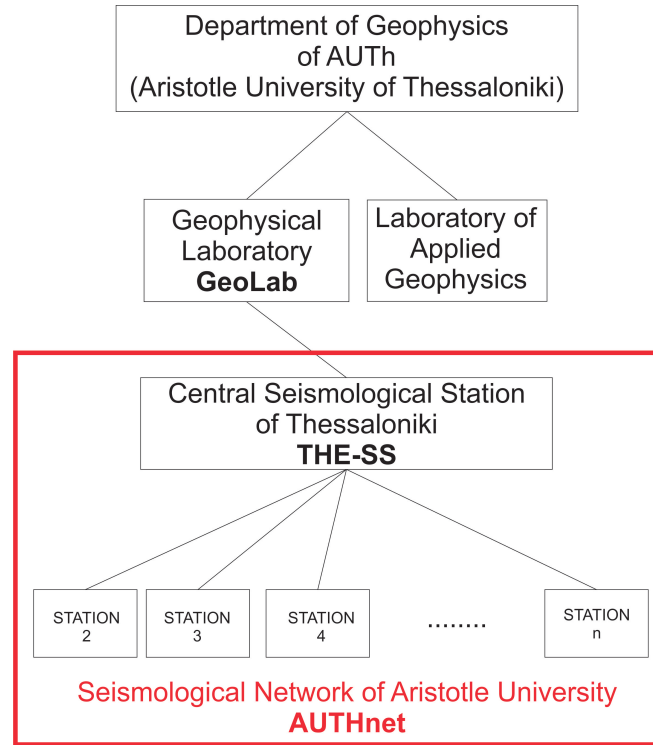
Figure 6.1: *Organisation chart of GeoLab, THE-SS and AUTHnet.*

by providing information to the authorities, the media and citizens about felt earthquakes, as well as by helping civilians to become more familiar with earthquakes and by teaching them how to be better protected.

6.1.1 Introduction

Seismic networks are necessary for scientists in order to monitor the seismic activity and to study the active tectonics of a region. Analysis of their records results in the compilation of reliable earthquake catalogues which are the basic tool for seismic hazard studies. To achieve this, records of large earthquakes as well as of smaller ones are necessary. The lower magnitude over which all earthquakes of a region will be detected and recorded by a network is an indicator of the network's detectability, strongly depending on the number of stations and on their geographical distribution.

On 20 June 1978 a strong earthquake ($M_w = 6.5$) occurred about 25 km NE of the city of Thessaloniki (*Papazachos and Papazachou*, 2003). The mainshock was preceded and followed by rich foreshock and aftershock sequences that lasted for months. This devastating earthquake was the first one in Greece to have occurred near a major city and to have had a significant impact on it. 45 people were killed, huge problems were caused in several sectors and it took months for the community to return to normal life. This earthquake triggered the installation of the seismological network of the Geophysical Laboratory of Aristotle University of Thessaloniki (AUTHnet). The network, in its first shape, was completed within 2 years and consisted of one central and 7 peripheral permanent stations located in Central Macedonia (N. Greece). On January 1st 1981, the network officially started operating. That was a big step forward for seismology in Greece and its surroundings as AUTHnet was the first telemetric seismic network supported by a mainframe computer, in the entire Balkan region.

Nowadays, (October 2019) AUTHnet consists of 51 permanent stations, covering a large part of the country. The network is registered to the International Federation of Digital Seismograph Networks (FDSN - `http://www.fdsn.org`) under the code HT, and holds the Digital Object Identifier `https://doi.org/10.7914/SN/HT`. The agency code at the ISC is THE.

6.1.2 Network Description

Time Evolution of AUTHnet

In 1979 the Central Seismological Station of Thessaloniki (THE-SS) was built at the Aristotle University of Thessaloniki and the first two seismometers, a S-13 3-component short period and a SL-220 3-component long-period, both by Teledyne-Geotech, were installed (station code THE).

By the end of 1980, the formation of AUTHnet in its initial shape was completed with the installation of seven peripheral stations at Sohos (SOH), Litochoro (LIT), Griva (GRG), Paliouri (PAIG), Kentriko (KNT), Ouranoupoli (OUR) and Serres (SRS). The region covered by the network was central Macedonia (N. Greece), with six stations on sites no more than about 100 km from Thessaloniki (Figure 6.2a).

The network expanded in several phases. The **1st phase** took place in **1989**, with four new stations installed in Igoumenitsa (IGT), Florina (FNA), Alexandroupoli (ALN) and Agios Georgios (AGG). Thus, AUTHnet expanded towards the East, West and South, at distances about 250 km from Thessaloniki, covering most of N. Greece and an area about five times larger than before. This step changed the profile of AUTHnet from a local to a regional network, significantly increasing its detectability.

While the continental part of N. Greece was well covered azimuthally, another region not far from Thessaloniki was practically out of coverage. The North Aegean Sea, an area with many catastrophic earthquakes in the last 2,500 years with continuous activity and great geotectonic interest, was the next target of AUTHnet. The **2nd phase** of the network's expansion took place in **1996**, with the installation of three new stations in Lemnos Island (LOS), Alonissos Island (AOS) and Xorichti (XOR) (Figure 6.2b).

Three years later, in **1999**, the network further expanded in western Greece **(3rd phase)**, with a new station installed on Lefkada Island (LKD), in the Ionian Sea. This is the area of the highest seismicity level not only in Greece but also in the whole central and eastern Eurasia.

During the next two years **(2000-2001)**, two more stations were installed **(4th phase)** in W. Macedonia at the areas of Kastania (KTI) and Metsovo (MEV) in order to improve the density of the network in its southwestern part.

In **2003** the first special network of GeoLab was installed in Santorini Island (south Aegean), far from the existing main network (**5th phase**, Fig. 6.2c). Santorini Island is of high scientific interest due to its famous active volcano (most recently activ in 1950). In collaboration with the Institute for the Study and Monitoring of the Santorini Volcano (I.S.MO.SA.V.), five new seismological stations were installed: THR1, THR4, THR6 on Thira Island, THR3 on Nea Kameni Island and THR5 on Thirasia Island. This local network strongly improved the detectability of AUTHnet in the S. Aegean, providing valuable data to the scientific community. In addition, it allowed continuous and detailed monitoring of

the microearthquake activity of the volcano, an increase of which might be connected to possible volcano activation.

In the same year, the older S-13 analogue short period seismometers started being replaced by new digital, 3-component, broad-band sensors (CMG-3ESP, Guralp Systems).

During **2006-2008**, the **6th and 7th phase** of the AUTHnet upgrade took place in an effort to further improve the network's azimuthal coverage and its performance. A new digital station was installed very close to the city of Thessaloniki, on Mount Hortiatis (HORT), to better monitor local activity, as the THE station was situated in a populated and noisy area. AUTHnet was also expanded to the central and eastern part of Aegean Sea, on the islands of Lesvos (SIGR) and Chios (CHOS), increasing the network's sensitivity for events in the central and north Aegean Sea as well as for the NW coast of Turkey. The installation of three new stations followed, in Kavala (KAVA), Nestorio (NEST) and on Thira Island (THR2). At the same time, LKD2 in Lefkada Island replaced the older LKD station, due to technical problems.

Based on the experience gained from the local network at Santorini, a new local network was installed on the Dodecanese islands (**7th phase**, Fig. 6.2d), in order to monitor the possible microearthquake activity associated with the known volcanic center of Nisyros Island. In collaboration with the regional authorities and the recently founded Volcanic Observatory of Nisyros, a seismological station was established in 2008 (NIS1) and three more (NIS2, NIS3 and NIS4) within the next year, covering the whole island of Nisyros. However, due to many technical problems, some of these stations remained closed for long periods.

In **2010 (8th phase)**, a new station was added to the local network of Santorini in Fira (THR7). At the same time, AUTHnet was extended to the south with a new station installed in Kranidi (KRND), E. Peloponnesus. In this way, AUTHnet with more than 30 stations covering the biggest part of the country and Aegean Sea became able to detect almost all events of M>2.0 in the broader area of Greece.

Another expansion **(9th phase)** took place in **2011**, with the installation of two new stations in Kipourio (KPRO), W. Macedonia, and in Thessaly, at the Larissa Observatory (LRSO). The existing network at Santorini was enhanced with new stations in Columbo (CMBO), Athinios (THT1), Monolithos (THR8), Imerovigli (THT2), Akrotiri (THR9) and Taxiarchis (STAX). This decision was very important, as a significant seismic swarm started in January 2011, strongly related to processes showing volcanic activity inside the caldera of Santorini (*Newman et al.*, 2012). Thanks to the dense local network of AUTHnet, with more than ten operating stations in about 200 km^2, more than 1,200 earthquakes were recorded in 2011 in Santorini, most of them (about 1,000) during May-December 2011, with magnitudes M<2.5.

In **2012 (10th phase)**, another station (THAS) was installed in the N. Aegean, on the island of Thassos, increasing the sensitivity of the network in this region. To the west, in the Ionian Sea, two new stations were added on Lefkada Island, in Evgiros (EVGI) and Tsoukalades (TSLK), supporting the older LKD2. In this way, the network could better monitor the seismic activity of the area with the highest seismicity in Greece. The recent seismic activity of 2014, with two strong earthquakes (M_w=6.1 and M_w=6.0) in eight days (*Karakostas et al.*, 2015), and their rich aftershock sequence, pushed this local network to the next step. Thus, two more stations were added on Lefkada Island (in Dragano (DRAG) and Nydri (NYDR)) and another two on Cephalonia Island (in Damoulianata (DMLN) and Pessada (PSDA)). This local network was very helpful for the study of the large earthquake of Lefkada Island (M_w=6.5) some
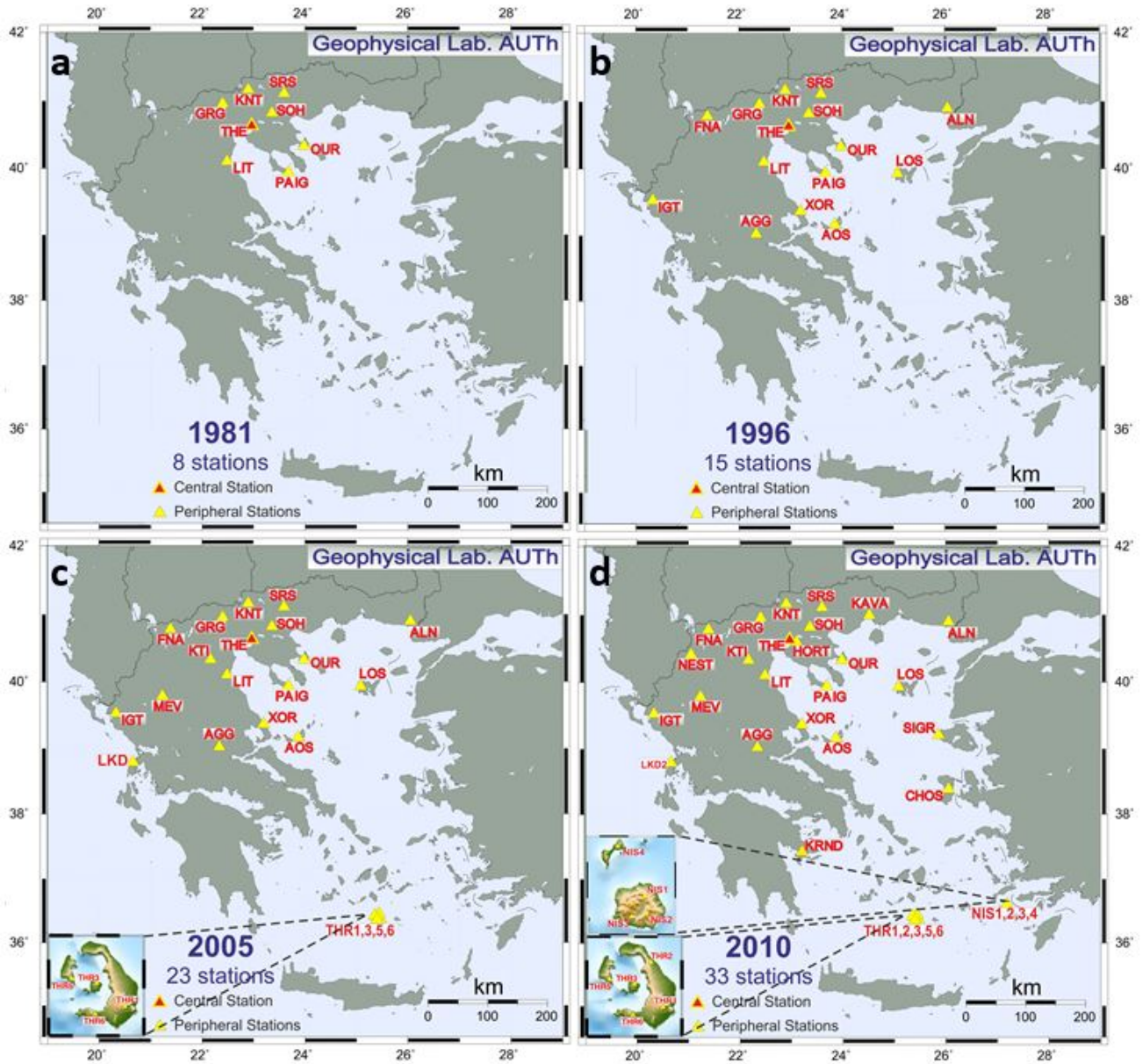
Figure 6.2: *Geographical distribution of AUTHnet stations in the past including maps for the two special local networks of Santorini and Nisyros (Vamvakaris, 2018).*
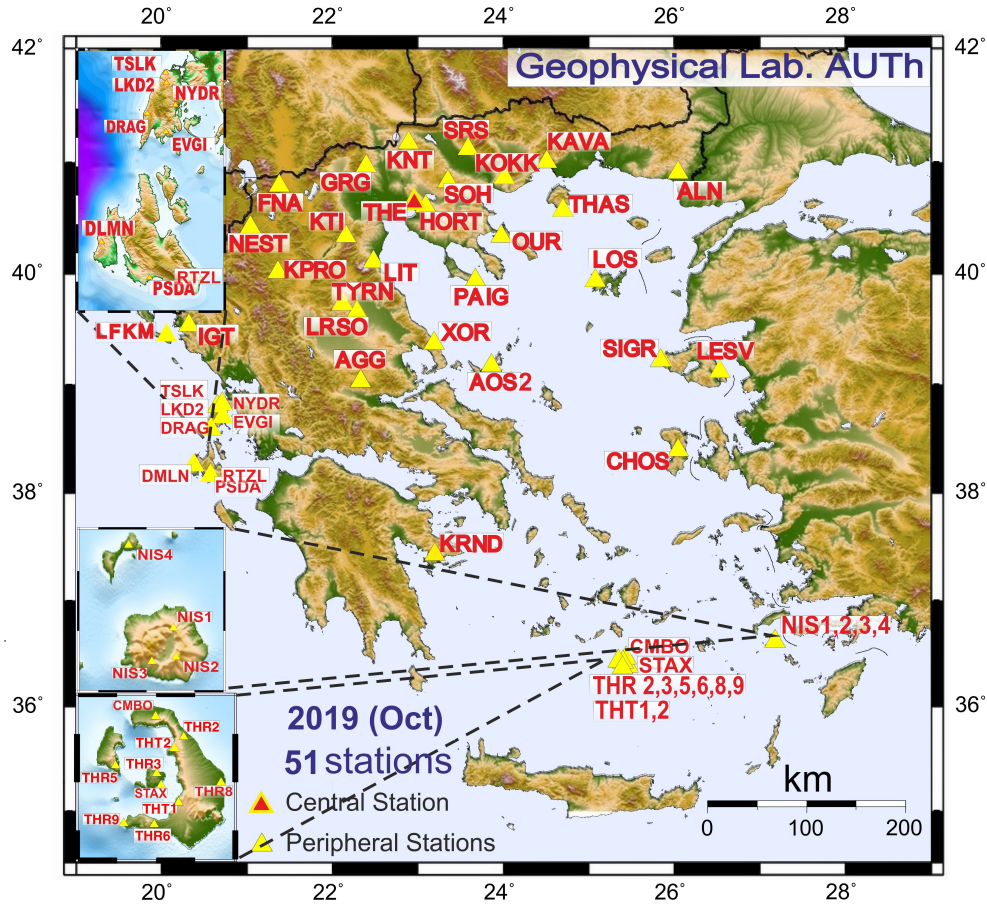
Figure 6.3: *Geographical distribution of the 51 AUTHnet stations in operation at the time of writing (October 2019). In the insets the special local networks of Cephalonia-Lefkada (top), Nisyros (centre) and Santorini (bottom) are also presented. Older, non-operating, stations are also shown (see Table 6.1) (modified from Vamvakaris, 2018).*

months later in 2015 (*Papadimitriou et al.*, 2017).

In **2015 (11th phase)**, two more stations were added in E. Macedonia, in Kokkinohori-Kavala (KOKK) improving the detectability in the area of the Strymon gulf (N. Aegean Sea) and in Tyrnavos (TYRN) in Thessaly.

In 2017 **(12th phase)**, a station was installed on Lesvos Island (LESV) just two weeks after the strong earthquake of $M_w = 6.3$ that hit the island. A couple of months later in **2018** two more stations on Cephalonia island in Ratzakli (RTZL) and on Corfu island in Lefkimi (LFKM) improved the local network on the Ionian Islands. Thus, AUTHnet counts (October 2019) 51 stations in total today.

Figure 6.2 represents the expansion of the network since its establishment in 1981, through a series of maps describing the geographical distribution of AUTHnet stations until 2010 during 4 significant periods (1981, 1996, 2005 and 2010). Its present form is outlined in Figure 6.3.

The change in the number of AUTHnet stations over time is presented in Figure 6.4, where the three basic phases of the network upgrade, in 1989, 1996 and 2003, can be clearly seen.
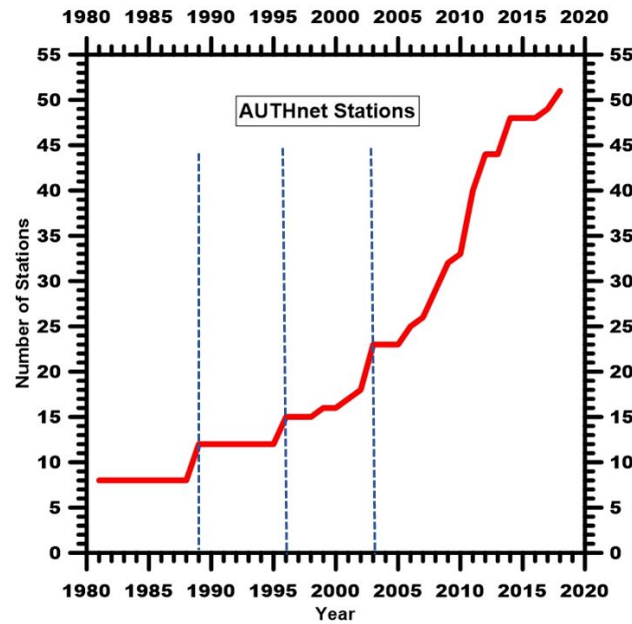
Figure 6.4: *Time evolution of the number of operating stations of AUTHnet, until Oct. 2019 (modified from Vamvakaris, 2018).*

Network Equipment

The initial network (1981) was equipped with 3-component short-period (1 s) analogue S-13 Teledyne-Geotech seismometers (set of 2 horizontals and 1 vertical), while in some cases only vertical S-13 seismometers were used. Additionally, three long-period (20 s) analogue SL-220 Teledyne-Geotech seismometers (one vertical, two horizontals) were installed at the Seismological Station of Thessaloniki (THE). Analogue signals were transmitted through telephone lines from the peripheral stations to the THE-SS. The analogue signal was recorded on a set of Teledyne-Geotech helicorder drums and on 16mm photographic films using a "Develocorder" (Teledyne-Geotech) but, at the same time, it was digitized using a 12-bit, 32-channel, AD converter and recorded to magnetic tapes. That process was managed by a 16-bit PDP11/34 mainframe computer (of Digital Equipment Corporation, DEC), making AUTHnet the first telemetric seismological network in the Balkan region, to be supported by a computer. This system was updated in 1989 with a DEC MicroVAX II 32-bit computer, running a VAX/VMS operating system, which was replaced about 10 years later by a DEC ALPHA 3100 running OpenVMS.

After 2003, modern broadband seismometers were installed in several stations of the network replacing the older short-period S-13. Most of them were CMG-3ESP (100 s – 50 Hz) by Guralp Systems and this is still the most common type of seismometers in AUTHnet stations. Alternatively, CMG-6T (30 s – 50 Hz) sensors were installed in the Nisyros network, CMG-40T (1 s – 100 Hz) and CMG-40T (30 s – 50 Hz) in the Cephalonia-Lefkada network (all by Guralp Systems). Recently, Trillium 120P, 3-component, broadband low-noise seismometers by Nanometrics Inc. were used in new installations. Due to its more suitable characteristics, this seismometer was also selected to replace the CMG-3ESP sensor of the THE-SS in 2014, which, in turn, had replaced the old analogue S-13 in 2005. Last year, a new-type Trillium 120C seismometer was installed at the KOKK and LESV stations.

During the first years of its operation, the network was pseudo-digital, as the transmitted signal was

analogue and then digitized at the receiving end (THE-SS). This situation was changed when the first 24-bit HRD-24 digitizers by Nanometrics were used in some stations, digitizing in-situ the signal and transmitting it to THE-SS. Later, Trident 24-bit digitizers with a typical dynamic range of 142 dB, working with a Janus-IP communication controller by Nanometrics, replaced some old HRD-24 digitizers. Since 2006, Taurus digitizers by Nanometrics were deployed as a portable 24-bit digital seismograph, working on 3 channels in a dynamic range of more than 141 dB. In some other cases, REFTEK RT130 by Trimble, wave24 by MicroStep-MIS, CMG-DM24 by Guralp Systems, Smart-24 by Geotech Instruments LLC, were used. Lately, 24-bit Centaur digital recorders by Nanometrics were obtained. Table 6.1 lists in detail the current instrumentation of all 51 operating stations of AUTHnet.

Table 6.1: *Current (October 2019) station list and instrumentation of the stations of AUTHnet*

#	Station	Lat deg	Long deg	Elevation m	Seismometer	Controler	Digitizer	Initial Installation
1	AGG	39.0211	22.3360	625	TRILLIUM 120P	JANUS	TRIDENT	1989
2	ALN	40.8957	26.0497	110	CMG-3ESP/100	JANUS	TRIDENT	1989
3	AOS	39.1654	23.8639	230	CMG-3ESP/100	-	TAURUS	1996
4	CHOS	38.3869	26.0506	854	CMG-3ESP/100	-	CENTAUR	2006
5	FNA	40.7817	21.3836	806	CMG-40T/30	-	HRD-24	1989
6	GRG	40.9558	22.4029	600	CMG-3ESP/100	-	TAURUS	1981
7	HORT	40.5978	23.0995	925	CMG-3ESP/100	JANUS	TRIDENT	2006
8	IGT	39.5315	20.3299	262	CMG-3ESP/100	-	HRD-24	1989
9	KAVA	40.9941	24.5119	95	TRILLIUM 120P	-	CENTAUR	2008
10	KNT	41.1620	22.8980	380	CMG-3ESP/100	-	HRD-24	1981
11	KOKK	40.8178	23.9992	261	TRILLIUM 120C	-	TAURUS	2015
12	KPRO	39.9549	21.3632	837	CMG-3ESP/100	-	TAURUS	2011
13	KRND	37.3830	23.1502	140	CMG-3ESP/100	-	TAURUS	2010
14	KTI	40.3929	22.1165	1329	S-13	JANUS	TRIDENT	2001
15	LESV	39.1074	26.5613	20	TRILLIUM 120C	-	TAURUS	2017
16	LIT	40.1033	22.4892	568	CMG-3ESP/100	JANUS	TRIDENT	1981
17	LOS	39.9330	25.0810	460	S-13	JANUS	TRIDENT	1996
18	LRSO	39.6713	22.3917	78	CMG-40T/1	-	REFTEK-130	2011
19	NEST	40.4147	21.0489	1056	TRILLIUM 120P	JANUS	TRIDENT	2008
20	OUR	40.3325	23.9791	117	CMG-3ESP/100	-	CENTAUR	1981
21	PAIG	39.9363	23.6768	217	CMG-3ESP/100	-	TAURUS	1981
22	SIGR	39.2114	25.8553	92	CMG-3ESP/100	JANUS	TRIDENT	2007
23	SOH	40.8206	23.3556	731	TRILLIUM 120P	-	TAURUS	1981
24	SRS	41.1087	23.5950	314	CMG-3ESP/100	JANUS	TRIDENT	1981
25	THAS	40.6064	24.7194	67	CMG-3ESP/100	-	TRIDENT	2012
26	THE	40.6319	22.9628	132	CMG-6T/30	JANUS	TRIDENT	1981
27	TYRN	39.7110	22.2325	151	TRILLIUM 120P	-	CENTAUR	2015
28	XOR	39.3660	23.1918	541	CMG-3ESP/100	-	TAURUS	1996
SANTORINI LOCAL NETWORK								
29	CMBO	36.4709	25.4056	108	TRILLIUM 120P	-	TAURUS	2011
30	STAX	36.3993	25.4045	20	CMG-40T/30	-	DM-24	2012
31	THR2	36.4469	25.4354	220	S-13	JANUS	TRIDENT	2008
32	THR3	36.4091	25.4008	71	S-13	JANUS	TRIDENT	2003
33	THR5	36.4172	25.3479	180	S-13	JANUS	TRIDENT	2003

#	Station	Lat deg	Long deg	Elevation m	Seismometer	Controler	Digitizer	Initial Installation
34	THR6	36.3562	25.3975	119	S-13	JANUS	TRIDENT	2003
35	THR8	36.4070	25.4788	30	S-13	JANUS	TRIDENT	2001
36	THR9	36.3577	25.3569	54	S-13	JANUS	TRIDENT	2011
37	THT1	36.3858	25.4296	0	S-13	-	SMART-24	2011
38	THT2	36.4351	25.4218	338	CMG-3ESP/120	-	REFTEK-130	2011
NISYROS LOCAL NETWORK								
39	NIS1	36.6023	27.1782	378	CMG-3ESP/100	-	TAURUS	2008
40	NIS2	36.5780	27.1808	400	CMG-6T/30	-	WAVE-24	2009
41	NIS3	36.5742	27.1557	271	CMG-6T/30	-	WAVE-24	2009
42	NIS4	36.6717	27.1314	-	CMG-6T/30	-	WAVE-24	2009
CEPHALONIA-LEFKADA LOCAL NETWORK								
43	DLMN	38.2385	20.3734	370	CMG-40T/1	-	REFTEK-130	2014
44	DRAG	38.6839	20.5746	348	CMG-40T/1	-	REFTEK-130	2014
45	EVGI	38.6210	20.6560	249	CMG-40T/30	-	REFTEK-130	2012
46	LKD2	38.7889	20.6578	485	CMG-3ESP/100	JANUS	TRIDENT	2008
47	NYDR	38.7135	20.6983	212	CMG-40T/1	-	REFTEK-130	2014
48	PSDA	38.1140	20.5841	48	CMG-40T/30	-	REFTEK-130	2014
49	TSLK	38.8249	20.6554	212	CMG-40T/1	-	REFTEK-130	2014
50	RTZL	38.0760	20.7715	103	TRILLIUM 120C	-	REFTEK-130	2018
51	LFKM	39.4465	20.0608	1	LE-3D/1sec	-	REFTEK-130	2018
OLDER STATIONS (NOT OPERATING)								
	LKD	38.7074	20.6505	1171				
	MEV	39.785	21.2290	1500				
	THR1	36.3712	25.4597	522				
	THR4	36.46	25.3974	220				
	THR7	36.4224	25.4284	315				

Data Transmission

Typical telephone lines (using carriers of 1020 Hz, 1360 Hz and 1700 Hz for the vertical, N-S and E-W components, respectively) and analogue modems (USRobotics and 3Com) were firstly used to transmit the signal from the seven initially installed peripheral stations (SOH, LIT, GRG, PAIG, KNT, OUR and SRS) to the Central Seismological Station in Thessaloniki (THE-SS).

Initially, the data from some stations (such as LOS, AOS and XOR) were delivered using radio modems (MR400 by RACOM), in the UHF band. Later on, as internet connectivity got faster, cheaper and easier to acquire, DSL connections (PSTN or ISDN) became prominent. Where necessary, RM4 multiplexers by Nanometrics were employed for the transmission over IP, while at several stations (e.g. AGG, KNT, SRS, CHOS, etc.) satellite links are used. Recently, communication over GSM/3G protocol was implemented at LIT.

6.1.3 Data Aquisition

Until 2005, there were four operational seismological networks monitoring the seismic activity in Greece: the networks of the Institute of Geodynamics of National Observatory of Athens (NOA), the Geophysical Laboratory of the Aristotle University of Thessaloniki (AUTH), the Seismological Laboratory of University of Athens (NKUA) and the Seismological Laboratory of University of Patras (UPAT). In 2005, a national project was carried out, financially supported by the Ministry of Development of Greece, in order to unify these networks into one dense national network named Hellenic Unified Seismic Network, HUSN. This project was completed in 2007 and the HUSN started its operation in 2008. Thus, data from all participating networks are now shared in real-time to all four participating institutions, giving them direct access to the records of a unified seismic network of more than 150 stations, all over Greece.

Moreover, in an effort to further improve its detectability, AUTHnet interacts with several European institutions such as GEOFON (Germany), MEDNET (Italy), KOERI (Turkey), IGEWE (Albania), NIGGG-BAS (Bulgaria), SOS (N. Macedonia) and SSS (Serbia) who provide their real-time data and receive data from selected AUTHnet stations. This interaction with neighbouring institutions is critical, mostly in cases of strong or damaging earthquakes out of or close to the network boundaries. At the same time, the opportunity for wider international scientific collaboration is offered.

Data Management

In order to manage all the seismological data transmitted to the THE-SS the NaqsServer system by Nanometrics was used for about 15 years until May 2019. It was working simultaneously on four acquisition servers (both physical and virtual), running on GNU/LINUX. The data acquisition system was receiving real-time data from digitizers through UDP/IP, distributing the data through TCP/IP, saving them on ringbuffers, creating and checking all the triggers and detecting the events. Finally, the Nanometrics acquisition system consists of several utilities to monitor the state-of-health for all the stations and to send calibration commands for the managed instruments remotely.

In May 2019, SeisComP3 software by GFZ Potsdam and Gempa GmbH replaced the outdated Naqs-Server. SeisComP3 is the most known open seismological software for data acquisition, processing, distribution and interactive analysis. The latest stable SeisComP3 version (Jakarta 2018.327.p17) is currently used in AUTHnet.

Seedlink protocol is used for data exchange in the Standard for the Exchange of Earthquake Data format (SEED) with other servers in real time, through TCP/IP. For data exchange with other acquisition systems (such as Nanometrics or Reftek), other appropriate plugins are used.

All real time data, including waveforms, are stored on two different servers running CentOS Linux 7. SeisComP3 uses a database to save all information related with station metadata and seismological data processing, such as arrival times, epicenter estimations, magnitude calculations etc. The database management used is the latest MariaDB Database Engine, a successor of MySQL.

Depth	Thickness km	Velocity km/s	References
Upper sed. layer	1.5	5.0	*Scordilis*, 1985
Layer 1	18.5	6.0	*Panagiotopoulos*, 1984
Layer 2	12.5	6.6	*Panagiotopoulos*, 1984
Half-space	-	7.9	*Panagiotopoulos*, 1984

Table 6.2: *Details on the two-layer over a half-space velocity model and the upper sediment layer used in the earthquake-location procedure.*

Analysis

For daily earthquake analysis SCOLV is used, which is the main interactive tool of SeisComP3 to revise or review the original information such as picks, locations, depths, time, magnitudes and event association. Earthquake parameters and arrival times are stored in the typical AUTOLOC3 format while preliminary bulletins and seismic catalogues are created. The events are analysed on a 24/7 basis. After review, final monthly bulletins are published.

The earthquake-location algorithm NonLinLoc (*Lomax et al.*, 2000) is used to manually estimate the focal parameters. This is a set of programs for velocity model construction, travel-time calculation and earthquake location in 3D structures. The selected velocity model is the one proposed by *Panagiotopoulos* (1984) and *Panagiotopoulos and Papazachos* (1985), which consists of two-layers over a half-space. Additionally, an upper sediment layer (*Scordilis*, 1985) is also considered (Table 6.2).

Near real-time automatic epicenter estimation is also provided by SeisComp3 using LocSat locator by *Bratt and Nagy* (1991). In this case, the IASP91 predefined travel-time table proposed by *Kennett and Engdahl* (1991) and the responsible IASPEI Sub-Commission is implemented for earthquake location and phase identification.

Storage

Raw data are stored in temporary ring-buffers with capacity of more than 90 days (depending on station), in 100 samples/s. Over 500 channels flow per day in ring-buffers resulting in a daily need of about 5.5 GB storage (about 2 TB per year). All located events are stored in the SeisComP3 database, in the SEED format. Additionally, all continuous data (waveforms) are also stored in the European Integrated Data Archive (EIDA, `http://www.orfeus-eu.org/eida/`) national node.

Magnitude calculation

During the earthquake analysis procedure the local magnitude (M_L) is calculated, adopting the multi-parametric equation initially proposed by *Bakun and Joyner* (1984):

$$M_L = \log(A) + n \cdot \log\left(\frac{R}{100}\right) + K(R - 100) + 3.0, \tag{6.1}$$

where A is the zero-to-peak amplitude (in mm) on a typical W-A seismograph (recorded or synthesized), R is the hypocentral distance (in km), n is the geometrical spreading factor and K is the anelastic

attenuation coefficient. For the routine analysis the values n=1.11 and K=0.00189, estimated by *Hutton and Boore* (1987) for earthquakes of California, are adopted. The amplitude used for each station corresponds to the mean value of the maximum zero-to-peak amplitudes measured on the two horizontal components of synthetic Wood-Anderson (SW-A) records. The final local magnitude, M_L, of each earthquake is calculated as the mathematical mean value of the individual magnitudes provided by each station, after applying 90 % confidence limits ($\pm$ 1.65 SD).

Recently, there was a study using a large number of SW-A records of the HUSN (Hellenic Unified Seismic Network) in an effort to define values of geometrical spreading factor n and of anelastic attenuation coefficient K representative for the area of Greece (*Scordilis et al.*, 2015). The final relation proposed in this work for M_L estimation in Greece is:

$$M_L = 1.319 \cdot \log\left(\frac{R}{100}\right) + 0.00226(R - 100) + 3 + c_i, \tag{6.2}$$

where c_i is the individual correction due to the site conditions of each station. We are currently running tests to evaluate Equation 6.2 in comparison with Equation 6.1.

Quality Analysis of GeoLab Bulletin

As a product of routine analysis, monthly bulletins starting from 1995 are published online on our website. The catalogue that is formed from these bulletins includes about 94,000 earthquakes that occurred within the area 33–43°N, 18–30°E.

The completeness of the catalogue, i.e. the magnitude value M_c above which a bulletin is expected to contain 100 % of seismic events, varies in space as well as with time. This is due to the inhomogeneous coverage of the region by seismological stations as well as to possible expansions of the participating seismological networks and/or development of more sophisticated sensors. Several methods have been proposed for the determination of completeness (e.g. *Wyss et al.*, 1999; *Wiemer and Wyss*, 2000; *Woessner and Wiemer*, 2005), essentially relying on the estimation when the reported seismicity no longer follows the Gutenberg-Richter relationship (*Zuniga and Wyss*, 1995). The catalogue's completeness was analysed by applying a combination of these methods.

Completeness variation with time

To determine the time-dependency of the catalogue's completeness, sample windows of several sizes were considered and repeated estimations after bootstrapping were attempted. Three methods have been applied, namely the maximum curvature method (MAXC), the goodness of fit method (GoF) with confidence limits 90 % and 95 % and the entire magnitude range method (EMR) with the help of the Zmap software package (*Wiemer*, 2001).

Figure 6.5 presents the time variation of the completeness magnitude, M_c, as obtained with the combination of the three methods, mentioned above. The examination of the corresponding plot suggests the presence of rather stable M_c values, for certain time intervals. On the basis of this temporal stability, the following general completeness time periods are proposed:

- 1995 – 2003, $M \geq 3.3$,
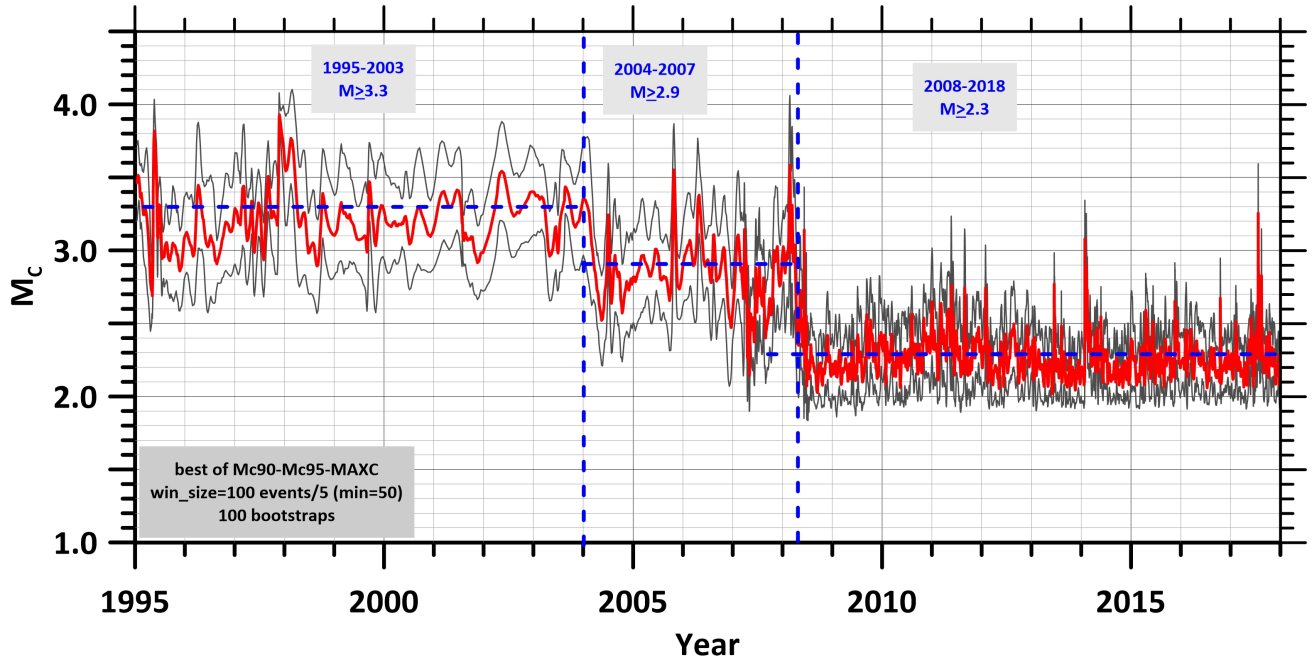
Figure 6.5: *Time variation of the completeness magnitude, Mc, for the AUTHnet catalogue after the combined application of the maximum curvature (MAXC), the goodness of fit (GoF) with confidence limits 90 % and 95 % and the entire magnitude range (EMR) methods (Zmap software, Wiemer, 2001). Gray lines represent the uncertainties revealed after resampling (sample size 100 with 100 bootstraps).*

- 2004 – 2007, $M \geq 2.9$,

- 2008 – 2018, $M \geq 2.3$.

The defined completeness periods are affected by the main expansion phases of AUTHnet. More specifically:

(a) The period (2004-2007) is affected by the 5th phase of the network's expansion that improved its detectability (see Chapter 6.1.2) reducing the completeness magnitude from M_c=3.3 to M_c=2.9.

(b) A further reduction of the completeness level to M_c=2.3 is observed after 2007 due to the 6th and 7th phases of the network's expansion.

Completeness Variation in Space

The spatial variation of the M_c values for each of the previously defined completeness periods has also been analysed, in order to further exhibit the temporal variations throughout the broader area of Greece (Figure 6.6).

A grid of 0.10°×0.10° covered the whole study region. For each complete time-period, circular areas of 100 km radius, centred at each node of the grid were considered. The M_c value corresponding to the earthquakes of each circular area was estimated again by the combination of MAXC, GoF 90 %, GoF 95 % and the EMR method (Zmap software package, *Wiemer*, 2001). The derived M_c values were used to produce contour maps showing its spatial distribution for each complete period (Figure 6.6).
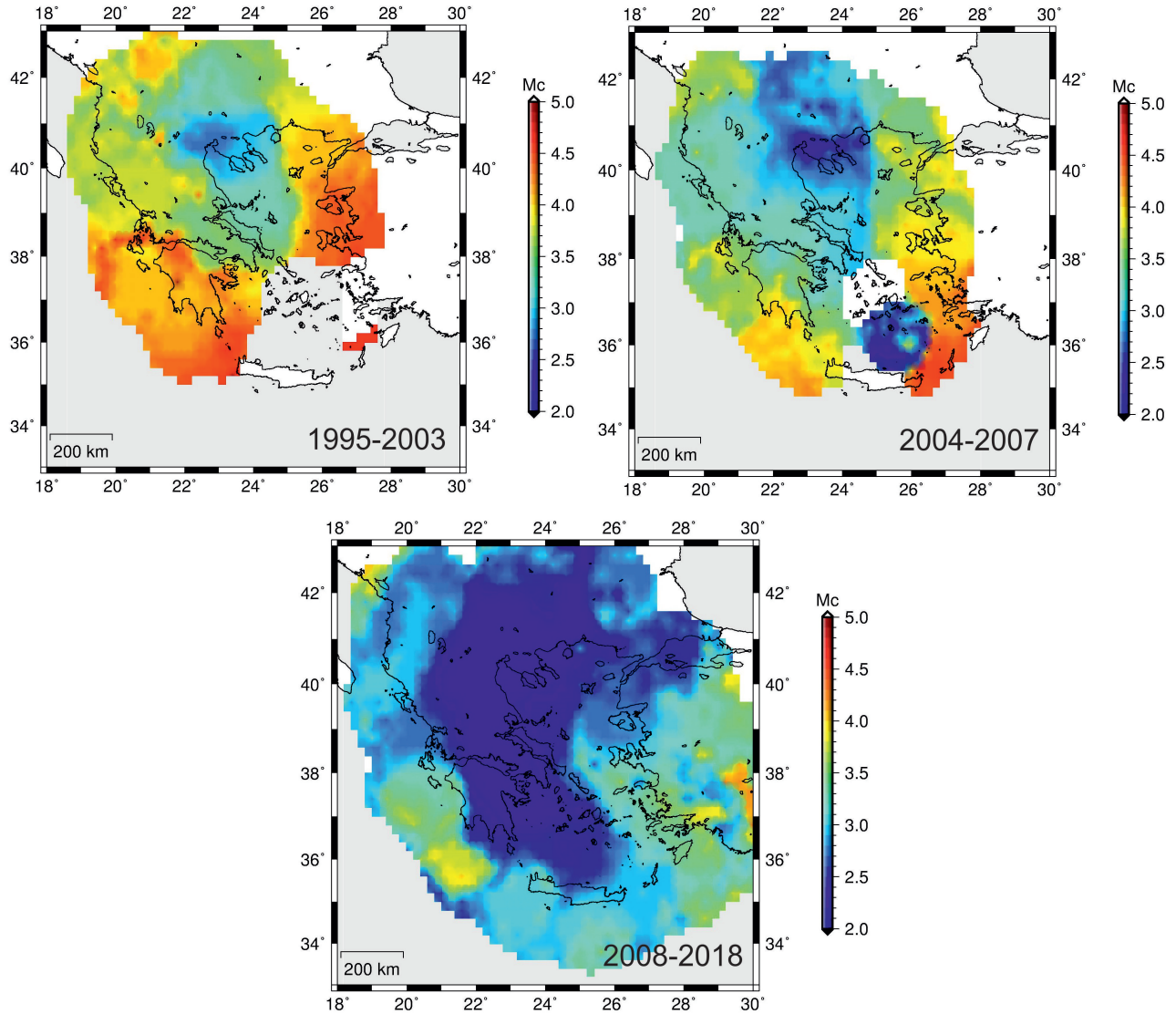
Figure 6.6: *Spatial variation of the completeness magnitude, Mc, of the catalogue produced by AUTHnet.*

6.1.4 Aims and Social Contribution

Aims and Services Provided

AUTHnet operates 24 hours per day, 365 days per year and its main purpose is the continuous near real-time monitoring and processing of seismic data. The dense network provides the opportunity for a rapid manual determination (in about 15–20 minutes) of the location and magnitude of all earthquakes (M>2.5) that occur in the broader area of Greece. Automatically produced preliminary determinations of the focal parameters (based on SeisComP software) for every event are also performed within one minute of the event's occurrence. In case of a destructive event, all available information is disseminated to national and local authorities, such as the Earthquake Planning and Protection Organization (E.P.P.O) and the General Secretariat of Civil Protection. It is also a priority for the staff of THE-SS to provide rapid and valid information to the media and to the public, preparing also announcements, whenever necessary, about the evaluation of on-going seismic activity.

Several types of information are presented on the THE-SS website (`http://seismology.geo.auth.gr/ss`), where both automatic (real-time) and revised (manual, near real-time) locations for the current seismic activity are presented on a map. In case of a disruptive earthquake (e.g. of $M > 4.0$) additional details are provided. As the network is now equipped with broadband sensors, near-real time moment tensor computations are performed and published online. Since 2013, a semi-automatic process for a near-real-time evaluation of the evolution of seismic excitations (*Teza*, 2011) is also applied. The respective results are published on-line and are updated daily until the end of the excitation under surveillance. Finally, seismicity maps, preliminary and revised earthquake catalogues as well as monthly earthquake bulletins are also available in the THE-SS website.

The international scientific community receives detailed information about the seismic activity in Greece as THE-SS shares this information with international seismological agencies dealing with the collection of such data (e.g. EMSC, ISC, NEIC). THE-SS also contributes phase readings of long-distance moderate to large earthquakes that occur globally.

The continuous technical and spatial upgrade of the network assures the high quality of the data collected. The number of recorded earthquakes is increasing, data of higher accuracy are produced, while the uncertainties on epicenter and depth determination are less than 5 km. At the same time, the network's detectability keeps improving due to the installation of new stations. Thus, in areas with azimuthal gaps of less than 180° the network's detectability is higher with the minimum recorded (detected) magnitude dropping below 2.0.

Thus, the completeness magnitude for the broader Thessaloniki area is M_c=2.9 since 1981 and M_c=2.4 since 1990 (*Vamvakaris et al.*, 2016). Recently, the completeness in this area is further improved with M_c=2.0, while for the rest of the network area the completeness magnitude increases to 2.5 or more, especially close to the network boundaries (Figure 6.6). In many cases, local networks (e.g. Santorini and Cephalonia-Lefkada networks) are able to provide reliable focal parameters for earthquakes with magnitudes even smaller than M=1.0.

Between 1995 and 2006, 1,000 to 1,500 regional events were recorded per year and analysed by AUTHnet. Some 4,200 earthquakes were recorded in 2007 (the annual number nearly quadrupled), while this number increased to 6,600 in the following year (2008). In 2013 the recorded earthquakes reached 7,200. During the last four years, the network detected more than 8,000 events/year, while in 2015 this number exceeded 9,000. This means that around 25 regional earthquakes were recorded daily, the focal parameters of which were manually calculated by GeoLab scientific staff. This large number of earthquakes is directly connected with the continuous qualitative and quantitative improvement of AUTHnet. Thus, from 2004 onward, it became feasible to conduct detailed studies on disturbing regional seismic excitations (e.g. in Andravida with M=6.5 in 2008; Lemnos with M=5.9 and Amfiklia with M=4.9 in 2013; Zakynthos with M=4.7, Cephalonia with M=6.1, Samothraki with M=6.3 and Evoikos gulf with M=5.3 in 2014; Lefkada with M=6.4 in 2015; Ioannina with M=5.3 in 2016; Lesvos with M=6.3 and Kos with M=6.6 in 2017; Zakynthos with M=6.8 in 2017).
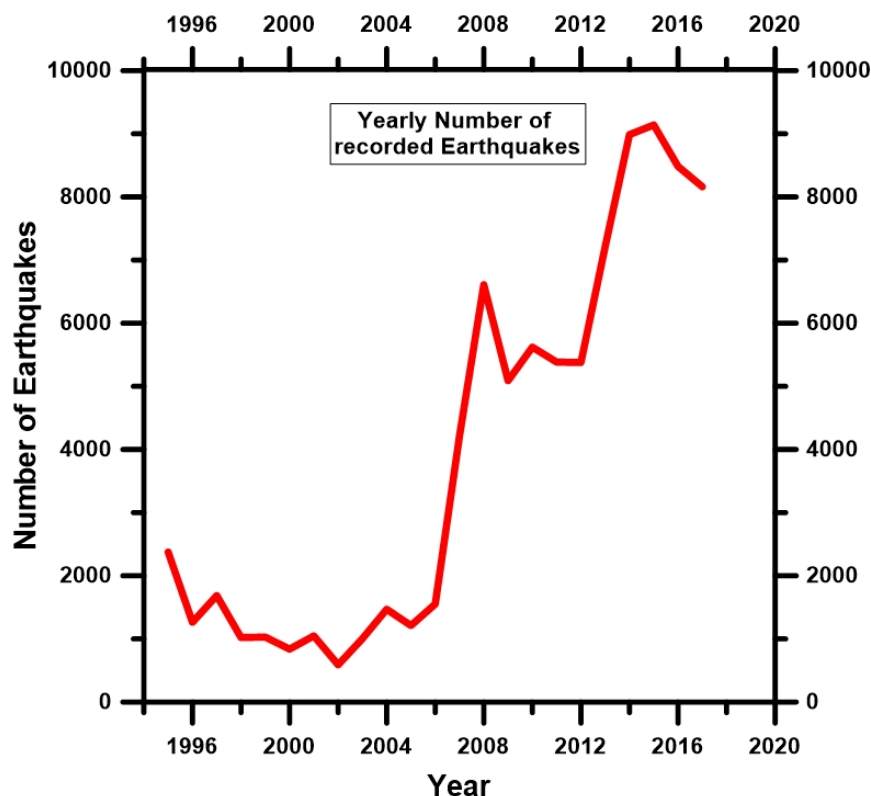
Figure 6.7: *Number of regional earthquakes recorded by AUTHnet, during the period 1995-2017 (Vamvakaris, 2018).*

AUTHnet Contribution to Society

Besides their research profile, GeoLab and THE-SS also have an educative mission. Thanks to the seismological network and its data collection, undergraduate students are involved with applied seismology and many postgraduate students and PhD candidates elaborate their theses and work on several seismological and geophysical projects. It is also important to note that in the framework of the continuous flow of information to the public, the scientists of THE-SS give several lectures to elementary and high school students, transferring knowledge about earthquakes and protection measures. Highschool students have the opportunity to visit the Central Seismological Station, see the instruments and experience the routine of a seismologist on duty. Lectures focused on specific topics are also given to rescue teams and members of the Civil Protection Organization of Greece.

In the last 5 years, taking advantage of the project "AUTH Sundays", organized by the Aristotle University, citizens have the opportunity to visit the Central Seismological Station and get more familiar with earthquakes, by watching relevant presentations and speaking with seismologists. The main target, through this permanent interaction with society, is to get people (and especially the young kids) more familiar with earthquakes by teaching them how to act and how to protect themselves when a strong earthquake occurs.

The Geophysical Laboratory is always open to invitations to participate in activities, exhibitions and festivals, aiming to better inform the public on seismic building codes and protection issues.

6.1.5   Future Plans

A continuous improvement of the geographical density of AUTHnet by installing more stations is always in the plans. An instrumental upgrade is coming soon, as new compact 3-component Trillium seismometers (120 s - 100 Hz) are already available to replace the older ones. The time of correspondence and reaction in case of felt earthquakes is very important, thus it is necessary to further reduce the time needed for accurate estimation of the focal parameters of disturbing earthquakes. In this sense, more reliable automatic alerts could be very helpful, mostly in cases of aftershock sequences. Another realistic target for the next period is to offer automatically produced near real-time shake maps, when a strong earthquake occurs. These maps could be very useful to the authorities, in order to have a more detailed instant view of possibly damaged sites and, therefore, to better prepare their actions.

AUTHnet plans to start permanent communication with selected persons of authorities by sending direct notice through e-mail or SMS, when an earthquake occurs. That service could be extended to the public, so everybody could receive an automatic e-mail informing them about the evolution of an ongoing seismic excitation.

Apart from the obvious contribution to earthquake monitoring, a result of the ongoing qualitative and quantitative improvement of the produced seismological data is the better understanding and interpreting of the geodynamic phenomena that take place in Greece. Such data are powerful tools for scientists who are involved with geodynamics to study the crustal structure, the complexity of lithosphere and the upper and deeper mantle, as well. These are significant research areas that can lead to important breakthroughs in better understanding the continental dynamics and earthquake mechanics.

Acknowledgements

References

Bakun, W.H. and W.B., Joyner (1984), The M_L scale in central California, *Bull. Seismol. Soc. Am.*, *74*, 1827–1843.

Bratt, S.R. and W. Nagy (1991), The LocSAT Program, *Science Applications International Corporation*, San Diego.

Hutton, L.K. and D.M., Boore (1987). The M_L scale in southern California, *Bull. Seismol. Soc. Am.*, *77*, 2074–2094.

Karakostas, V., E. Papadimitriou, M. Mesimeri, Ch. Gkarlaouni, and P. Paradisopoulou (2015), The

2014 Kefalonia Doublet (M_W 6.1 and M_W 6.0), Central Ionian Islands, Greece: Seismotectonic Implications along the Kefalonia Transform Fault Zone, *Acta Geophysica*, `https://doi.org/10.2478/s11600-014-0227-4`.

Kennett, B.L.N. and E.R. Engdahl (1991), Traveltimes for global earthquake location and phase identification, *Geophys. J. Int*, *105*(2), 429–465, `https://doi.org/10.1111/j.1365-246X.1991.tb06724.x`.

Lomax, A., J. Virieux, P. Volant and C. Berge, (2000), Probabilistic earthquake location in 3D and layered models: Introduction of a Metropolis-Gibbs method and comparison with linear locations, in: *Advances in Seismic Event Location*, Thurber, C.H., and N. Rabinowitz (eds.), Kluwer, Amsterdam, 101-134.

Newman, A.V., S. Stiros, L. Feng, P. Psimoulis, F. Moschas, V. Saltogianni, Y. Jiang, C. Papazachos, D. Panagiotopoulos, E. Karagianni and D. Vamvakaris (2012), Recent Geodetic Unrest at Santorini Caldera, Greece, *Geophys. Res. Lett.*, *39*, L06309, `https://doi.org/10.1029/2012GL051286`.

Panagiotopoulos, D.G. (1984), Travel time curves and crustal structure in the southern Balkan region, Ph.D. Thesis, University of Thessaloniki, pp. 173 (in Greek).

Panagiotopoulos, D. G. and B. C. Papazachos (1985), Travel times of Pn-waves in the Aegean and surrounding area, *Geophys. J. R. astr. Soc.*, *80*, 165–176.

Papadimitriou, E., V. Karakostas, M. Mesimeri, G. Chouliaras and Ch. Kourouklas (2017), The M_W6.5 17 November 2015 Lefkada (Greece) Earthquake: Structural Interpretation by Means of the Aftershock Analysis, *Pure and Applied Geophysics*, *174*(10), 3869–3888, `https://doi.org/10.1007/s00024-017-1601-3`.

Papazachos, B.C. and C.B. Papazachou (2003), The earthquakes of Greece, Ziti Publications, Thessaloniki, (in Greek).

Scordilis, E.M. (1985), A microseismic study of Servomacedonian zone and the surrounding area, Ph.D. Thesis, Aristotle University of Thessaloniki, pp. 250.

Scordilis, E.M., D. Kementzetzidou and B.C. Papazachos (2015), Local magnitude calibration of the Hellenic Unified Seismic Network, *J. Seismol.*, *20*(1), 319–332, `https://doi.org/10.1007/s10950-015-9529-5`.

Teza, E. (2011), Automated procedure validating the possible evolution of a seismic excitation, MSc Thesis, Aristotle University of Thessaloniki (in Greek).

Vamvakaris, D. A., C.B. Papazachos, C.A. Papaioannou, E.M. Scordilis and G.F. Karakaisis (2016), A detailed seismic zonation model for shallow earthquakes in the broader Aegean area, *Nat. Hazards Earth Syst. Sci.*, 16(1), 55–84, `https://doi.org/10.5194/nhess-16-55-2016`.

Vamvakaris, D. A. (2018), Aristotle University of Thessaloniki telemetric seismological network (AU-THnet); a brief description, *Proceedings of the 9th International INQUA Meeting on Paleoseismology, Active Tectonics and Archeoseismology (PATA)*, *9*, 303–307.

Wiemer, S. and M. Wyss (2000), Minimum magnitude of complete reporting in earthquake catalogues: examples from Alaska, the western United States, and Japan, *Bull. Seism. Soc. Am.*, *90*(4), 859–869,

`https://doi.org/10.1785/0119990114`.

Wiemer, S. (2001), A software package to analyze seismicity: ZMAP, *Seism. Res. Lett.*, *72*(3), 373–382, `https://doi.org/10.1785/gssrl.72.3.373`.

Woessner, J. and S. Wiemer (2005), Assessing the quality of earthquake catalogues: Estimating the magnitude of completeness and its uncertainty, *Bull. Seism. Soc. Am.*, *95*, `https://doi.org/10.1785/012040,007`.

Wyss, M., A. Hasegawa, S. Wiemer and N. Umino (1999), Quantitative mapping of precursory seismic quiescence before the 1989, M7.1 off-Sanriku earthquake, Japan, *Annali Di Geofisica*, *42*(5), 851–869, `https://doi.org/10.4401/ag-3765`.

Zuniga, F. and M. Wyss (1995), Inadvertent changes in magnitude reported in earthquake catalogues: Their evaluation through b-value estimates, *Bull. Seism. Soc. Am.*, *85*, 1858–1866.

6.2 Seismological Monitoring in Latvia

Valerijs G. Ņikuļins

Latvian Environment, Geology and Meteorology Center, Riga, Latvia

The development of modern seismological monitoring in Latvia was set up after the Kaliningrad earthquake on September 21, 2004 where the magnitude of the main shock reached $M_W = 5.2$ (*Gregersen et al.*, 2007) and the intensity of shaking at the epicentre was 6.5 points according to the MSK-64 scale (*Nikonov et al.*, 2005). In the south of Latvia (village of Kalni and town of Saldus), the intensity of shaking reached 5 points on the EMS-98 scale (*Nikulin*, 2005). In October 2006, the Slītere station was created in the north-west of Latvia, which became part of the GEOFON international seismic network of GFZ Potsdam, Germany. Thanks to the cooperation agreement between the Latvian Environment, Geology and Meteorology Center (LEGMC) and GFZ Potsdam, it became possible not only to create a seismological station with modern instruments and equipment, but also to use other stations of the GEOFON network as well as some stations of national networks in the Baltic region to localise seismic events in the East Baltic Region (EBR), which covers Estonia, Latvia, Lithuania, the Kaliningrad region of Russia and the adjacent part of the Baltic Sea (Lat: 53.9° – 59.7° N; Lon: 19,4°E – 29.6°E, see box in Figure 6.8). This article describes the history of seismological monitoring in Latvia, presents the characteristics of the data acquisition (since 2006) and processing, gives some review of the natural and technogenic seismicity of the East Baltic region and briefly discusses the problems of monitoring tectonic earthquakes and man-made seismic phenomena. Prospects for optimizing the seismological monitoring are outlined as well.

6.2.1 Regional Seismicity and History of Seismological Monitoring in Latvia

Latvia is located in the west of the East European Platform (EEP) with a very low level of natural seismic activity (*Nikulins*, 2011). Its territory is more than 1800 km away from the divergent border in the North Atlantic and the convergent border in the Mediterranean Sea. However, there is intraplate, natural seismicity.

In Latvia, historical earthquakes occurred in 1616 in the Bauska region, in 1821 in the Koknese region, in 1857 in the Irben Strait and in 1896 in the Jelgava region (*Doss*, 1909; *Avotinja et al.*, 1988). In Estonia, historical earthquakes occurred in 1670 in the Pärnu region, in 1823 in the Kuigatsi region, in 1827 in the Haapsalu region, and in 1881 in the Narva region. Modern EBR earthquakes occurred in

1976 on the island of Osmussaare, in the shelf zone of Estonia (M = 4.7) (*Kondorskaya et al.*, 1988), and in 2004 in the Kaliningrad region of Russia (M_W = 5.0 and 5.2) (*Gregersen et al.*, 2007).

Since the Kaliningrad earthquakes caused damage in the territory of Latvia, the need arose to monitor the seismic regime throughout the territory of the EBR to assess the seismic hazard of the territory of Latvia. This chapter provides an overview of the development of seismological observations in Latvia.

The Early History of Seismological Observations in Latvia

The beginning of seismological observations in Latvia dates back to the 1960s when, with the help of the Department of Earth Physics of Moscow State University, the seismic station "Baldone" operated in the territory of the Radio-Astrophysical Observatory of the Academy of Sciences of Latvia until 1991. A long-period seismograph SD-1 was installed at the station. Teleseismic and strong earthquakes were recorded together with other stations in Minsk, Moscow and Pulkovo, and the deep structure of the Earth's crust and mantle was estimated based on the analysis of converted phases and the determination of dispersion curves of phase and group velocities of surface waves (*Hot'ko*, 1974).

The second stage of seismological observations dates back to 1994, when the State Geological Survey of Latvia created the short-period, analogue seismic station Skujas in the Valmiera region in the north-east of Latvia. In addition, a three-component seismic recorder (GBV-316) was installed at the station in 2000. Skujas station operated until 2013 and was then closed. The station recorded over 2,900 seismic events, including over 1,400 teleseismic and 550 regional seismic events. 600 seismic events could not be identified as man-made seismic events or tectonic earthquakes because only one analogue seismic station was used.

The Modern Stage of Seismological Observations

The third stage of instrumental observations in Latvia began after the Kaliningrad earthquakes in 2004, when the Latvian Environment, Geology and Meteorology Center, together with GFZ Potsdam, created the Slitere seismic station in northwestern Latvia. Participation in the GEOFON network allowed access to seismic stations in the Baltic region and the creation of the Baltic Virtual Seismic Network (BAVSEN). BAVSEN includes its own Slitere station (SLIT), a number of stations of the GEOFON network (PABE, PBUR, VSU, PUL), as well as some stations of national networks of countries in the Baltic region (Fig. 6.8), in particular stations of Finland (MEF, RAF), Estonia (MTSE, ARBE), Denmark (BSD) and Poland (SUW). To localise regional EBR seismic events, 6 stations were mainly used (SLIT, VSU, MTSE, ARBE, MEF, RAF).

The Finnish stations (MEF and RAF) play an important role in the localization of regional seismic events in EBR, since they are located on the crystalline basement of the Fennoscandian shield in very favourable seismic and geological conditions. Often, the first P-wave can be confidently identified on the records of these stations. However, in 2019, data availability from the RAF station was sometimes limited. Lithuanian stations (PABE, PBUR) were used much less frequently for localization of seismic events in EBR. Almost no stations were used in Poland (SUW) and Denmark (BSD) for localization of regional seismic events in EBR. In addition, some stations stopped registering (SRPE - Estonia),
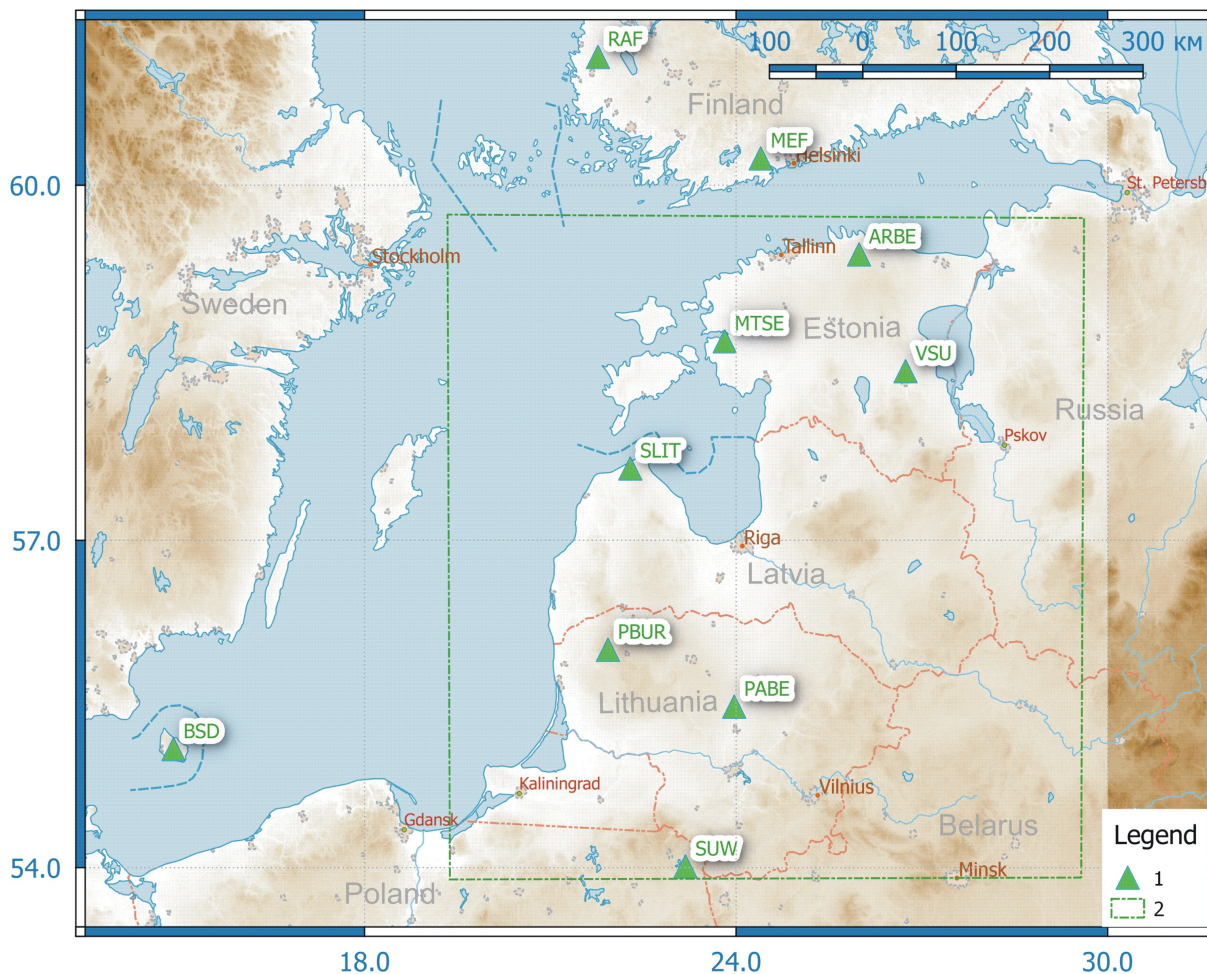
Figure 6.8: *Baltic virtual seismic network BAVSEN. Labels: 1 - seismic stations; 2 - border of the East Baltic region (Estonia, Latvia, Lithuania, Kaliningrad region of Russia, western part of the Pskov region of Russia, northwestern Belarus, part of north-east Poland, adjacent waters of the Baltic Sea.*

or access to the data of these stations from the GFZ Potsdam server (PUL - Russia) was terminated. Therefore, from 2015 it was necessary to switch to high-frequency HH* channels, although from 2008 to 2015 broadband BH* channels were used for localisation.

For the localization of teleseismic events with magnitudes greater than 5.5, a larger number of stations were used, including PABE, PBUR, SUW and BSD. However, the quality of hypocentre localization of remote seismic events was low because of the large azimuthal gap for BAVSEN network stations. The Latvian seismic station Slitere is located in the north-west of Latvia in the Kurzeme region. The station is located 5.5 km from the coast of the Baltic Sea in the territory of the Slitere lighthouse (Fig. 6.9). The sensor is located at a depth of 6.5 m from the surface of the ground in moraine deposits.

6.2.2 Data Aquisition

The Slitere station, like other stations of the GEOFON network, is equipped with typical seismological equipment, which consists of the following main elements (Fig. 6.10): STS-2 sensors, PS6 Earth Data 24 analogue-to-digital converter, SeisComp software and communications unit, GPS antenna. SeisComp is seismological software for the collection, processing, dissemination and interactive analysis of data,

Figure 6.9: *Seismic station Slitere (Latvia). 1 - lighthouse "Slitere"; 2 - entrance to the instrumental bunker; 3 - tool house; 4 - SeisComp unit and analogue-to-digital converter PS6 Earth Data 24; 5 - a view of the STS-2 sensor from the height of the upper compartment; 6 - a view of the STS-2 sensor from the height of the middle compartment.*
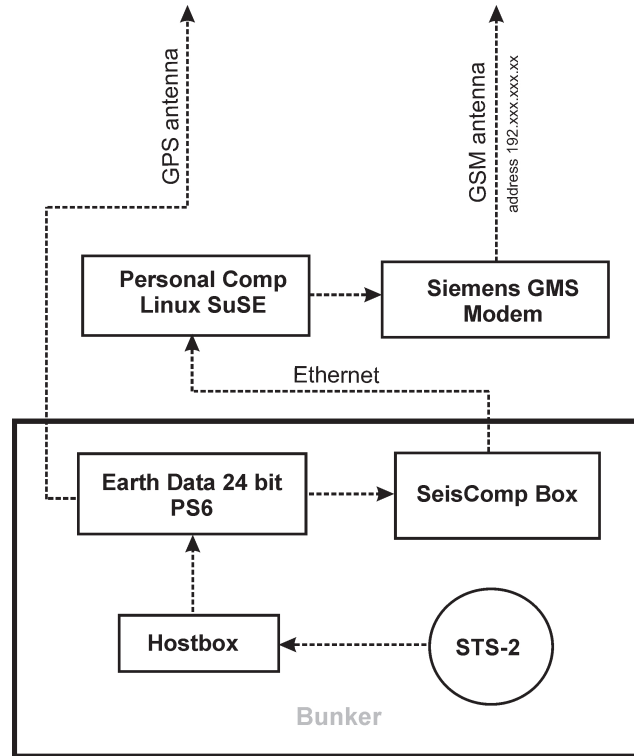
Figure 6.10: *Scheme of typical equipment of a GEOFON seismic network station.*

developed at Potsdam by the German Geoscience Research Center GFZ and gempa GmbH. A schematic diagram of a typical GEOFON station is presented in Figure 6.10.

The Streckeisen STS-2 Broadband Sensor has three inertial pendulums with angular geometry. In the vertical plane, the axis of the pendulums are oriented at an angle of 54.7° relative to the vertical axis. In the horizontal plane, the axis of the pendulums are oriented approximately at an angle of 120° from each other. The generator constant has a value of 1500 ± 15 V · s/m. The frequency range covers the band from 0.00833 to more than 50 Hz. Many stations in the GEOFON network use high-frequency HH*, broadband BH*, low-frequency LH*, and ultra-low-frequency VH* channels.

The seismological data is sent as MiniSeed from the stations to the servers at GFZ Potsdam via internet, and from Slitere to the LEGMC processing center (Fig. 6.11).

The download for the several stations required for the localisation of events takes place automatically from the GFZ Potsdam server in accordance with the SeedLink data transfer protocol.

6.2.3   Analysis

At the next stage, seismic events are sampled in GSE1.0 format using SeismicHandler (*Stammler*, 1993). Further, initial information is processed in the environment of Seisan (*Havskov and Ottemöller*, 1999), a seismic analysis system consisting of a set of programs and a database.

For hypocentre location, a modified version of the Hypocenter program is used (*Lienert et al.*, 1986; *Lienert and Havskov*, 1995). The main modification is the ability to use more phases of seismic waves, localise teleseismic events and use the Nordic format directly from the database. Four seismic velocity
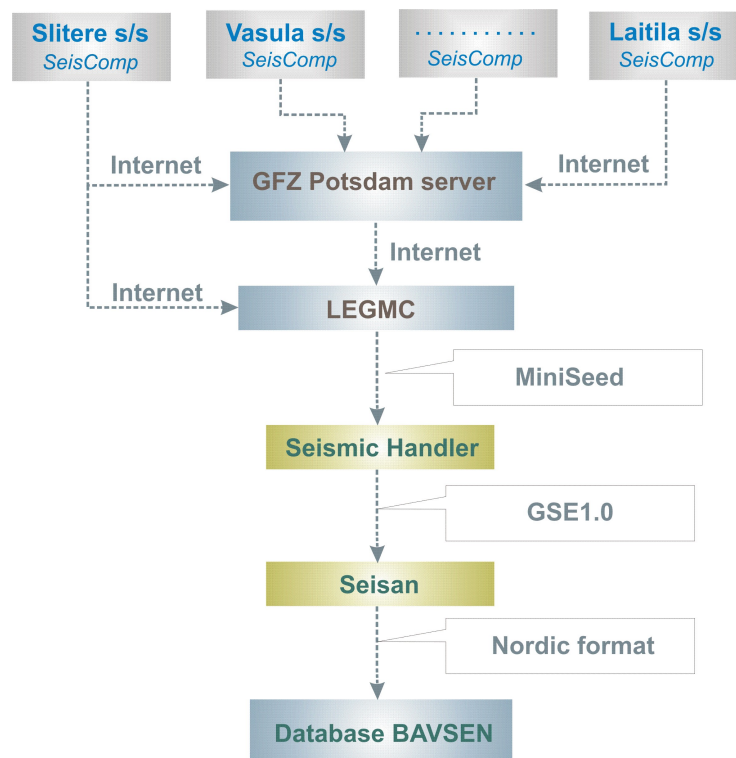
Figure 6.11: *Flow chart of transmission of seismological information from the stations to the servers, data formats, software and processing steps.*

models are used for locating regional seismic events: iasp91 (*Kennett and Engdahl*, 1991), Helsinki model – hel (Institute of Seismology, University of Helsinki), Fennoscandian model (fen) and proprietary model baltic08.

The baltic08 regional velocity model was created based on the results of deep seismic sounding using the Sovetsk – Riga – Kohtla-Järve 563.4 km long geo-traverse (*Sadov and Penzina*, 1986). According to these studies, the deep geological structure of the East Baltic region has the following features: (1) the Earth's crust is characterised by a depression; (2) the Mohorovičić discontinuity can be distinguished into three parts: northern (PK 600 - PK 420, PK = pickets, km along seismic profile), central (PK420 - PK170) and southern (PK170 - PK130); (3) the crust in the northern and southern parts is less thick (46 and 40 km) than in the central part, where it shows an anomalous deep base of the Earth's crust with 64 km; (4) five layers can be distinguished within the Earth's lithosphere: M1 - crust-mantle-boundary; M2 - intramantle border; IV, II' and II - intracrustal borders. The baltic08 model consists of 5 layers shown in Table 6.3.

Seismic Background Noise Characteristic

The characteristics of the seismic background noise gives an idea of the capabilities of the seismic stations of the BAVSEN network. Figure 6.12 shows the spectral power density of seismic noise in busy periods (daytime, during working hours (May 22, 2019 from 09:20 to 09:40 - red curve) and quiet periods (at night during the weekend (May 25, 2019 from 23:20 to 23:40 - blue curve) for stations of the BAVSEN network, mainly located in the EBR.
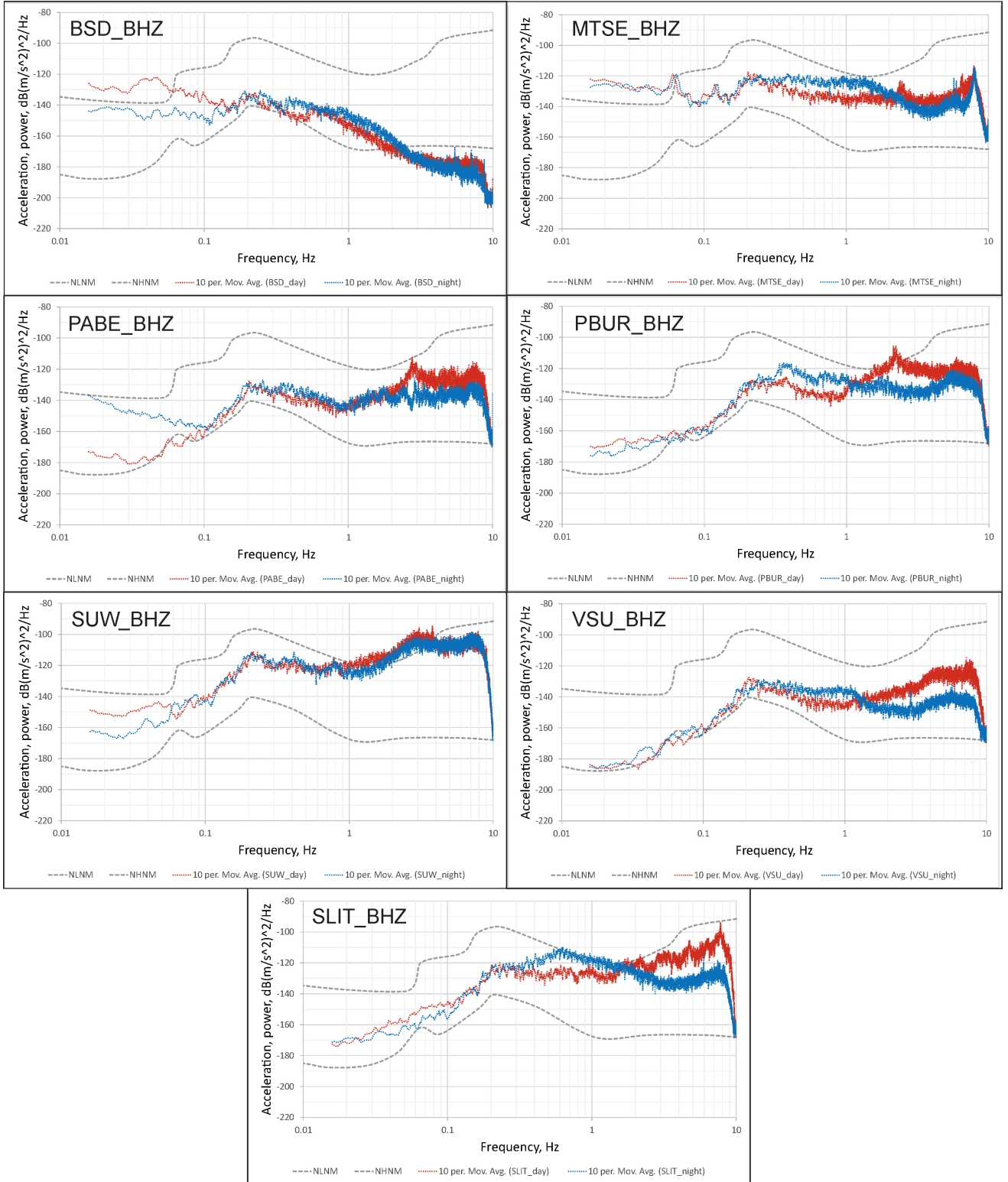
Figure 6.12: *Spectral power density of seismic background noise at BAVSEN stations during day time (red curve) and night time (blue curve). Dashed lines: Spectral power density of noise for NLNM (bottom) and NHNM (top) according to* Peterson *(1993).*

Layer	Depth of base km	Velocity km/s	Composition
h1	1.0	2.3	Sedimentary
h2	20.0	6.1	Metamorphic granite
h3	42.0	6.6	Diorite-granulite
h4	57.0	7.1	Granite-granulite
h5	70.0	8.2	Gabbro-peridotite-pyroxene
	>70.0	8.5	

*Table 6.3: baltic08 velocity model. The composition of the deeper layers are based on information about the geological structure of the Karelian-Kola region by V.V.Yakovleva (*Ankudinov and Dvoretskaya*, 1984;* Ankudinov et al.*, 1991).*

Only the BSD station is located on the Scandinavian shield. This station has a low noise level at high frequencies, starting from 2 Hz, but at low frequencies, less than 0.1 Hz, the noise level is quite high. BSD is located in the Baltic Sea, on the island of Bornholm. At stations located within the East Baltic region (SUW, SLIT, PABE, PBUR, MTSE and VSU), the noise level at high frequencies is significant and a technogenic impact in the daytime during working hours at SLIT, PABE, PBUR and VSU stations is obvious. Despite the fact that at many stations (SUW, VSU, PBUR, PABE, SLIT, PUL) in the EBR the sensors are located at depths from 2 to 10 m, this does not significantly reduce the background noise in the band above 1 Hz. In sedimentary cover and especially unconsolidated Quaternary sediments, there are adverse conditions that significantly reduce the effectiveness of seismological monitoring. The solution could be to install the sensors into deep pits and wells, which would increase the efficiency of seismic monitoring in the EBR.

EBR Regional Tectonic Earthquakes from 2008 to 2019

During the instrumental observation period from 2008 to 2019 in the EBR, low seismic activity caused by tectonic earthquakes was observed (Fig. 6.13).

During this period, only 8 tectonic earthquakes occurred in the indicated EBR territory, which were localised using the BAVSEN network. The magnitude range of earthquakes was 1.3 – 2.5. Mostly, the EBR earthquake centres were located along the western and northern coasts of Estonia, in the Gulf of Finland and in the area of Lake Võrtsjärv, in Estonia. The localization results according to BAVSEN data were compared with Institute of Seismology University of Helsinki (ISUH) data (for more information on the Finnish National Seismic Network see *Kortström, Uski and Oinonen*, (2018)). The results showed a satisfactory similarity. Thus, most of the modern tectonic earthquakes of the EBR, for the period from 2008 to 2019, are confined to the coastal and shelf zones of Estonia. In the past, historical earthquakes occurred in these areas, which is evidence of the preservation of a certain level of seismic activity.

Regional man-made Seismicity of the EBR from 2008 to 2019

Man-made seismicity is the predominant type of seismicity in EBR. It is due to the action of a large number of industrial quarries, as well as seismic sources located in the Baltic Sea. About 50 industrial
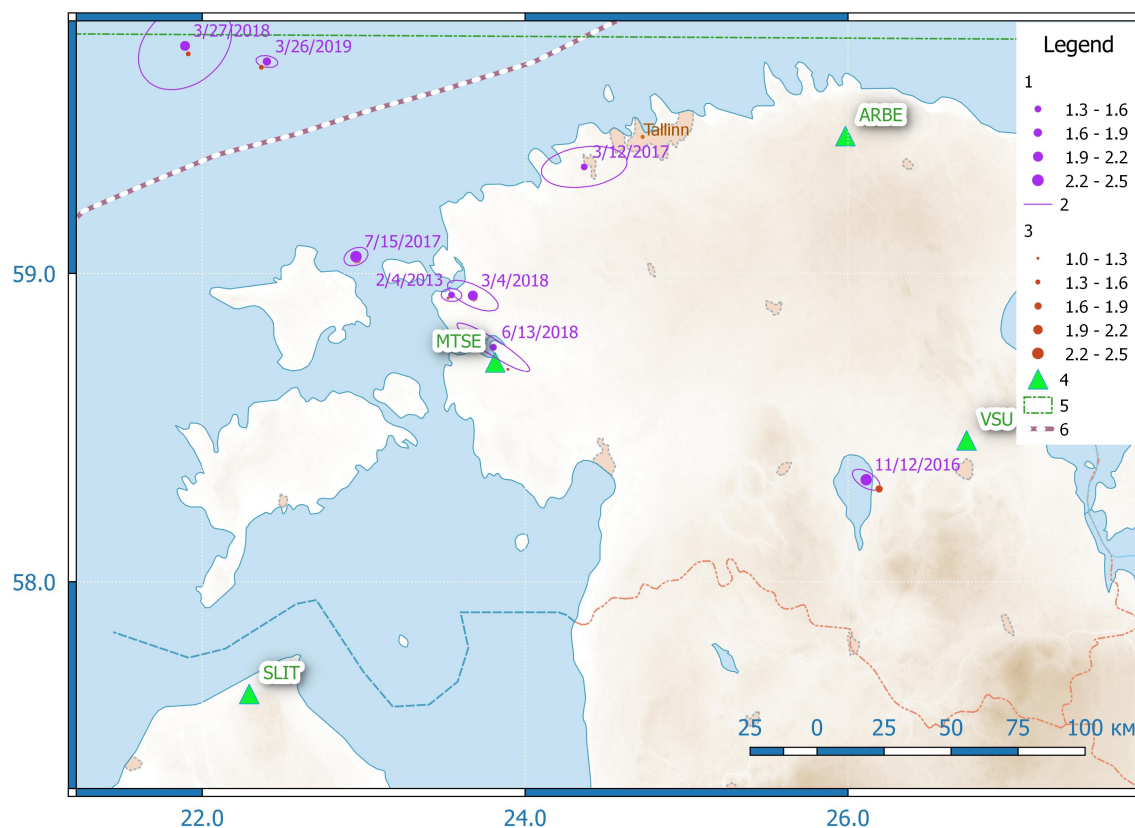
Figure 6.13: *Comparison of earthquake hypocentres of the East Baltic region according to BAVSEN and ISUH data for the period from 2008 to 2019. Labels: 1 - local magnitudes according to BAVSEN; 2 - error ellipse for BAVSEN data; 3 - local magnitudes according to ISUH; 4 - BAVSEN network; 5 - East-Baltic region border; 6 - Nord Stream gas pipeline.*

quarries are located on the territory of the EBR, including several mines in Estonia (*Nikulins*, 2017). Explosions are used in industrial quarries and mines to mine oil shale, dolomite, limestone and gypsum. But the number of explosions carried out in quarries in the EBR changed significantly over time and decreased due to the ongoing economic crisis. In some quarries, the explosions stopped. Active development of oil shale is still ongoing in the north-east of Estonia, in the areas of Mustanina, Kiviõli and Aidu-Liiva. In Latvia, only the Aiviekste quarry, where dolomite is mined, continues to maintain a stable operation. Explosions in other quarries of Latvia and Lithuania are rare at the moment.

The average local magnitude is 1.8 with a standard deviation of $\pm$ 0.42. The distribution map of instrumental-recorded, anthropogenic seismic events of the EBR from 2008 to 2019 is shown in Figure 6.14.

Over the indicated period of time (2008 - 2019), 5778 seismic events (including tectonic events) were localised in the EBR. Man-made events included all events that did not have confirmation as tectonic earthquakes from other seismic networks, for example, ISUH. The total number of regional seismic events in the entire Baltic region, localised by the BAVSEN network from 2008 to November 2019 reaches 12449 (with an epicenter distance of up to 800 - 1000 km). Several zones of concentration of epicentres of seismic events can be noted, with man-made seismic events being confined to quarries and the coastal zone of the EBR where blasting operations also occur. The distribution of seismic events during the day clearly indicates their predominantly man-made genesis (Fig. 6.15).
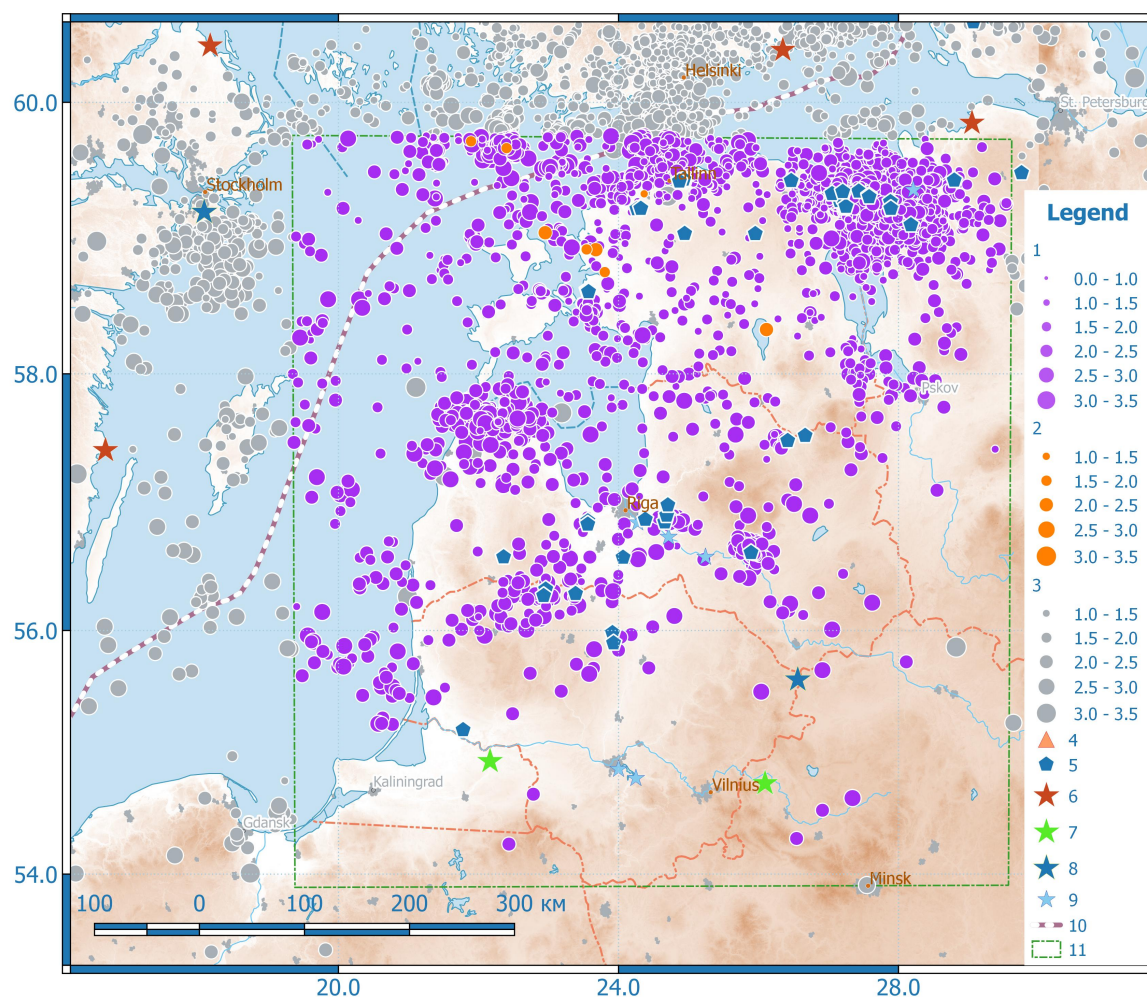
Figure 6.14: *Integrated seismicity of the East Baltic region from 2008 to 2019 according to the BAVSEN network. Labels: 1 - local magnitude of technogenic seismic events (explosions); 2 - local magnitude of tectonic earthquakes; 3 - local magnitude of summary seismic events outside the East Baltic region; 4 - seismic stations of the BAVSEN network; 5 - quarries in which blasting may be carried out; 6 - operating nuclear power plants (NPP); 7 - NPPs under construction; 8 - closed NPPs; 9 - hydroelectric power station; 10 - Nord Stream gas pipeline; 11 - East Baltic region's contour.*
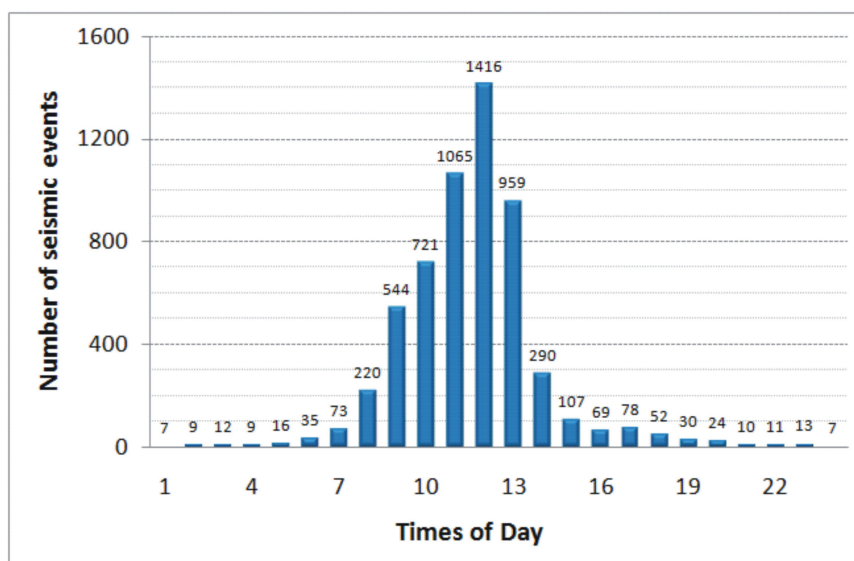
Figure 6.15: *The daily distribution of seismic events in the East Baltic region from 2008 to 2019.*

Agency	Origin time	Lat deg	Lon deg	Depth km	Mag
LEGMC	2015/06/12 08:18:28	55.461	21.357	0.0	2.6 ML
UHIS	2015/06/12 08:18:28	55.489	21.450	0.0	2.5 ML
SNSN	2015/06/12 08:18:29	55.420	21.502	0.4	2.6 ML
NORSAR Automatic GBF	2015/06/12 08:18:29	55.490	21.690	-	2.51
EST	2015/06/12 08:18:27	55.486	21.417	0.0	-
GEUS	2015/06/12 08:18:27	55.435	21.488	0.0	-

Table 6.4: *Hypocentres of an induced event in Lithuania. Notation: LEGMC - Latvian Environment (latest relocation), Geology and Meteorology Center; UHIS - University of Helsinki Institute of Seismology; SNSN - Sweden National Seismic Network; NORSAR - Norwegian Seismic Array; EST - Geological Survey of Estonia; GEUS - Geological Survey of Denmark and Greenland*

Most seismic events (96% - 97%) occur during daylight hours. Even those seismic events that occurred before the start (6 a.m.) or after the end (5 p.m.) of the working day could also be associated with anthropogenic sources, including marine explosions. Marine explosions can occur at any time of the day or week. These are associated with technical, geophysical work at sea, operations on the destruction of WWI and WWII sea mines and naval exercises.

Another example of man-made seismicity is the event on June 12, 2015 (08:18:26 GMT) that was identified as a probable induced earthquake caused by the production of geothermal resources in Lithuania, near Klaipeda (*Nikulins and Assinovskaya*, 2018). The local magnitude of this event reached 2.6 and the depth of the hypocentre 0.9 km. This event was also localised by Finnish, Swedish seismic networks and the Norwegian array NORSAR (Tab. 6.4).

The effectiveness of the applied velocity models was investigated based on reliable explosions in the Aiviekste quarry. Between 2013 and 2019, a data set of 60 explosions was accumulated. The standard deviation of the seismic event epicenter from the quarry position according to the BAVSEN network data is 10.8 km. Comparing the hypocentres to those of other agencies is difficult as the Regional Reviewed Bulletin of NORSAR (RRB NORSAR) does not contain those events because it includes only reliably defined seismic events which were localised and confirmed by at least three seismic arrays. The events are listed in NORSAR's GBF Bulletin, which hypocentres show much larger deviations to the quarry location as the BAVSEN hypocentres, but as this is an automatic, unchecked bulletin it cannot be used for this purpose. The UHIS seismic network practically does not cover the East Baltic region south of 56°N and localises only quarry blasts in the Aiviekste quarry with relatively large magnitudes (> 2.0). About 77% of all explosions in the Aiviekste quarry were localised by the BAVSEN network using the baltic08 model. In 17% of cases, the explosions were better localised using the fen model. Thus, the baltic08 model turned out to be more effective when localizing seismic events within the central part of the East Baltic region.

The Problem of Identifying the Genesis of Regional Seismic Events

For EBR, the problem of recognizing the nature of seismic events is very relevant. A significant factor that makes it difficult to recognize the nature of seismic events is the geological structure. The reflecting and refracting seismic boundaries of the sedimentary cover contribute to the appearance of a complex

interference and wave pattern. The main reference, reflecting horizon is the surface of the Ordovician, which lies at depths of 800 - 2050 m (*Sadov and Penzina*, 1986) and can be traced over most of the territory of the EBR. To a lesser extent, reflecting seismic properties are inherent in the surface of the Silurian and, especially, the surface of Devonian, which are fragmentarily traced in the sections.

Due to the presence of numerous reflecting boundaries in the sedimentary cover, the first P-waves from regional seismic events are weakened and therefore it is difficult to distinguish them in seismograms. For regional seismic events, the first P-wave arrival is most often determined by the BAVSEN network stations located on the Scandinavian shield (MEF and RAF). At stations located in the EBR, the arrival of the first P-wave is difficult to distinguish, and sometimes almost impossible. At the same time, many methods for identifying the nature of seismic events are based precisely on the first P-waves. The large distances between the BAVSEN network stations, the low magnitudes of regional seismic events (from 1.3 to 2.3) and the limited number of waveforms from regional EBR earthquakes, due to the low level of seismic activity, also complicate the identification of the nature of seismic events. Testing of various identification methods (spectral characteristics, P/S ratio, spectral-time analysis (STA) and complexity (ratio of integrated power of the P and S wave) have not yet revealed reliable discriminators (*Nikulins*, 2017).

Teleseismic Earthquakes and man-made Seismic Events

During 2008 - 2019, 1172 teleseismic events were localised, mainly strong earthquakes with magnitudes greater than 5.5. These were mainly tectonic earthquakes. At the same time, several nuclear explosions from North Korea were recorded.

The possibility of identifying nuclear explosions on a remote, regional seismic network was tested (*Nikulins*, 2019b), where the ratio of magnitudes MS/Mb was used as a discriminator (Fig. 6.16). The number of nuclear explosions recorded by the BAVSEN network for an 11 year period was limited. From 2006 to 2017, the power of Korean nuclear explosions gradually increased and only for the last three explosions was it possible to determine the corresponding magnitudes.

The results of the identification of nuclear explosions according to the BAVSEN network were compared with similar results obtained using the Aswan Seismic Network (ASN) in Egypt (*Kebeasy et al.*, 1998). In the case of studies of the Aswan network, the epicentres of nuclear explosions were located in Russia (Novaya Zemlya), China and Kazakhstan. Epicentral distances varied between 5,600 and 8,700 km. The records were obtained by the Aswan seismic network, but the parameters for these explosions were taken from the NEIC (National Earthquake Information Center) catalogues.

In the case of the BAVSEN network research, the epicentres of nuclear explosions were located in North Korea. Epicentral distances reached 11,500 km. Thus, for a sufficiently large range of distances, the discriminator MS/Mb can be used to identify nuclear explosions. Both studies show similar results regarding the linear regression of the magnitude ratios MS/Mb (Fig. 6.16).
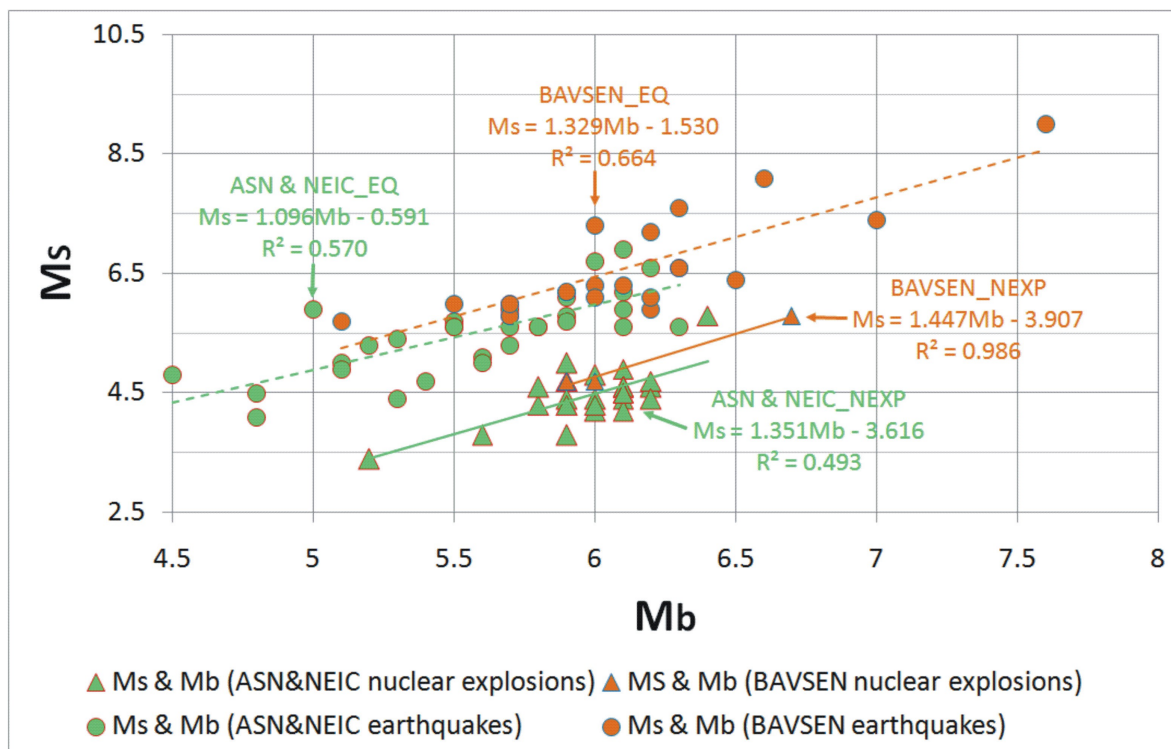
Figure 6.16: *Correlation between the magnitude types Ms and Mb for teleseismic earthquakes and nuclear explosions according to BAVSEN (orange) and ASN (green) seismic network data.*

6.2.4 Seismic Hazard of Latvia

The ultimate goal of seismic monitoring is to assess the seismic hazard of a particular area, that is, to conduct seismic zoning. Areas for monitoring in Latvia are the areas around the Plavinu hydroelectric power station and the densely populated Riga agglomeration. Plavinu hydroelectric station is located almost inside an active graben structure which is formed by two tectonic faults. One of the faults is directly adjacent to the station's dam. The tectonic structure only became known years after the construction of the Plavinu hydroelectric station. Through the territory of Riga, the Olaine-Inčukalns fault extends with signs of geodynamic activity (*Nikulin*, 2019a).

Latvia's seismic hazard was evaluated twice, in 1998 and 2007. In 1998, the Latvian Geological Survey, together with the Crimean Seismology Department of the Institute of Geophysics of the Academy of Sciences of Ukraine, prepared a map of seismic zoning at a scale of 1:1,000,000 (*Safronovs and Nikulins*, 1999). Due to insufficient numbers of tectonic earthquakes in the East Baltic region two methods were used to estimate the maximum magnitude, PSHA and a method to assess the seismotectonic potential that is based on a number of geological and geophysical parameters which is more suitable for areas with low to moderate seismicity (*Borissoff et al.*, 1976; *Reisner et al.*, 1991; *Reisner and Ioganson*, 1992). Three types of seismogenic zones were identified: zones of occurrence of earthquake foci (ZOEF), potential zones of occurrence of earthquake foci (PZOEF) and seismotectonic zones (STZ). As a result, 6 ZOEF, 7 PZOEF and 5 STZ were allocated. The intensity of seismic tremors in two ZOEF (Daugavpils and Bauska) was estimated at VII points on the MSK-64 scale while the intensity of seismic shocks in the remaining ZOEF, PZVOZ and STZ zones was estimated at VI points on the MSK-64 scale. The 1998 studies had several drawbacks, namely: 1) the studies were based on the deterministic method,
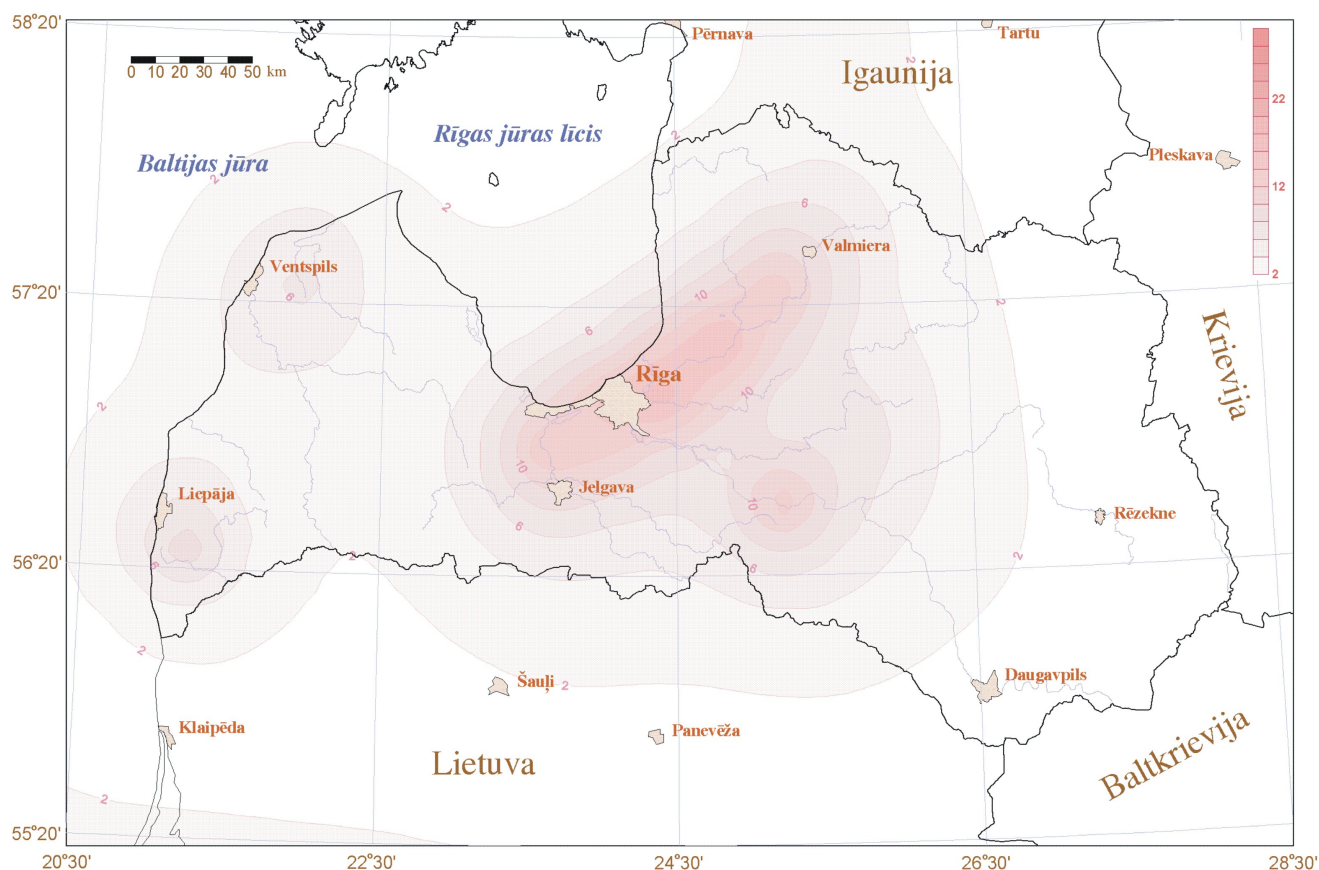
Figure 6.17: *Map of maximum horizontal acceleration (PGA) on solid ground (in cm/s2), with a 10% probability of exceedance in 50 years.*

which did not allow reliable estimates of the recurrence of earthquakes; 2) the studies used tectonic maps issued before 1991, which did not have a reliable topographic reference; 3) the catalogue of earthquakes used for analysis included several technogenic seismic events, in particular in 1995; 4) magnitudes were not unified and reduced to a single magnitude scale (for example Mw).

Given the above drawbacks, in 2007, under an agreement with the Ministry of Economy of Latvia, a second version of the seismic zoning of Latvia was prepared (*Nikulins*, 2011). In addition to eliminating the above-mentioned drawbacks of the 1998 version, the new 2007 version took into account the damping function. Seismotectonic analysis made it possible to identify eight seismogenic zones in the territory of Latvia and another eight seismogenic zones in the East Baltic region. As a result of the calculations, a set of maps of maximum horizontal acceleration in solid ground (PGA) was prepared with a probability of 10%, 5%, 1% and 0.5% over 50 years. With a probability of 10% over 50 years on solid pre-Quaternary deposits of Latvia, the PGA can exceed 10–13 cm/s2 in Sigulda, Riga, Olaine, Aizkraukle, Cesis and their environs (Fig. 6.17).

6.2.5 Data Distribution

Data distribution is an important part of the exchange of information within the international seismological community. The LEGMC first shared its data with the European-Mediterranean Seismological Centre (EMSC) and provided the East-Baltic seismic event bulletins from 2008 to 2010. The EMSC

uses real-time data for their Earthquake Notification Service for potentially devastating earthquakes in the Euro-Mediterranean region, and disseminates messages to users within an hour after the earthquake. Since the LEGMC does not provide real-time epicenter determinations, the EMSC recommended that the LEGMC collaborates with the ISC to share seismological data.

Therefore, in 2012, LEGMC began to send their bulletins to the International Seismological Centre (ISC) under the agency code LVSN. LEGMC currently provides bulletins of seismic events in the Eastern Baltic region from January 2012 to December 2017 (`http://www.isc.ac.uk/cgi-bin/collect?Reporter=LVSN`). General information on the seismicity of the East Baltic region is also located on the LEGMC page (`https://www.meteo.lv/lapas/geologija/monitorings/monitorings-geologija?id=1759&nid=826`). Information on seismic events in the East Baltic region is available only on LEGMC's internal work resources.

6.2.6 Conclusion and Future Steps

Modern seismological studies carried out in Latvia during 2008 - 2019 have made it possible to localise a few tectonic earthquakes and a great amount of man-made seismic events in industrial quarries and in the Baltic Sea using a Baltic Virtual Seismic Network. Low natural seismic activity was noted along the western and northern coasts of Estonia, in the Gulf of Finland and in the area of Lake Võrtsjärv, in Estonia. Man-made seismicity is predominant in EBR. This is mainly due to explosions in open industrial quarries and marine explosions. The problem of identifying the genesis of seismic events in the EBR has not yet been resolved for a number of objective reasons, among which the seismic-geological factor due to sedimentary cover, a sparse seismic network (average distances between stations from 120 to 280 km) and only small seismic events should be highlighted. To reduce the high level of seismic noise the seismic sensors were buried a little deeper between 2 and 10 m, which did not reduce the noise sufficiently. Calibrated explosions in the Aivikste quarry made it possible to choose the optimal model of seismic wave propagation velocity for the central part of the EBR (Latvia). To detect nuclear explosions in North Korea on the BAVSEN remote regional seismic network the Ms/Mb ratio was tested as a discriminator.

For the further development and optimization of seismological monitoring in EBR, the following tasks need to be solved: 1) expansion of the database of waveforms of regional earthquakes and explosions in EBR; 2) search for optimal discriminators, including amplitude P/S ratios, spectral ratios, STA, complexity and other methods for identifying the genesis of weak, regional seismic events (ML <2.5); 3) optimization of the velocity model based on the collection of data on calibrated seismic sources; 4) expansion of the seismic network with uniform coverage by seismic stations of the studied territory of the EBR; 5) the use of geophones placed in deep pits or wells to increase the effective sensitivity of observations; 6) the creation of the National Data Center of Latvia to access the data of the International Monitoring System and the International Data Center (CTBTO), to obtain additional information (e.g. waveforms, radionuclide data and infrasound data).

References

Ankudinov, S.A. and L.M. Dvoretskaya (1984), Report on regional seismic surveys of the GSZ-MOV in the Kola superdeep well area and within the Kola megablock, *NW TGF* (in Russian).

Ankudinov, S.A., H.S. Brio and A.S. Sadov (1991), The deep structure of the Earth's crust on the territory of the republics of the Baltic states according to the data of DSS seismic exploration works, *Belarusian Seismological Bulletin, 1*, 111 – 117 (in Russian).

Avotinja, I.Ja., A.M. Boborykin, A.P. Emel'janov and H.H. Sil'dvjeje H.H. (1988), Catalog of historical earthquakes of Belarus and the Baltic States, *Seismological Bulletin of the seismic stations "Minsk" (Pleshchenitsy) and "Naroch" for 1984*, Minsk, 126 – 137 (in Russian).

Borissoff, B.A., G.I. Reisner and V.N. Sholpo (1976), Tectonics and maximum magnitudes of earthquakes, *Tectonophysics, 33*(1-2), 167 – 185.

Doss, B. (1909), Die historisch beglaubigten Einsturzbeben und seismisch-akustischen Phänomene der russische Ostseeprovinzen, *Sonderabdruck aus Gerlands u. Rudolphs Beiträgen zur Geophysik, X*(1), Leipzig, 1 – 121 (in German).

Hot'ko, Z.P. (1974), The deep structure of the territory of Belarus and the Baltic States according to geophysics, Minsk, *Science and Technique.*

Gregersen, S., P. Wiejacz, W. Debski, B. Domanski, B. Assinovskaya, B. Guterch, P. Mantyniemi, V.G. Nikulin, A. Pacesa, V. Puura, A.G. Aronov, T.I. Aronova, G. Grunthal, E.S. Husebye and S. Sliaupa (2007), The exceptional earthquakes in Kaliningrad district, Russia on September 21, 2004, *Phys. Earth Planet. Inter, 164*(1–2), 63–74, `https://doi.org/10.1016/j.pepi.2007.06.005`.

Havskov, J. and L. Ottemöller (1999), SeisAn Earthquake analysis software, *Seis. Res. Lett., 70*(5), 532–534, `https://doi.org/10.1785/gssrl.70.5.532`.

Kebeasy, R. M., A.I. Hussein and S.A. Dahy (1998), Discrimination between natural earthquakes and nuclear explosions using the Aswan Seismic Network, *Annali di Geofisica, 41*(2), 127 – 140.

Kennett, B.L.N. and E.R. Engdahl (1991), Travel times for global earthquake location and phase association, *Geophys. J. Int, 105*(2), 429 – 465, `https://doi.org/10.1111/j.1365-246X.1991.tb06724.x`.

Kondorskaya, N.V., A.A. Nikonov, I.V. Ananyin, D.V. Dolgopolov, H. Korhonen, K. Arhe and H.H. Sildvee (1988), Osmussaar earthquake in the East Baltics of 1976. Recent seismological investigation in Europe, *Proceedings of the XIX General Assembly of the European Seismological Commission, Moscow, Nauka*, 376 – 387.

Kortström, J., M. Uski and K. Oinonen (2018), The Finnish National Seismic Network, *Summ. Bull. Internatl. Seismol. Cent.*, January - June 2015, *52*(I), 41 – 52, `https://doi.org/10.31905/59QRNANC`.

Lienert, B.R.E., E. Berg and L.N. Frazer (1986), Hypocenter: An earthquake location method using centered, scaled, and adaptively least squares, *BSSA, 76*(3), 771 – 783.

Lienert, B.R.E. and J. Havskov J. (1995), A computer program for locating earthquakes both locally and globally, *Seismol. Res. Lett., 66*(5), 26 – 36, `https://doi.org/10.1785/gssrl.66.5.26`.

Nikonov, A.A., F.F. Aptikaev, A.S. Aleshin, B.A. Assinovskaya, V.V. Pogrebchenko and O.N. Ponomareva (2005), Kaliningrad earthquake of September 21, 2004, macroseismic data for near and mesoseismal zones, Kaliningrad earthquake September 21, 2004, Workshop Material, Tartu, 26 – 29.

Nikulins, V. (2005), Estimation of seismic effects in Latvia from the Kaliningrad earthquake of September 21, 2004, Kaliningrad earthquake September 21, 2004, Workshop Material, Tartu, 30 - 31.

Nikulins, V. (2011), Assessment of the seismic hazard in Latvia, *Scientific Journal of Riga Technical University. Material Science and Applied Chemistry*, *1*(24), 110–115.

Nikulins, V. (2017), Seismicity of the East Baltic region and application-oriented methods in the conditions of low seismicity, *LU Akademiskais apgads*, Riga, 291 p.

Nikulins, V. and B. Assinovskaya (2018), Seismicity of the East Baltic region after the Kaliningrad earthquakes on 21 September 2004, *Baltica*, *42*(1), 35 – 48.

Nikulins, V. (2019a), Geodynamic Hazard Factors of Latvia: Experimental Data and Computational Analysis, *Baltic Journal of Modern Computing*, *1*, 151 - 170, `https:doi.org/10.22364/bjmc.2019.7.1.11`.

Nikulins, V (2019b), Detection of Nuclear Explosions by Remote Regional Seismic Network, *SnT 2019 Book of Abstracts*, Vienna, Austia, CTBTO, p. 77.

Peterson, J. (1993), Observations and Modeling of Seismic Background Noise, *USGS Open-File Report 93-322*, `https://doi.org/10.3133/ofr93322`.

Reisner, G.I., L.I. Ioganson, O.N. Safronovs and V.I. Semova (1991), Seismotectonic zoning of platform areas (on the example of the southern part of the East European platform), *Belarusian Seismological Bulletin*, Academy of Sciences of Belarus Institute of Geochemistry and Geophysics, Minsk, *1*, 86 – 108 (in Russian).

Reisner, G.I. and L.I. Ioganson (1992), Seismic potential of the Crimean-Caucasian region and adjacent southern regions of the Russian plate, *Belarusian Seismological Bulletin*, Academy of Sciences of Belarus Institute of Geochemistry and Geophysics, Minsk, *2*, 56 – 83 (in Russian).

Sadov, A.S. and V.N. Penzina (1986), The study of the deep structure of the earth's crust (regional seismic exploration works of Deep Seismic Sounding) for the Sovetsk-Riga-Kohtla-Jarve geotraverse, *PGO Sevzapgeologija Kaliningrad complex geophysical expedition*, Riga, *1*, p. 208 (in Russian).

Safronovs, O.N. and V.G. Nikulins (1999), General seismic zoning of Latvia, *Latvijas geologijas vestis*, *6*, 30 – 35 (in Latvian).

Stammler, K. (1993), Seismic Handler – Programmable multichannel data handler for interactive and automatic processing of seismological analyses, *Computers & Geosciences*, *19*(2), 135 – 140, `https://doi.org/10.1016/0098-3004(93)90110-Q`.

7

Summary of Seismicity, January - June 2017

Compared to the time period covered by the previous Summary (July - December 2016) that showed ten events with a magnitude of $M_W \geq 7$, this Summary's time period appears to be much quieter with only three earthquakes larger than M_W 7 (Fig. 7.2). However, the seismic sequence that substantially damaged central Italy in August 2016 is still ongoing and raised the most interest in the scientific community in the first half of 2017. Between January and June 2017 there are 4 registered events in the ISC Event Bibliography (*Di Giacomo et al.*, 2014; *International Seismological Centre*, 2020) with more than ten related scientific articles to date, all of them discussing events of the seismic sequence in Italy. In comparison, the time period July - December 2016 showed 12 events with more than ten articles to date in the ISC Event Bibliography (including three events with more than 100 articles).

Three other events that were discussed in the scientific community with seven related articles each in the ISC Event Bibliography are the M_W 6.9 event that ruptured the megathrust in Central Chile near Valparaiso (2017/04/24 21:38:28.99, 33.0626°S, 72.0346°W, 21.3 km, 2069 stations (ISC)) and the M_W 6.4 Lesvos Island event in Greece (2017/06/12 12:28:38.66 (UTC), 38.8846°N, 26.3440°E, 9.7 km, 2751 stations (ISC)). While both these events occurred in regions that usually show a high seismicity, the third event, however, is a rather rare large intracrustal event in Botswana (2017/04/03 17:40:16.93 (UTC), 22.6666°S, 25.2166°E, 20.5 km, 2887 stations (ISC)). With a magnitude of M_W 6.5 this is the second largest earthquake to have occurred in Botswana. Results of *Fadel et al.* (2020) suggest that fluids from the East African Rift System in the upper mantle triggered the intraplate earthquake as part of the ongoing rifting in southern Africa.

The number of events in this Bulletin Summary categorised by type are given in Table 7.1.

The period between January and June 2017 produced 3 earthquakes with $M_W \geq 7$; these are listed in Table 7.2.

Figure 7.1 shows the number of moderate and large earthquakes in the first half of 2017. The distribution of the number of earthquakes should follow the Gutenberg-Richter law.

Figures 7.2 to 7.5 show the geographical distribution of moderate and large earthquakes in various magnitude ranges.

Table 7.1: *Summary of events by type between January and June 2017.*

felt earthquake	293
known earthquake	259493
known chemical explosion	6997
known induced event	3208
known mine explosion	1226
known rockburst	508
known experimental explosion	116
suspected collapse	1
suspected earthquake	51517
suspected chemical explosion	3025
suspected induced event	41
suspected mine explosion	5635
suspected rockburst	153
unknown	2
total	332215

Table 7.2: *Summary of the earthquakes of magnitude $Mw \geq 7$ between January and June 2017.*

Date	lat	lon	depth	Mw	Flinn-Engdahl Region
2017-01-22 04:30:24	-6.23	155.07	156	7.9	Bougainville-Solomon Islands region
2017-01-10 06:13:47	4.41	122.56	628	7.3	Celebes Sea
2017-02-24 17:28:44	-23.37	-178.83	415	7.0	South of Fiji Islands
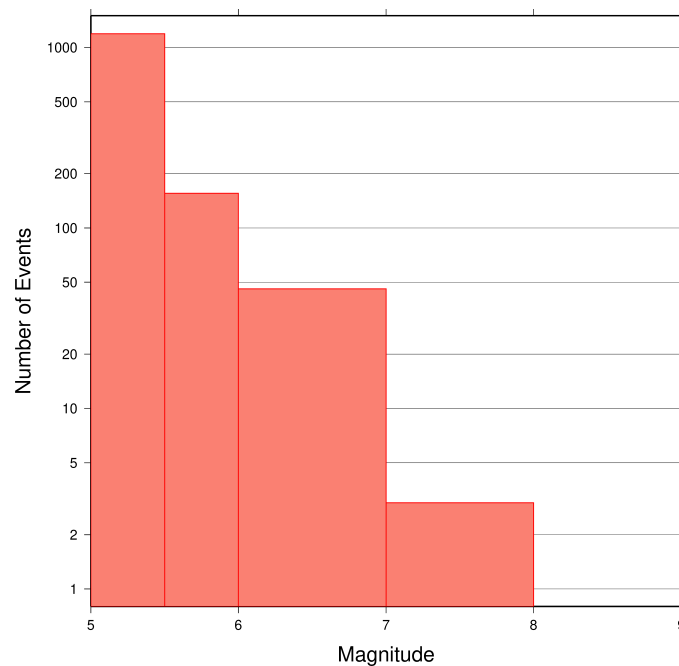
Figure 7.1: *Number of moderate and large earthquakes between January and June 2017. The non-uniform magnitude bias here correspond with the magnitude intervals used in Figures 7.2 to 7.5.*

MW 5 – 5.5, 1190 Events
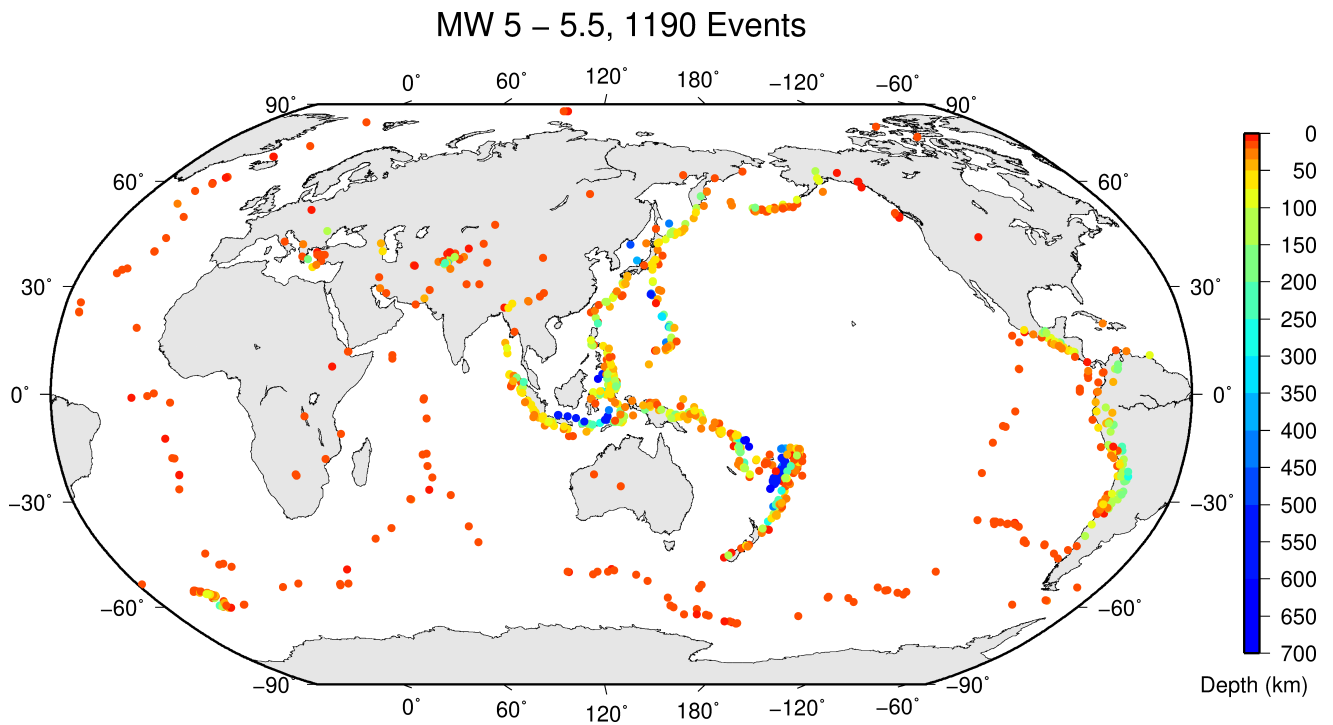
Figure 7.2: *Geographic distribution of magnitude 5-5.5 earthquakes between January and June 2017.*

MW 5.5 – 6, 156 Events
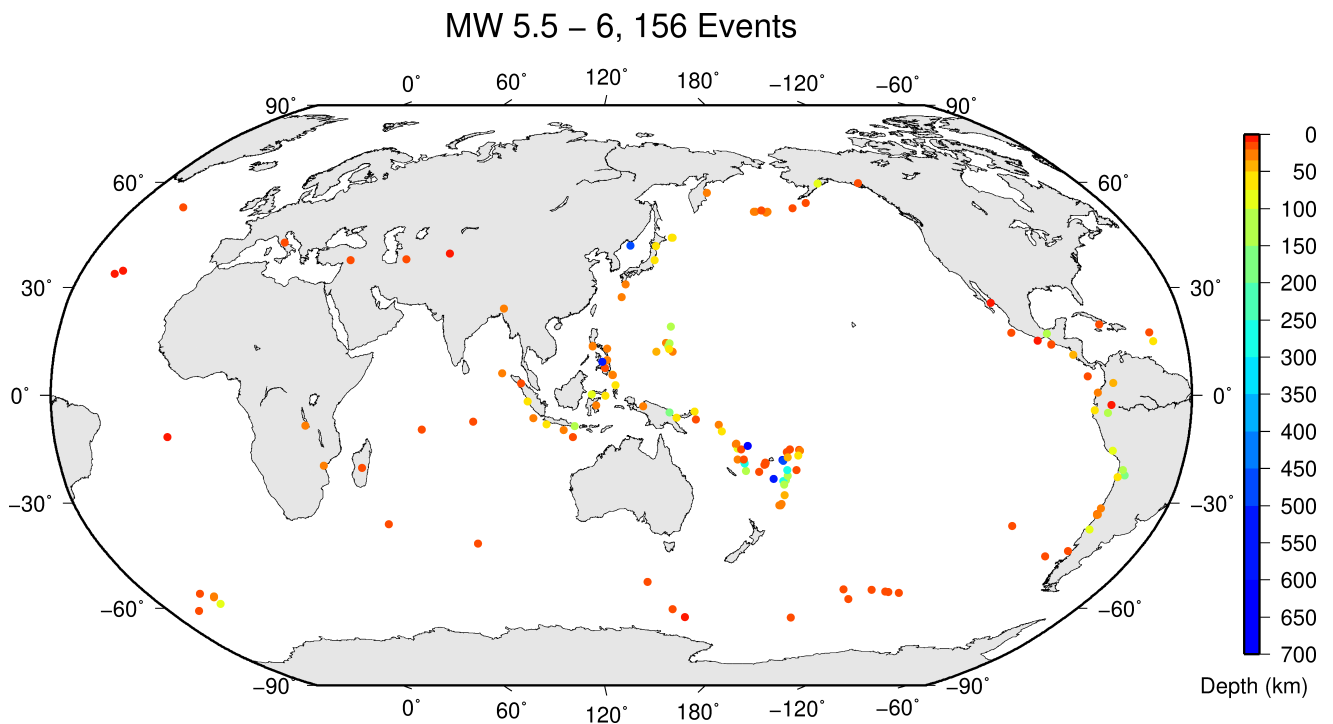
Figure 7.3: *Geographic distribution of magnitude 5.5-6 earthquakes between January and June 2017.*
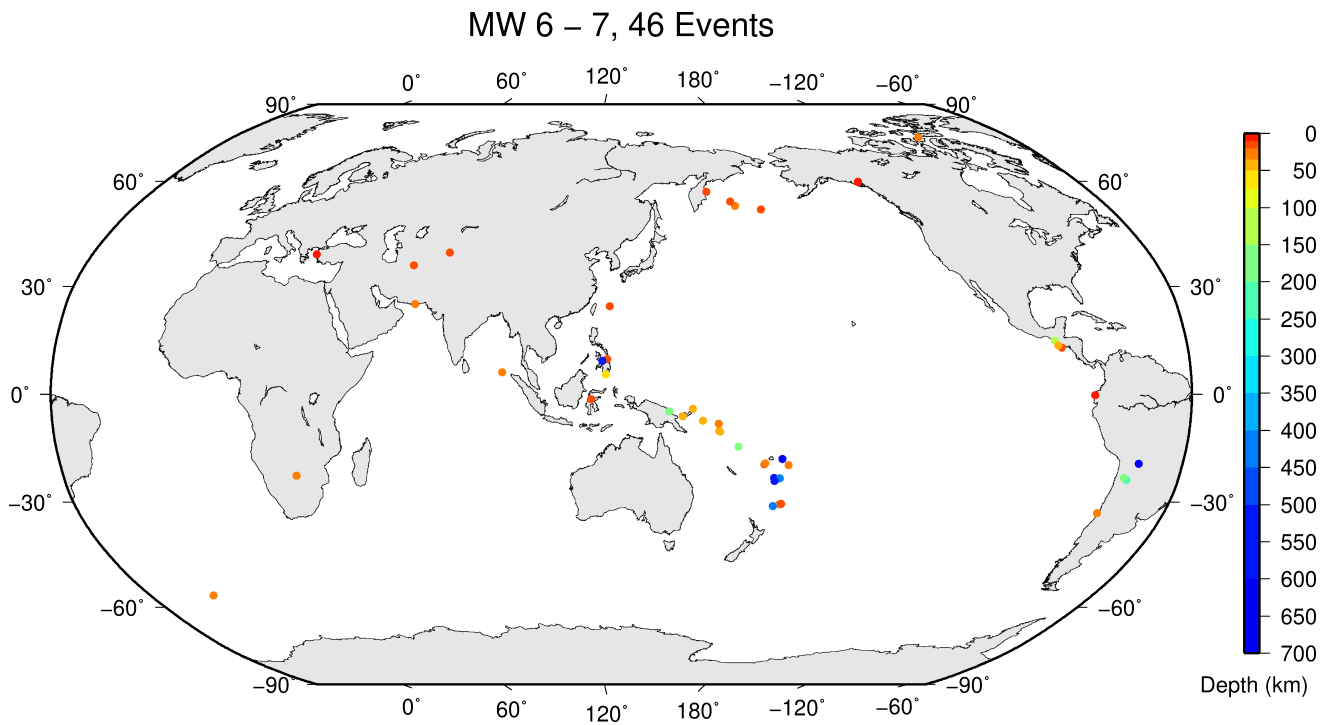
Figure 7.4: *Geographic distribution of magnitude 6-7 earthquakes between January and June 2017.*
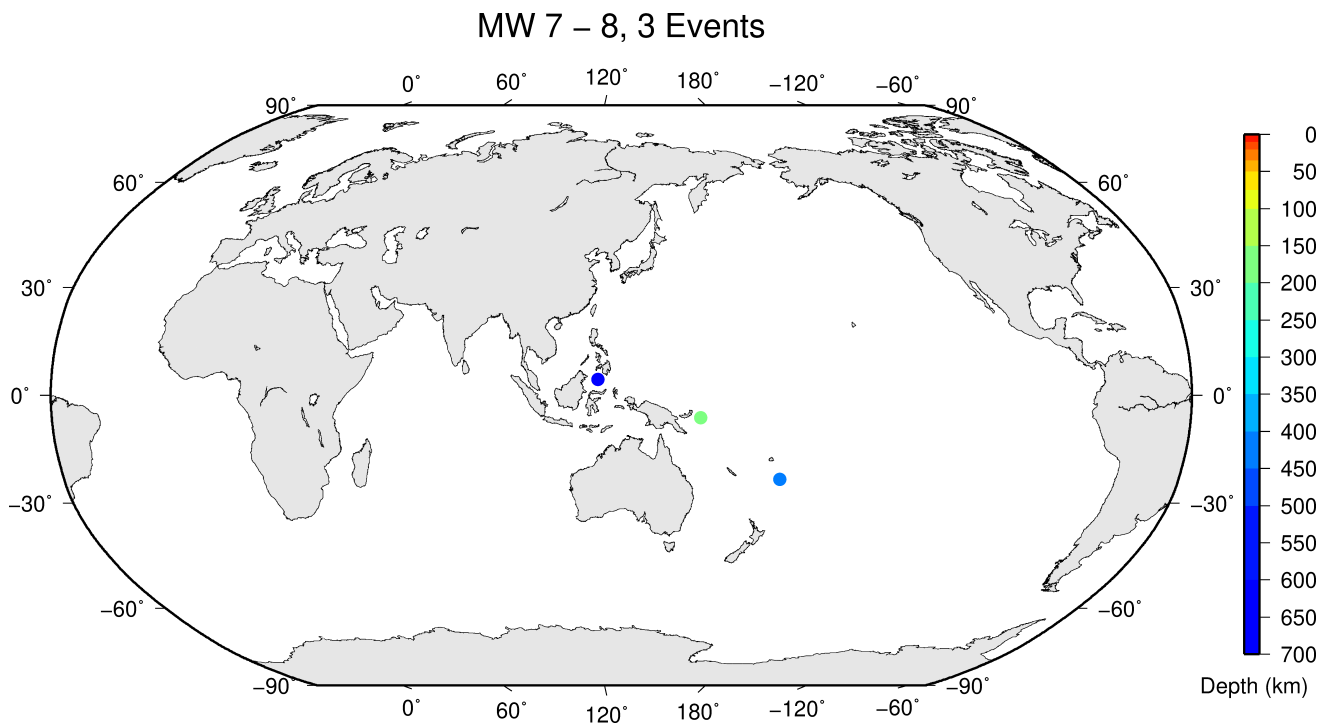
Figure 7.5: *Geographic distribution of magnitude 7-8 earthquakes between January and June 2017.*

References

Di Giacomo, D., D.A. Storchak, N. Safronova, P. Ozgo, J. Harris, R. Verney and I. Bondár (2014), A New ISC Service: The Bibliography of Seismic Events, *Seismol. Res. Lett.*, *85*(2), 354–360, `https://doi.org/10.1785/0220130143`.

Fadel, I., H. Paulssen, M. van der Meijde, M. Kwadiba, O. Ntibinyane, A. Nyblade and R. Durrheim (2020), Crustal and upper mantle shear wave velocity structure of Botswana: The 3 April 2017 central Botswana earthquake linked to the East African Rift System, *Geophys. Res. Lett.*, *47*, e2019GL085598, `https://doi.org/10.1029/2019GL085598`.

International Seismological Centre (2019), On-line Event Bibliography, `http://www.isc.ac.uk/event_bibliography`, Internatl. Seis. Cent., Thatcham, United Kingdom.

8

Statistics of Collected Data

8.1   Introduction

The ISC Bulletin is based on the parametric data reports received from seismological agencies around the world. With rare exceptions, these reports include the results of waveform review done by analysts at network data centres and observatories. These reports include combinations of various bulletin elements such as event hypocentre estimates, moment tensors, magnitudes, event type and felt and damaging data as well as observations of the various seismic waves recorded at seismic stations.

Data reports are received in different formats that are often agency specific. Once an authorship is recognised, the data are automatically parsed into the ISC database and the original reports filed away to be accessed when necessary. Any reports not recognised or processed automatically are manually checked, corrected and re-processed. This chapter describes the data that are received at the ISC before the production of the reviewed Bulletin.

Notably, the ISC integrates all newly received data reports into the automatic ISC Bulletin (available on-line) soon after these reports are made available to ISC, provided it is done before the submission deadline that currently stands at 12 months following an event occurrence.

With data constantly being reported to the ISC, even after the ISC has published its review, the total data shown as collected, in this chapter, is limited to two years after the time of the associated reading or event, i.e. any hypocentre data collected two years after the event are not reflected in the figures below.

8.2   Summary of Agency Reports to the ISC

A total of 147 agencies have reported data for January 2017 to June 2017. The parsing of these reports into the ISC database is summarised in Table 8.1.

Table 8.1: *Summary of the parsing of reports received by the ISC from a total of 147 agencies, containing data for this summary period.*

	Number of reports
Total collected	4238
Automatically parsed	3184
Manually parsed	1054

Data collected by the ISC consists of multiple data types. These are typically one of:

- Bulletin, hypocentres with associated phase arrival observations.

- Catalogue, hypocentres only.

- Unassociated phase arrival observations.

In Table 8.2, the number of different data types reported to the ISC by each agency is listed. The number of each data type reported by each agency is also listed. Agencies reporting indirectly have their data type additionally listed for the agency that reported it. The agencies reporting indirectly may also have 'hypocentres with associated phases' but with no associated phases listed - this is because the association is being made by the agency reporting directly to the ISC. Summary maps of the agencies and the types of data reported are shown in Figure 8.1 and Figure 8.2.

Table 8.2: *Agencies reporting to the ISC for this summary period. Entries in bold are for new or renewed reporting by agencies since the previous six-month period.*

Agency	Country	Directly or indirectly reporting (D/I)	Hypocentres with associated phases	Hypocentres without associated phases	Associated phases	Unassociated phases	Amplitudes
TIR	Albania	D	314	0	4311	67	869
CRAAG	Algeria	D	231	0	978	167	0
LPA	Argentina	D	0	0	0	715	0
SJA	Argentina	D	949	1	41205	0	11191
NSSP	Armenia	D	51	0	706	0	0
ADE	**Australia**	**D**	**0**	**0**	**0**	**36**	**0**
AUST	Australia	D	809	69	18942	0	0
CUPWA	Australia	D	60	0	934	0	0
IDC	Austria	D	17401	1	543991	0	501173
VIE	Austria	D	4521	84	42074	1125	42469
AZER	Azerbaijan	D	199	0	7846	0	0
UCC	Belgium	D	1046	0	7587	37	1889
SCB	Bolivia	D	734	0	11265	0	1820
RHSSO	Bosnia and Herzegovina	D	967	0	19898	8034	0
VAO	Brazil	D	1093	25	32819	0	0
SOF	Bulgaria	D	184	0	1306	2237	0
SOMC	Cameroon	D	0	0	0	27	0
OTT	Canada	D	2527	193	70127	0	3679
PGC	Canada	I OTT	1759	1	53511	0	0
GUC	Chile	D	4462	540	155117	5634	42897
BJI	China	D	1332	1	115260	36059	77967
ASIES	Chinese Taipei	D	0	105	0	0	0
TAP	Chinese Taipei	D	16682	0	695311	0	0
RSNC	Colombia	D	8403	0	181864	17634	54066
ICE	**Costa Rica**	**I UCR**	**0**	**1**	**0**	**0**	**0**
UCR	Costa Rica	D	350	1	17634	0	0
ZAG	Croatia	D	1	0	0	37568	0
SSNC	Cuba	D	922	4	9600	0	3716
NIC	Cyprus	D	453	0	14088	0	7853
IPEC	Czech Republic	D	554	0	3625	21533	1658
PRU	Czech Republic	D	4981	21	44674	255	11216
WBNET	Czech Republic	D	317	0	6124	0	6067
KEA	Democratic People's Republic of Korea	D	209	0	2888	0	1367
DNK	Denmark	D	2437	1388	30353	23643	8808
OSPL	Dominican Republic	D	489	12	4649	0	1394
SDD	**Dominican Republic**	**D**	**534**	**0**	**11962**	**0**	**0**
IGQ	Ecuador	D	0	46	3031	0	0
HLW	Egypt	D	989	0	7299	0	0
SNET	El Salvador	D	1548	6	26411	115	3217

Table 8.2: *(continued)*

Agency	Country	Directly or indirectly reporting (D/I)	Hypocentres with associated phases	Hypocentres without associated phases	Associated phases	Unassociated phases	Amplitudes
EST	Estonia	I HEL	298	13	0	0	0
AAE	Ethiopia	D	154	0	1468	361	186
SKO	FYR Macedonia	D	1504	0	16114	3866	3027
FIA0	Finland	I HEL	3	2	0	0	0
HEL	Finland	D	8367	544	198411	0	34691
CSEM	France	I BGR	2021	719	0	0	0
LDG	France	D	2812	85	51500	2	21830
STR	France	D	2898	0	55310	3	0
PPT	French Polynesia	D	1183	3	9643	209	9750
TIF	Georgia	D	1	251	1	5399	0
AWI	Germany	D	2202	4	9429	2640	2505
BGR	Germany	D	600	208	17172	0	6301
BNS	Germany	I BGR	2	26	0	0	0
BRG	Germany	D	0	0	0	8048	4138
BUG	Germany	I BGR	6	19	0	0	0
CLL	Germany	D	2	0	91	8431	2780
GDNRW	Germany	I BGR	1	9	0	0	0
GFZ	Germany	I PRE	87	0	0	0	0
LEDBW	Germany	I BGR	18	1	0	0	0
ATH	Greece	D	8178	29	236219	0	82606
THE	Greece	D	5141	2	99967	6122	32807
UPSL	Greece	D	0	4	0	0	0
GCG	Guatemala	D	460	0	2889	0	0
HKC	Hong Kong	D	0	0	0	18	0
KRSZO	Hungary	D	247	135	5753	0	2298
REY	Iceland	D	72	0	3040	0	0
HYB	India	D	513	12	1296	3	200
NDI	India	D	454	341	12176	1641	3392
DJA	Indonesia	D	4255	49	67468	0	86187
TEH	Iran	D	1708	1	31589	0	0
THR	Iran	D	20	0	507	0	138
ISN	Iraq	D	290	0	1944	0	755
GII	Israel	D	572	0	10222	0	0
GEN	Italy	D	616	0	13883	0	0
MED_RCMT	Italy	D	0	168	0	0	0
RISSC	Italy	D	3	0	24	0	0
ROM	Italy	D	32449	97	3313788	857268	2319701
TRI	Italy	D	0	0	0	9037	0
LIC	Ivory Coast	D	359	0	1077	0	1066
JSN	Jamaica	D	164	0	861	10	0
JMA	Japan	D	130624	6597	790302	0	13357
NIED	Japan	D	0	598	0	0	0
SYO	Japan	D	0	0	0	376	0
JSO	Jordan	D	144	0	2251	0	0
NNC	Kazakhstan	D	9809	0	113779	0	105135
SOME	Kazakhstan	D	6356	94	88925	0	80677
KNET	Kyrgyzstan	D	1369	0	11966	0	4057
KRNET	Kyrgyzstan	D	3448	0	64708	0	0
LVSN	Latvia	D	248	0	3808	0	2147
GRAL	Lebanon	D	253	0	2147	480	0
LIT	Lithuania	D	415	406	3746	1822	112
MCO	Macao, China	D	0	0	0	30	0
TAN	Madagascar	D	0	0	0	153	0
GSDM	Malawi	D	0	0	0	202	0
KLM	Malaysia	D	99	0	342	0	0
ECX	Mexico	D	707	0	17801	0	3333
MEX	Mexico	D	7495	142	133722	0	0
MOLD	Moldova	D	0	0	0	1824	1008
PDG	Montenegro	D	368	0	7897	20	3984
CNRM	Morocco	D	1556	0	15796	0	0
NAM	Namibia	D	1	0	7	0	0
DMN	Nepal	D	1421	0	13184	0	9535

Table 8.2: *(continued)*

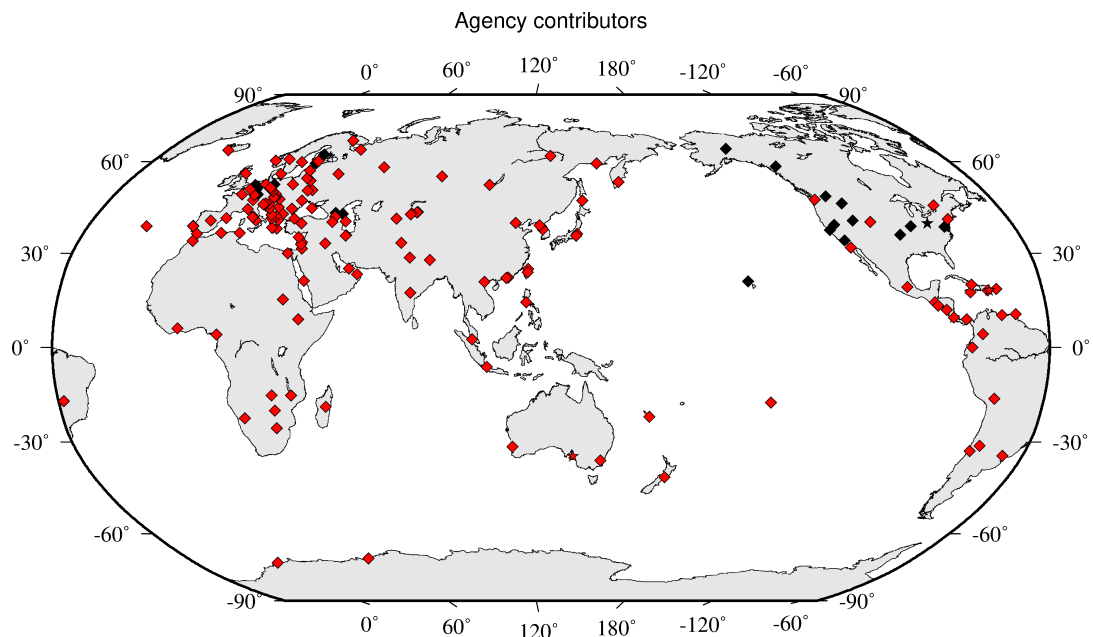| Agency	Country	Directly or indirectly reporting (D/I)	Hypocentres with associated phases	Hypocentres without associated phases	Associated phases	Unassociated phases	Amplitudes
DBN	Netherlands	I BGR	0	3	0	0	0
NOU	New Caledonia	D	4243	58	69923	0	5945
WEL	New Zealand	D	11277	109	385114	478	337356
INET	Nicaragua	D	657	8	6374	0	131
BER	Norway	D	3056	1561	54889	5111	13473
NAO	Norway	D	2070	856	5633	0	1872
OMAN	Oman	D	460	0	20232	0	0
MSSP	Pakistan	D	0	0	0	1035	0
UPA	Panama	D	691	0	10148	13	67
MAN	Philippines	D	0	4705	0	87692	16407
WAR	Poland	D	0	0	0	7844	315
IGIL	Portugal	D	538	0	2615	455	1021
INMG	Portugal	D	1292	1	41554	1240	13996
SVSA	Portugal	D	563	0	12659	4116	6292
BELR	Republic of Belarus	D	0	0	0	23307	7799
CFUSG	Republic of Crimea	D	102	0	1961	945	1745
KMA	Republic of Korea	D	87	0	1637	0	0
BUC	Romania	D	772	35	18328	61217	5766
ASRS	Russia	D	107	0	3172	0	1081
BYKL	Russia	D	68	0	8132	0	2640
DRS	Russia	I MOS	179	142	0	0	0
IEPN	Russia	D	208	0	2165	4546	1771
KOLA	Russia	D	736	0	6524	0	0
KRSC	Russia	D	650	0	20209	0	0
MIRAS	Russia	D	111	0	2931	0	1413
MOS	Russia	D	1986	288	313260	0	109798
NERS	Russia	D	32	0	1004	0	471
NORS	Russia	I MOS	29	146	0	0	0
SKHL	Russia	D	1076	1079	23199	0	10908
YARS	Russia	D	440	1	5821	0	4294
SGS	Saudi Arabia	D	37	0	594	0	0
BEO	Serbia	D	1324	0	25188	0	6
BRA	Slovakia	D	0	0	0	20758	0
LJU	Slovenia	D	1017	370	14219	2466	4795
PRE	South Africa	D	872	0	26948	0	9273
MDD	Spain	D	2554	1	53731	0	15037
MRB	Spain	D	1590	0	37386	0	16420
SFS	Spain	D	1170	4	19399	0	0
SSN	Sudan	D	93	0	415	0	4
UPP	Sweden	D	2100	1379	23646	0	0
ZUR	Switzerland	D	657	0	10456	0	6779
TRN	Trinidad and Tobago	D	0	2067	0	43995	0
TUN	Tunisia	D	59	2	245	0	0
DDA	Turkey	D	19117	3	411593	0	135912
ISK	Turkey	D	17028	0	264799	3137	157988
AEIC	U.S.A.	I NEIC	1195	1499	29080	0	0
ANF	U.S.A.	I IRIS	196	1391	0	0	0
BUT	U.S.A.	I NEIC	3	16	381	0	0
GCMT	U.S.A.	D	0	2084	0	0	0
HVO	U.S.A.	I NEIC	210	7	10919	0	0
IRIS	U.S.A.	D	3347	1391	331738	0	0
LDO	U.S.A.	I NEIC	8	5	137	0	0
NCEDC	U.S.A.	I NEIC	79	7	8450	0	0
NEIC	U.S.A.	D	13917	7998	1289342	0	605443
OGSO	**U.S.A.**	**I NEIC**	**0**	**2**	**0**	**0**	**0**
PAS	U.S.A.	I NEIC	72	1	10745	0	0
PNSN	U.S.A.	D	0	114	0	0	0
REN	U.S.A.	I NEIC	102	11	2872	0	0
RSPR	U.S.A.	D	1994	641	29606	12	0
SCEDC	U.S.A.	I IRIS	2	0	0	0	0

Table 8.2: (continued)

Agency	Country	Directly or indirectly reporting (D/I)	Hypocentres with associated phases	Hypocentres without associated phases	Associated phases	Unassociated phases	Amplitudes
SEA	U.S.A.	I NEIC	45	3	3572	0	0
SLM	U.S.A.	I NEIC	59	1	2108	0	0
TUL	U.S.A.	I NEIC	483	0	0	0	0
UUSS	U.S.A.	I NEIC	59	2	1046	0	0
MCSM	Ukraine	D	89	0	2182	0	178
SIGU	Ukraine	D	47	33	1421	0	529
DSN	United Arab Emirates	D	415	0	5349	0	0
BGS	United Kingdom	D	301	12	8600	124	3357
ISU	Uzbekistan	D	433	0	4544	0	0
CAR	Venezuela	I NEIC	0	1	0	0	0
FUNV	Venezuela	D	664	0	9256	0	0
PLV	Viet Nam	D	11	8	112	0	50
LSZ	Zambia	D	69	0	233	7	24
BUL	Zimbabwe	D	976	0	7157	223	0

Figure 8.1: *Map of agencies that have contributed data to the ISC for this summary period. Agencies that have reported directly to the ISC are shown in red. Those that have reported indirectly (via another agency) are shown in black. Any new or renewed agencies, since the last six-month period, are shown by a star. Each agency is listed in Table 8.2.*

Types of reports to the ISC for data from 2017/01/01 to 2017/06/30
○ Hypocentres associated to phase data: 147 agencies
● Phases associated to hypocentres: 134 agencies
● Hypocentres without directly associated phase data: 88 agencies
▢ Unassociated phases - phase data not directly associated with a hypocentre: 62 agencies
◆ Moment tensor solutions: 9 agencies
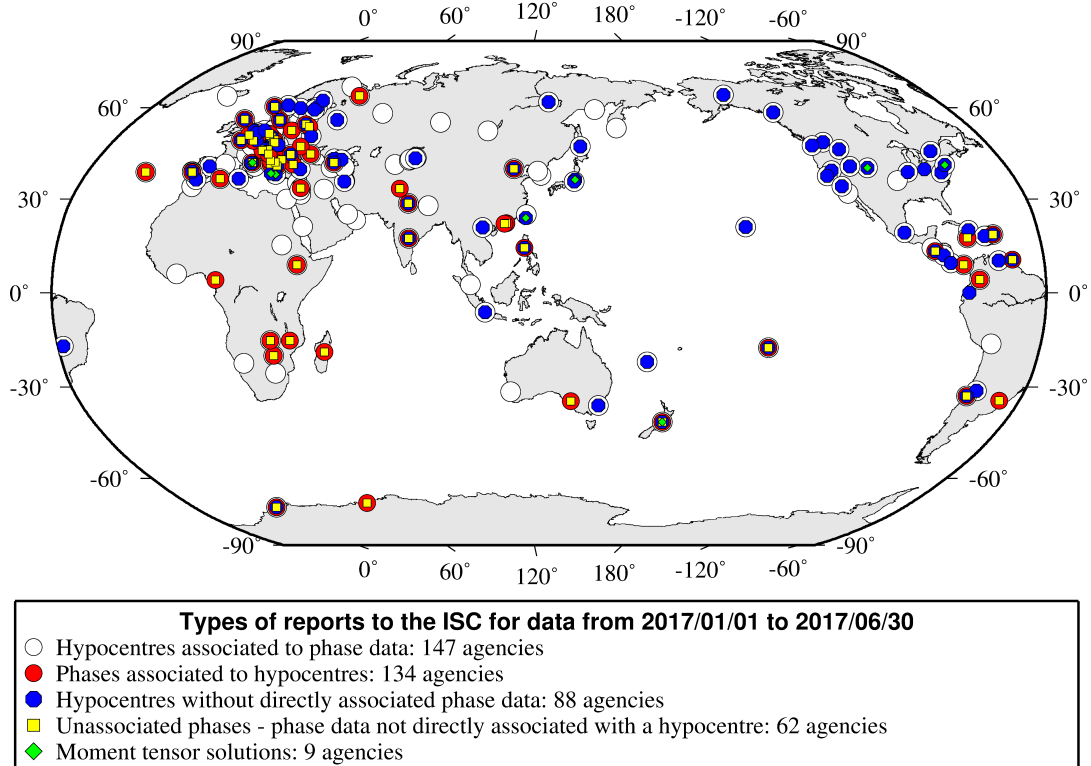
Figure 8.2: *Map of the different data types reported by agencies to the ISC. A full list of the data types reported by each agency is shown in Table 8.2.*

8.3 Arrival Observations

The collection of phase arrival observations at the ISC has increased dramatically with time. The increase in reported phase arrival observations is shown in Figure 8.3.

The reports with phase data are summarised in Table 8.3. This table is split into three sections, providing information on the reports themselves, the phase data, and the stations reporting the phase data. A map of the stations contributing these phase data is shown in Figure 8.4.

The ISC encourages the reporting of phase arrival times together with amplitude and period measurements whenever feasible. Figure 8.5 shows the percentage of events for which phase arrival times from each station are accompanied with amplitude and period measurements.

Figure 8.6 indicates the number of amplitude and period measurement for each station.

Together with the increase in the number of phases (Figure 8.3), there has been an increase in the number of stations reported to the ISC. The increase in the number of stations is shown in Figure 8.7. This increase can also be seen on the maps for stations reported each decade in Figure 8.8.
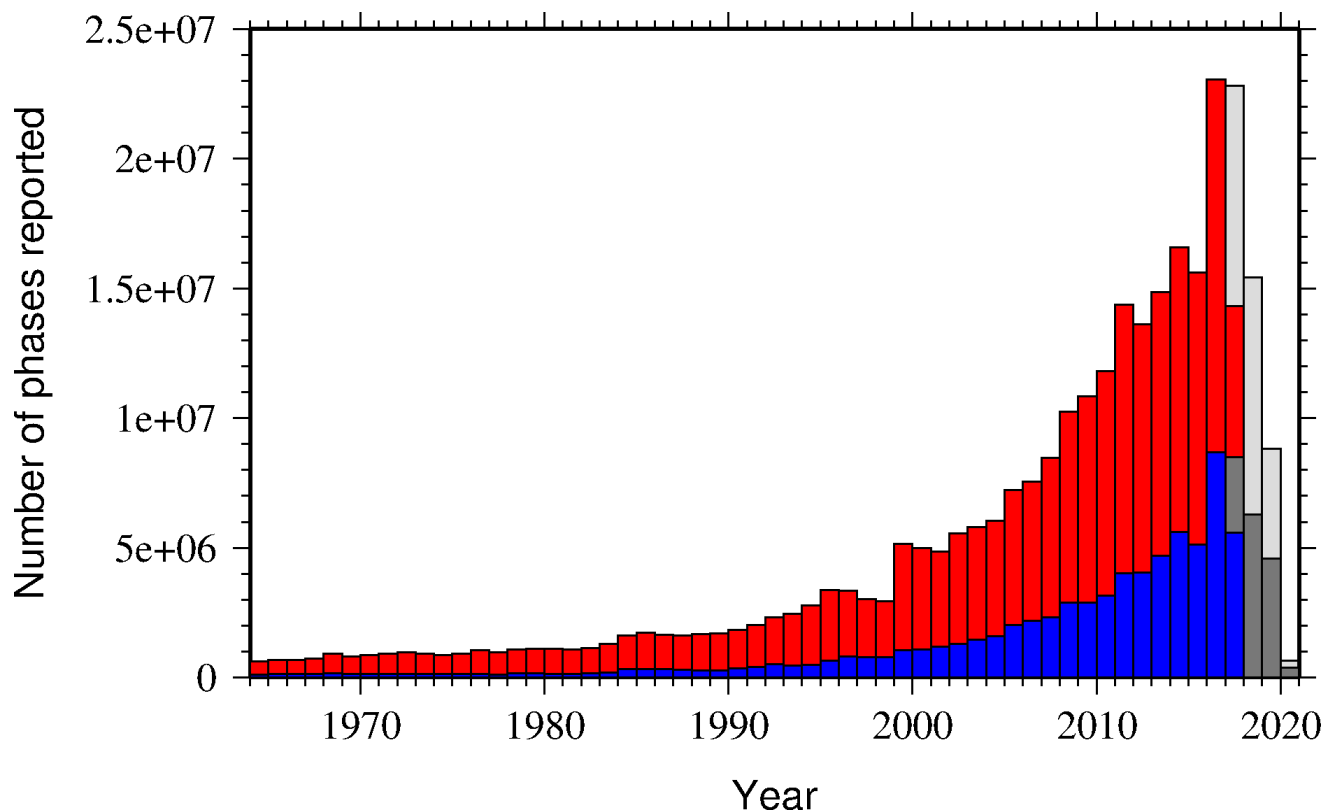
Figure 8.3: *Histogram showing the number of phases (red) and number of amplitudes (blue) collected by the ISC for events each year since 1964. The data in grey covers the current period where data are still being collected before the ISC review takes place and is accurate at the time of publication.*

Table 8.3: *Summary of reports containing phase arrival observations.*

Reports with phase arrivals	4139
Reports with phase arrivals including amplitudes	1563
Reports with only phase arrivals (no hypocentres reported)	231
Total phase arrivals received	12250883
Total phase arrival-times received	9767684
Number of duplicate phase arrival-times	1058198 (10.8%)
Number of amplitudes received	5019958
Stations reporting phase arrivals	8672
Stations reporting phase arrivals with amplitude data	4872
Max number of stations per report	2218

Data were collected by the ISC from 4906 stations for the decade starting in 2020
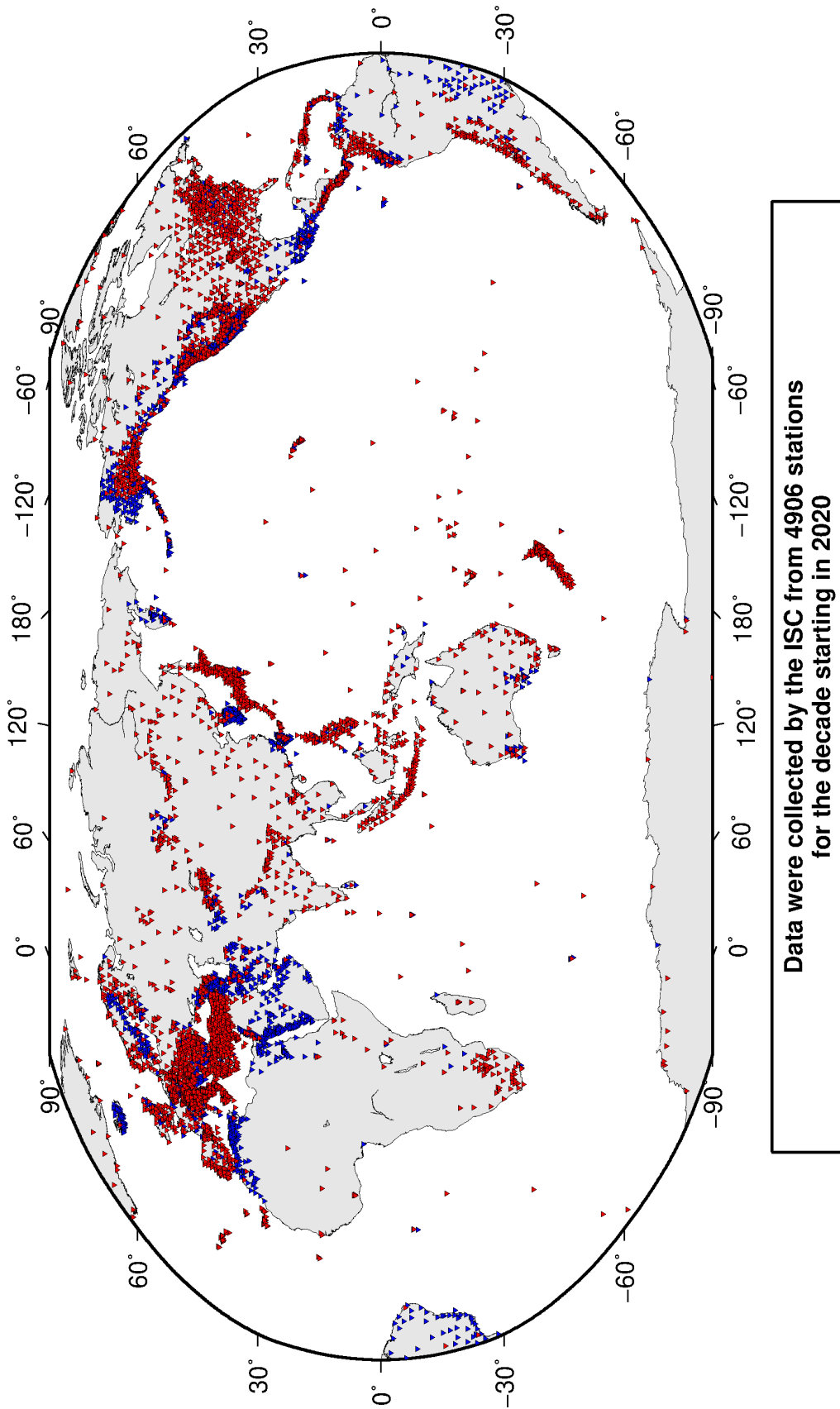
Figure 8.4: Stations contributing phase data to the ISC for readings from January 2017 to the end of June 2017. Stations in blue provided phase arrival times only; stations in red provided both phase arrival times and amplitude data.
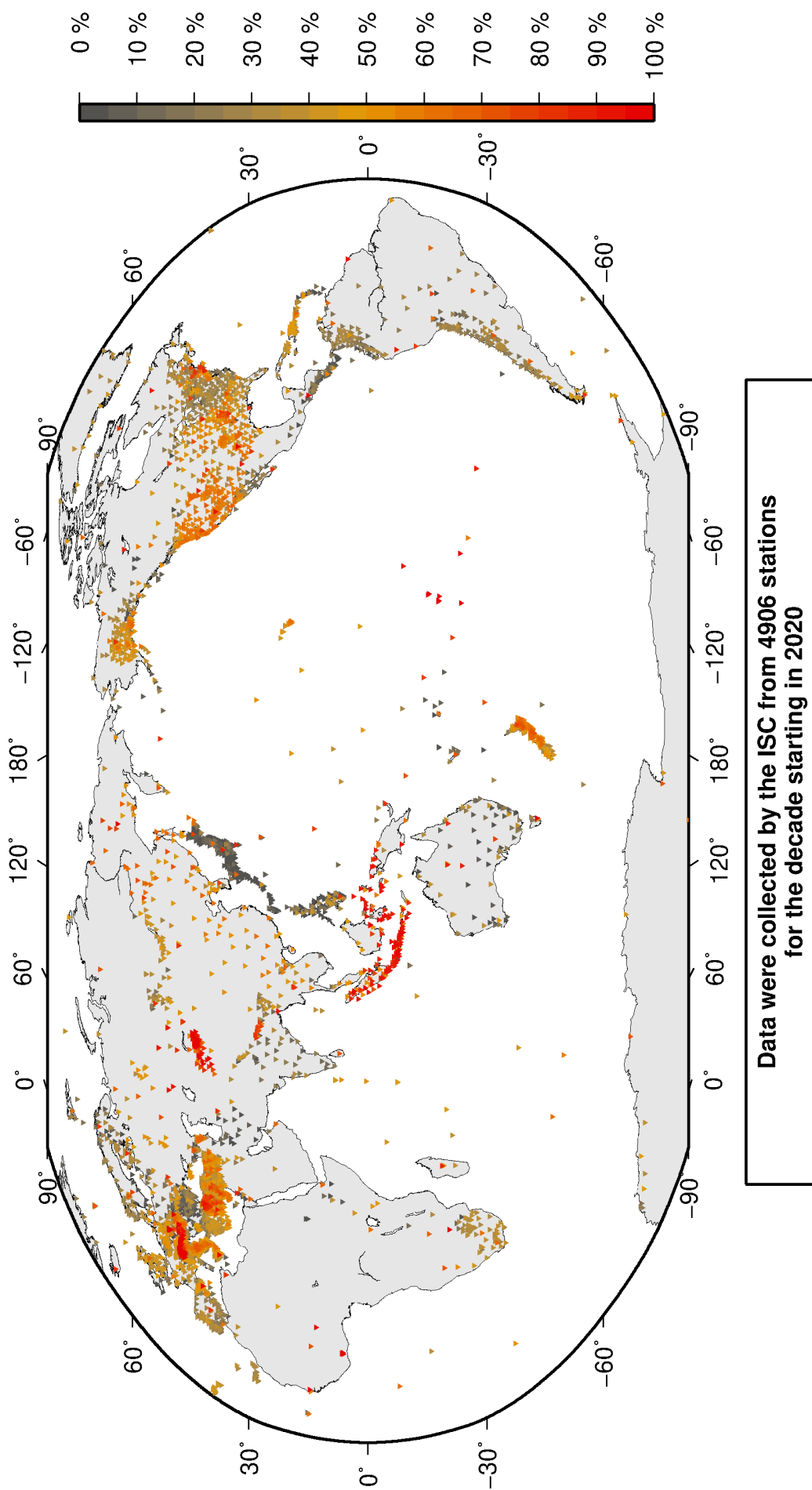
Figure 8.5: *Percentage of events for which phase arrival times from each station are accompanied with amplitude and period measurements.*

Data were collected by the ISC from 4906 stations for the decade starting in 2020

Number of Amplitudes

Number
of Amplitudes

**Data were collected by the ISC from 4906 stations
for the decade starting in 2020**
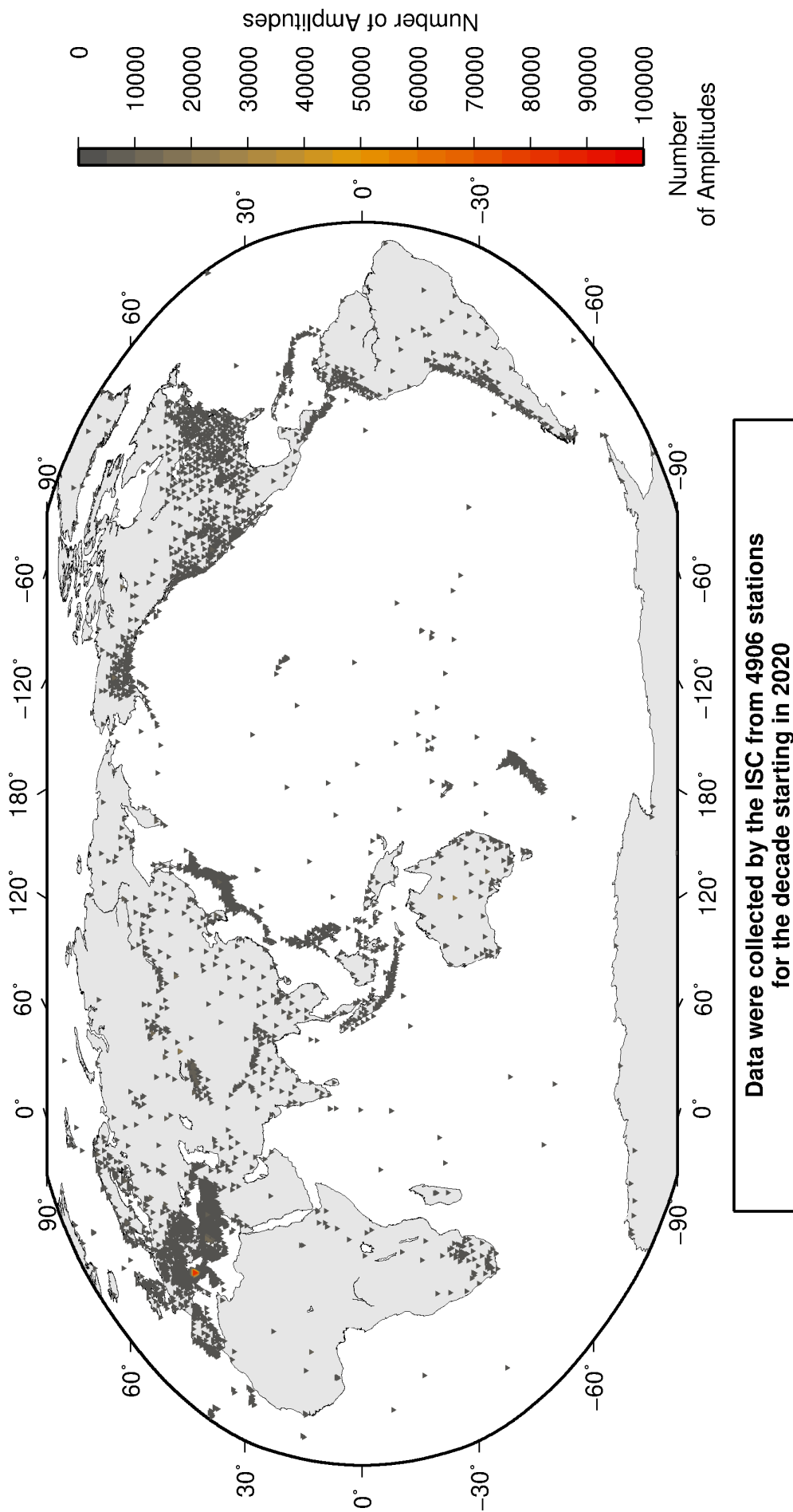
Figure 8.6: Number of amplitude and period measurements for each station.
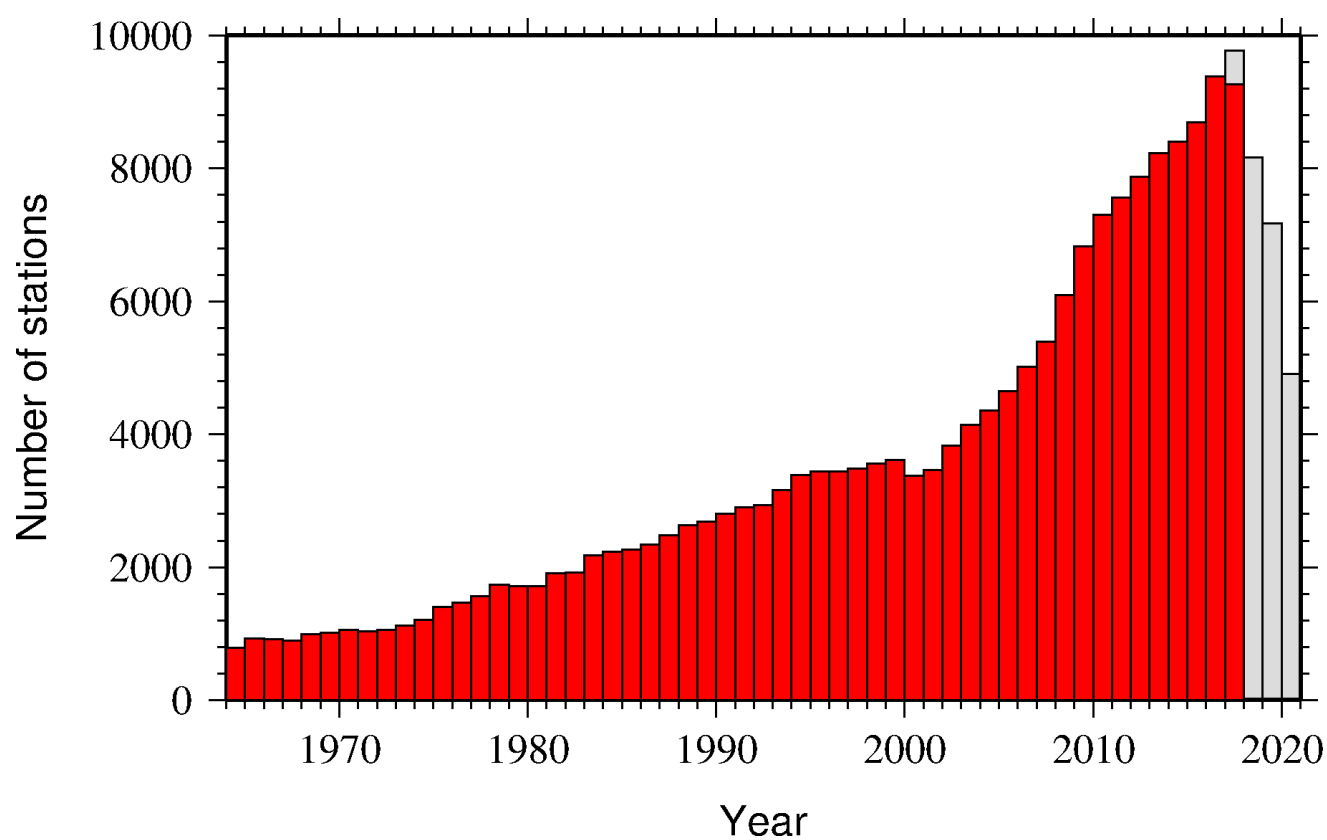
Figure 8.7: *Histogram showing the number of stations reporting to the ISC each year since 1964. The data in grey covers the current period where station information is still being collected before the ISC review of events takes place and is accurate at the time of publication.*
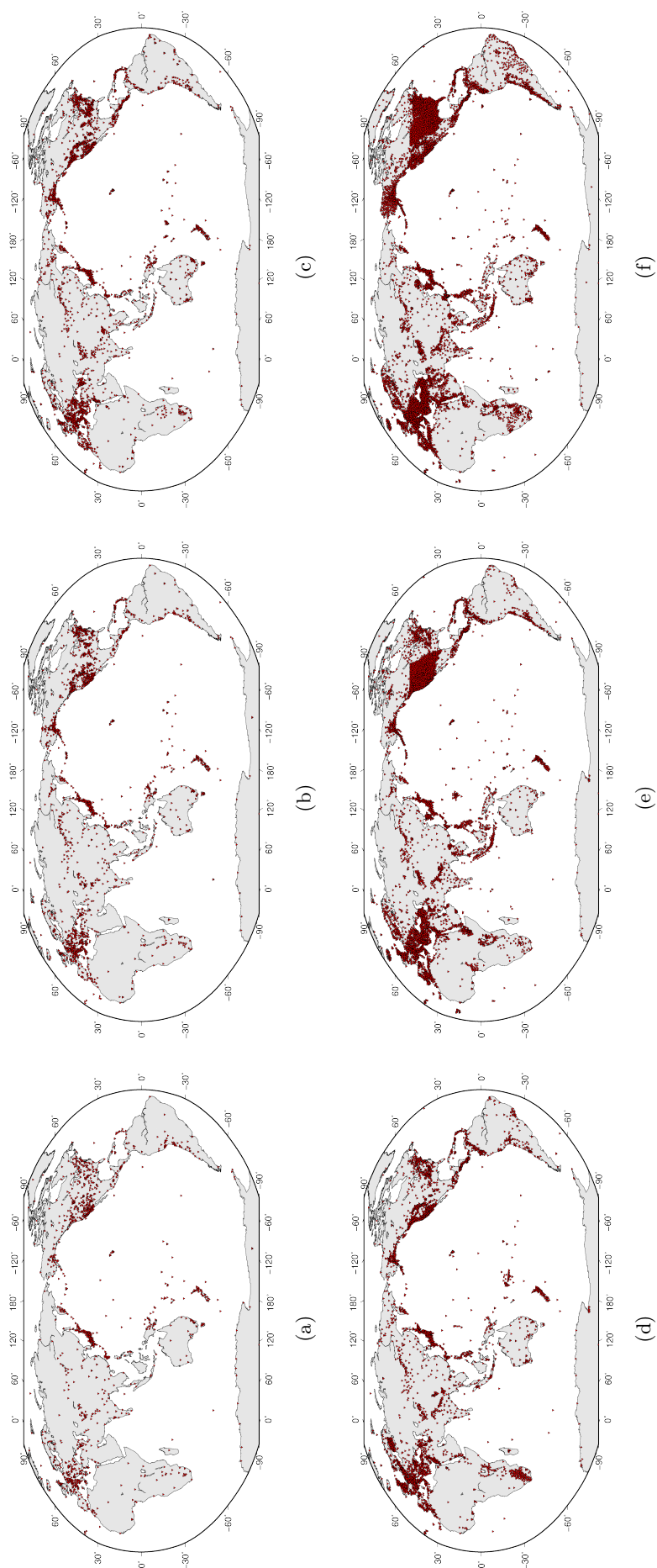
Figure 8.8: *Maps showing the stations reported to the ISC for each decade since 1960. Note that the last map covers a shorter time period.*

8.4 Hypocentres Collected

The ISC Bulletin groups multiple estimates of hypocentres into individual events, with an appropriate prime hypocentre solution selected. The collection of these hypocentre estimates are described in this section.

The reports containing hypocentres are summarised in Table 8.4. The number of hypocentres collected by the ISC has also increased significantly since 1964, as shown in Figure 8.9. A map of all hypocentres reported to the ISC for this summary period is shown in Figure 8.10. Where a network magnitude was reported with the hypocentre, this is also shown on the map, with preference given to reported values, first of M_W followed by M_S, m_b and M_L respectively (where more than one network magnitude was reported).

Table 8.4: *Summary of the reports containing hypocentres.*

Reports with hypocentres	4007
Reports of hypocentres only (no phase readings)	99
Total hypocentres received	443452
Number of duplicate hypocentres	9343 (2.1%)
Agencies determining hypocentres	160
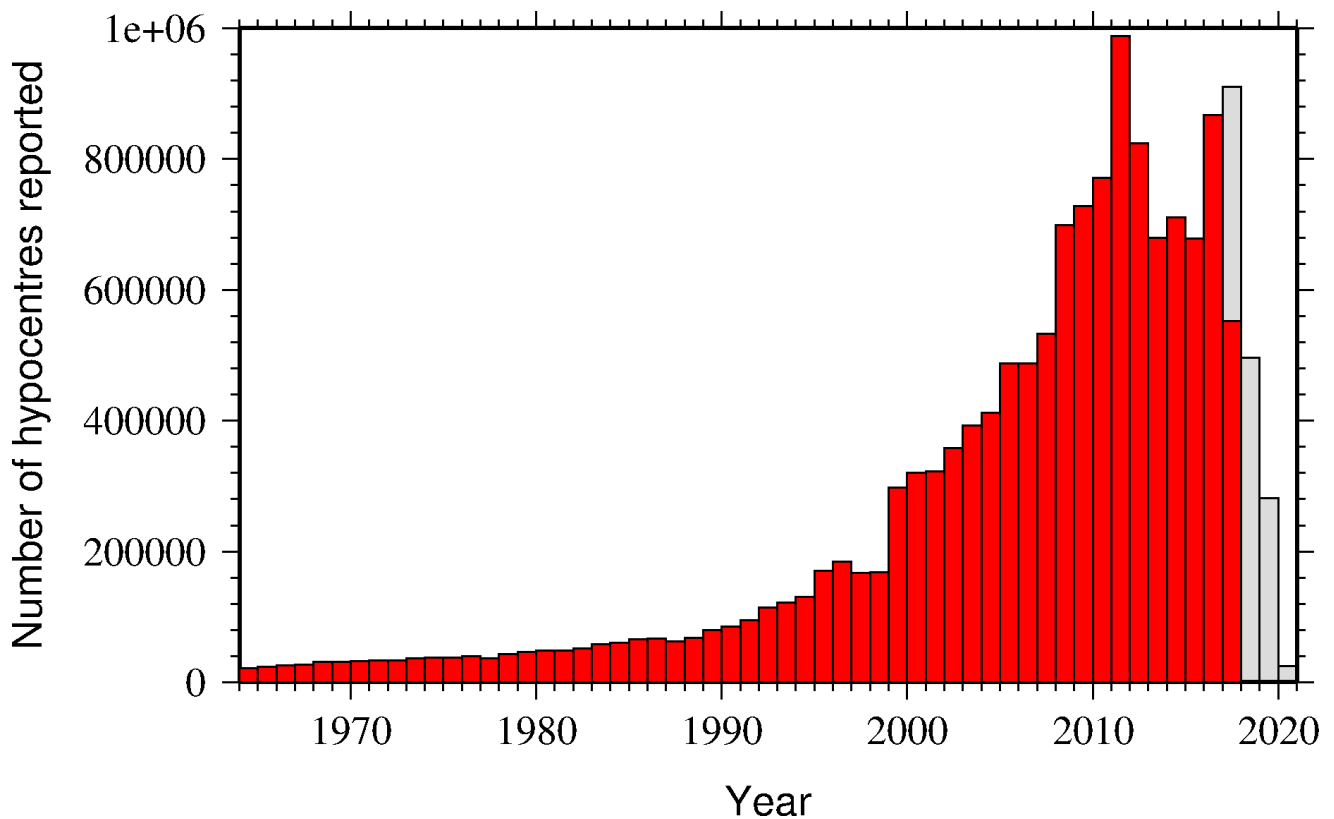
Figure 8.9: *Histogram showing the number of hypocentres collected by the ISC for events each year since 1964. For each event, multiple hypocentres may be reported.*

All the hypocentres that are reported to the ISC are automatically grouped into events, which form the basis of the ISC Bulletin. For this summary period 463620 hypocentres (including ISC) were grouped
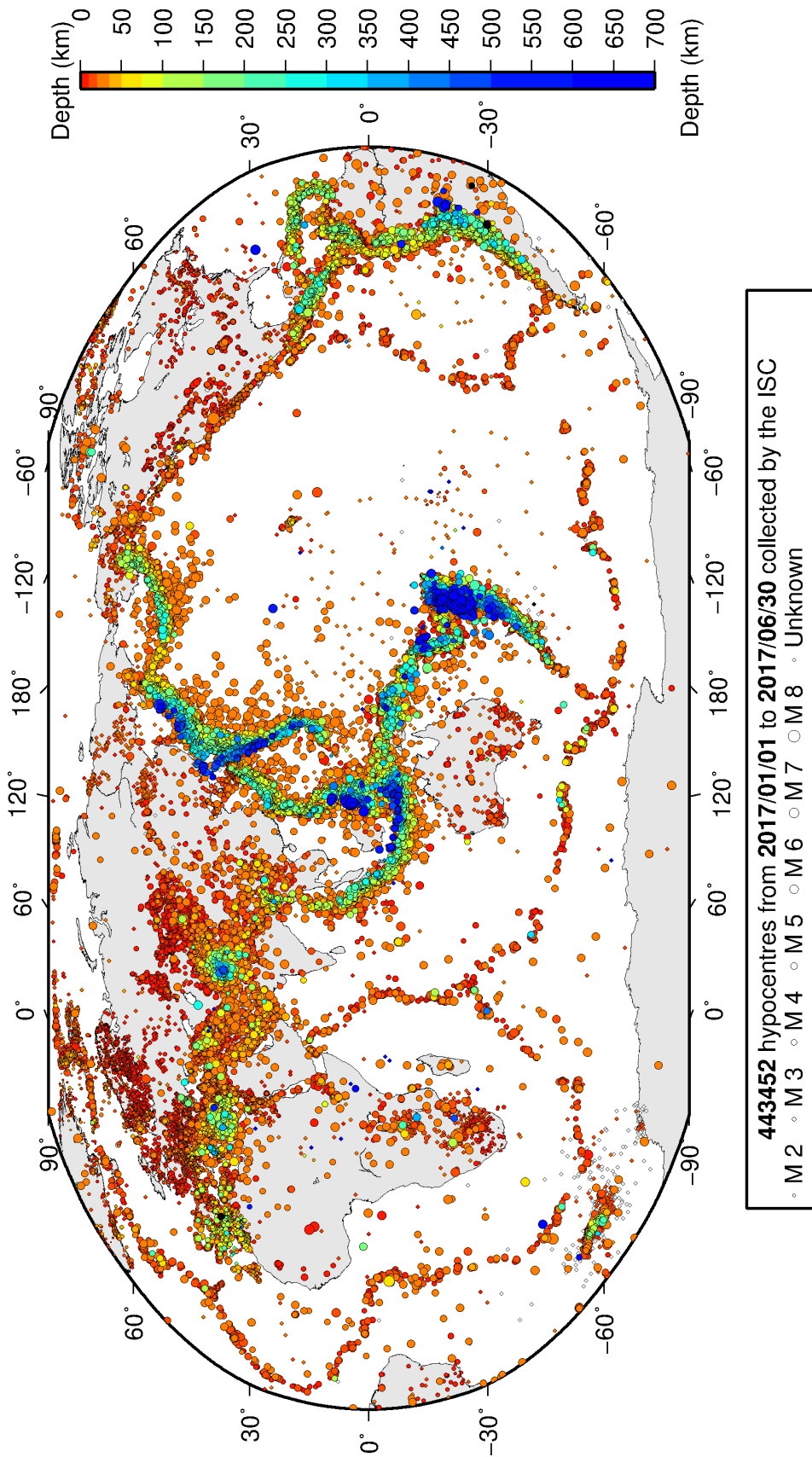
Figure 8.10: *Map of all hypocentres collected by the ISC. The scatter shows the large variation of the multiple hypocentres that are reported for each event. The magnitude corresponds with the reported network magnitude. If more than one network magnitude type was reported, preference was given to values of M_W, M_S, m_b and M_L respectively. Compare with Figure 9.2*

into 338769 events, the largest of these having 58 hypocentres in one event. The total number of events shown here is the result of an automatic grouping algorithm, and will differ from the total events in the published ISC Bulletin, where both the number of events and the number of hypocentre estimates will have changed due to further analysis. The process of grouping is detailed in Section 11.1.3. Figure 9.2 on page 98 shows a map of all prime hypocentres.

8.5   Collection of Network Magnitude Data

Data contributing agencies normally report earthquake hypocentre solutions along with magnitude estimates. For each seismic event, each agency may report one or more magnitudes of the same or different types. This stems from variability in observational practices at regional, national and global level in computing magnitudes based on a multitude of wave types. Differences in the amplitude measurement algorithm, seismogram component(s) used, frequency range, station distance range as well as the instrument type contribute to the diversity of magnitude types. Table 8.5 provides an overview of the complexity of reported network magnitudes reported for seismic events during the summary period.

Table 8.5: *Statistics of magnitude reports to the ISC; M – average magnitude of estimates reported for each event.*

	M<3.0	3.0≤M<5.0	M≥5.0
Number of seismic events	274000	39607	439
Average number of magnitude estimates per event	1.3	3.2	19.3
Average number of magnitudes (by the same agency) per event	1.1	1.9	2.7
Average number of magnitude types per event	1.2	2.5	9.2
Number of magnitude types	28	38	35

Table 8.6 gives the basic description, main features and scientific paper references for the most commonly reported magnitude types.

Table 8.6: *Description of the most common magnitude types reported to the ISC.*

Magnitude type	Description	References	Comments
M	Unspecified		Often used in real or near-real time magnitude estimations
mB	Medium-period and Broad-band body-wave magnitude	*Gutenberg (1945a); Gutenberg (1945b); IASPEI (2005); IASPEI (2013); Bormann et al. (2009); Bormann and Dewey (2012)*	
mb	Short-period body-wave magnitude	*IASPEI (2005); IASPEI (2013); Bormann et al. (2009); Bormann and Dewey (2012)*	Classical mb based on stations between 21°-100° distance

Table 8.6: *continued*

Magnitude type	Description	References	Comments
mb1	Short-period body-wave magnitude	*IDC* (1999) and references therein	Reported only by the IDC; also includes stations at distances less than 21°
mb1mx	Maximum likelihood short-period body-wave magnitude	*Ringdal* (1976); *IDC* (1999) and references therein	Reported only by the IDC
mbtmp	short-period body-wave magnitude with depth fixed at the surface	*IDC* (1999) and references therein	Reported only by the IDC
mbLg	Lg-wave magnitude	*Nuttli* (1973); *IASPEI* (2005); *IASPEI* (2013); *Bormann and Dewey* (2012)	Also reported as MN
Mc	Coda magnitude		
MD (Md)	Duration magnitude	*Bisztricsany* (1958); *Lee et al.* (1972)	
ME (Me)	Energy magnitude	*Choy and Boatwright* (1995)	Reported only by NEIC
MJMA	JMA magnitude	*Tsuboi* (1954)	Reported only by JMA
ML (Ml)	Local (Richter) magnitude	*Richter* (1935); *Hutton and Boore* (1987); *IASPEI* (2005); *IASPEI* (2013)	
MLSn	Local magnitude calculated for Sn phases	*Balfour et al.* (2008)	Reported by PGC only for earthquakes west of the Cascadia subduction zone
MLv	Local (Richter) magnitude computed from the vertical component		Reported only by DJA and BKK
MN (Mn)	Lg-wave magnitude	*Nuttli* (1973); *IASPEI* (2005)	Also reported as mbLg
MS (Ms)	Surface-wave magnitude	*Gutenberg* (1945c); *Vaněk et al.* (1962); *IASPEI* (2005)	Classical surface-wave magnitude computed from station between 20°-160° distance
Ms1	Surface-wave magnitude	*IDC* (1999) and references therein	Reported only by the IDC; also includes stations at distances less than 20°
ms1mx	Maximum likelihood surface-wave magnitude	*Ringdal* (1976); *IDC* (1999) and references therein	Reported only by the IDC

Table 8.6: *continued*

Magnitude type	Description	References	Comments
Ms7	Surface-wave magnitude	*Bormann et al.* (2007)	Reported only by BJI and computed from records of a Chinese-made long-period seismograph in the distance range 3°-177°
MW (Mw)	Moment magnitude	*Kanamori* (1977); *Dziewonski et al.* (1981)	Computed according to the *IASPEI* (2005) and *IASPEI* (2013) standard formula
Mw(mB)	Proxy Mw based on mB	*Bormann and Saul* (2008)	Reported only by DJA and BKK
Mwp	Moment magnitude from P-waves	*Tsuboi et al.* (1995)	Reported only by DJA and BKK and used in rapid response
mbh	Unknown		
mbv	Unknown		
MG	Unspecified type		Contact contributor
Mm	Unknown		
msh	Unknown		
MSV	Unknown		

Table 8.7 lists all magnitude types reported, the corresponding number of events in the ISC Bulletin and the agency codes along with the number of earthquakes.

Table 8.7: *Summary of magnitude types in the ISC Bulletin for this summary period. The number of events with values for each magnitude type is listed. The agencies reporting these magnitude types are listed, together with the total number of values reported.*

Magnitude type	Events	Agencies reporting magnitude type (number of values)
M	10852	WEL (10780), PRU (40), RSPR (32), FDF (1)
mB	1730	BJI (1117), DJA (721), WEL (169), IASPEI (1), NOU (1), SFS (1)
MB	1	IPEC (1)
mb	28353	IDC (15668), NEIC (6397), NNC (5060), MAN (4601), KR-NET (3442), MOS (1512), VIE (1477), DJA (1358), BJI (1062), VAO (543), NOU (370), BGR (256), MDD (124), IASPEI (98), OMAN (71), CFUSG (63), GII (58), NAO (57), MCSM (39), SIGU (27), SFS (22), NDI (17), DSN (17), PGC (10), PRE (6), DMN (6), DNK (5), BGS (3), ROM (3), IGIL (3), BER (3), CSEM (2), RSNC (2), INMG (1), SSNC (1), CRAAG (1), PDG (1), YARS (1), STR (1)
mb(Pn)	189	BER (189)
mB_BB	28	BGR (28)
mb_Lg	3096	MDD (2412), NEIC (669), OTT (16), TEH (1)
mBc	1	DJA (1)
mbR	85	VAO (85)

Table 8.7: *Continued.*

Magnitude type	Events	Agencies reporting magnitude type (number of values)
mbtmp	17105	IDC (17105)
MC	24	DDA (24)
Mc	52	KRSC (45), DNK (5), BER (1), OSPL (1)
MD	11315	RSPR (2098), TRN (1943), LDG (1940), ROM (1078), SSNC (865), HLW (700), ECX (699), SDD (529), GCG (459), TIR (297), JMA (277), GRAL (252), GII (189), SOF (173), MEX (138), PNSN (109), JSN (105), PDG (88), UPA (66), TUN (61), LSZ (60), SLM (58), INET (36), BUG (20), HVO (15), INMG (13), SIGU (8), NCEDC (7), SNET (6), NIC (5), ISK (4), UUSS (1), SEA (1), SJA (1), NDI (1)
Mjma	15	DJA (14), WEL (1)
ML	154430	ROM (31241), DDA (18640), ISK (17020), TAP (16680), WEL (10355), IDC (9217), HEL (8549), RSNC (8401), ATH (8121), THE (5138), GUC (4849), MAN (4675), NEIC (3548), UPP (3092), AEIC (2684), LDG (2595), VIE (2424), BER (2412), PGC (1710), TEH (1706), MRB (1590), SNET (1549), ANF (1541), SFS (1439), DNK (1411), SKO (1396), INMG (1372), BEO (1320), CNRM (1003), LJU (988), RHSSO (966), SSNC (867), SJA (867), PRE (796), BUC (769), SCB (725), ECX (704), KOLA (701), KRSC (646), IPEC (553), GEN (537), SDD (499), OSPL (488), TUL (482), NIC (449), HLW (447), IGIL (377), PDG (326), WBNET (317), NAO (309), KNET (293), ISN (290), TIR (264), LVSN (245), KRSZO (215), HVO (203), OTT (199), CRAAG (193), NDI (173), OMAN (170), DSN (140), BGS (129), BJI (127), UCC (122), KEA (117), BGR (109), MI-RAS (106), ASIES (105), INET (90), REN (73), PAS (67), PPT (65), NOU (61), UUSS (60), SEA (47), MCSM (46), UPA (45), SGS (37), CUPWA (35), BNS (28), DJA (28), NCEDC (28), DMN (27), BUT (24), BUG (24), AAE (22), THR (20), PLV (17), DRS (17), LSZ (15), LDO (12), FIA0 (5), VAO (3), RISSC (3), SIGU (3), RSPR (3), ASRS (3), OGSO (2), AUST (2), CLL (1), CSEM (1)
MLh	667	ZUR (565), ASRS (102)
MLSn	369	PGC (369)
MLv	19007	WEL (10804), DJA (3510), STR (2897), NOU (1557), SFS (919), KRSZO (15), MCSM (4), ASRS (1)
Mm	454	GII (454)
MN	410	OTT (410)
mpv	5448	NNC (5448)
MPVA	244	MOS (216), NORS (175)
MS	12073	IDC (7689), MAN (4667), BJI (811), MOS (382), BGR (141), NSSP (51), IASPEI (46), SOME (35), OMAN (18), VIE (12), NDI (2), DNK (2), DSN (2), IGIL (1), RSNC (1), YARS (1), IPEC (1), BER (1)
Ms(BB)	12	DJA (12)
Ms7	803	BJI (803)
Ms_20	161	NEIC (161)

Table 8.7: *Continued.*

Magnitude type	Events	Agencies reporting magnitude type (number of values)
MV	128184	JMA (128184)
MW	6393	GCMT (1042), SJA (865), FUNV (664), UPA (639), NIED (598), SSNC (573), INET (550), DDA (422), PGC (395), UCR (295), SCB (259), RSNC (245), ASIES (105), WEL (99), JMA (97), SDD (86), MED_RCMT (84), DJA (60), ROM (53), ATH (27), BER (9), MEX (6), GFZ (5), CSEM (4), UPSL (4), AAE (3), IEC (2), OTT (1), DNK (1), PDG (1), SNET (1)
Mw(mB)	170	WEL (169), SFS (1)
Mwb	192	NEIC (192)
Mwc	13	NEIC (13)
Mwp	113	DJA (105), OMAN (6), ROM (2)
Mwr	511	NEIC (387), GUC (108), OTT (33), SLM (28), NCEDC (26), REN (11), VIE (9), PAS (5), ROM (2), CAR (1)
Mww	364	NEIC (363), GUC (9)

The most commonly reported magnitude types are short-period body-wave, surface-wave, local (or Richter), moment, duration and JMA magnitude type. For a given earthquake, the number and type of reported magnitudes greatly vary depending on its size and location. The large earthquake of October 25, 2010 gives an example of the multitude of reported magnitude types for large earthquakes (Listing 8.1). Different magnitude estimates come from global monitoring agencies such as the IDC, NEIC and GCMT, a local agency (GUC) and other agencies, such as MOS and BJI, providing estimates based on the analysis of their networks. The same agency may report different magnitude types as well as several estimates of the same magnitude type, such as NEIC estimates of Mw obtained from W-phase, centroid and body-wave inversions.

Listing 8.1: *Example of reported magnitudes for a large event*

```
Event     15264887 Southern Sumatera
    Date         Time      Err   RMS Latitude Longitude  Smaj  Smin  Az Depth    Err Ndef Nsta Gap   mdist  Mdist Qual   Author        OrigID
2010/10/25 14:42:22.18   0.27 1.813  -3.5248  100.1042 4.045 3.327  54  20.0   1.37 2102 2149  23    0.76 176.43 m i de ISC          01346132
  (#PRIME)

Magnitude   Err Nsta Author      OrigID
mb     6.1         61 BJI       15548963
mB     6.9         68 BJI       15548963
Ms     7.7         85 BJI       15548963
Ms7    7.5         86 BJI       15548963
mb     5.3 0.1     48 IDC       16686694
mb1    5.3 0.1     51 IDC       16686694
mb1mx  5.3 0.0     52 IDC       16686694
mbtmp  5.3 0.1     51 IDC       16686694
ML     5.1 0.2      2 IDC       16686694
MS     7.1 0.0     31 IDC       16686694
Ms1    7.1 0.0     31 IDC       16686694
ms1mx  6.9 0.1     44 IDC       16686694
mb     6.1        243 ISCJB     01677901
MS     7.3        228 ISCJB     01677901
M      7.1        117 DJA       01268475
mb     6.1 0.2    115 DJA       01268475
mB     7.1 0.1    117 DJA       01268475
MLv    7.0 0.2     26 DJA       01268475
       7.1 0.4    117 DJA       01268475
Mwp    6.9 0.2    102 DJA       01268475
mb     6.4         49 MOS       16742129
MS     7.2         70 MOS       16742129
mb     6.5        110 NEIC      01288303
ME     7.3            NEIC      01288303
MS     7.3        143 NEIC      01288303
MW     7.7            NEIC      01288303
MW     7.8        130 GCMT      00125427
mb     5.9            KLM       00255772
ML     6.7            KLM       00255772
MS     7.6            KLM       00255772
mb     6.4         20 BGR       16815854
Ms     7.2          2 BGR       16815854
mb     6.3 0.3    250 ISC       01346132
MS     7.3 0.1    237 ISC       01346132
```

An example of a relatively small earthquake that occurred in northern Italy for which we received

magnitude reports of mostly local and duration type from six agencies in Italy, France and Austria is given in Listing 8.2.

Listing 8.2: Example of reported magnitudes for a small event

```
Event 15089710 Northern Italy
   Date       Time      Err   RMS Latitude Longitude  Smaj  Smin  Az Depth    Err Ndef Nsta Gap  mdist  Mdist Qual   Author     OrigID
2010/08/08 15:20:46.22  0.94 0.778  45.4846    8.3212 2.900 2.539 110  28.6   9.22  172  110  82   0.41   5.35 m i ke ISC        01249414
 (#PRIME)

Magnitude  Err Nsta Author      OrigID
ML    2.4         10 ZUR       15925566
Md    2.6 0.2     19 ROM       16861451
Ml    2.2 0.2      9 ROM       16861451
ML    2.5            GEN       00554757
ML    2.6 0.3     28 CSEM      00554756
Md    2.3 0.0      3 LDG       14797570
Ml    2.6 0.3     32 LDG       14797570
```

Figure 8.11 shows a distribution of the number of agencies reporting magnitude estimates to the ISC according to the magnitude value. The peak of the distribution corresponds to small earthquakes where many local agencies report local and/or duration magnitudes. The number of contributing agencies rapidly decreases for earthquakes of approximately magnitude 5.5 and above, where magnitudes are mostly given by global monitoring agencies.
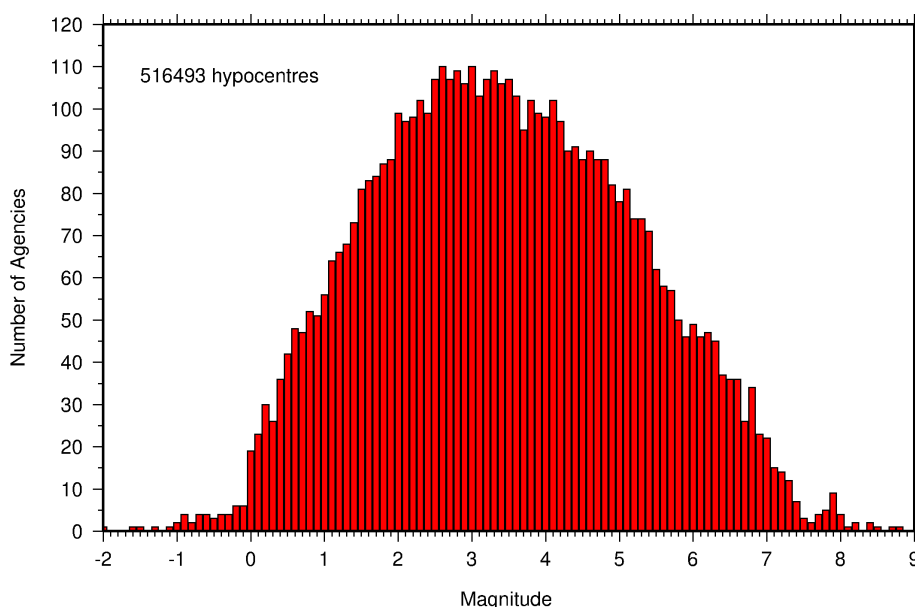
Figure 8.11: Histogram showing the number of agencies that reported network magnitude values. All magnitude types are included.

8.6   Moment Tensor Solutions

The ISC Bulletin publishes moment tensor solutions, which are reported to the ISC by other agencies. The collection of moment tensor solutions is summarised in Table 8.8. A histogram showing all moment tensor solutions collected throughout the ISC history is shown in Figure 8.12. Several moment tensor solutions from different authors and different moment tensor solutions calculated by different methods from the same agency may be present for the same event.

The number of moment tensors for this summary period, reported by each agency, is shown in Table 8.9. The moment tensor solutions are plotted in Figure 8.14.

Table 8.8: *Summary of reports containing moment tensor solutions.*

Reports with Moment Tensors	100
Total moment tensors received	18289
Agencies reporting moment tensors	9
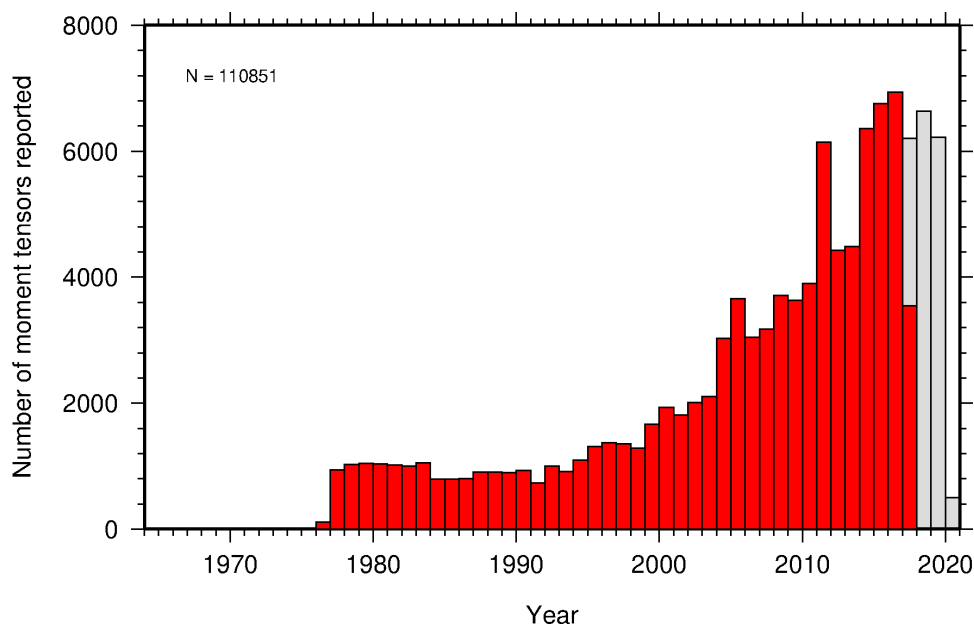
Figure 8.12: *Histogram showing the number of moment tensors reported to the ISC since 1964. The regions in grey represent data that are still being actively collected.*
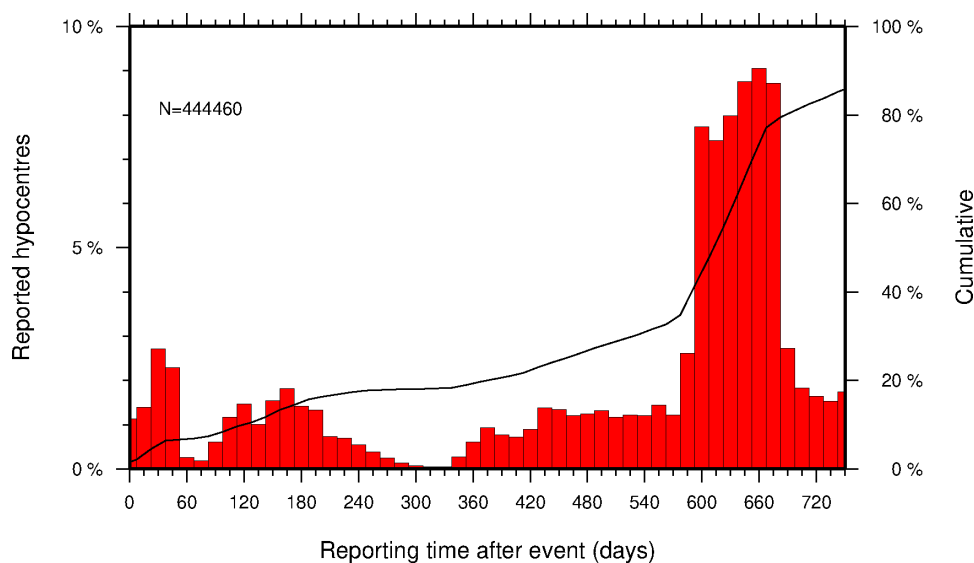
Figure 8.13: *Histogram showing the timing of final reports of the hypocentres (total of N) to the ISC. The cumulative frequency is shown by the solid line.*
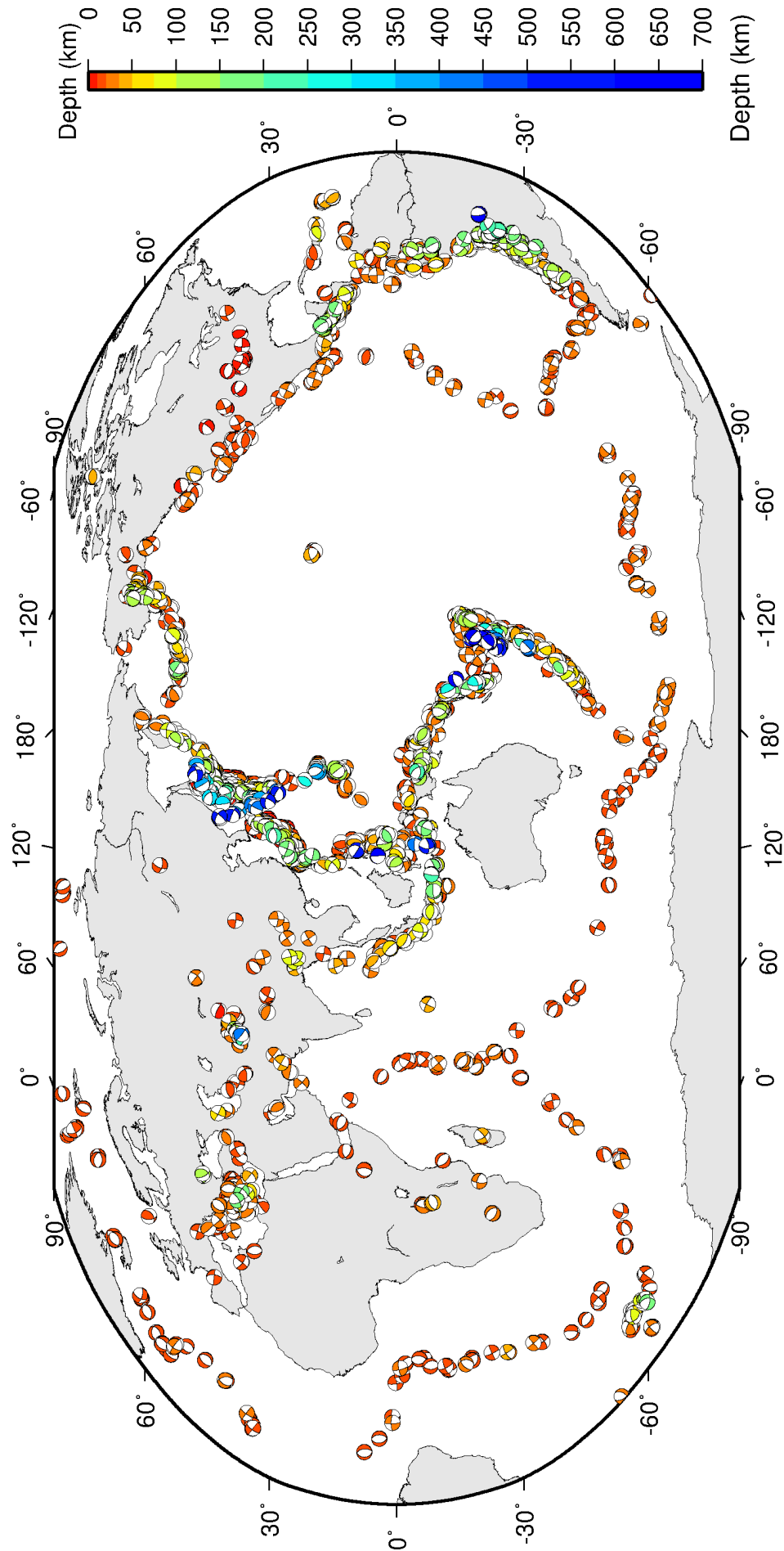
ISC Bulletin: **3051** focal mechanism solutions for **2128** events from **2017/01/01** to **2017/06/30**

Figure 8.14: *Map of all moment tensor solutions in the ISC Bulletin for this summary period.*

Table 8.9: *Summary of moment tensor solutions in the ISC Bulletin reported by each agency.*

Agency	Number of moment tensor solutions
ISC	1144
GCMT	1042
NEIC	1040
NIED	598
PNSN	109
ASIES	105
WEL	99
MED_RCMT	84
RSNC	70
ROM	52
ATH	27
SDD	17
UPA	15
ECX	14
PRE	10
MOS	6
UPSL	4
IEC	4
UCR	3
DNK	1
GUC	1
OSPL	1
BER	1
MEX	1
INET	1

8.7 Timing of Data Collection

Here we present the timing of reports to the ISC. Please note, this does not include provisional alerts, which are replaced at a later stage. Instead, it reflects the final data sent to the ISC. The absolute timing of all hypocentre reports, regardless of magnitude, is shown in Figure 8.13. In Figure 8.15 the reports are grouped into one of six categories - from within three days of an event origin time, to over one year. The histogram shows the distribution with magnitude (for hypocentres where a network magnitude was reported) for each category, whilst the map shows the geographic distribution of the reported hypocentres.
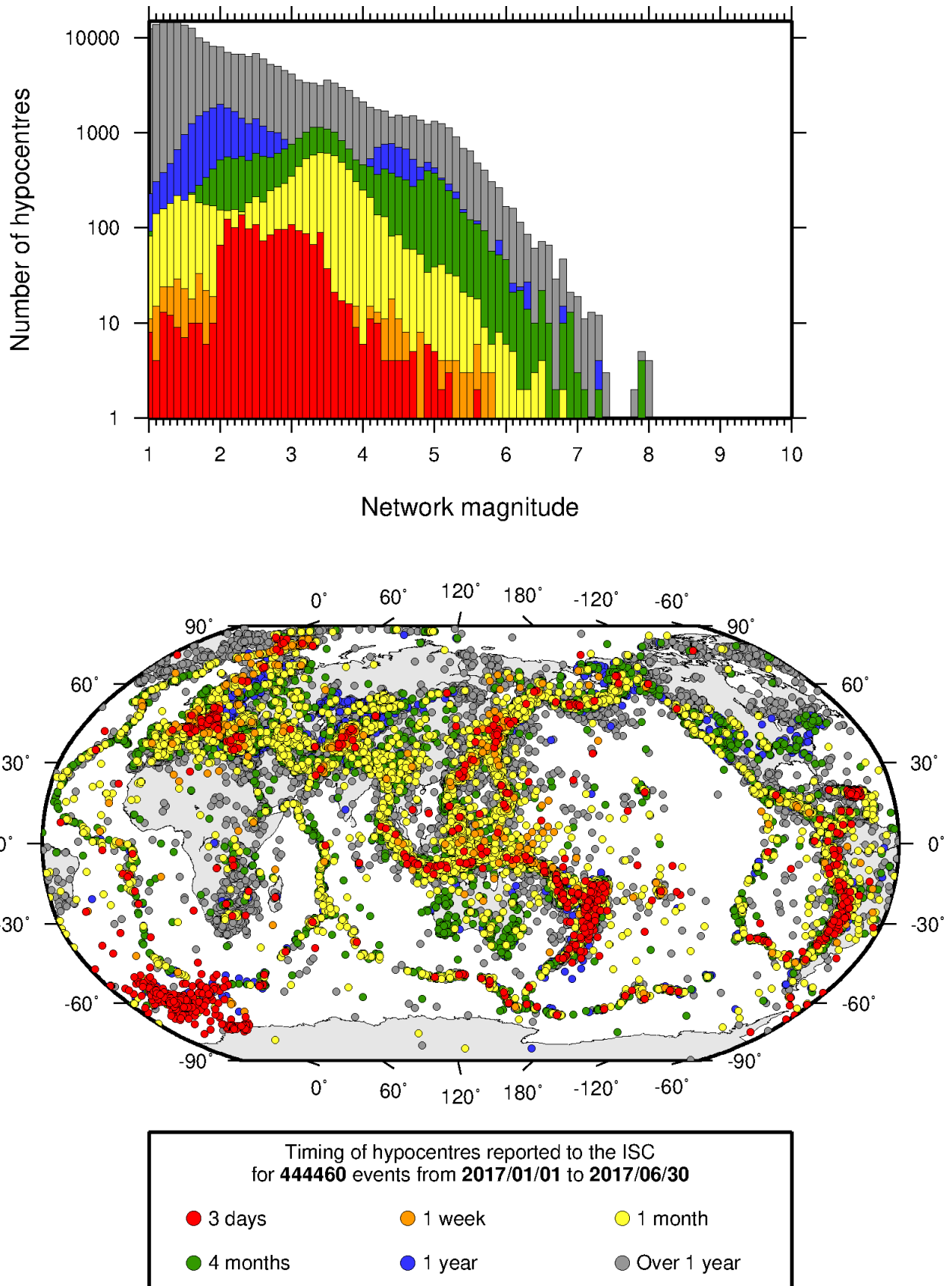
Figure 8.15: *Timing of hypocentres reported to the ISC. The colours show the time after the origin time that the corresponding hypocentre was reported. The histogram shows the distribution with magnitude. If more than one network magnitude was reported, preference was given to a value of M_W followed by M_S, m_b and M_L respectively; all reported hypocentres are included on the map. Note: early reported hypocentres are plotted over later reported hypocentres, on both the map and histogram.*

9

Overview of the ISC Bulletin

This chapter provides an overview of the seismic event data in the ISC Bulletin. We indicate the differences between all ISC events and those ISC events that are reviewed or located. We describe the wealth of phase arrivals and phase amplitudes and periods observed at seismic stations worldwide, reported in the ISC Bulletin and often used in the ISC location and magnitude determination. Finally, we make some comparisons of the ISC magnitudes with those reported by other agencies, and discuss magnitude completeness of the ISC Bulletin.

9.1 Events

The ISC Bulletin had 332215 reported events in the summary period between January and June 2017. Some 93% (311303) of the events were identified as earthquakes, the rest (20912) were of anthropogenic origin (including mining and other chemical explosions, rockbursts and induced events) or of unknown origin. As discussed in Section 11.1.3, typically about 15% of the events are selected for ISC review, and about half of the events selected for review are located by the ISC. In this summary period 8% of the events were reviewed and 5% of the events were located by the ISC. For events that are not located by the ISC, the prime hypocentre is identified according to the rules described in Section 11.1.3.

Of the 12588822 reported phase observations, 29% are associated to ISC-reviewed events, and 27% are associated to events selected for ISC location. Note that all large events are reviewed and located by the ISC. Since large events are globally recorded and thus reported by stations worldwide, they will provide the bulk of observations. This explains why only about one-fifth of the events in any given month is reviewed although the number of phases associated to reviewed events has increased nearly exponentially in the past decades.

Figure 9.1 shows the daily number of events throughout the summary period. Figure 9.2 shows the locations of the events in the ISC Bulletin; the locations of ISC-reviewed and ISC-located events are shown in Figures 9.3 and 9.4, respectively.

Figure 9.5 shows the hypocentral depth distributions of events in the ISC Bulletin for the summary period. The vast majority of events occur in the Earth's crust. Note that the peaks at 0, 10, 35 km, and at every 50 km intervals deeper than 100 km are artifacts of analyst practices of fixing the depth to a nominal value when the depth cannot be reliably resolved.

Figure 9.6 shows the depth distribution of free-depth solutions in the ISC Bulletin. The depth of a hypocentre reported to the ISC is assumed to be determined as a free parameter, unless it is explicitly labelled as a fixed-depth solution. On the other hand, as described in Section 11.1.4, the ISC locator attempts to get a free-depth solution if, and only if, there is resolution for the depth in the data, i.e. if
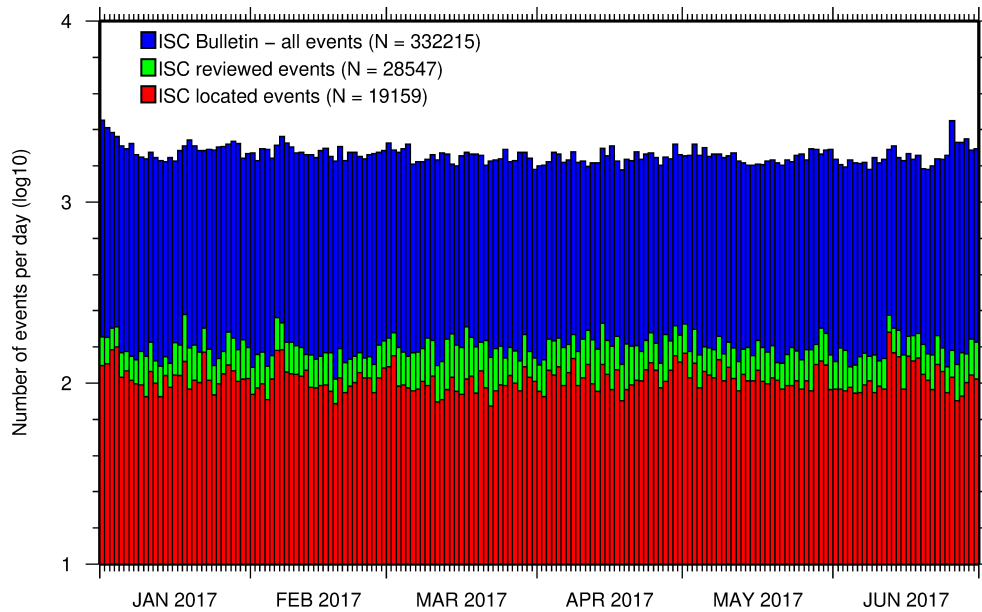
Figure 9.1: *Histogram showing the number of events in the ISC Bulletin for the current summary period. The vertical scale is logarithmic.*

there is a local network and/or sufficient depth-sensitive phases are reported.

Figure 9.7 shows the depth distribution of fixed-depth solutions in the ISC Bulletin. Except for a fraction of events whose depth is fixed to a shallow depth, this set comprises mostly ISC-located events. If there is no resolution for depth in the data, the ISC locator fixes the depth to a value obtained from the ISC default depth grid file, or if no default depth exists for that location, to a nominal default depth assigned to each Flinn-Engdahl region (see details in Section 11.1.4). During the ISC review editors are inclined to accept the depth obtained from the default depth grid, but they typically change the depth of those solutions that have a nominal (10 or 35 km) depth. When doing so, they usually fix the depth to a round number, preferably divisible by 50.

For events selected for ISC location, the number of stations typically increases as arrival data reported by several agencies are grouped together and associated to the prime hypocentre. Consequently, the network geometry, characterised by the secondary azimuthal gap (the largest azimuthal gap a single station closes), is typically improved. Figure 9.8 illustrates that the secondary azimuthal gap is indeed generally smaller for ISC-located events than that for all events in the ISC Bulletin. Figure 9.9 shows the distribution of the number of associated stations. For large events the number of associated stations is usually larger for ISC-located events than for any of the reported event bulletins. On the other hand, events with just a few reporting stations are rarely selected for ISC location. The same is true for the number of defining stations (stations with at least one defining phase that were used in the location). Figure 9.10 indicates that because the reported observations from multiple agencies are associated to the prime, large ISC-located events typically have a larger number of defining stations than any of the reported event bulletins.

The formal uncertainty estimates are also typically smaller for ISC-located events. Figure 9.11 shows the distribution of the area of the 90% confidence error ellipse for ISC-located events during the summary period. The distribution suffers from a long tail indicating a few poorly constrained event locations. Nevertheless, half of the events are characterised by an error ellipse with an area less than 173 km^2, 90%
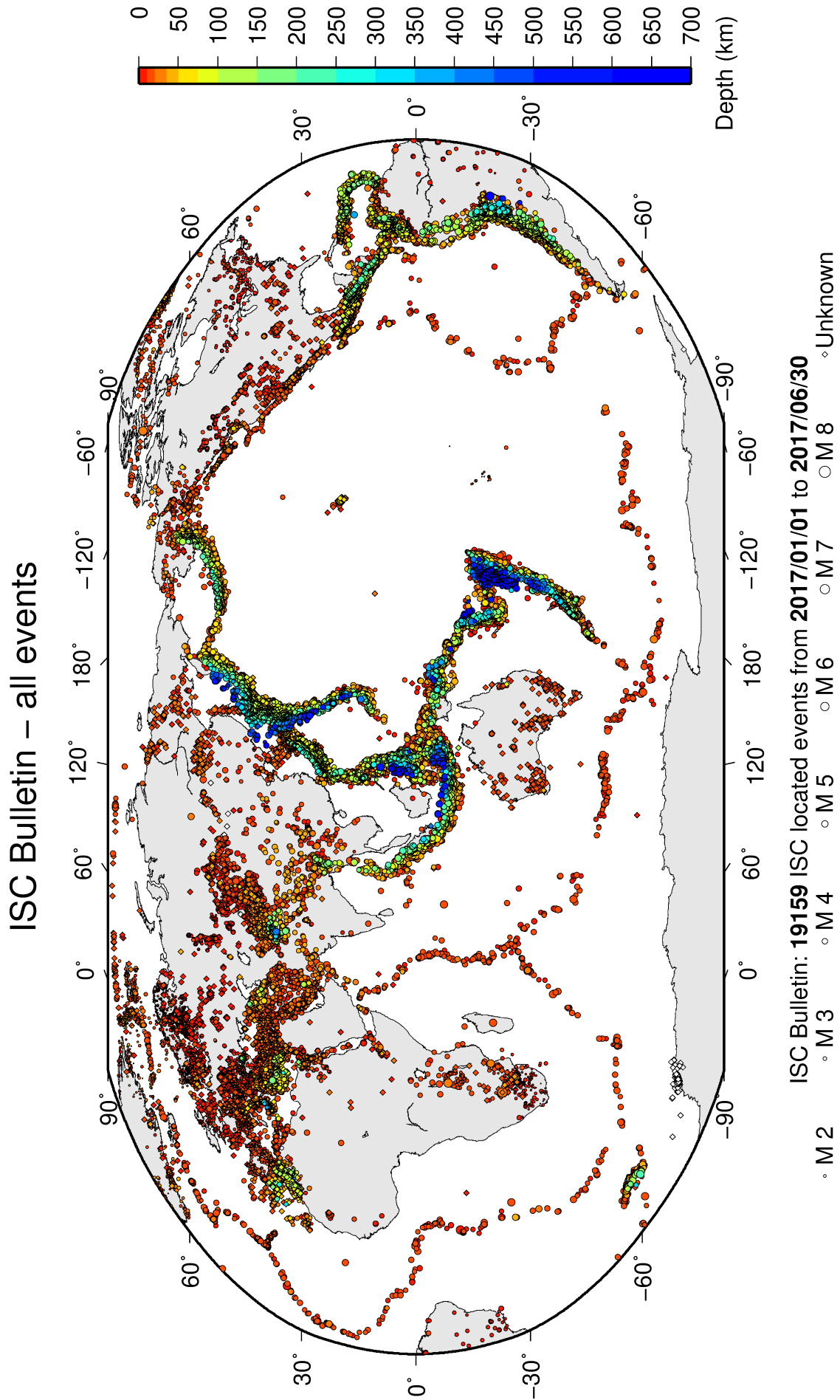
Figure 9.2: *Map of all events in the ISC Bulletin. Prime hypocentre locations are shown. Compare with Figure 8.10.*
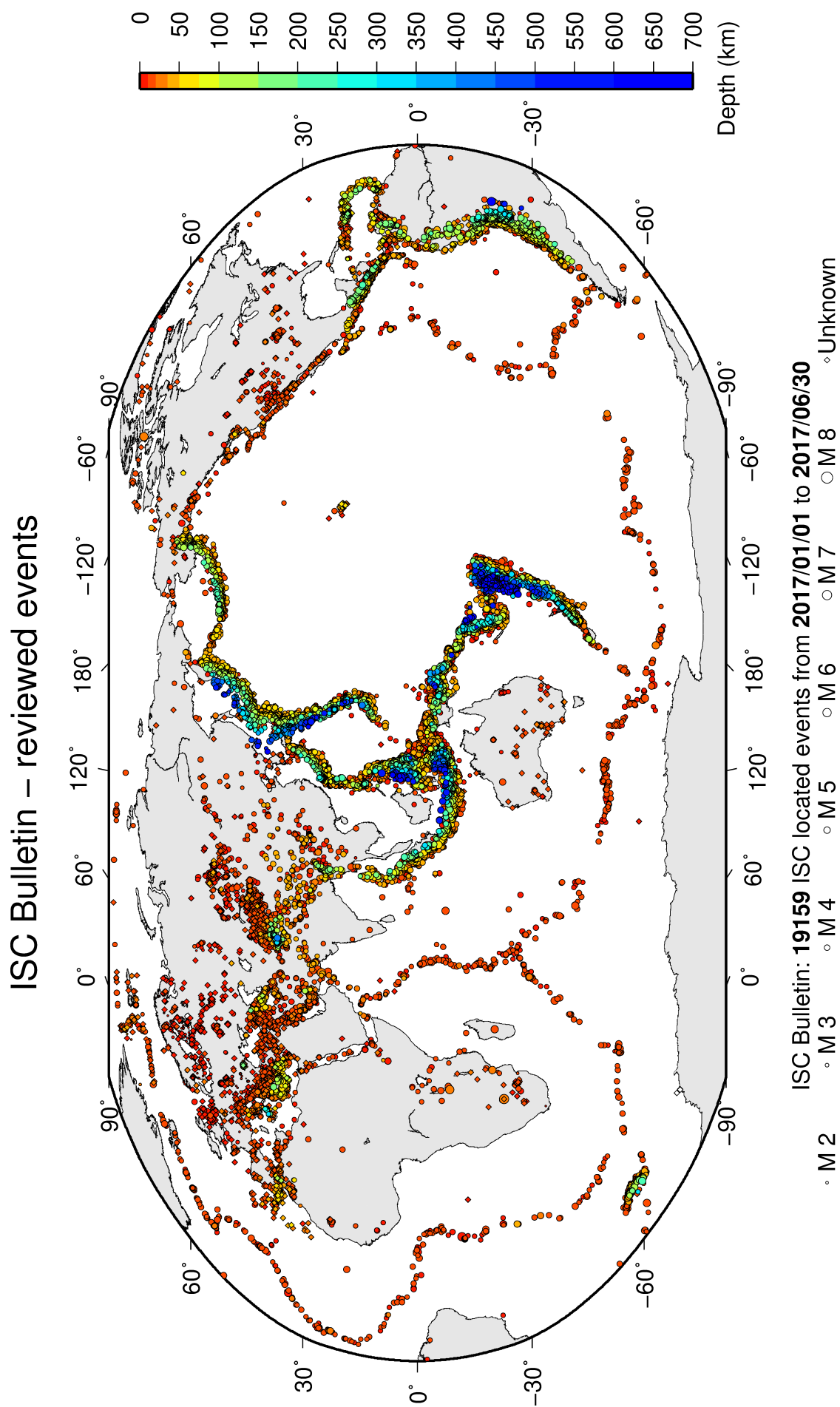
Figure 9.3: *Map of all events reviewed by the ISC for this time period. Prime hypocentre locations are shown.*

ISC Bulletin – ISC located events

ISC Bulletin: **19159** ISC located events from **2017/01/01** to **2017/06/30**
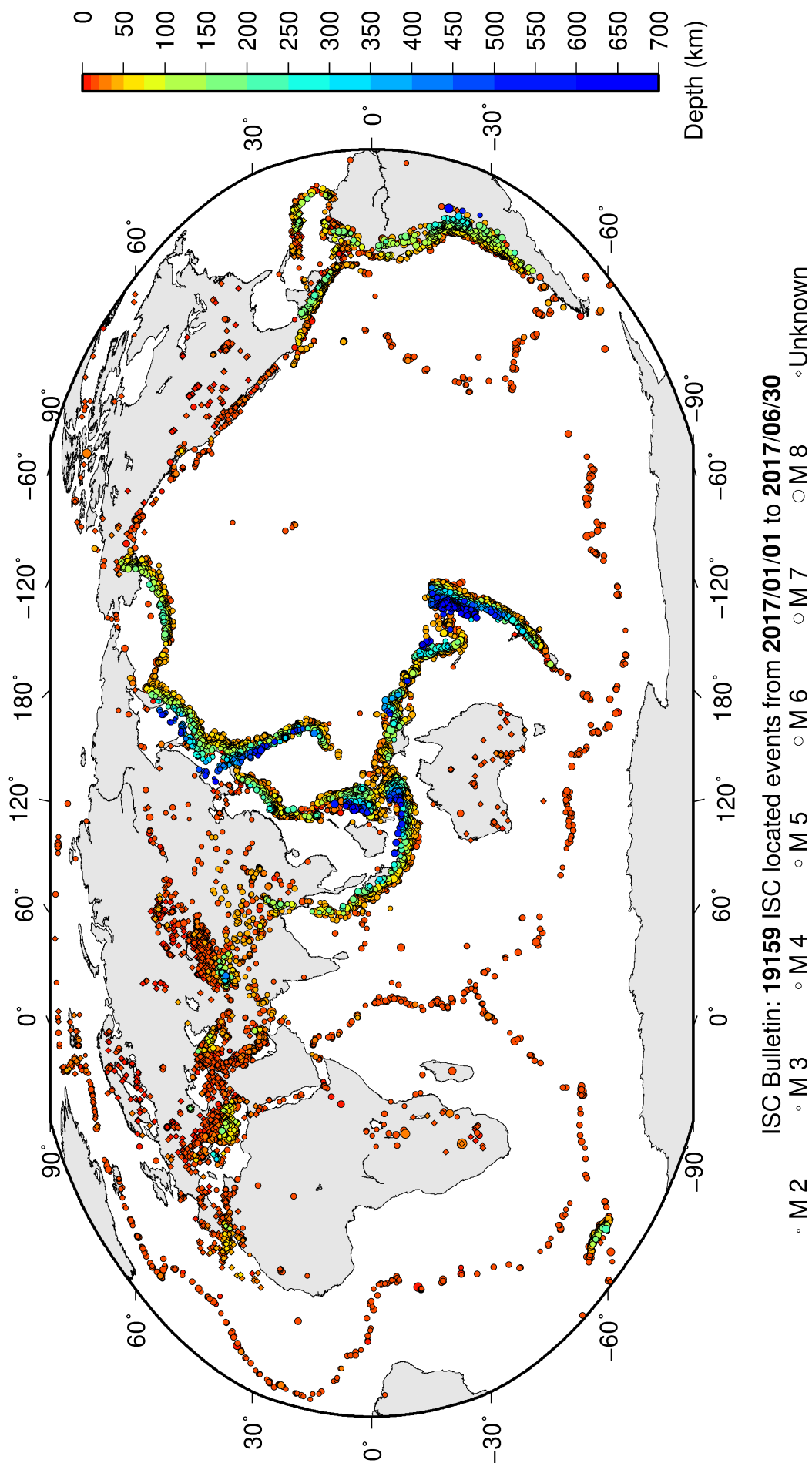
Figure 9.4: *Map of all events located by the ISC for this time period. ISC determined hypocentre locations are shown.*
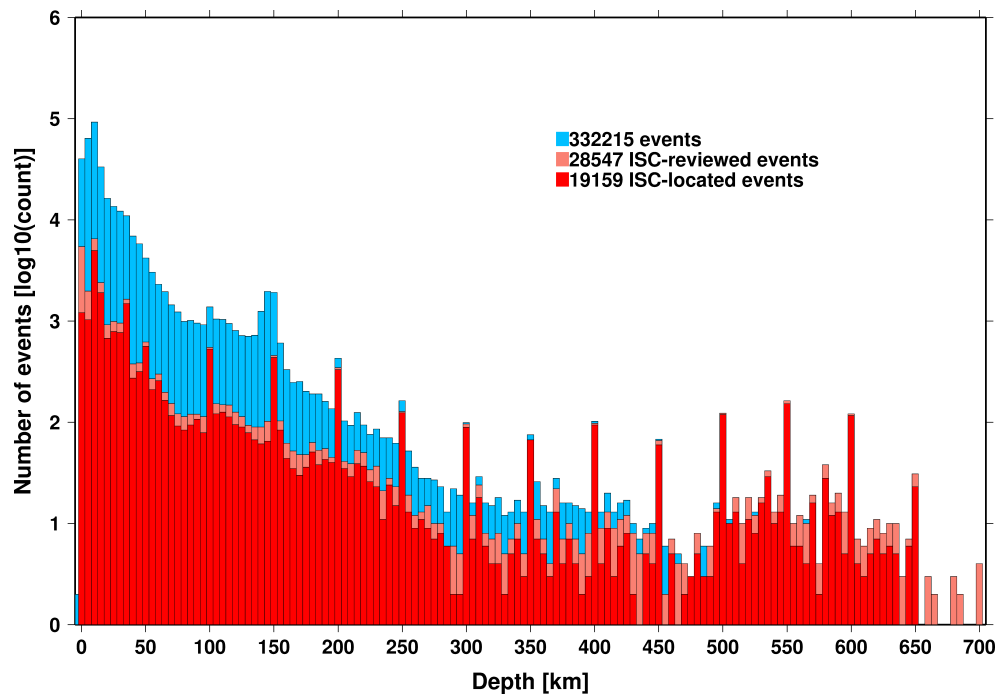
Figure 9.5: *Distribution of event depths in the ISC Bulletin (blue) and for the ISC-reviewed (pink) and the ISC-located (red) events during the summary period. All ISC-located events are reviewed, but not all reviewed events are located by the ISC. The vertical scale is logarithmic.*
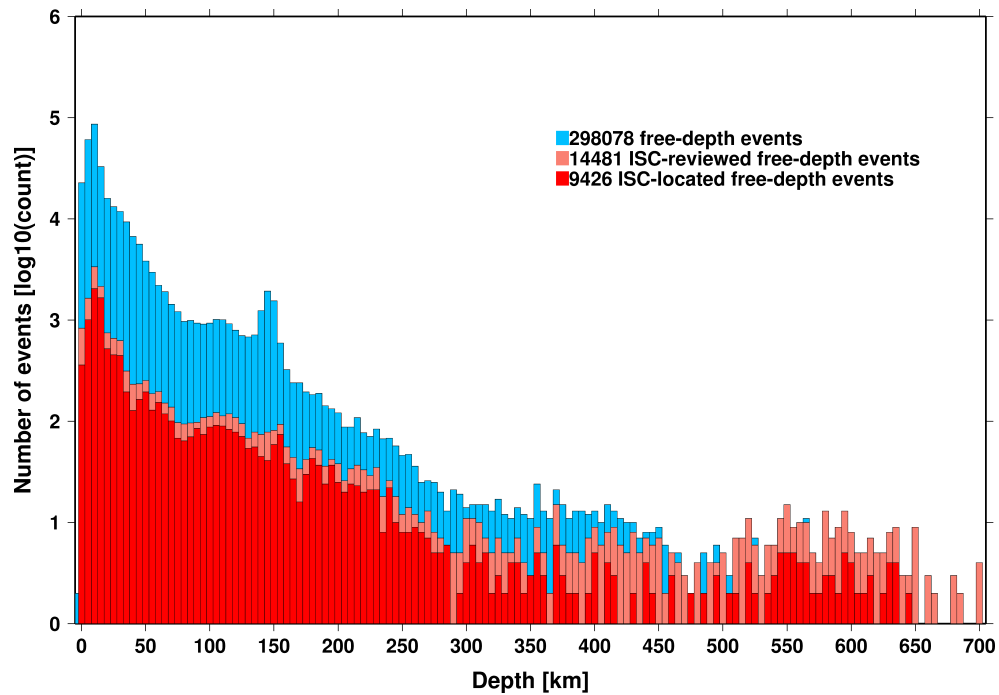
Figure 9.6: *Hypocentral depth distribution of events where the prime hypocentres are reported/located with a free-depth solution in the ISC Bulletin. The vertical scale is logarithmic.*
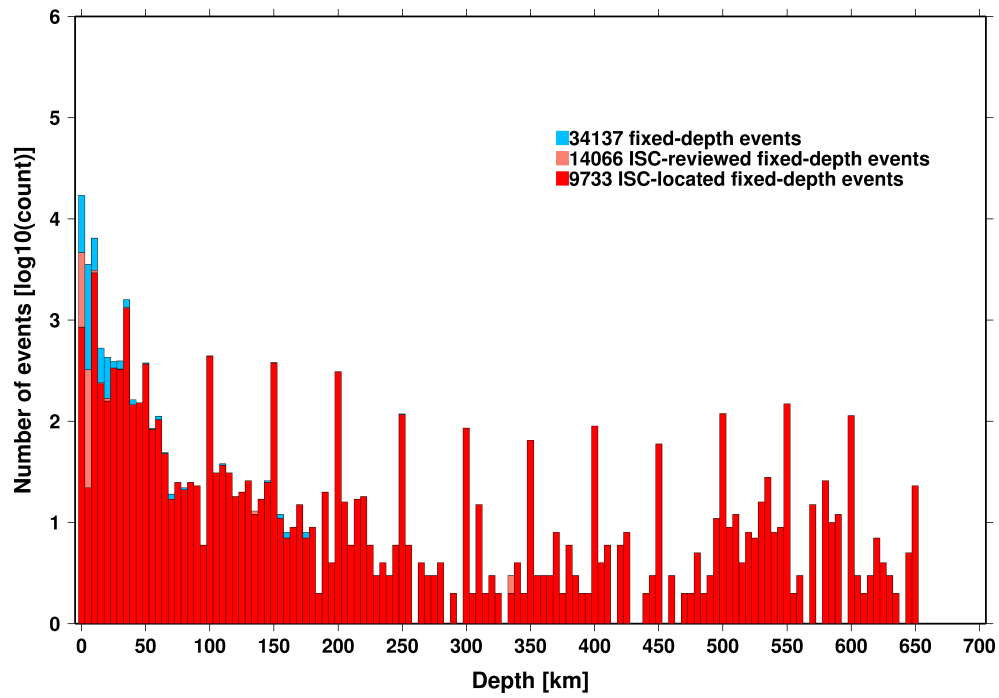
Figure 9.7: *Hypocentral depth distribution of events where the prime hypocentres are reported/located with a fixed-depth solution in the ISC Bulletin. The vertical scale is logarithmic.*
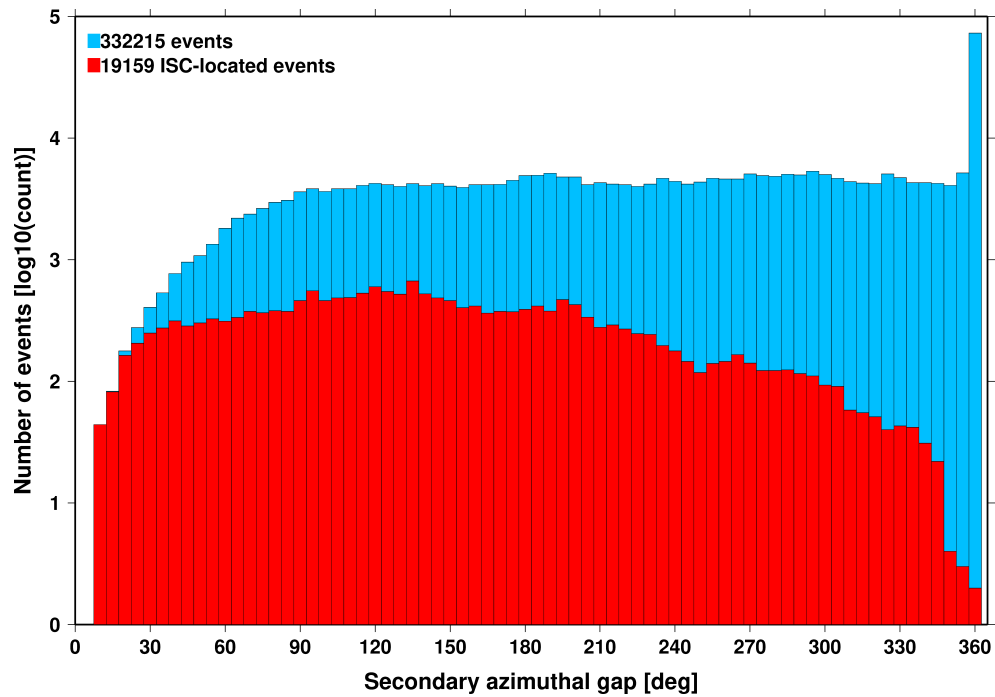
Figure 9.8: *Distribution of secondary azimuthal gap for events in the ISC Bulletin (blue) and those selected for ISC location (red). The vertical scale is logarithmic.*
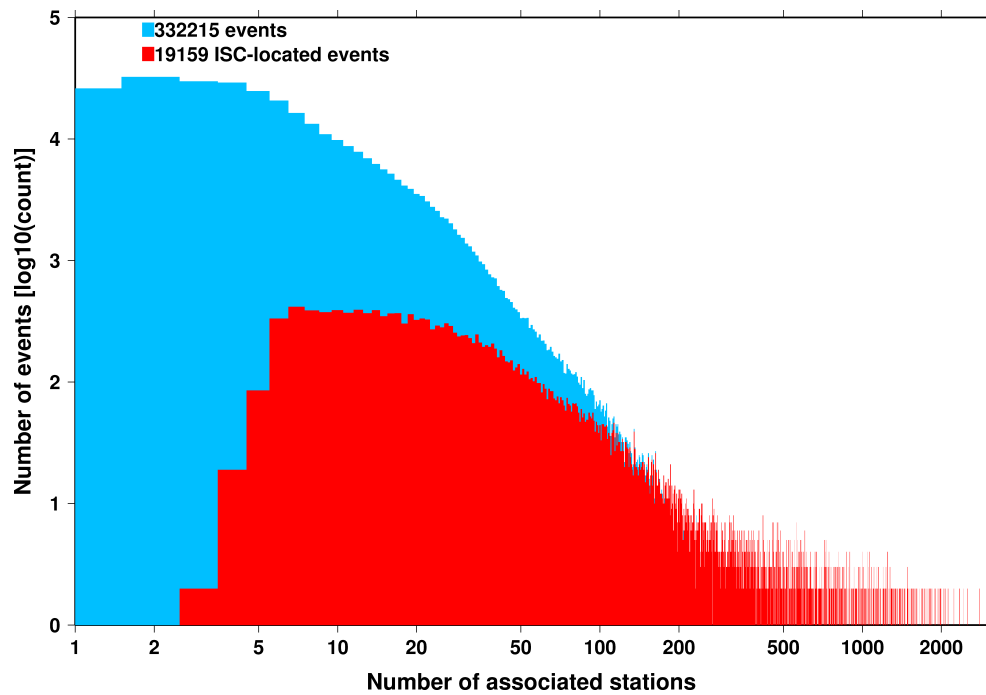
Figure 9.9: *Distribution of the number of associated stations for events in the ISC Bulletin (blue) and those selected for ISC location (red). The vertical scale is logarithmic.*
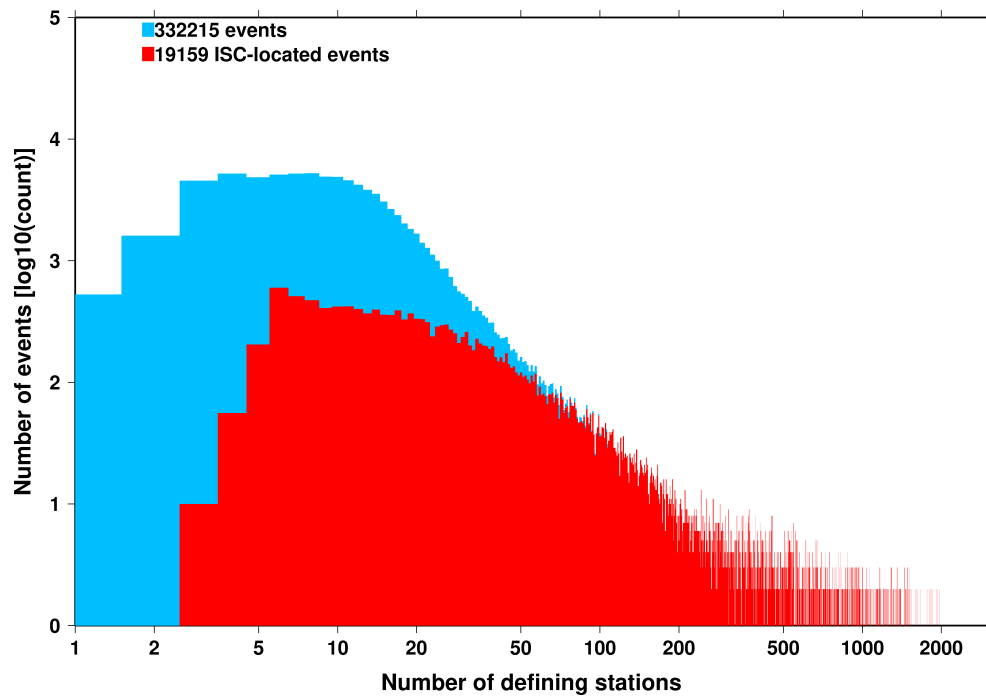
Figure 9.10: *Distribution of the number of defining stations for events in the ISC Bulletin (blue) and those selected for ISC location (red). The vertical scale is logarithmic.*

of the events have an error ellipse area less than 1240 km^2, and 95% of the events have an error ellipse area less than 2109 km^2.
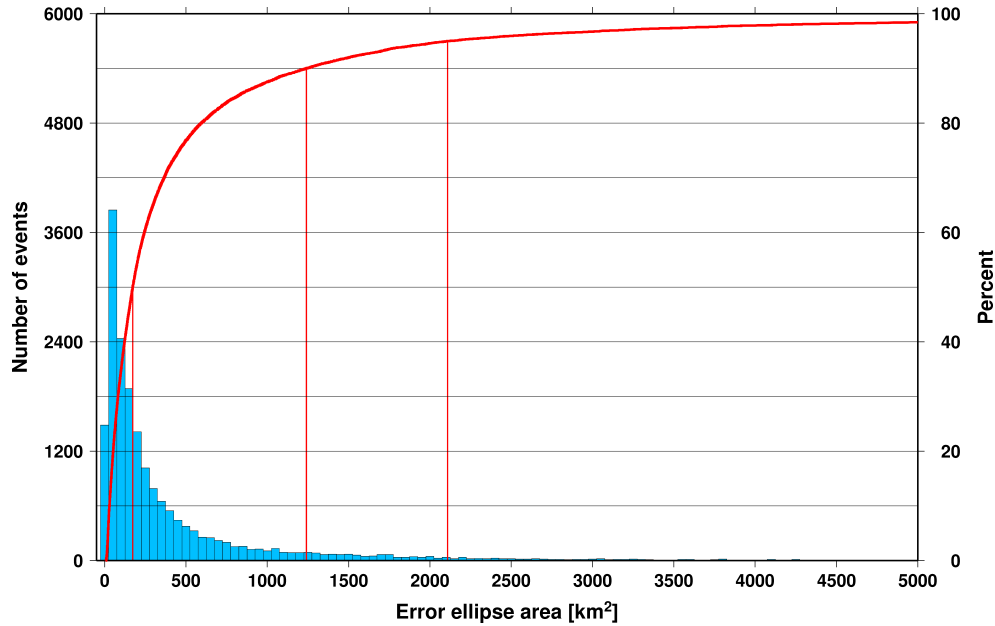
Figure 9.11: *Distribution of the area of the 90% confidence error ellipse of the ISC-located events. Vertical red lines indicate the 50th, 90th and 95th percentile values.*

Figure 9.12 shows one of the major characteristic features of the ISC location algorithm (Bondár and Storchak, 2011). Because the ISC locator accounts for correlated travel-time prediction errors due to unmodelled velocity heterogeneities along similar ray paths, the area of the 90% confidence error ellipse does not decrease indefinitely with increasing number of stations, but levels off once the information carried by the network geometry is exhausted, thus providing more realistic uncertainty estimates.
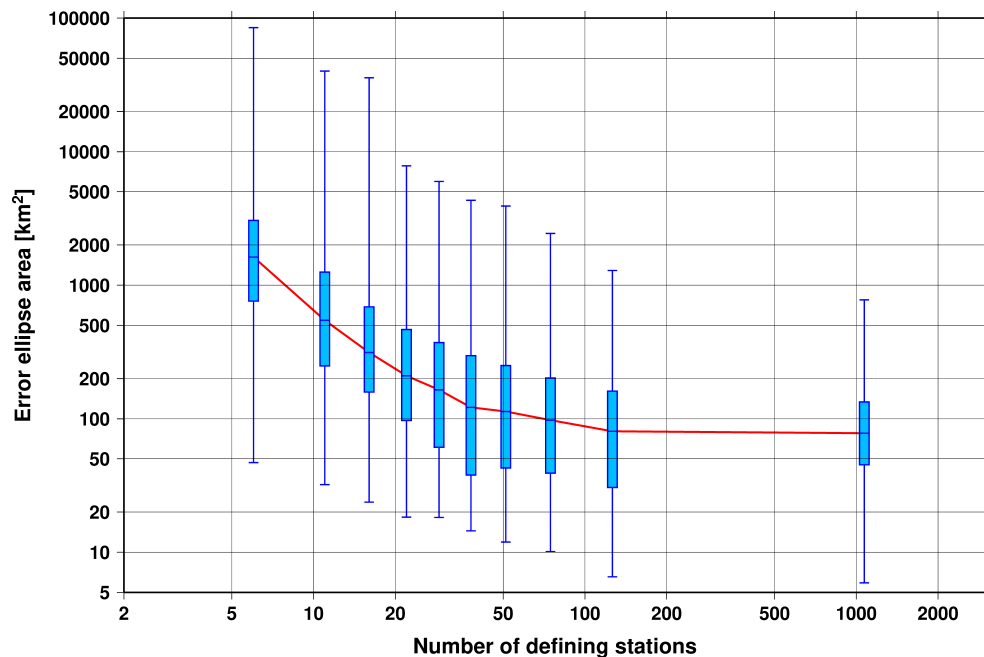
Figure 9.12: *Box-and-whisker plot of the area of the 90% confidence error ellipse of the ISC-located events as a function of the number of defining stations. Each box represents one-tenth-worth of the total number of data. The red line indicates the median 90% confidence error ellipse area.*

9.2 Seismic Phases and Travel-Time Residuals

The number of phases that are associated to events over the summary period in the ISC Bulletin is shown in Figure 9.13. Phase types and their total number in the ISC Bulletin is shown in the Appendix, Table 11.3. A summary of phase types is indicated in Figure 9.14.
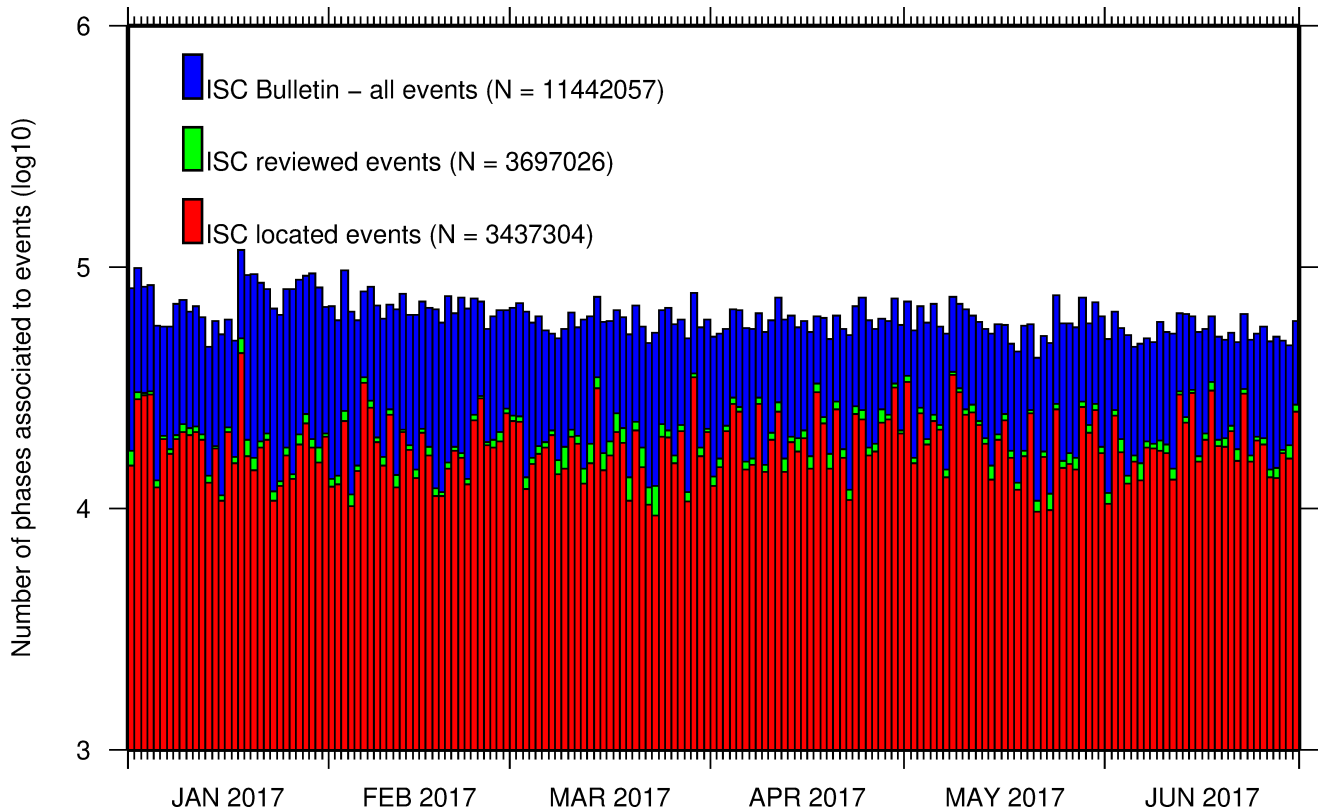
Figure 9.13: *Histogram showing the number of phases (N) that the ISC has associated to events within the ISC Bulletin for the current summary period.*

In computing ISC locations, the current (for events since 2009) ISC location algorithm (*Bondár and Storchak*, 2011) uses all *ak135* phases where possible. Within the Bulletin, the phases that contribute to an ISC location are labelled as *time defining*. In this section, we summarise these time defining phases.

In Figure 9.15, the number of defining phases is shown in a histogram over the summary period. Each defining phase is listed in Table 9.1, which also provides a summary of the number of defining phases per event. A pie chart showing the proportion of defining phases is shown in Figure 9.16. Figure 9.17 shows travel times of seismic waves. The distribution of residuals for these defining phases is shown for the top five phases in Figures 9.18 through 9.22.

Table 9.1: *Numbers of 'time defining' phases (N) within the ISC Bulletin for 19159 ISC located events.*

Phase	Number of 'defining' phases	Number of events	Max per event	Median per event
P	986564	12878	2498	12
Pn	624843	17698	812	17
Sn	172033	15271	208	5
Pb	96343	8705	217	6
Pg	87011	7104	157	8
Sg	60290	6558	143	6
Sb	59605	7973	123	5
PKPdf	54108	3795	558	2

Table 9.1: (continued)

Phase	Number of 'defining' phases	Number of events	Max per event	Median per event
S	43824	3450	806	3
PKiKP	33598	2999	472	2
PKPbc	25122	3109	273	2
PKPab	15828	2417	201	2
PcP	13207	3534	73	2
pP	12115	1559	213	3
Pdif	8759	916	633	2
PP	8120	1278	168	2
sP	4531	1309	51	2
ScP	4464	1250	78	2
SS	3983	1047	47	2
SKSac	2098	425	80	2
pwP	1852	621	41	2
PKKPbc	1741	429	74	2
ScS	1289	472	158	1
SnSn	1162	576	15	1
PnPn	1123	538	18	1
pPKPdf	1040	373	61	1
sS	971	454	10	1
SKPbc	948	296	43	2
SKiKP	520	296	19	1
P'P'df	505	139	44	2
PS	446	190	25	2
PcS	406	323	4	1
PKKPdf	398	202	28	1
PKKPab	377	190	22	1
pPKPbc	376	201	15	1
pPKPab	358	137	24	1
SKSdf	287	172	17	1
SKKSac	271	142	14	1
sPKPdf	255	159	11	1
SKPab	232	127	17	1
SKPdf	221	76	44	1
PnS	164	124	8	1
PKSdf	152	95	7	1
pS	123	100	4	1
sPKPab	103	49	16	1
SP	102	50	13	1
Sdif	98	57	12	1
sPKPbc	97	72	4	1
SKKPbc	81	29	12	1
pPKiKP	78	38	9	1
SKKSdf	69	65	2	1
pPdif	59	41	9	1
P'P'bc	54	38	4	1
SKKPab	31	11	8	2
P'P'ab	28	16	11	1
PbPb	23	17	3	1
SKKPdf	19	14	5	1
sPdif	14	9	6	1
sPn	10	4	5	2
SbSb	9	8	2	1
sSKSac	9	7	2	1
SPn	9	9	1	1
PgPg	7	7	1	1
PKSbc	7	4	3	2
pPn	4	4	1	1
S'S'ac	4	4	1	1
PKSab	4	3	2	1
sPKiKP	4	3	2	1
sSdif	2	2	1	1
sPb	2	2	1	1
PgS	1	1	1	1
SgSg	1	1	1	1
sSKSdf	1	1	1	1
PKKSbc	1	1	1	1

ISC Bulletin
Total phases: 11442057

- P 32%
- Pn 20%
- IAmb 6%
- Sn 6%
- AML 5%
- LR 4%
- Pg 4%
- pmax 4%
- Pb 3%
- Sg 2%
- Sb 2%
- PKPdf 2%
- S 1%
- Others 9%
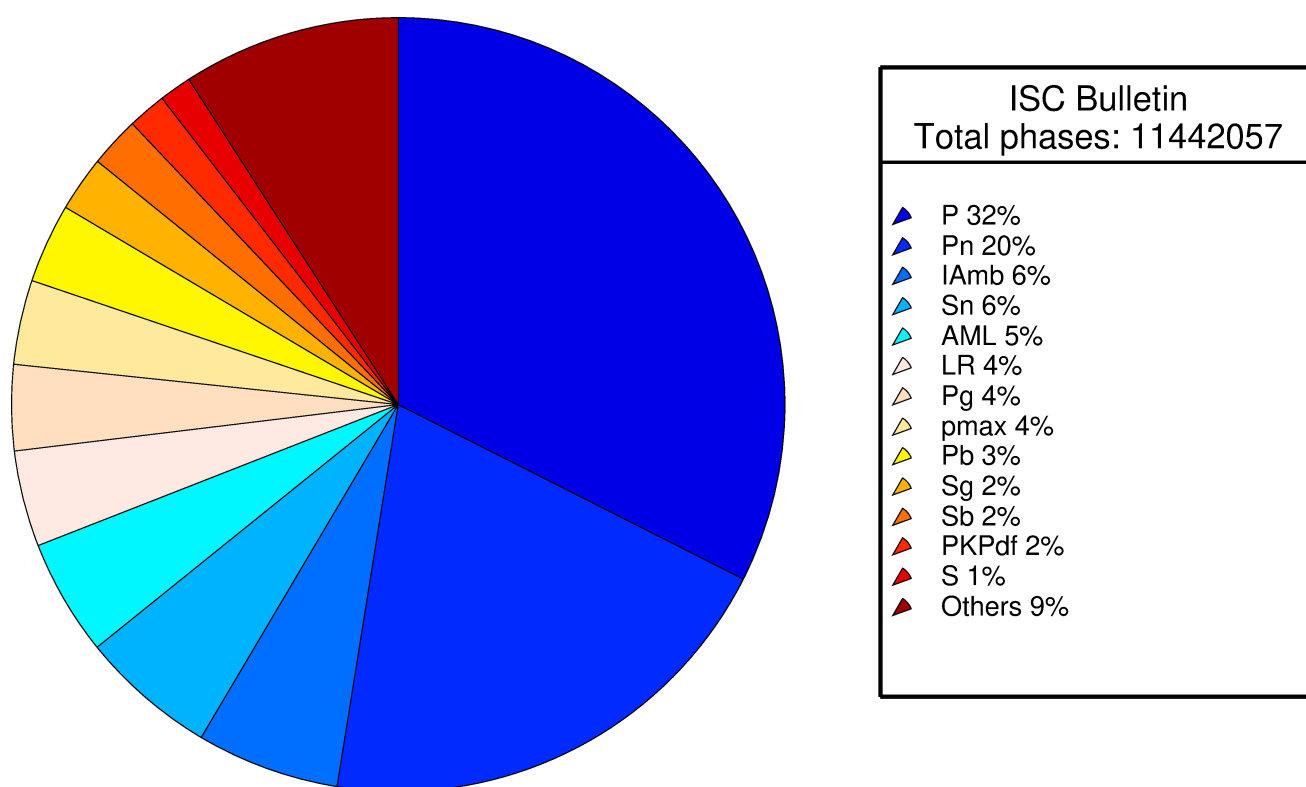
Figure 9.14: *Pie chart showing the fraction of various phase types in the ISC Bulletin for this summary period.*
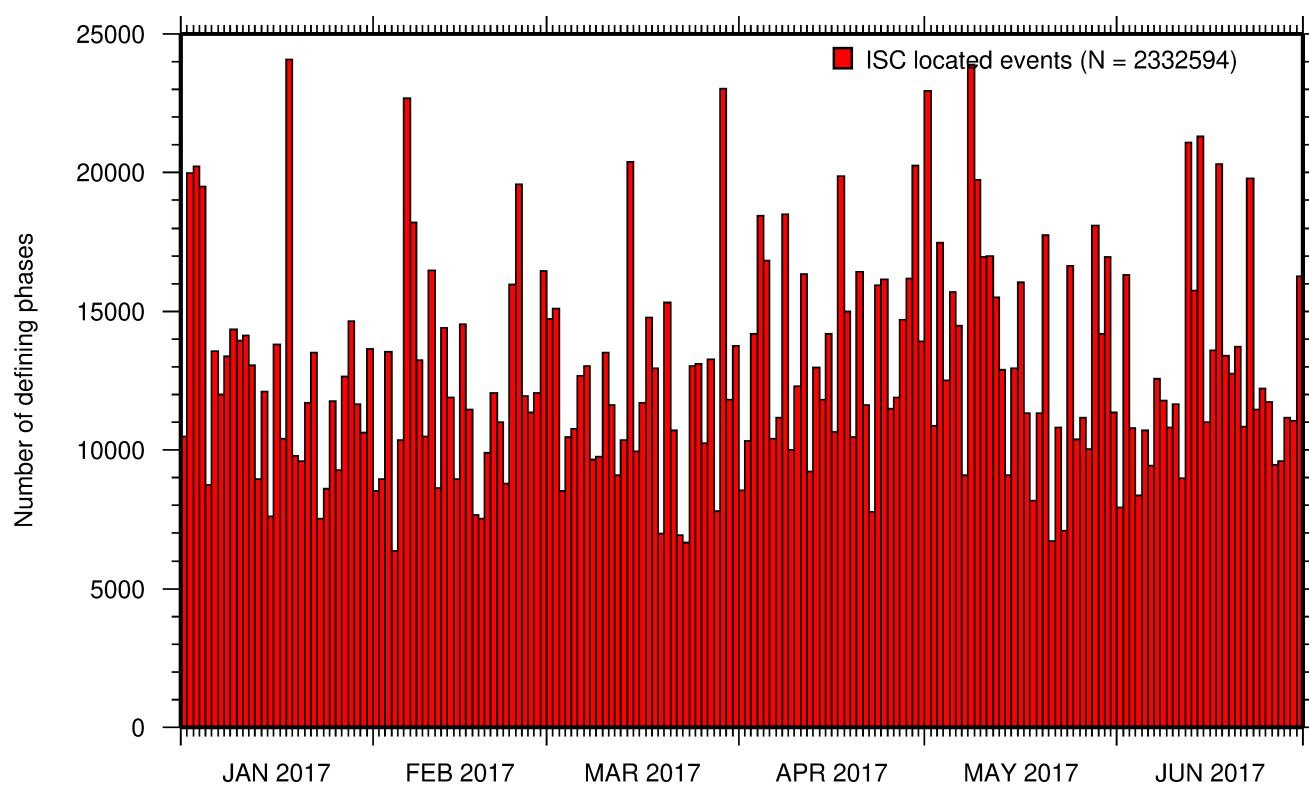
Figure 9.15: *Histogram showing the number of defining phases in the ISC Bulletin, for events located by the ISC.*
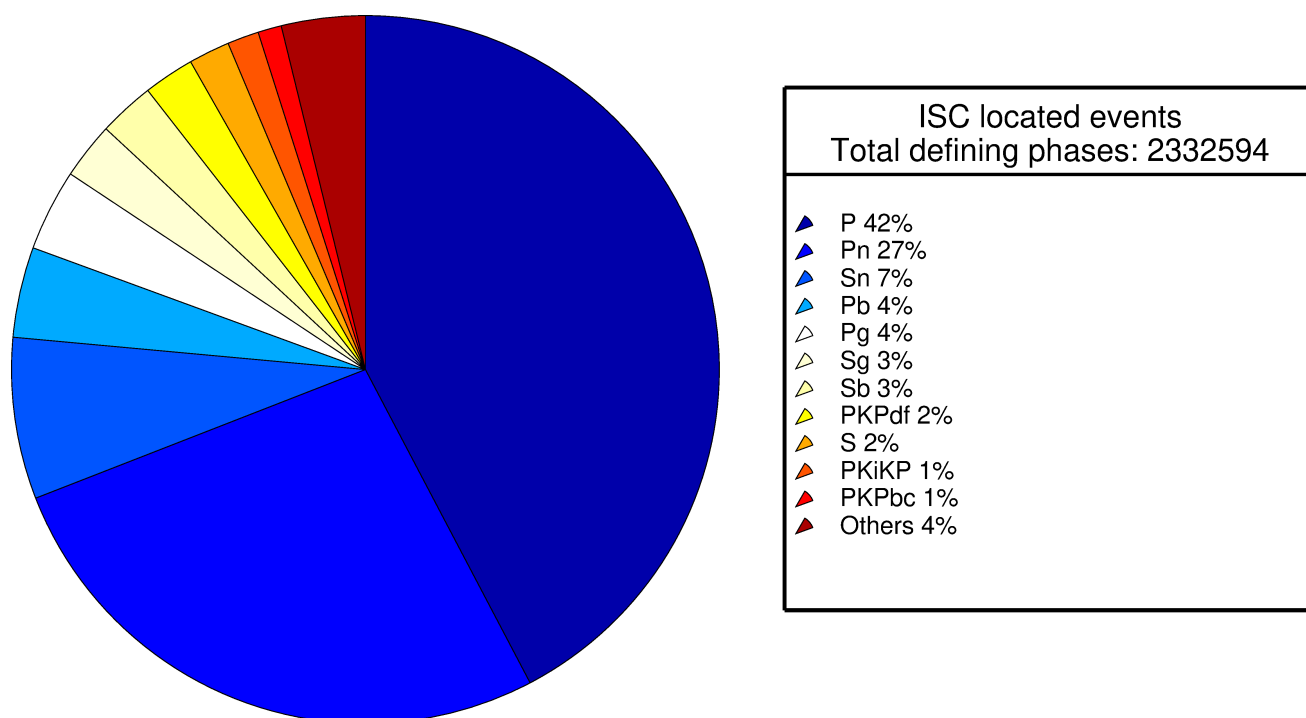
Figure 9.16: *Pie chart showing the defining phases in the ISC Bulletin, for events located by the ISC. A complete list of defining phases is shown in Table 9.1.*
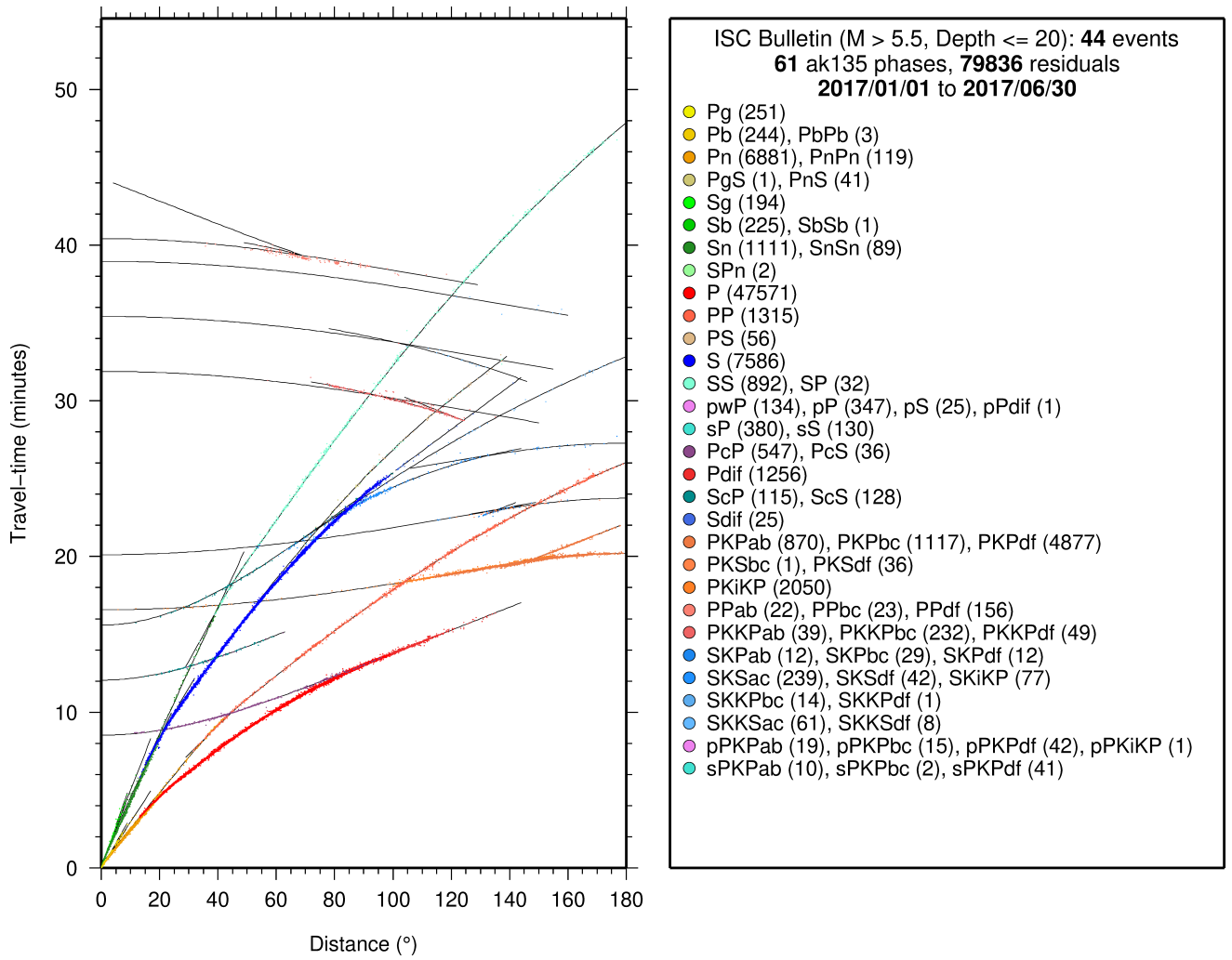
Figure 9.17: *Distribution of travel-time observations in the ISC Bulletin for events with M > 5.5 and depth less than 20 km. The travel-time observations are shown relative to a 0 km source and compared with the theoretical ak135 travel-time curves (solid lines). The legend lists the number of each phase plotted.*
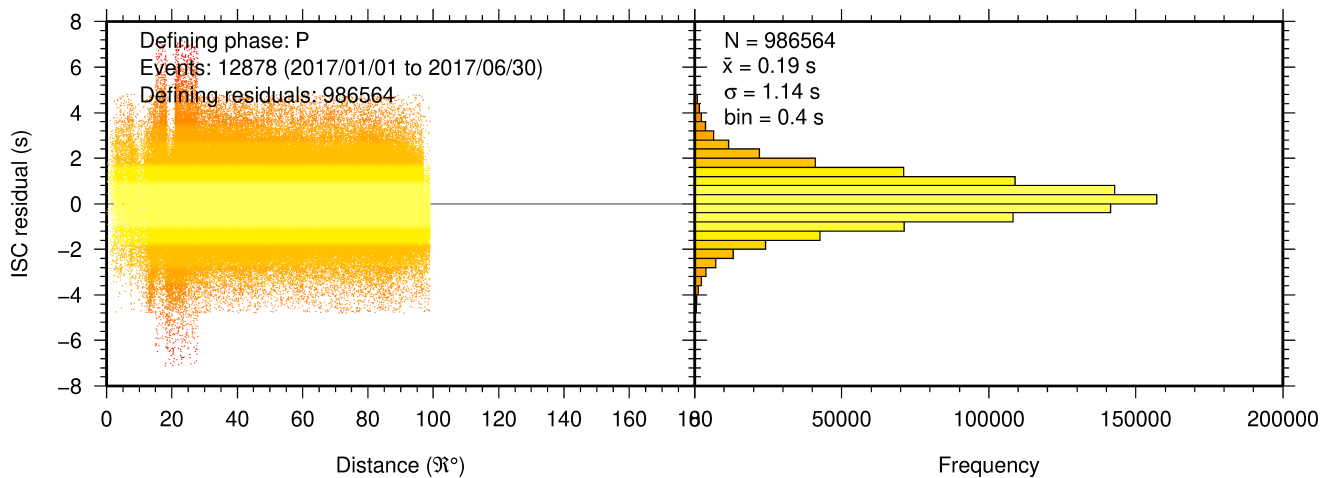
Figure 9.18: *Distribution of travel-time residuals for the defining P phases used in the computation of ISC located events in the Bulletin.*
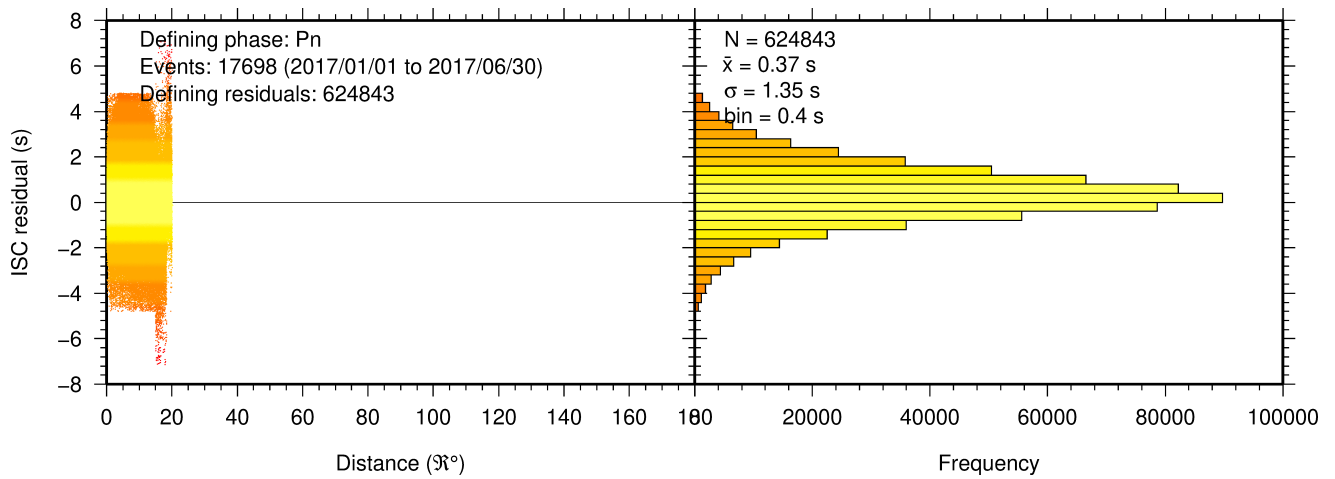
Figure 9.19: *Distribution of travel-time residuals for the defining Pn phases used in the computation of ISC located events in the Bulletin.*
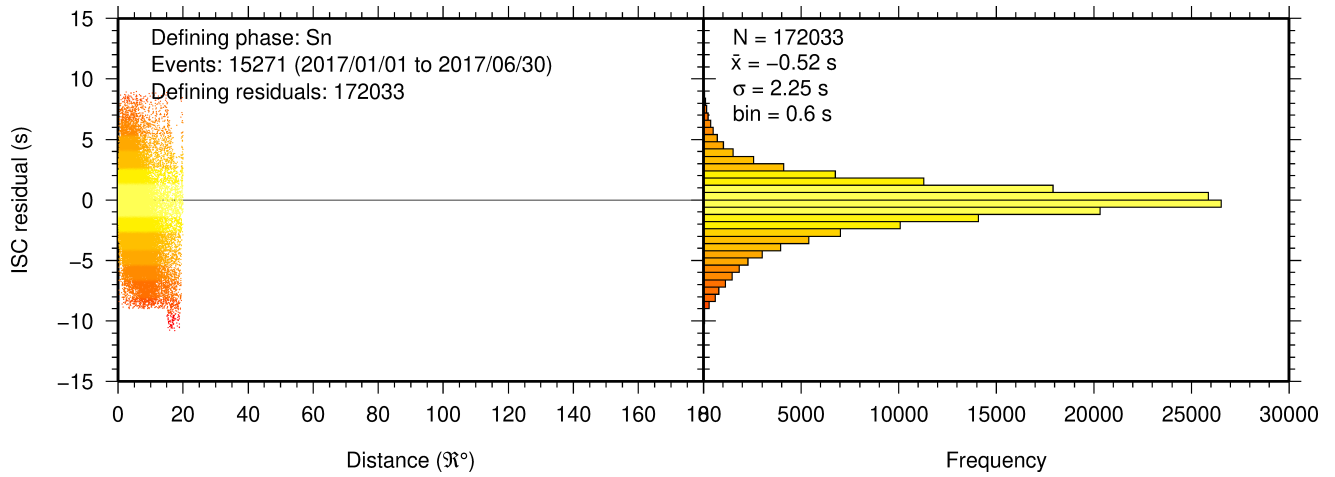
Figure 9.20: *Distribution of travel-time residuals for the defining Sn phases used in the computation of ISC located events in the Bulletin.*
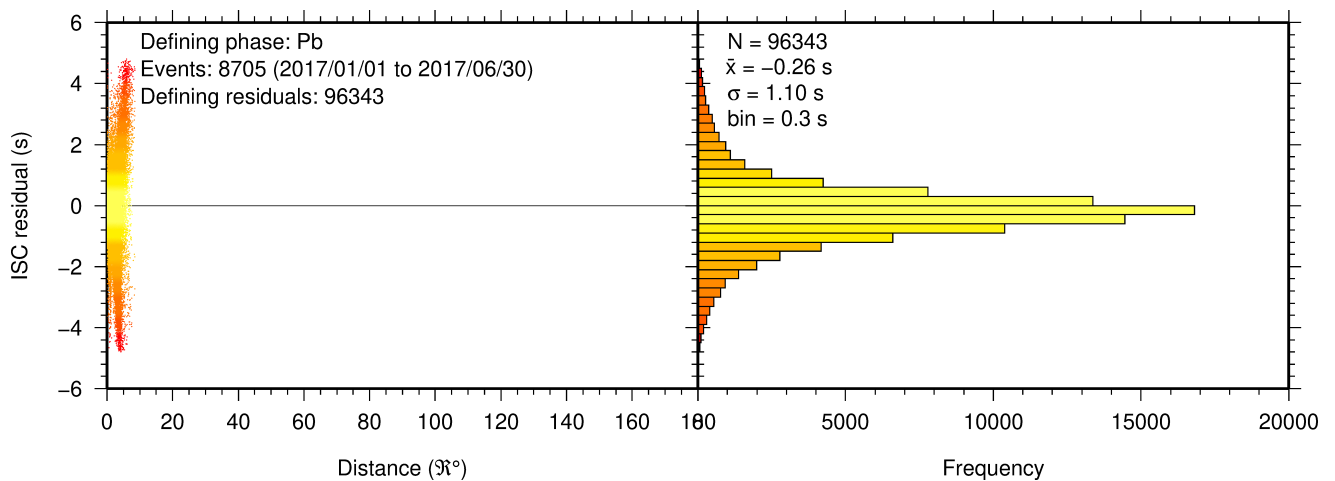
Figure 9.21: *Distribution of travel-time residuals for the defining Pb phases used in the computation of ISC located events in the Bulletin.*
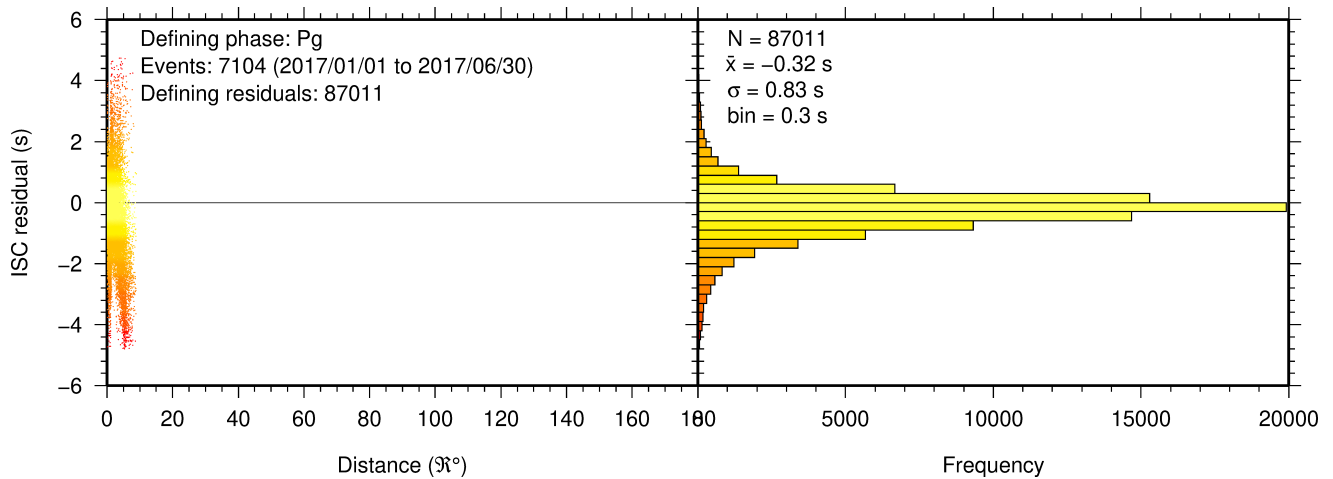
Figure 9.22: *Distribution of travel-time residuals for the defining Pg phases used in the computation of ISC located events in the Bulletin.*

9.3 Seismic Wave Amplitudes and Periods

The ISC Bulletin contains a variety of seismic wave amplitudes and periods measured by reporting agencies. For this Bulletin Summary, the total of collected amplitudes and periods is 550989 (see Section 8.3). For the determination of the ISC magnitudes MS and mb, only a fraction of such data can be used. Indeed, the ISC network magnitudes are computed only for ISC located events. Here we recall the main features of the ISC procedure for MS and mb computation (see detailed description in Section 11.1.4). For each amplitude-period pair in a reading the ISC algorithm computes the magnitude (a reading can include several amplitude-period measurements) and the reading magnitude is assigned to the maximum A/T in the reading. If more than one reading magnitude is available for a station, the station magnitude is the median of the reading magnitudes. The network magnitude is computed then as the 20% alpha-trimmed median of the station magnitudes (at least three required). MS is computed for shallow earthquakes (depth $\leq$ 60 km) only and using amplitudes and periods on all three components (when available) if the period is within 10-60 s and the epicentral distance is between 20° and 160°. mb is computed also for deep earthquakes (depth down to 700 km) but only with amplitudes on the vertical component measured at periods $\leq$ 3 s in the distance range 21°-100°.

Table 9.2 is a summary of the amplitude and period data that contributed to the computation of station and ISC MS and mb network magnitudes for this Bulletin Summary.

Table 9.2: *Summary of the amplitude-period data used by the ISC Locator to compute MS and mb.*

	MS	mb
Number of amplitude-period data	131351	419638
Number of readings	112588	415789
Percentage of readings in the ISC located events with qualifying data for magnitude computation	13.9	40.0
Number of station magnitudes	107873	379670
Number of network magnitudes	3283	11233

A small percentage of the readings with qualifying data for MS and mb calculation have more than

one amplitude-period pair. Notably, only 13.9% of the readings for the ISC located (shallow) events included qualifying data for MS computation, whereas for mb the percentage is much higher at 40%. This is due to the seismological practice of reporting agencies. Agencies contributing systematic reports of amplitude and period data are listed in Appendix Table 11.4. Obviously the ISC Bulletin would benefit if more agencies included surface wave amplitude-period data in their reports.

Figure 9.23 shows the distribution of the number of station magnitudes versus distance. For mb there is a significant increase in the distance range 70°-90°, whereas for MS most of the contributing stations are below 100°. The increase in number of station magnitude between 70°-90° for mb is partly due to the very dense distribution of seismic stations in North America and Europe with respect to earthquake occurring in various subduction zones around the Pacific Ocean.
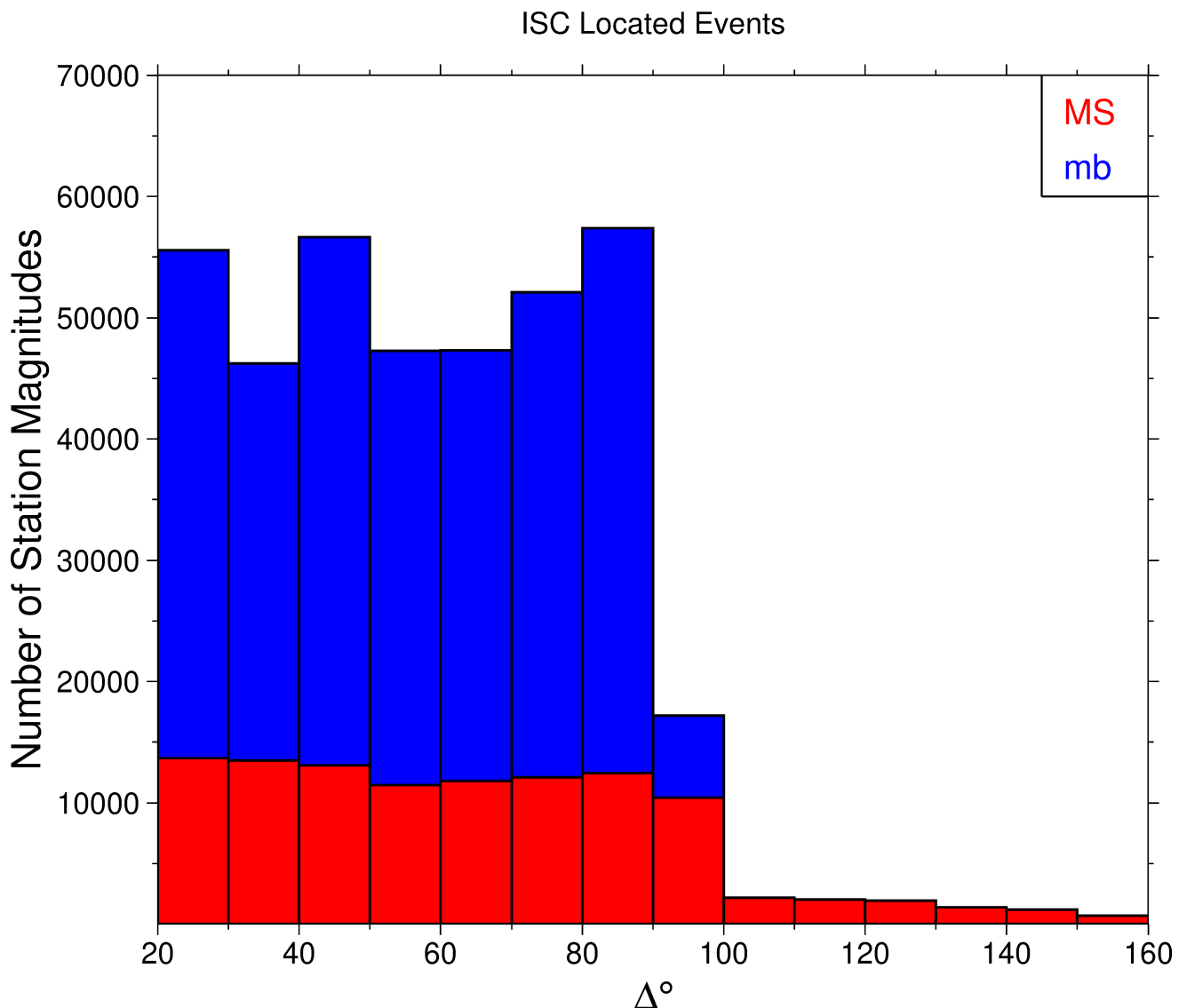
Figure 9.23: *Distribution of the number of station magnitudes computed by the ISC Locator for mb (blue) and MS (red) versus distance.*

Finally, Figure 9.24 shows the distribution of network MS and mb as well as the median number of stations for magnitude bins of 0.2. Clearly with increasing magnitude the number of events is smaller but with a general tendency of having more stations contributing to the network magnitude.
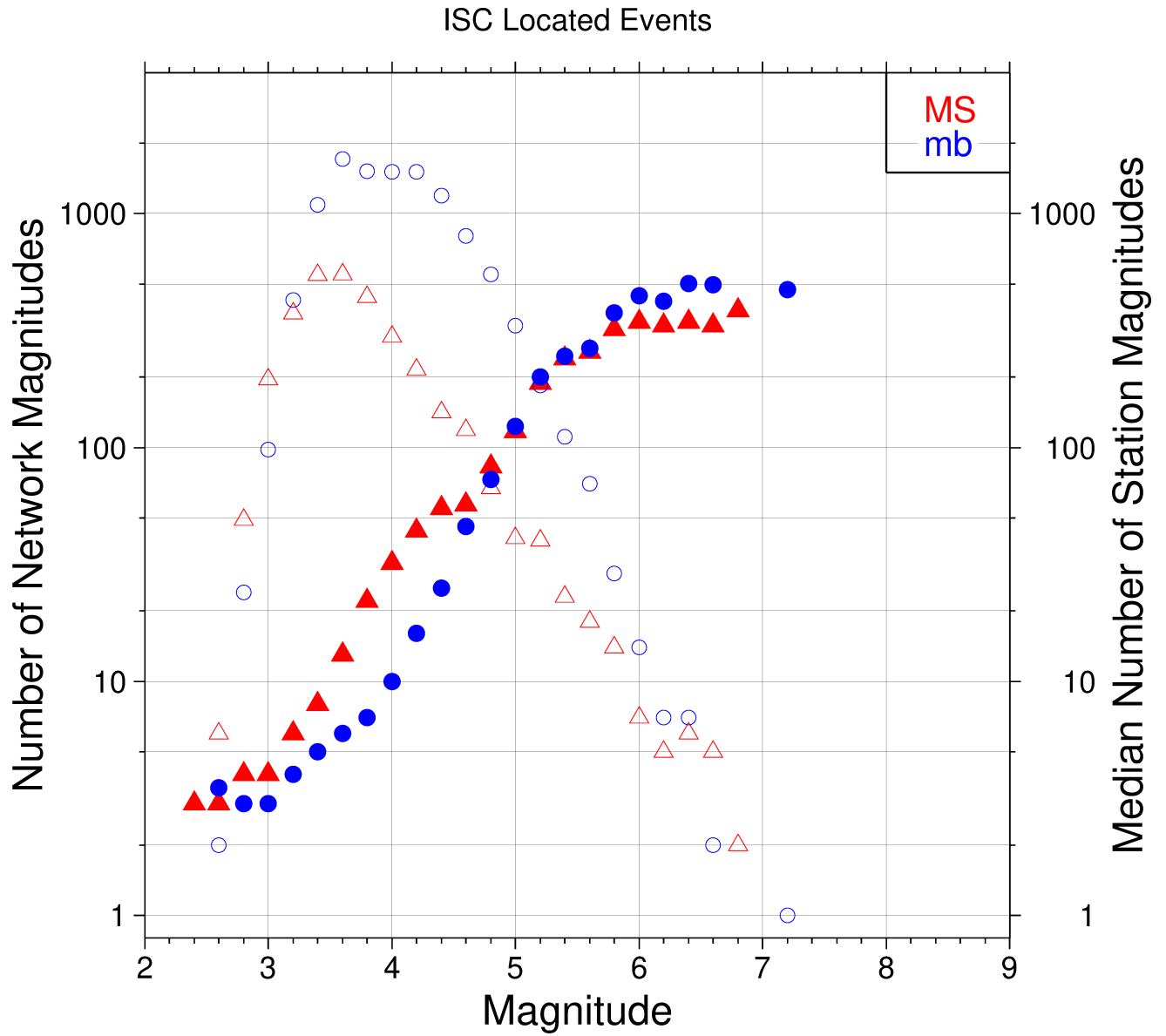
Figure 9.24: *Number of network magnitudes (open symbols) and median number of stations magnitudes (filled symbols). Blue circles refer to mb and red triangles to MS. The width of the magnitude interval δM is 0.2, and each symbol includes data with magnitude in M ± δM/2.*

9.4   Completeness of the ISC Bulletin

We define the magnitude of completeness (hereafter M_C) as the lowest magnitude threshold above which all events are believed to be recorded. The Bulletin with events bigger than the defined M_C is assumed to be complete.

Until Issue 53, Volume II (July - December 2016) of the Summary of the ISC an estimation of M_C was computed only with the maximum curvature technique (*Woessner and Wiemer*, 2005). After the completion of the Rebuild Project and relocation of ISC hypocenters from data years 1964 to 2010 (*Storchak et al.*, 2017), the estimate of M_C for the entire ISC Bulletin is re-computed using four catalogue based methodologies (*Adamaki*, 2017, and references therein): the previously used maximum curvature for comparison (maxC), Mc based on the b-value stability (MBS technique), the Goodness of Fit Test with a 90% level of fit (GFT90) and the modified Goodness of Fit Test (mGFT). Further details on each of these methodologies and their statistical behaviour can be found in *Leptokaropoulos et al.* (2018).

The magnitudes of completeness of the ISC Bulletin for this Summary period is shown in Figure 9.25. How M_C varies for the ISC Bulletin over the years is shown in Figure 9.26. The step change in 1996 corresponds with the inclusion of the Prototype IDC (EIDC) Bulletin, followed by the Reviewed Event Bulletin (REB) of the IDC.
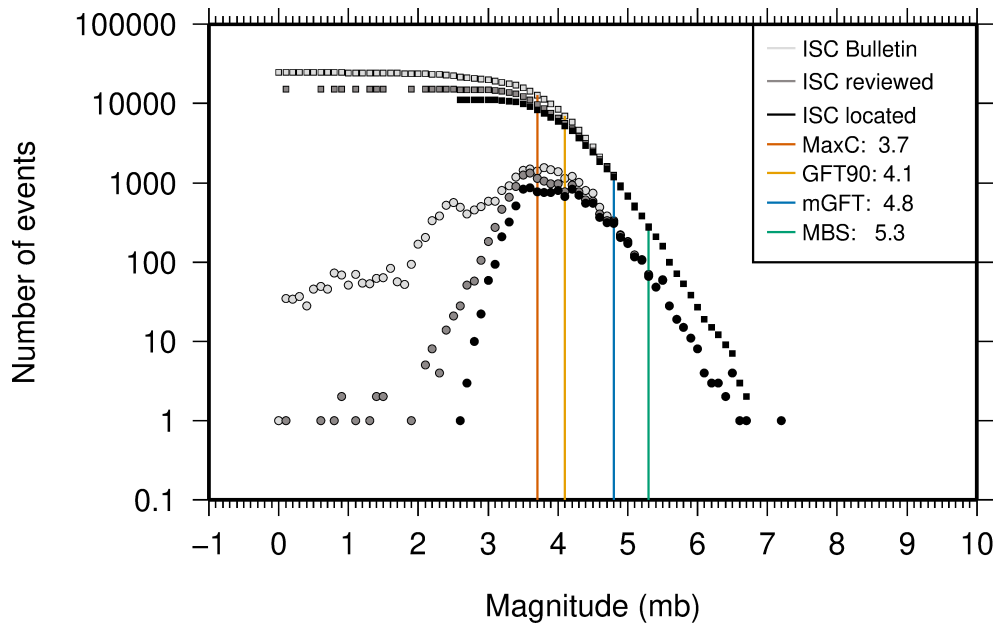
Figure 9.25: *Frequency (circles) and cumulative frequency (squares) magnitude distribution for all events in the ISC Bulletin, ISC reviewed events and events located by the ISC. The magnitudes of completeness (M_C) are shown for the ISC Bulletin. Note: only events with values of mb are represented in the figure.*
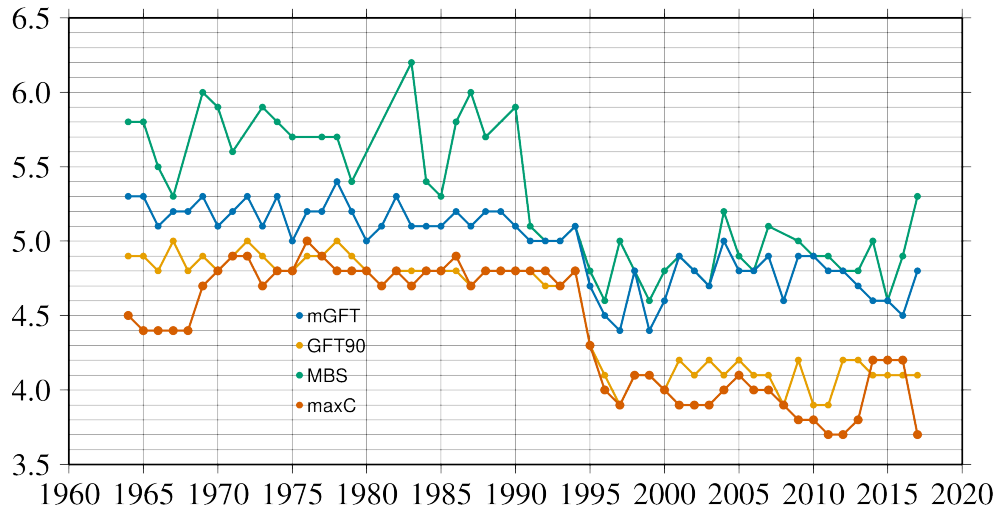
Figure 9.26: *Variation of magnitudes of completeness (M_C) for each year in the ISC Bulletin. Note: M_C is calculated only using those events with values of mb.*

9.5 Magnitude Comparisons

The ISC Bulletin publishes network magnitudes reported by multiple agencies to the ISC. For events that have been located by the ISC, where enough amplitude data has been collected, the MS and mb magnitudes are calculated by the ISC (MS is computed only for depths $\leq$ 60 km). In this section, ISC magnitudes and some other reported magnitudes in the ISC Bulletin are compared.

The comparison between MS and mb computed by the ISC locator for events in this summary period is shown in Figure 9.27, where the large number of data pairs allows a colour coding of the data density. The scatter in the data reflects the fundamental differences between these magnitude scales.

Similar plots are shown in Figure 9.28 and 9.29, respectively, for comparisons of ISC mb and ISC MS with M_W from the GCMT catalogue. Since M_W is not often available below magnitude 5, these distributions are mostly for larger, global events. Not surprisingly, the scatter between mb and M_W is larger than the scatter between MS and M_W. Also, the saturation effect of mb is clearly visible for earthquakes with $M_W > 6.5$. In contrast, MS scales well with $M_W > 6$, whereas for smaller magnitudes MS appears to be systematically smaller than M_W.

In Figure 9.30 ISC values of mb are compared with all reported values of mb, values of mb reported by NEIC and values of mb reported by IDC. Similarly in Figure 9.31, ISC values of MS are compared with all reported values of MS, values of MS reported by NEIC and values of MS reported by IDC. There is a large scatter between the ISC magnitudes and the mb and MS reported by all other agencies.

The scatter decreases both for mb and MS when ISC magnitudes are compared just with NEIC and IDC magnitudes. This is not surprising as the latter two agencies provide most of the amplitudes and periods used by the ISC locator to compute MS and mb. However, ISC mb appears to be smaller than NEIC mb for $mb < 4$ and larger than IDC mb for $mb > 4$. Since NEIC does not include IDC amplitudes, it seems these features originate from observations at the high-gain, low-noise sites reported by the IDC. For the MS comparisons between ISC and NEIC a similar but smaller effect is observed for $MS < 4.5$, whereas a good scaling is generally observed for the MS comparisons between ISC and IDC.

Figure 9.27: *Comparison of ISC values of MS with mb for common event pairs.*
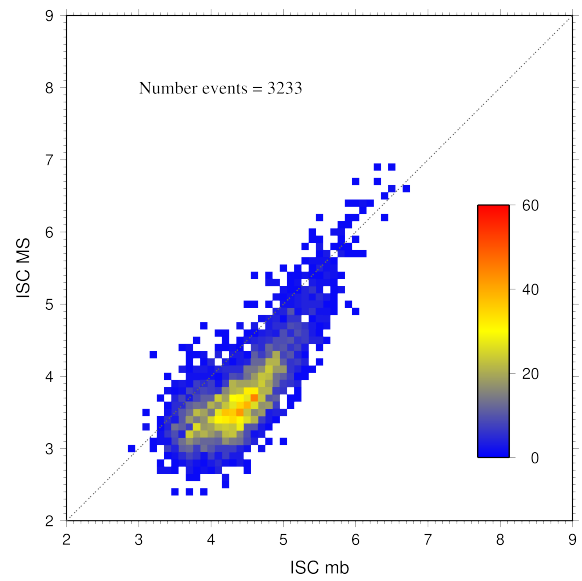
Figure 9.28: *Comparison of ISC values of mb with GCMT M_W for common event pairs.*
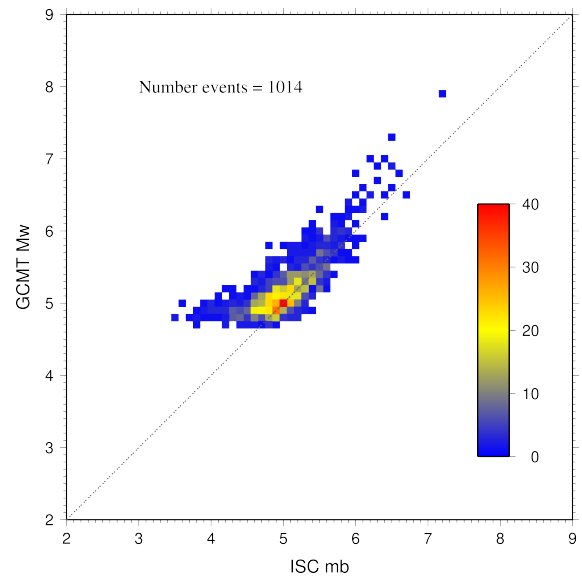
Figure 9.29: *Comparison of ISC values of MS with GCMT M_W for common event pairs.*
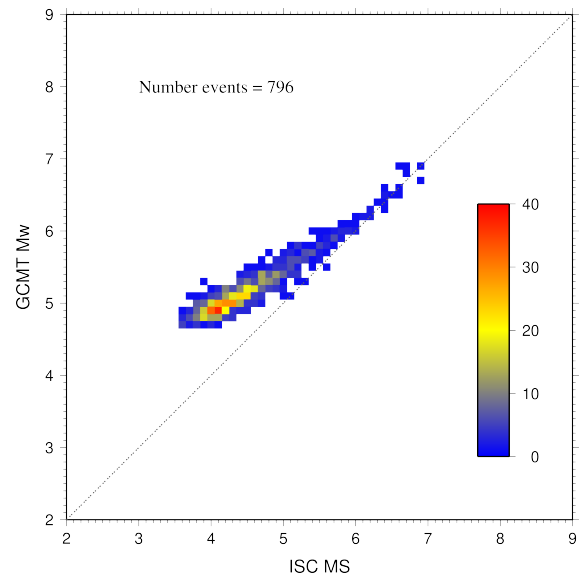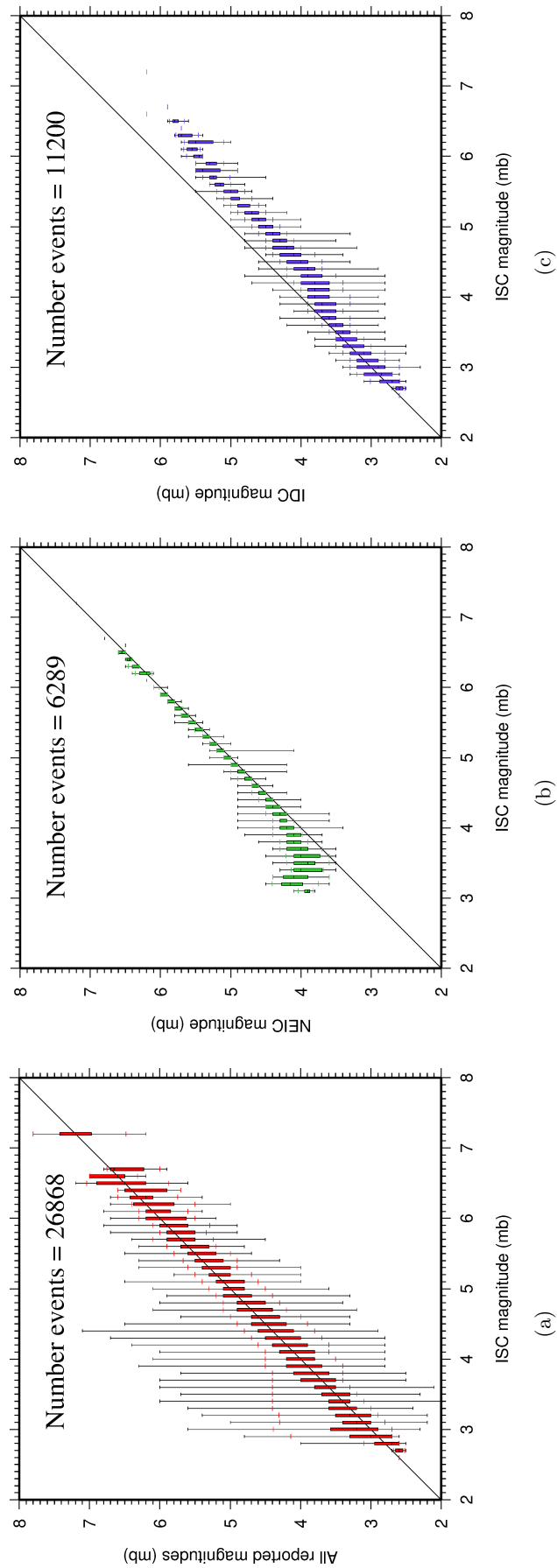
Figure 9.30: *Comparison of ISC magnitude data (mb) with additional agency magnitudes (mb). The statistical summary is shown in box-and-whisker plots where the 10th and 90th percentiles are shown in addition to the max and min values. (a): All magnitudes reported; (b): NEIC magnitudes; (c): IDC magnitudes.*
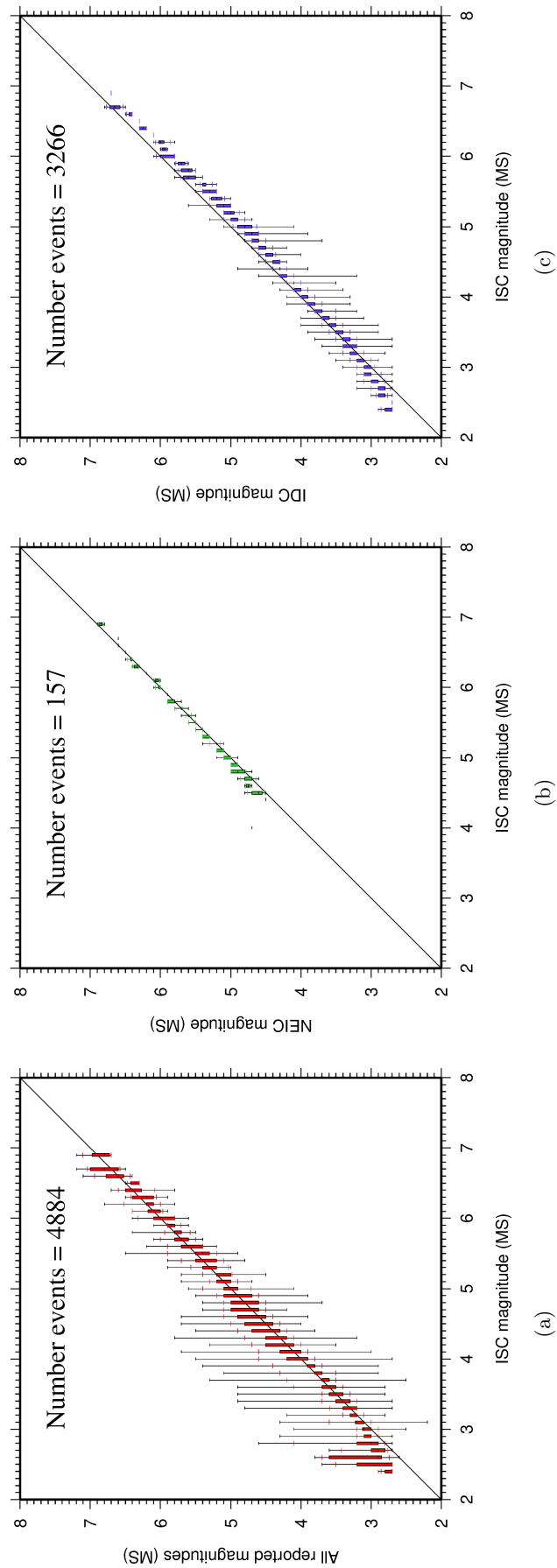
Figure 9.31: *Comparison of ISC magnitude data (MS) with additional agency magnitudes (MS). The statistical summary is shown in the box-and-whisker plots where the 10th and 90th percentiles are shown in addition to the max and min values. (a): All magnitudes reported; (b): NEIC magnitudes; (c): IDC magnitudes.*

10

The Leading Data Contributors

For the current six-month period, 147 agencies reported related bulletin data. Although we are grateful for every report, we nevertheless would like to acknowledge those agencies that made the most useful or distinct contributions to the contents of the ISC Bulletin. Here we note those agencies that:

- provided a comparatively large volume of parametric data (see Section 10.1),

- reported data that helped quite considerably to improve the quality of the ISC locations or magnitude determinations (see Section 10.2),

- helped the ISC by consistently reporting data in one of the standard recognised formats and in-line with the ISC data collection schedule (see Section 10.3).

We do not aim to discourage those numerous small networks who provide comparatively smaller yet still most essential volumes of regional data regularly, consistently and accurately. Without these reports the ISC Bulletin would not be as comprehensive and complete as it is today.

10.1   The Largest Data Contributors

We acknowledge the contribution of IDC, NEIC, USArray, MOS, BJI, CLL, DJA and a few others (Figure 10.1) that reported the majority of moderate to large events recorded at teleseismic distances. The contributions of NEIC, IDC, MEX, JMA, and several others are also acknowledged with respect to smaller seismic events. The contributions of JMA, ROM, DDA, TAP, ISK, WEL and a number of others are also acknowledged with respect to small seismic events. Note that the NEIC bulletin accumulates a contribution of all regional networks in the USA. Several agencies monitoring highly seismic regions routinely report large volumes of small to moderate magnitude events, such as those in Japan, Chinese Taipei, Turkey, Italy, Greece, New Zealand, Mexico and Columbia. Contributions of small magnitude events by agencies in regions of low seismicity, such as Finland are also gratefully received.

We also would like to acknowledge contributions of those agencies that report a large portion of arrival time and amplitude data (Figure 10.2). For small magnitude events, these are local agencies in charge of monitoring local and regional seismicity. For moderate to large events, contributions of IDC, USArray, NEIC, MOS are especially acknowledged. Notably, three agencies (IDC, NEIC and MOS) together reported over 70% of all amplitude measurements made for teleseismically recorded events. We hope that other agencies would also be able to update their monitoring routines in the future to include the amplitude reports for teleseismic events compliant with the IASPEI standards.
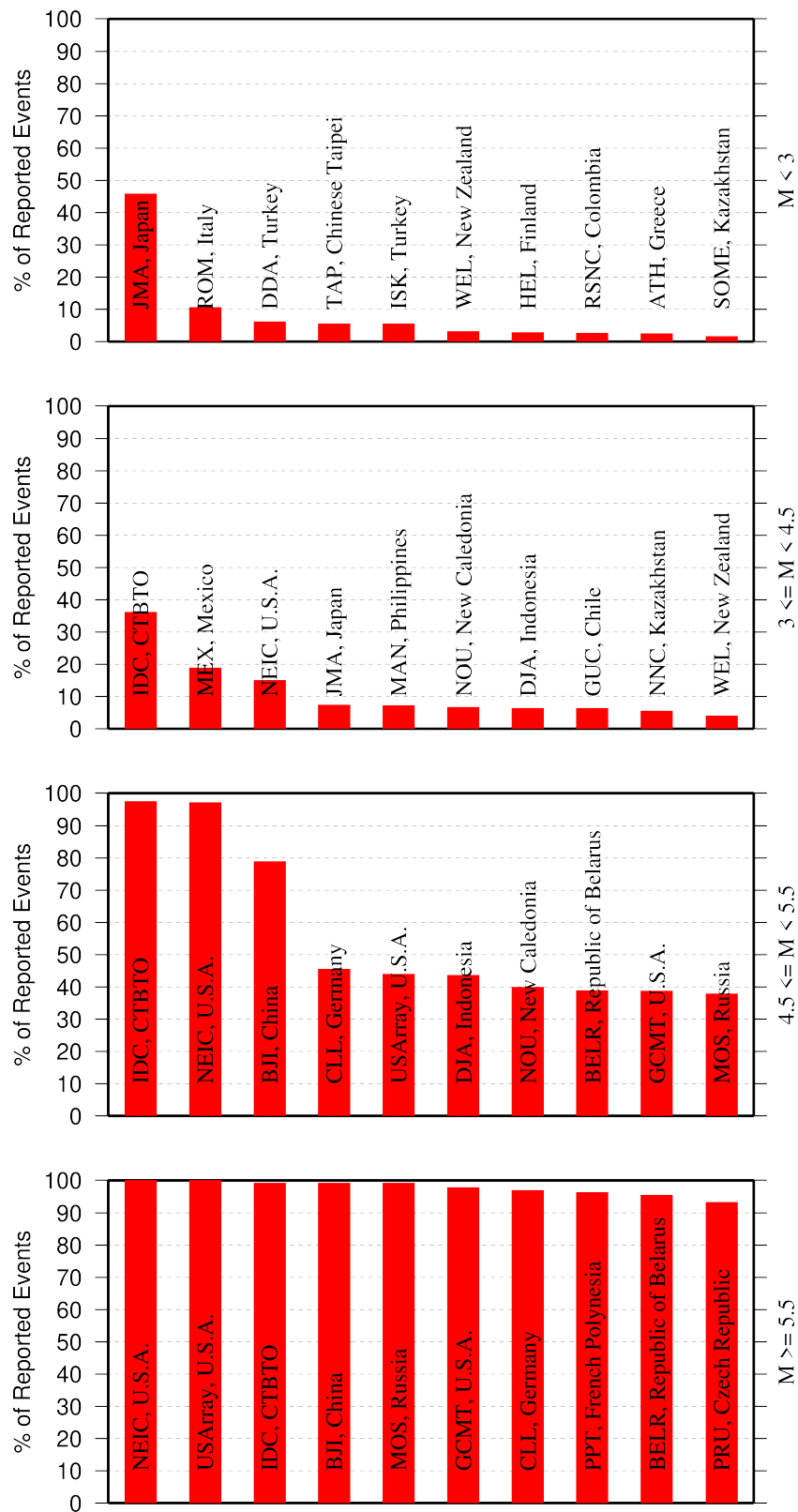
Figure 10.1: *Frequency of events in the ISC Bulletin for which an agency reported at least one item of data: a moment tensor, a hypocentre, a station arrival time or an amplitude. The top ten agencies are shown for four magnitude intervals.*
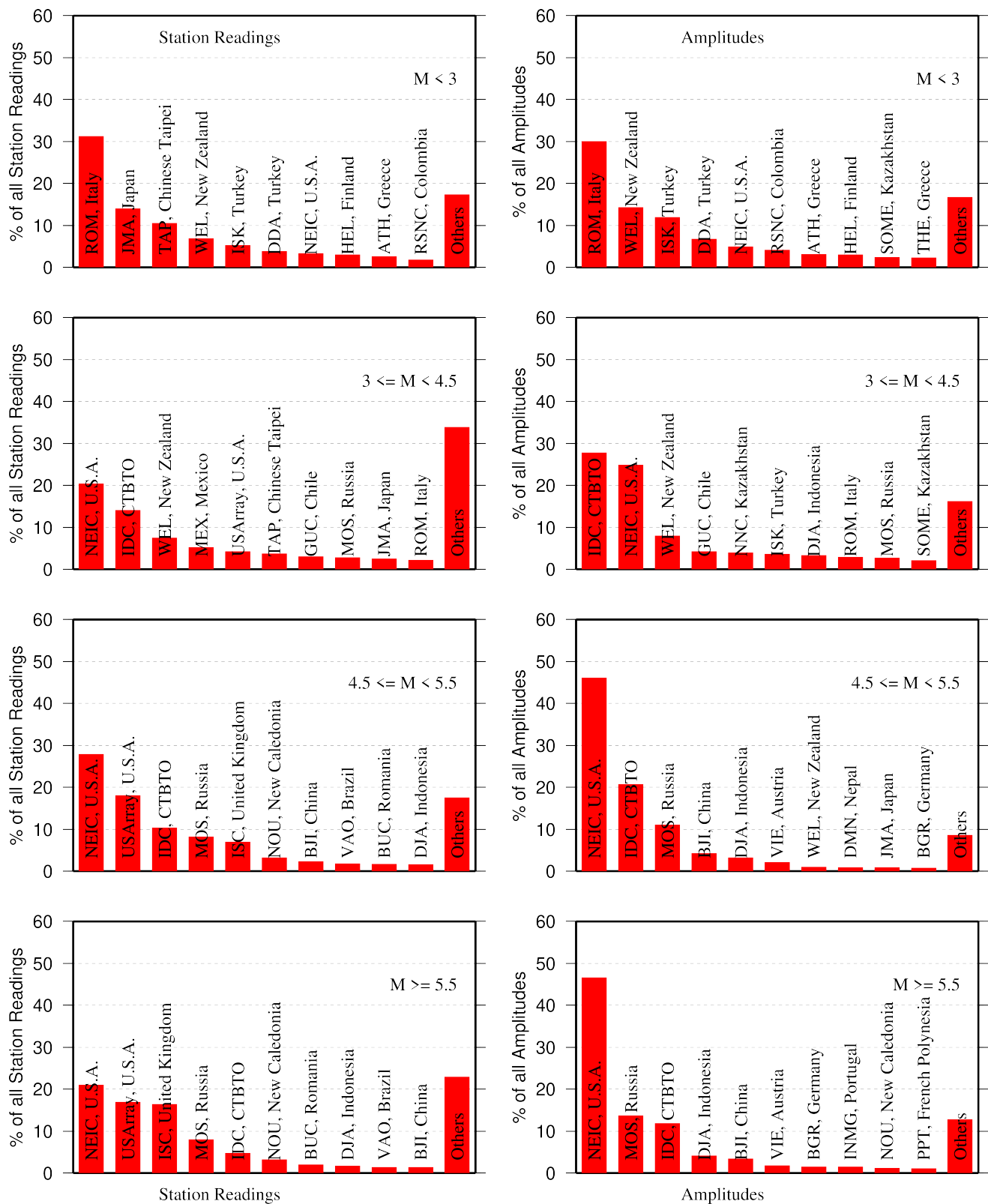
Figure 10.2: *Contributions of station arrival time readings (left) and amplitudes (right) of agencies to the ISC Bulletin. Top ten agencies are shown for four magnitude intervals.*

10.2 Contributors Reporting the Most Valuable Parameters

One of the main ISC duties is to re-calculate hypocentre estimates for those seismic events where a collective wealth of all station reports received from all agencies is likely to improve either the event location or depth compared to the hypocentre solution from each single agency. For areas with a sparse local seismic network or an unfavourable station configuration, readings made by other networks at teleseismic distances are very important. All events near mid-oceanic ridges as well as those in the majority of subduction zones around the world fall into this category. Hence we greatly appreciate the effort made by many agencies that report data for remote earthquakes (Figure 10.3). For some agencies, such as the IDC and the NEIC, it is part of their mission. For instance, the IDC reports almost every seismic event that is large enough to be recorded at teleseismic distance (20 degrees and beyond). This is largely because the International Monitoring System of primary arrays and broadband instruments is distributed at quiet sites around the world in order to be able to detect possible violations of the Comprehensive Nuclear-Test-Ban Treaty. The NEIC reported almost 40% of those events as their mission requires them to report events above magnitude 4.5 outside the United States of America. For other agencies reporting distant events it is an extra effort that they undertake to notify their governments and relief agencies as well as to help the ISC and academic research in general. Hence these agencies usually report on the larger magnitude events. BJI, NAO, CLL, MOS, NOU, USArray, VIE and BELR each reported individual station arrivals for several percent of all relevant events. We encourage other agencies to report distant events to us.
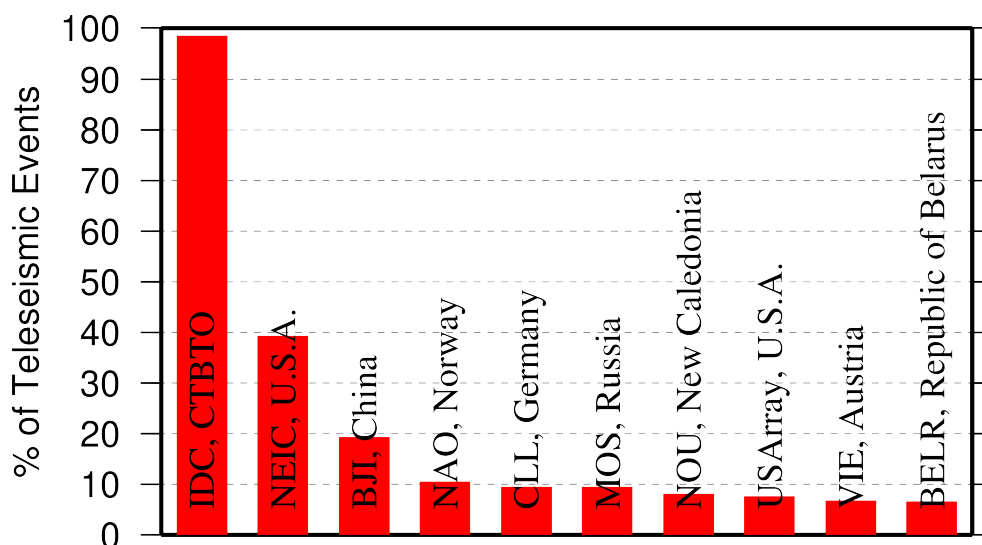
Figure 10.3: *Top ten agencies that reported teleseismic phase arrivals for a large portion of ISC events.*

In addition to the first arriving phase we encourage reporters to contribute observations of secondary seismic phases that help constrain the event location and depth: S, Sn, Sg and pP, sP, PcP (Figure 10.4). We expect though that these observations are actually made from waveforms, rather than just predicted by standard velocity models and modern software programs. It is especially important that these arrivals are manually reviewed by an operator (as we know takes place at the IDC and NEIC), as opposed to some lesser attempts to provide automatic phase readings that are later rejected by the ISC due to a generally poor quality of unreviewed picking.
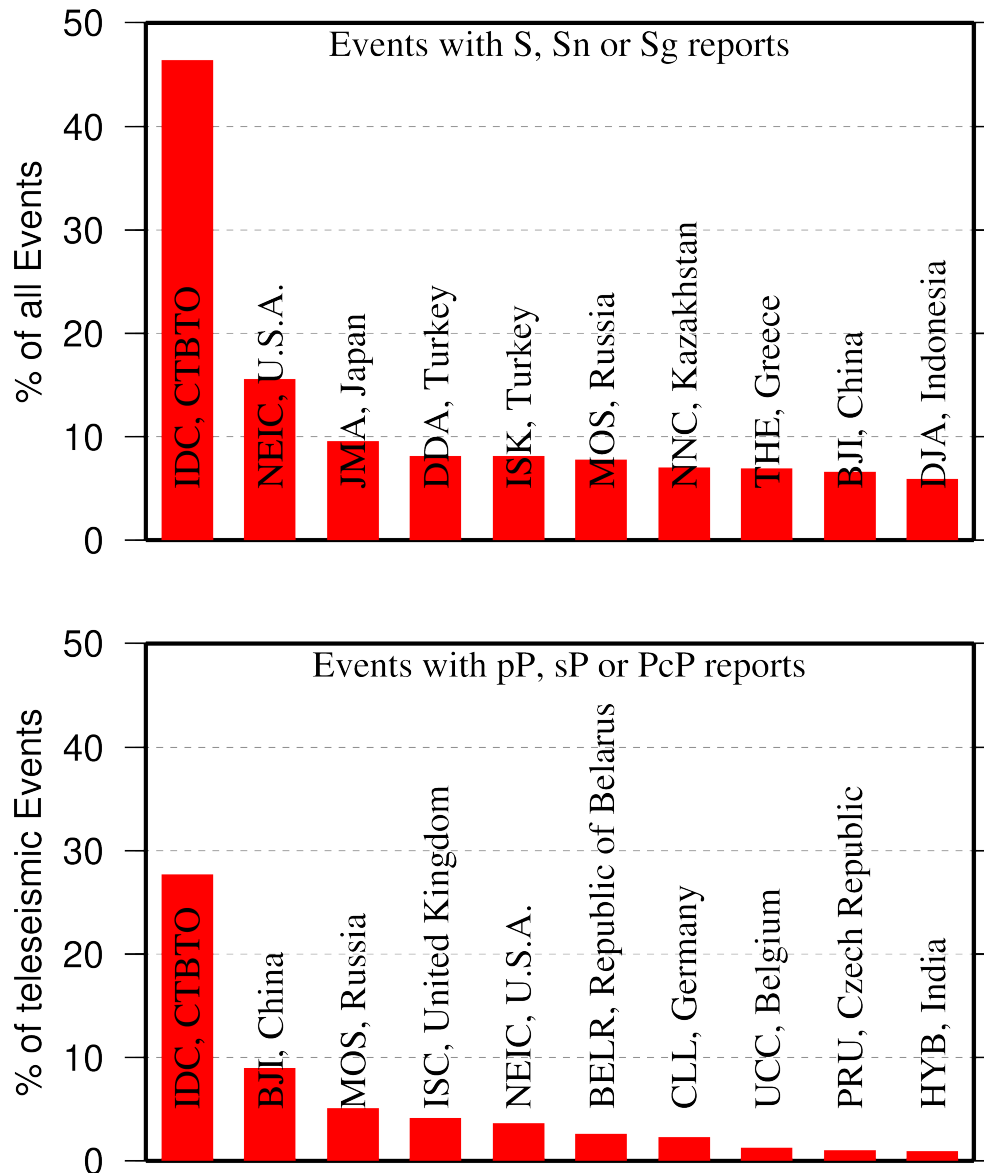
Figure 10.4: *Top ten agencies that reported secondary phases important for an accurate epicentre location (top) and focal depth determination (bottom); notably, the ISC's recent dedicated effort of picking depth phases from moderate to large earthquakes using openly available waveforms, currently makes it the 4th largest contributor of such data.*

Another important long-term task that the ISC performs is to compute the most definitive values of MS and mb network magnitudes that are considered reliable due to removal of outliers and consequent averaging (using alpha-trimmed median) across the largest network of stations, generally not feasible for a single agency. Despite concern over the bias at the lower end of mb introduced by the body wave amplitude data from the IDC, other agencies are also known to bias the results. This topic is further discussed in Section 9.5.

Notably, the IDC reports almost 100% of all events for which *MS* and *mb* are estimated. This is due to the standard routine that requires determination of body and surface wave magnitudes useful for discrimination purposes. NEIC, BJI, MOS, PPT, NAO and a few other agencies (Figure 10.5) are also responsible for the majority of the amplitude and period reports that contribute towards the ISC magnitudes.

The ISC only recently started to determine source mechanisms in addition to those reported by other agencies. For moment tensor magnitudes we rely on reports from other agencies (Figure 10.6).
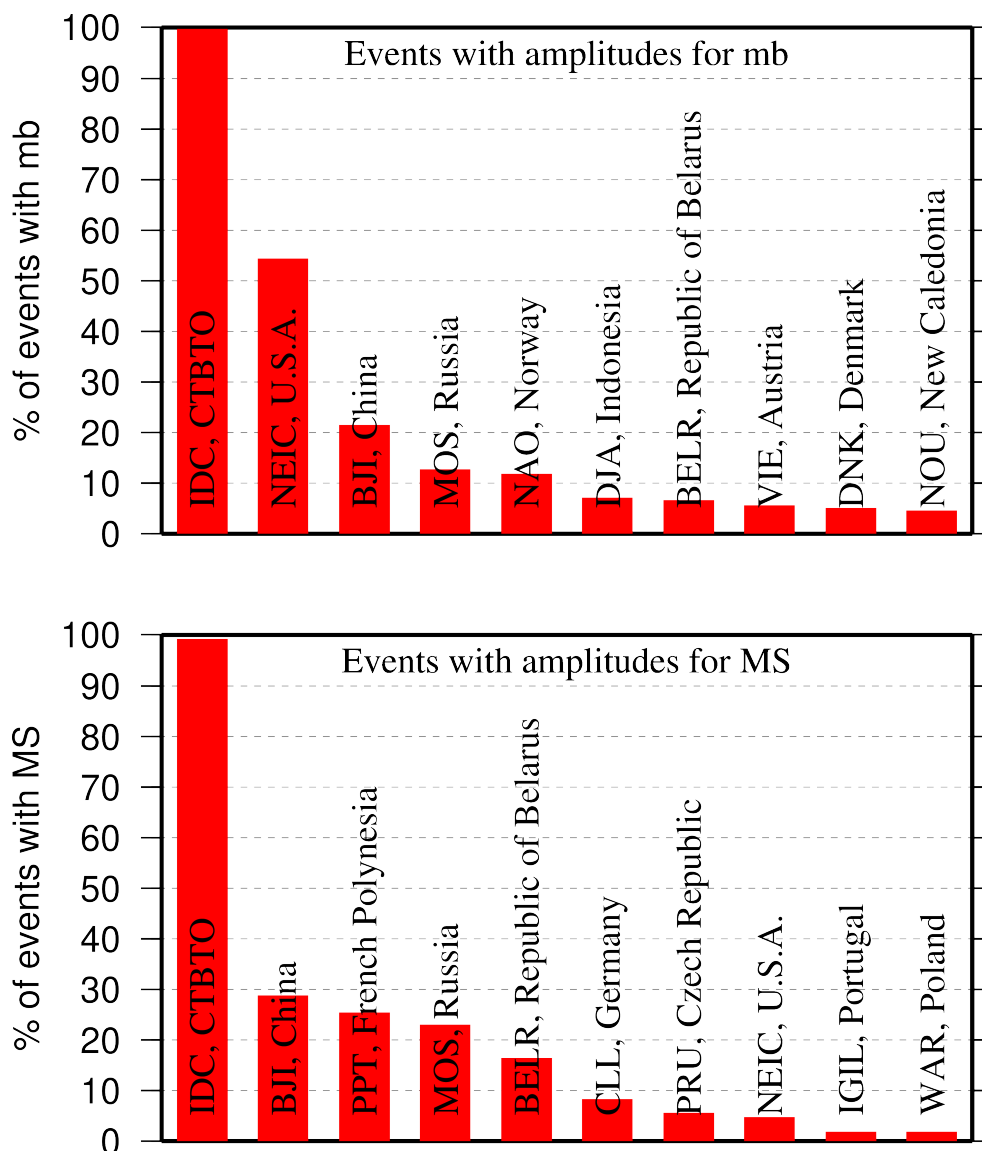
Figure 10.5: *Agencies that report defining body (top) and surface (bottom) wave amplitudes and periods for the largest fraction of those ISC Bulletin events with MS/mb determinations.*

Among other event parameters the ISC Bulletin also contains information on event type. We cannot independently verify the type of each event in the Bulletin and thus rely on other agencies to report the event type to us. Practices of reporting non-tectonic events vary greatly from country to country. Many agencies do not include anthropogenic events in their reports. Suppression of such events from reports to the ISC may lead to a situation where a neighbouring agency reports the anthropogenic event as an earthquake for which expected data are missing. This in turn is detrimental to ISC Bulletin users studying natural seismic hazard. Hence we encourage all agencies to join the agencies listed on Figure 10.7 and several others in reporting both natural and anthropogenic events to the ISC.

The ISC Bulletin also contains felt and damaging information when local agencies have reported it to us. Agencies listed on Figure 10.8 provide such information for the majority of all felt or damaging events in the ISC Bulletin.
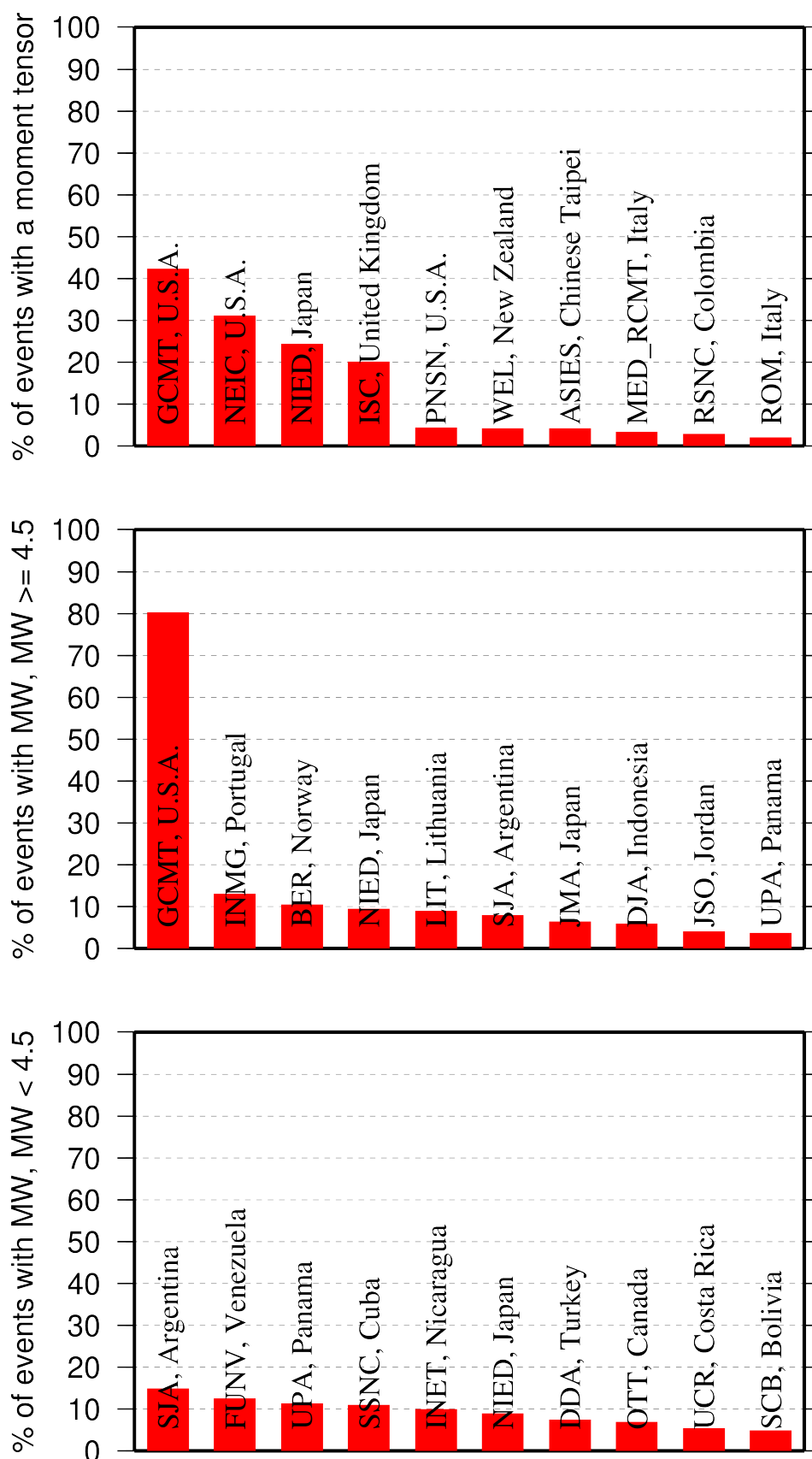
Figure 10.6: *Top ten agencies that most frequently report determinations of seismic moment tensor (top) and moment magnitude (middle/bottom for M greater/smaller than 4.5); notably, the ISC's recent dedicated effort of determination of source mechanisms based on automated picking of first arrival polarities, currently makes it the 4th largest contributor of such data.*
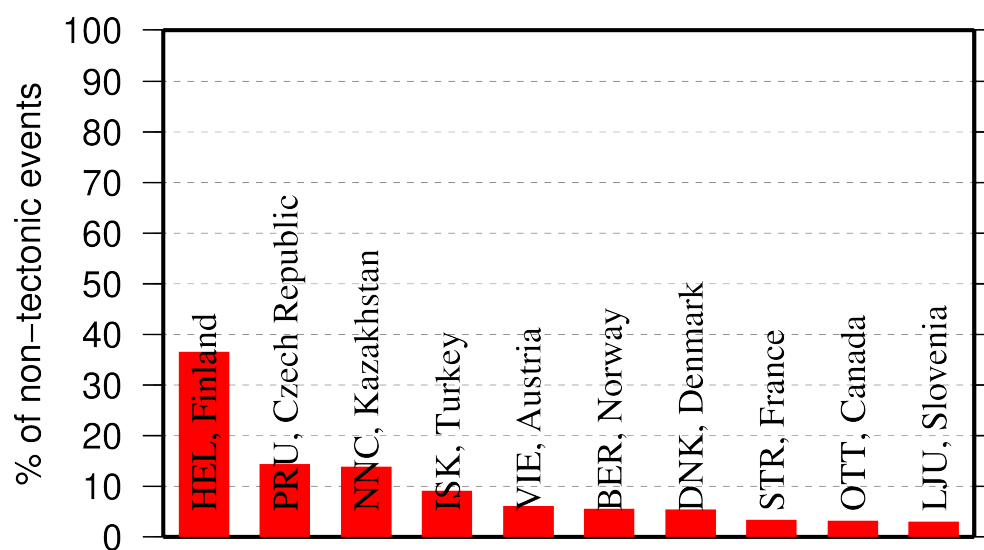
Figure 10.7: *Top ten agencies that most frequently report non-tectonic seismic events to the ISC.*
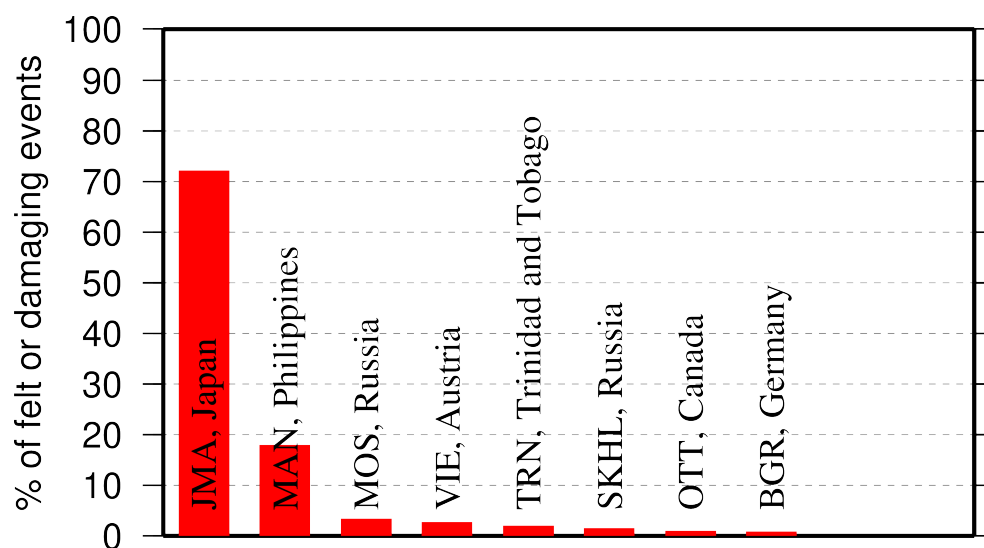
Figure 10.8: *Top ten agencies that most frequently report macroseismic information to the ISC.*

10.3 The Most Consistent and Punctual Contributors

During this six-month period, 29 agencies reported their bulletin data in one of the standard seismic formats (ISF, IMS, GSE, Nordic or QuakeML) and within the current 12-month deadline. Here we must reiterate that the ISC accepts reviewed bulletin data after a final analysis as soon as they are ready. These data, even if they arrive before the deadline, are immediately parsed into the ISC database, grouped with other data and become available to the ISC users on-line as part of the preliminary ISC Bulletin. There is no reason to wait until the deadline to send the data to the ISC. Table 10.1 lists all agencies that have been helpful to the ISC in this respect during the six-month period.

Table 10.1: *Agencies that contributed reviewed bulletin data to the ISC in one of the standard international formats before the submission deadline.*

Agency Code	Country	Average Delay from real time (days)
ZUR	Switzerland	13
ATH	Greece	15
PPT	French Polynesia	26
LDG	France	27
NAO	Norway	30
IGIL	Portugal	31
ECX	Mexico	31
KNET	Kyrgyzstan	33
LIC	Ivory Coast	34
BUC	Romania	41
IDC	Austria	47
INMG	Portugal	60
ISN	Iraq	63
SVSA	Portugal	89
AUST	Australia	92
BGS	United Kingdom	113
THE	Greece	139
PRE	South Africa	142
BJI	China	144
UCC	Belgium	171
ISK	Turkey	182
NEIC	U.S.A.	194
NIC	Cyprus	216
VIE	Austria	257
NAM	Namibia	290
MOS	Russia	316
BER	Norway	325
IRIS	U.S.A.	325
IPEC	Czech Republic	347

11

Appendix

11.1 ISC Operational Procedures

11.1.1 Introduction

The relational database at the ISC is the primary source for the ISC Bulletin. This database is also the source for the ISC web-based search, the ISC CD-ROMs and this printed Summary. The ISC database is also mirrored at several institutions such as the Data Management Center of the Incorporated Research Institutions for Seismology (IRIS DMC), Earthquake Research Institute (ERI) of the University of Tokyo and a few others.

The database holds information about ISC events, both natural and anthropogenic. Information on each event may include hypocentre estimates, moment tensors, event type, felt and damaging reports and associated station observations reported by different agencies and grouped together per physical event.

The majority of the ISC events ($\sim$80%) are small and are not reviewed by the ISC analysts. Those that are reviewed ($\sim$20%, usually magnitude greater than 3.5) may or may not include an ISC hypocentre solution and magnitude estimates. The decision depends on whether the wealth of combined information from several agencies as compared to the data of each single agency alone warrants the ISC location. The events are called ISC events regardless of whether they have been reviewed or located by the ISC or not.

All events located by the ISC are reviewed by the ISC analysts but not the other way round. Analyst review involves an examination of the integrity of all reported parametric information. It does not involve review of waveforms. Even if waveforms from all of the $\sim$6,000 stations included in a typical recent month of the ISC Bulletin were freely available, it would be an unmanageable task to inspect them all.

We shall now describe briefly current processes and procedures involved in producing the Bulletin of the International Seismological Centre. These have been developed from former practices described in the Introduction to earlier issues of the ISC Bulletin to account for modern methods and technologies of data collection and analysis.

11.1.2 Data Collection

Parametric data, mainly comprising seismic event hypocentre solutions, phase arrival observations and associated magnitude data, are now mostly emailed to the ISC (seismo@isc.ac.uk) by agencies around the world. Other macroseismic and source information associated with seismic events may also be incorporated in accordance with modern standards. The process of data collection at the ISC involves

the automatic parsing of these data into the ISC relational database. The ISC now has over 200 individual parsers to account for legacy and current bulletin data formats used by data reporters.

Figure 11.1 shows the 313 agencies that have reported bulletin data to the ISC, directly or via regional data centres, during the entire period of the ISC existence: these agencies are also listed in Table 11.2 of the Appendix. In Figure 11.1, corresponding countries are shown shaded in red. Please note that the continent of Antarctica appears white on the map despite a steady stream of bulletin data from Antarctic stations: the agencies that run these stations are based elsewhere.
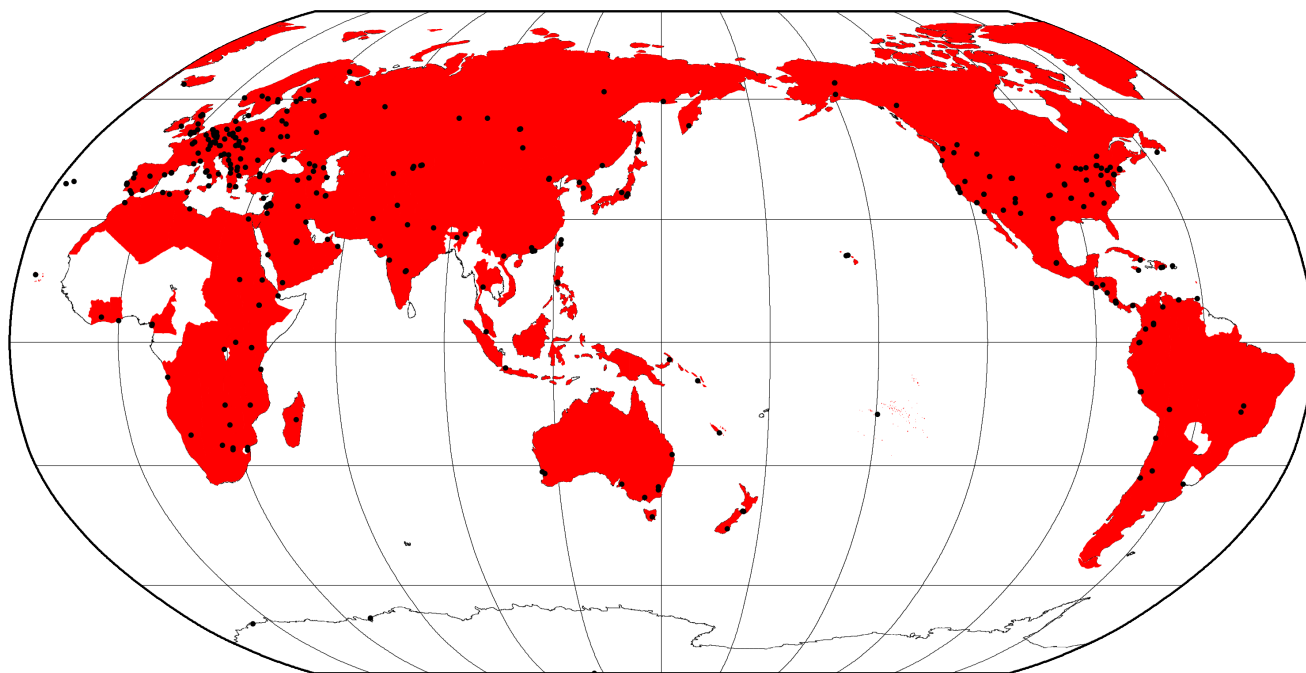
Figure 11.1: *Map of 313 agencies and corresponding countries that have reported seismic bulletin data to the ISC at least once during the entire period of the ISC operations, either directly or via regional data centres. Corresponding countries are shaded in red.*

11.1.3 ISC Automatic Procedures

Grouping

Grouping is the automatic process by which the many hypocentre solutions sent by the agencies reporting to the ISC for the same physical event are merged together into a single ISC event. This process possibly begins with an alert message and ends before a final review by ISC analysts. The process periodically runs through a set time interval of the input data stream, typically one day, looking for hypocentres in newly received data that are not yet grouped into an ISC event. Thus it considers only data more recent than the last data month reviewed by the ISC analysts. Immediately after grouping the seismic arrival associator is run on the same time interval, dealing with new phase arrival data not associated with any hypocentre.

The first stage of grouping gets a score where possible for each hypocentre to determine whether the reported hypocentre will be considered to be the primary estimate, or prime, for an ISC event. This score is based on the station arrival times reported in association with the hypocentre in four epicentral

distance zones that characterise the networks of stations reporting:

1. Whole network

2. Local, 0 - 150 km

3. Near-regional, 3° - 10°

4. Teleseismic, 28° - 180°

For each distance zone, the azimuthal gap, the secondary azimuthal gap (the largest azimuthal gap filled by a single station), the minimum and maximum epicentral distance and number of stations are all used to calculate the value of dU, the normalised absolute deviation from best fitting uniformly distributed stations (*Bondár and McLaughlin*, 2009a). Clearly, this procedure can only use:

1. Bulletin data with hypocentres and sufficient associated seismic arrivals

2. Data for stations that are in the International Registry (IR)

3. Station data that are actually reported to ISC: CENC (China), for example, reports at most 24 stations, whilst many more may have been used to determine the hypocentre.

The hypocentres are then each considered in turn for grouping using one of two methods, the first by searching for a similar hypocentre, and the second by searching for the best fit of the reported phase arrival data that are associated with the candidate hypocentre. The method chosen for a reporter is based on feedback gained from ISC analysts.

For finding similar hypocentres, three sets of limits for origin-time difference and epicentral separation are used according to the type of bulletin data, be it alert, provisional or final: these limits are, respectively:

- ± 2 minutes and 10°

- ± 2 minutes and 4°

- ± 1 minutes and 2°

If there is no overlap with the hypocentre of an existing ISC event, a new event is formed. For each candidate hypocentre, a proximity score is otherwise calculated based on differences in time, t, and distance, s, between the candidate hypocentre and a hypocentre in an event with which it could potentially be grouped.

Proximity score $= 2 - (dt/dt_{max}) - (ds/ds_{max})$

where ds_{max} is the maximum distance between hypocentres and dt_{max} the maximum difference in origin time.

As long as there is no duplication of hypocentre (with the same author, origin time and location within tight limits) the candidate hypocentre together with the associated phase data is grouped with the prime

hypocentre of the event and the initial dU score is used to reassess the prime hypocentre designation. Apparent duplicated hypocentre estimations, including preliminary solutions relayed by other agencies, need to be assessed to determine whether they should really be split between different events. Should there be two or more equally valid events, these can be assessed in turn and may eventually be merged together.

Grouping by fit of the associated phase arrival data is simpler. The residuals of the arrival data are calculated using ak135 travel times for all suitable prime hypocentres within the widest proximity limits given above for similar hypocentres. The hypocentre and associated phase arrival data is then grouped with the event with the best fitting prime hypocentre, which may similarly be re-designated according to the dU scores. Associations of phase arrival data are updated to be with the prime hypocentre estimate of each ISC event.

It follows that a hypocentre and associated phase arrival data submitted by a reporter will have the reported hypocentre set as the prime hypocentre in the ISC event if no other submitted hypocentre estimate is a closer match. It follows also that a hypocentre submitted without phase data can only be grouped with a similar hypocentre. Generally, early arriving data may be superseded by later arriving data: the data will still be in the ISC database but be deprecated, that is, marked as being no longer useful for further processes.

Association

Association is the automatic procedure, run routinely after grouping, that links reported phase arrivals at IR stations with the prime hypocentres of ISC events. As grouping took care of those phases associated with reported hypocentres, by associating the phases to the respective prime hypocentres of the ISC events without further checks, this procedure is only required for phase arrival observations that were sent without any association of event made for them by the reporter. Currently only 5% of arrival data is sent unassociated compared with 25% ten years ago.

If a phase arrival is found to be very similar to another already reported, it is placed in the same event, otherwise the procedure below is followed.

For associating a phase arrival, suitable events are sought with prime hypocentre origin-times in the window 40 minutes before and 100 s after the arrival time. For each phase arrival and prime hypocentre an ak135 travel-time residual is calculated for either the reported arrival phase name or an alternative from a default list if appropriate. Possible timing errors that are multiples of 60 s (a minute) are considered if the phase arrival is at a station not known to be digitally recording. A reporting likelihood is then determined based on the reported event magnitude: a magnitude default of 3.0 is used if no magnitude is given.

A final score is calculated from the residuals, from the likelihood of the phase observations for the magnitude of the event and from the S-P misfit. A phase arrival along with all other phase arrivals in that reading for the station is then associated with the prime hypocentre with the best score. If no suitable match is found, the reading remains unassociated but may be used at some later stage.

Thresholding

Thresholding is the process determining which events are to be reviewed by the ISC analysts. In former times, before email transmission of data was convenient, all events were reviewed, with magnitudes nearly always 3.5 or above. Nowadays, data contributors are encouraged to send all their data, which are stored in the ISC database. The overwhelming amount of data, including that for many more smaller events and from many more seismograph stations, led to the advent of ISC Comprehensive Bulletin, for all events, and the ISC Reviewed Bulletin, for selected events reviewed by ISC analysts. Thresholding has been under constant review since the start of the 1999 data year.

Several criteria are considered to decide which events merit review. Once a decision is made, whether or not an event is to be reviewed, further criteria are not considered.

In this section, M is the maximum magnitude reported by any agency for the event. The sequence of tests in the automatic decision process for reviewing events is currently:

- All events reported by the International Data Centre (IDC) of the Comprehensive Nuclear-Test-Ban Treaty Organization (CTBTO) are reviewed.

- If M is greater than or equal to 3.5, the event is reviewed.

- If M is less than 2.5, the event is not reviewed.

- If M is unknown, the number of data sources of hypocentres and phase arrivals is used. Care is taken here to avoid counting indirect reports arriving via agencies such as NEIC, CSEM and CASC, which compile regional and global data:

  - If the number of hypocentre authors is greater than two and the maximum epicentral distance of arrival data is greater than 10°, the event is reviewed.

  - If the number of arrival authors is greater than two and the maximum epicentral distance of arrival data is greater than 10°, the event is reviewed.

  - Otherwise the event is not reviewed.

- If M is between 2.5 and 3.5:

  - If the number of hypocentre and seismic arrival authors is less than two, the event is not reviewed.

  - If any bulletin contributing to the event has at least ten stations within 3° and the secondary azimuthal gap (the largest azimuthal gap filled by a single station) is less than 135°, the event is not reviewed.

Location by the ISC

The automatic processes group and associate incoming data into ISC events as indicated above. These data are available to users before review by the ISC analysts but there will be no ISC hypocentre solutions for any of the events. The candidate events due for review by the ISC analysts are determined by the

thresholding process, which is why many smaller events remain without an ISC hypocentre solution even after the analyst review.

Several further checks of the data are made in preparation for the analyst review, and initial trial estimates for ISC hypocentres are then generated using the accumulated data. If sufficiently robust, the ISC hypocentre estimation will be retained and be made the prime solution for the event, but this, of course, will itself be subject to the analyst review.

It is important to note that not all reviewed events will have an ISC hypocentre. For the reviewed events certain criteria must be met for an initial ISC location of an event to be made. These criteria are shown below:

- All events with an IDC hypocentre, unless IDC is the only hypocentre author and there are less than six associated phases.

- Two or more reporters of data

- Phase data at epicentral distance $\geq 20°$

The ISC locator also needs an intial seed location; in all events except those with eight or more reporters of data where the existing prime is used, this is calculated using a Neighbourhood Algorithm (NA) (*Sambridge*, 1999; *Sambridge and Kennett*, 2001). More information about the ISC location algorithm and initial seed is given in the next section.

11.1.4   ISC Location Algorithm

The new ISC location algorithm is described in detail in *Bondár and Storchak* (2011) (doi: 10.1111/j.1365-246X.2011.05107.x, Manual www.isc.ac.uk/iscbulletin/iscloc/); here we give a short summary of the major features. Ever since the ISC came into existence in 1964, it has been committed to providing a homogeneous bulletin that benefits scientific research. Hence the location algorithm used by the ISC, except for some minor modifications, has remained largely unchanged for the past 40 years (*Adams et al.*, 1982; *Bolt*, 1960). While the ISC location procedures have served the scientific community well in the past, they can certainly be improved.

Linearised location algorithms are very sensitive to the initial starting point for the location. The old procedures made the assumption that a good initial hypocentre is available among the reported hypocentres. However, there is no guarantee that any of the reported hypocentres are close to the global minimum in the search space. Furthermore, attempting to find a free-depth solution was futile when the data had no resolving power for depth (e.g. when the first arrival is not within the inflection point of the P travel-time curve). When there was no depth resolution, the algorithm would simply pick a point on the origin time – depth trade-off curve. The old ISC locator assumed that the observational errors are independent. The recent years have seen a phenomenal growth both in the number of reported events and phases, owing to the ever-increasing number of stations worldwide. Similar ray paths will produce correlated travel-time prediction errors due to unmodelled heterogeneities in the Earth, resulting in underestimated location uncertainties and for unfavourable network geometries, location bias. Hence,

accounting for correlated travel-time prediction errors becomes imperative if we want to improve (or simply maintain) location accuracy as station networks become progressively denser. Finally, publishing network magnitudes that may have been derived from a single station measurement was rather prone to producing erroneous event magnitude estimates.

To meet the challenge imposed by the ever-increasing data volume from heavily unbalanced networks we introduced a new ISC location algorithm to ensure the efficient handling of data and to further improve the location accuracy of events reviewed by the ISC. The new ISC location algorithm

- Uses all ak135 (*Kennett et al.*, 1995) predicted phases (including depth phases) in the location;

- Obtains the initial hypocentre guess via the Neighbourhood Algorithm (NA) (*Sambridge*, 1999; *Sambridge and Kennett*, 2001);

- Performs iterative linearised inversion using an *a priori* estimate of the full data covariance matrix to account for correlated model errors (*Bondár and McLaughlin*, 2009b);

- Attempts a free-depth solution if and only if there is depth resolution, otherwise it fixes the depth to a region-dependent default depth;

- Scales uncertainties to 90% confidence level and calculates location quality metrics for various distance ranges;

- Obtains a depth-phase depth estimate based on reported surface reflections via depth-phase stacking (*Murphy and Barker*, 2006);

- Provides robust network magnitude estimates with uncertainties.

Seismic Phases

One of the major advantages of using the ak135 travel-time predictions (*Kennett et al.*, 1995) is that they do not suffer from the baseline difference between P, S and PKP phases compared with the Jeffreys-Bullen tables (*Jeffreys and Bullen*, 1940). Furthermore, ak135 offers an abundance of phases from the IASPEI Standard Seismic List (*Storchak et al.*, 2003; 2011) that can be used in the location, most notably the PKP branches and depth-sensitive phases. Elevation and ellipticity corrections (*Dziewonski and Gilbert*, 1976; *Engdahl et al.*, 1998; *Kennett et al.*, 1996), using the WG84 ellipsoid parameters, are added to the ak135 predictions. For depth phases, bounce point (elevation correction at the surface reflection point) and water depth (for pwP) corrections are calculated using the algorithm of *Engdahl et al.* (1998). We use the ETOPO1 global relief model (*Amante and Eakins*, 2009) to obtain the elevation or the water depth at the bounce point.

Phase picking errors are described by *a priori* measurement error estimates derived from the inspection of the distribution of ground truth residuals (residuals calculated with respect to the ground truth location) from the IASPEI Reference Event List (*Bondár and McLaughlin*, 2009a). For phases that do not have a sufficient number of observations in the ground truth database we establish *a priori* measurement errors so that the consistency of the relative weighting schema is maintained. First-arriving P-type phases (P, Pn, Pb, Pg) are picked more accurately than later phases, so their measurement error estimates are

the smallest, 0.8 s. The measurement error for first-arriving S-phases (S, Sn, Sb, Sg) is set to 1.5 s. Phases traversing through or reflecting from the inner/outer core of the Earth have somewhat larger (1.3 s for PKP, PKS, PKKP, PKKS and P'P' branches as well as PKiKP, PcP and PcS, and 1.8 s for SKP, SKS, SKKP, SKKS and S'S' branches as well as SKiKP, ScP and ScS) measurement error estimates to account for possible identification errors among the various branches. Free-surface reflections and conversions (PnPn, PbPb, PgPg, PS, PnS, PgS and SnSn, SbSb, SgSg, SP, SPn, SPg) are observed less frequently and with larger uncertainty, and therefore suffer from large, 2.5 s, measurement errors. Similarly, a measurement error of 2.8 s is assigned to the longer period and typically emergent diffracted phases (Pdif, Sdif, PKPdif). The *a priori* measurement error for the commonly observed depth phases (pP, sP, pS, sS and pwP) is set to 1.3 s, while the remaining depth phases (pPKP, sPKP, pSKS, sSKS branches and pPb, sPb, sSb, pPn, sPn, sSn) have the measurement error estimate set to 1.8 s. We set the measurement error estimate to 2.5 s for the less reliable depth phases (pPg, sPg, sSg, pPdif, pSdif, sPdif and sSdif). Note that we also allow for distance-dependent measurement errors. For instance, to account for possible phase identification errors at far-regional distances the *a priori* measurement error for Pn and P is increased from 0.8 s to 1.2 s and for Sn and S from 1.5 s to 1.8 s between 15° and 28°. The measurement errors between 40° and 180° are set to 1.3 s and 1.8 s for the prominent PP and SS arrivals respectively, but they are increased to 1.8 s and 2.5 s between 25° and 40°.

The relative weighting scheme (Figure 11.2) described above ensures that arrivals picked less reliably or prone to phase identification errors are down-weighted in the location algorithm. Since the ISC works with reported parametric data with wildly varying quality, we opted for a rather conservative set of *a priori* measurement error estimates.

Correlated Travel-Time Prediction Error Structure

Most location algorithms, either linearised or non-linear, assume that all observational errors are independent. This assumption is violated when the separation between stations is less than the scale length of local velocity heterogeneities. When correlated travel-time prediction errors are present, the data covariance matrix is no longer diagonal, and the redundancy in the observations reduces the effective number of degrees of freedom. Thus, ignoring the correlated error structure inevitably results in underestimated location uncertainty estimates. For events located by an unbalanced seismic network this may also lead to a biased location estimate. *Chang et al.* (1983) demonstrated that accounting for correlated error structure in a linearised location algorithm is relatively straightforward once an estimate of the non-diagonal data covariance matrix is available. To determine the data covariance matrix we follow the approach described by *Bondár and McLaughlin* (2009b). They assume that the similarity between ray paths is well approximated by the station separation. This simplifying assumption allows for the estimation of covariances between station pairs from a generic P variogram model derived from ground truth residuals. Because the overwhelming number of phases in the ISC Bulletin is teleseismic P, we expect that the generic variogram model will perform reasonably well anywhere on the globe.

Since in this representation the covariances depend only on station separations, the covariance matrix (and its inverse) needs to be calculated only once. We assume that different phases owing to the different ray paths they travel along as well as station pairs with a separation larger than 1000 km are uncorrelated. Hence, the data covariance matrix is a sparse, block-diagonal matrix. Furthermore, if the stations in

Figure 11.2: A priori *measurement error estimates for phases used in the location algorithm. The red coloured errors are distance-dependent, which are applied for distances when phase identification errors may occur (see text).*
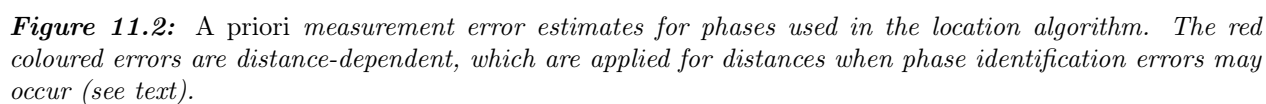
each phase block are ordered by their nearest neighbour distance, the phase blocks themselves become block-diagonal. To reduce the computational time of inverting large matrices we exploit the inherent block-diagonal structure by inverting the covariance matrix block-by-block. The *a priori* measurement error variances are added to the diagonal of the data covariance matrix.

Depth Resolution

In principle, depth can be resolved if there is a mixture of upgoing and downgoing waves emanating from the source, that is, if there are stations covering the distance range where the vertical partial derivative of the travel-time of the first-arriving phase changes sign (local networks), or if there are phases with vertical slowness of opposite sign (depth phases). Core reflections, such as PcP, and to a lesser extent, secondary phases (S in particular) could also help in resolving the depth.

We developed a number of criteria to test whether the reported data for an event have sufficient depth resolution:

- local network: one or more stations within 0.2° with time-defining phases

- depth phases: five or more time-defining depth phases reported by at least two agencies (to reduce a chance of misinterpretation by a single inexperienced analyst)

- core reflections: five or more time-defining core reflections (PcP, ScS) reported by at least two agencies

- local/near regional S: five or more time-defining S and P pairs within 3°

We attempt a free-depth solution if any of the above criteria are satisfied; otherwise we fix the depth to a default depth dependent on the epicentre location. The default depth grid was derived from the EHB (*Engdahl et al.*, 1998) free-depth solutions, including the fixed-depth EHB earthquakes that were flagged as having reliable depth estimate (personal communication with Bob Engdahl), as well as from free-depth solutions obtained by the new locator when locating the entire ISC Bulletin data-set. As Figure 11.3 indicates, the default depth grid provides a reasonable depth estimate where seismicity is well established. Note that the depths of known anthropogenic events and landslides are fixed to the surface.

Depth-Phase Stack

While we use depth phases directly in the location, the depth-phase stacking method (*Murphy and Barker*, 2006) provides an independent means to obtain robust depth estimates. Because the depth obtained from the depth-phase stacking method implicitly depends on the epicentre itself, we perform the depth-phase stack only twice: first, with respect to the initial location in order to obtain a reasonable starting point for the depth in the grid search described in the following section; second, with respect to the final location to obtain the final estimate for the depth-phase constrained depth.

ISC Default Depth Grid
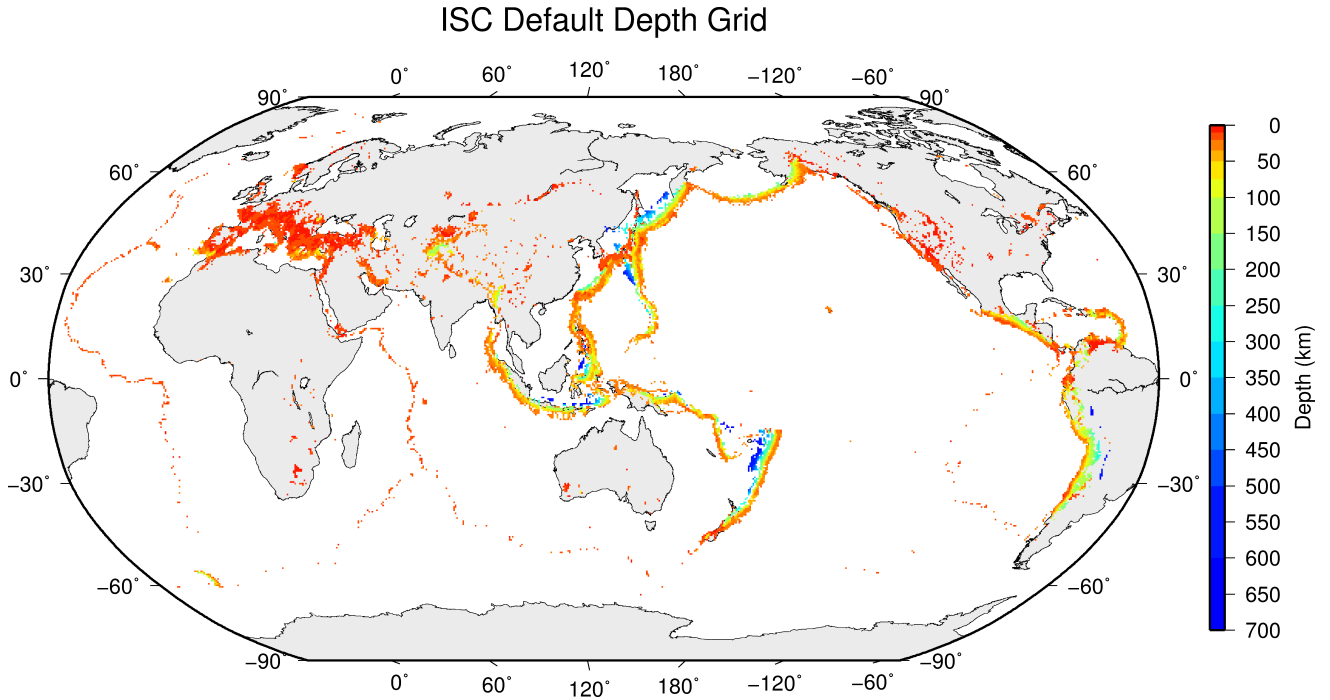
Figure 11.3: *Default depths on a 0.5×0.5 degree grid derived from EHB free-depth solutions and EHB events flagged as reliable depth, as well as free-depth solutions from the entire ISC Bulletin located with the new locator.*

Initial Hypocentre

For poorly recorded events the reported hypocentres may exhibit a large scatter and they could suffer from large location errors, especially if they are only recorded teleseismically. In order to obtain a good initial hypocentre guess for the linearised location algorithm we employ the Neighbourhood Algorithm (NA) (*Sambridge*, 1999; *Sambridge and Kennett*, 2001). NA is a nonlinear grid search method capable of exploring a large search space and rapidly closing in on the global optimum. *Kennett* (2006) discusses in detail the NA algorithm and its use for locating earthquakes.

We perform a search around the median of reported hypocentre parameters with a generously defined search region – within a 2° radius circle around the median epicentre, 10 s around the median origin time and 150 km around the median reported depth. These default search parameters were obtained by trial-and-error runs to achieve a compromise between execution time and allowance for gross errors in the median reported hypocentre parameters. Note that if our test for depth resolution fails, we fix the depth to the region-dependent default depth. The initial hypocentre estimate will be the one with the smallest L1-norm misfit among the NA trial hypocentres. Once close to the global optimum, we proceed with the linearised location algorithm to obtain the final solution and corresponding formal uncertainties.

Iterative Linearised Location Algorithm

We adopt the location algorithm described in detail in *Bondár and McLaughlin* (2009b). Recall that in the presence of correlated travel-time prediction errors the data covariance matrix is no longer diagonal. Using the singular value decomposition of the data covariance matrix we construct a projection matrix

that orthogonalises the data set and projects redundant observations into the null space. In other words, we solve the inversion problem in the eigen coordinate system in which the transformed observations are independent.

The model covariance matrix yields the four-dimensional error ellipsoid whose projections provide the two-dimensional error ellipse and one-dimensional errors for depth and origin time. These uncertainties are scaled to the 90% confidence level. Note that since we projected the system of equations into the eigen coordinate system, the number of independent observations is less than the total number of observations. Hence, the estimated location error ellipses necessarily become larger, providing a more realistic representation of the location uncertainties. The major advantage of this approach is that the projection matrix is calculated only once for each event location.

Validation Tests

To demonstrate improvements due to the new location procedures, we located some 7,200 GT0-5 events in the IASPEI Reference Event List (*Bondár and McLaughlin*, 2009a) both with the old ISC locator (which constitutes the baseline) and with the new location algorithm. We also located the entire (1960-2010) ISC Bulletin, including four years of the International Seismological Summary (ISS, the predecessor of the ISC) catalogue (*Villaseñor and Engdahl*, 2005; 2007).

The location of GT events demonstrated that the new ISC location algorithm provides small but consistent location improvements, considerable improvements in depth determination and significantly more accurate formal uncertainty estimates. Even using a 1-D model and a variogram model that fits teleseismic observations we could achieve realistic uncertainty estimates, as the 90% confidence error ellipses cover the true locations 80-85% of the time. The default depth grid provides reasonable depth estimates where there is seismicity. We have shown that the location and depth accuracy obtained by the new algorithm matches or surpasses the EHB accuracy.

We noted above that the location improvements for the ground truth events are consistent, but minor. This is not surprising as most of the events in the IASPEI Reference Event List are very well-recorded with a small azimuthal gap and dominated by P-type phases. In these circumstances we could expect significant location improvements only for heavily unbalanced networks where large numbers of correlated ray paths conspire to introduce location bias. On the other hand, the ISC Bulletin represents a plethora of station configurations ranging from reasonable to the most unfavourable network geometries. Hence, we could expect more dramatic location improvements when locating the entire ISC Bulletin. Although in this case we cannot measure the improvement in location accuracy due to the lack of ground truth information, we show that with the new locator we obtain significantly better clustering of event locations (Figure 11.4), thus providing an improved view of the seismicity of the Earth.

Magnitude Calculation

Currently the ISC locator calculates body and surface wave magnitudes. MS is calculated for shallow events (depth < 60 km) only. At least three station magnitudes are required for a network (mb or MS) magnitude. The network magnitude is defined as the median of the station magnitudes, and its
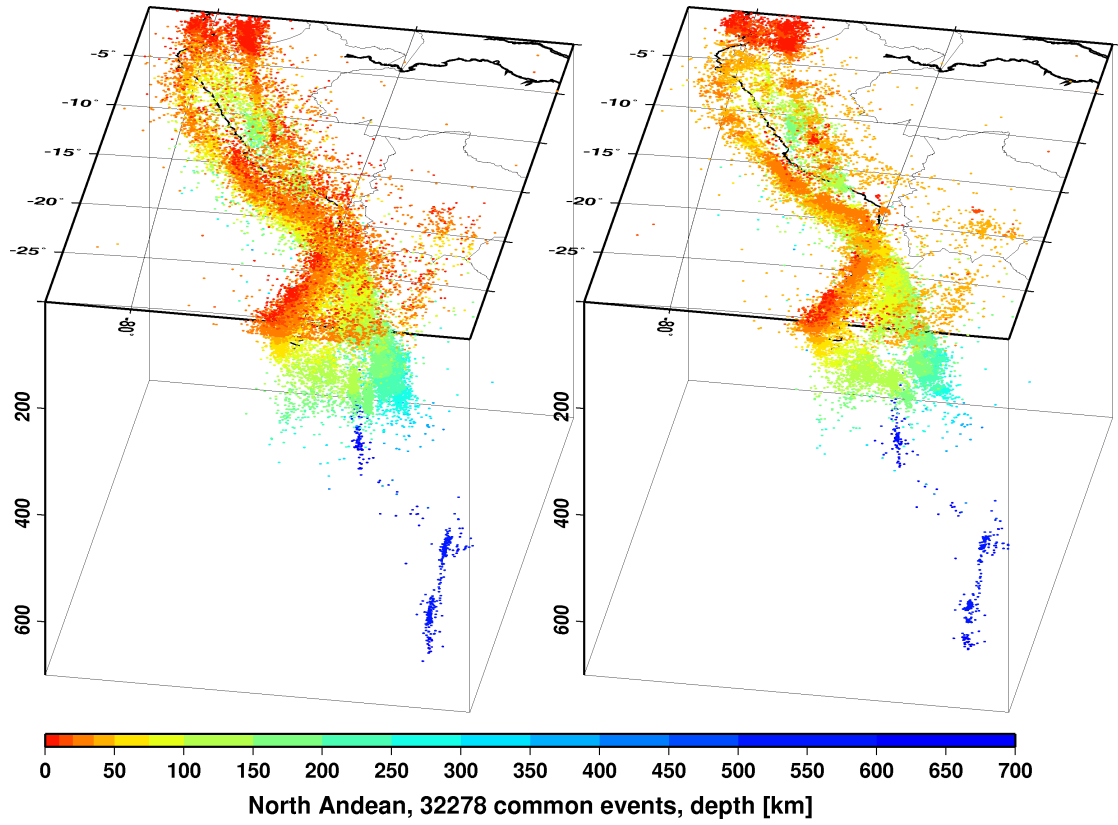
(a)
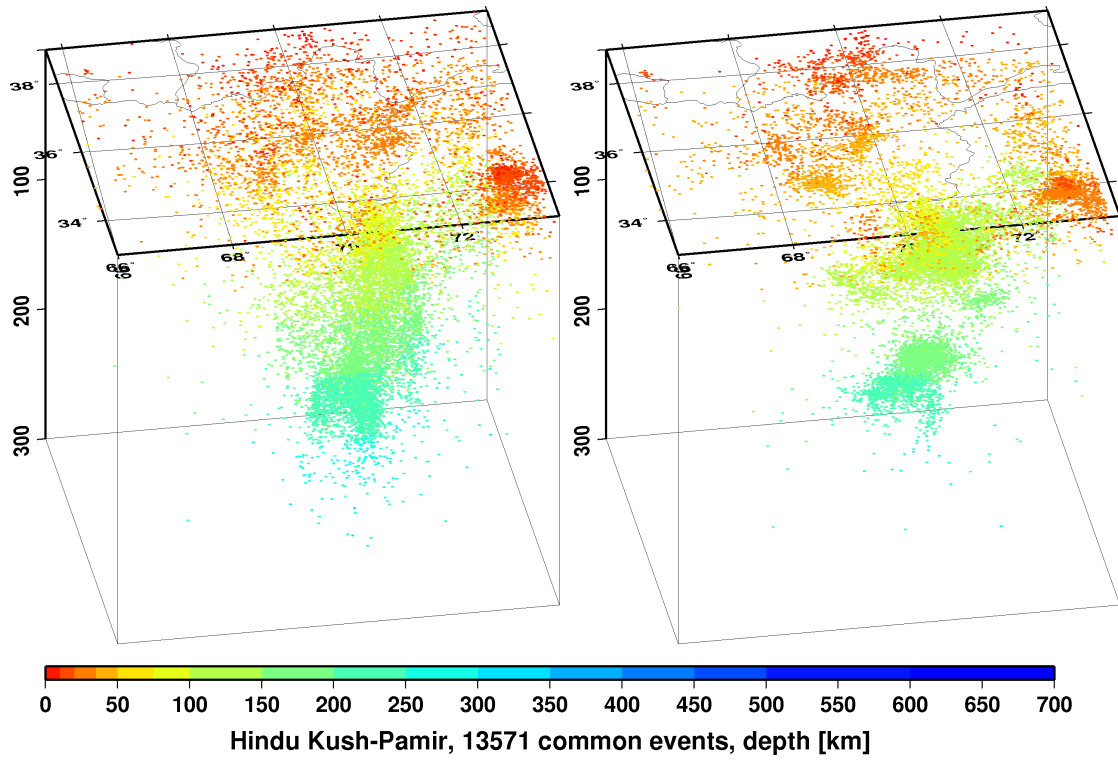
(b)

Figure 11.4: *Comparison of seismicity maps for common events in the reviewed ISC Bulletin (old locator, left) and the located ISC Bulletin (new locator, right) for the North Andean (a) and Hindu Kush - Pamir regions (b). The events are better clustered when located with the new locator.*

uncertainty is defined as the standard median absolute deviation (SMAD) of the alpha-trimmed (*alpha* = 20%) station magnitudes.

The station magnitude is defined as the median of reading magnitudes for a station. The reading magnitude is defined as the magnitude computed from the maximal log(A/T) in a reading. Amplitude magnitudes are calculated for each reported amplitude-period pair.

Body-Wave Magnitudes

Body-wave magnitudes are calculated for each reported amplitude-period pair, provided that the phase is in the list of phases that can contribute to mb (P, pP, sP, AMB, IAmb, pmax), the station is between the epicentral distances $21 - 100°$ and the period is less than 3 s.

A reading contains all parametric data reported by a single agency for an event at a station, and it may have several reported amplitude and periods. The amplitudes are measured as zero-to-peak values in nanometres. For each pair an amplitude mb is calculated.

$$mb_{amp} = log(A/T) + Q(\Delta, h) - 3 \tag{11.1}$$

If no amplitude-period pairs are reported for a reading, the body-wave magnitude is calculated using the reported logat values for $log(A/T)$.

$$mb_{amp} = logat + Q(\Delta, h) - 3 \tag{11.2}$$

where the magnitude attenuation $Q(\Delta, h)$ value is calculated using the Gutenberg-Richter tables (*Gutenberg and Richter*, 1956).

For each reading the ISC locator finds the reported amplitude-period pair for which A/T is maximal:

$$mb_{rd} = log(max(A/T)) + Q(\Delta, h) - 3 \tag{11.3}$$

Or, if no amplitude-period pairs were reported for the reading:

$$mb_{rd} = max(logat) + Q(\Delta, h) - 3 \tag{11.4}$$

Several agencies may report data from the same station. The station magnitude is defined as the median of the reading magnitudes for a station.

$$mb_{sta} = median(mb_{rd}) \tag{11.5}$$

Once all station mb values are determined, the station magnitudes are sorted and the lower and upper alpha percentiles are made non-defining. The network mb and its uncertainty are then calculated as the median and the standard median absolute deviation (SMAD) of the alpha-trimmed station magnitudes, respectively.

Surface-Wave Magnitudes

Surface-wave magnitudes are calculated for each reported amplitude-period pair, provided that the phase is in the list of phases that can contribute to MS (*AMS, IAMs_20, LR, MLR, M, L*), the station is between the epicentral distances $20 - 160°$ and the period is between $10 - 60$ s.

For each reported amplitude-period pair MS is calculated using the Prague formula (*Vaněk et al.*, 1962). Amplitude MS is calculated for each component (Z, E, N) separately.

$$MS_{amp} = log(A/T) + 1.66 * log(\Delta) + 0.3 \tag{11.6}$$

To calculate the reading MS, the ISC locator first finds the reported amplitude-period pair for which A/T is maximal on the vertical component.

$$MS_Z = log(max(A_Z/T_Z)) + 1.66 * log(\Delta) + 0.3 \tag{11.7}$$

Then it finds the max(A/T) for the E and N components for which the period measured on the horizontal components is within ± 5s from the period measured on the vertical component.

$$MS_E = log(max(A_E/T_E)) + 1.66 * log(\Delta) + 0.3 \tag{11.8}$$

$$MS_N = log(max(A_N/T_N)) + 1.66 * log(\Delta) + 0.3 \tag{11.9}$$

The horizontal MS is calculated as

$$max(A/T)h = \begin{cases} \sqrt{2(max(A_E/T_E))^2} & \text{if } MS_N \text{ does not exist} \\ \sqrt{(max(A_E/T_E))^2 + (max(A_N/T_N))^2} & \text{if } MS_E \text{ and } MS_N \text{ exist} \\ \sqrt{2(max(A_N/T_N))^2} & \text{if } MS_E \text{ does not exist} \end{cases} \tag{11.10}$$

$$MS_H = log(max(A/T)_H) + 1.66 * log(\Delta) + 0.3 \tag{11.11}$$

The reading MS is defined as

$$MS = \begin{cases} (MS_Z + MS_H)/2 & \text{if } MS_Z \text{ and } MS_H \text{ exist} \\ MS_H & \text{if } MS_Z \text{ does not exist} \\ MS_Z & \text{if } MS_H \text{ does not exist} \end{cases} \tag{11.12}$$

Several agencies may report data from the same station. The station magnitude is defined as the median of the reading magnitudes for a station.

$$MS_{sta} = median(MS_{rd}) \tag{11.13}$$

Once all station MS values are determined, the station magnitudes are sorted and the lower and upper alpha percentiles are made non-defining. The network MS and its uncertainty are calculated as the median and the standard median absolute deviation (SMAD) of the alpha-trimmed station magnitudes, respectively.

11.1.5 Review Process

Typically, for each month, the ISC analysts now review approximately 20% of the events in the ISC database, currently 3,500-5,000 per data month. This review is done about 24 months behind real time to allow for the comprehensive collection of data from networks and data centres worldwide.

Users of the ISC Bulletin can be assured that all ISC Bulletin events with an ISC hypocentre solution have been reviewed by the ISC analysts. Not all reviewed events will end up having an ISC hypocentre solution, but events that have not been reviewed are flagged accordingly.

An automatic process creates a monthly listing of the events for the analysts to review. The analysis is performed in batches: thus, events are generally not finalised one at a time, and a completed month of events is published after all the analysis is finished.

The first batch of editing involves careful examination of all events selected for review for the month. The entire month is then reprocessed incorporating the editing changes deemed necessary by the analysts. The analysts next review the same events again in a second pass through the data, checking for each event where there is a change that the result was as could be expected by comparing the revised solution against the initial solution. When the analysts are satisfied with an event, it is no longer revised in a subsequent pass but analysis continues in several passes until all events are considered satisfactory.

The analysts initially print the entire monthly listing, which is split into sections each with about 150 events. Each event, uniquely identified in the monthly printout, shows the reported hypocentres, magnitudes and phase arrivals grouped and associated for the event, as well as an ISC solution of hypocentre, if there is one, along with quality metrics, error estimates, redetermined magnitudes and phase arrival-time residuals. Ancillary information including the geographic region and reported macroseismic observations is also present in the listing for each pass.

The analysts have the capability to execute a variety of commands that can be used to merge or split events, to move phase arrivals or hypocentres from one event to another or to modify the reported phase names. Each of these changes initiates a new revision of the relevant events and ISC hypocentre solutions. There are also several commands to change the starting depth or location in the location algorithm.

The main tasks in reviewing the ISC Bulletin are to:

1. Check that the grouping of hypocentres and association of phase arrivals is appropriate.

2. Check that the depth and location is appropriate for the region and reported phase arrivals.

3. Check that no data are missing for an event, given the region and magnitude, and that included data are appropriate.

4. Examine the phase arrival-time residuals to check that the ISC hypocentre solution is appropriate.

5. Look for outliers in the observations and for misassociated phases.

As well as examining each event closely, it is also important to scan the hypocentres and phase arrivals of adjacent events, close in time and space, to ensure that there is uniformity in the composition of the events. In some cases, two events should be merged into one event, as apparent in some other case. In other cases, one apparent event needs to be split into two events, when the automatic grouping has erroneously created one event with more than one reported hypocentre out of the observations for two real events that are distinct but closely occurring.

Misassociated phase arrivals are returned to the unassociated data stream, if not immediately placed by the analyst in another event where they belong, These unassociated phases are then available to be associated with some other event if the time and location is appropriate. The analysts also check that no phase is associated to more than one event.

Towards the end of the monthly analysis, the ISC 'Search' procedure runs, attempting to build events from the remaining set of unassociated phase arrivals. The algorithm is based on the methodology of *Engdahl and Gunst* (1966). Candidate events are validated or rejected by attempting to find ISC hypocentres for them using the ISC locator. The surviving events are then reviewed. Those events with phase arrival observations reported by stations from at least two networks are added to the ISC Bulletin if the solutions meet the standards set by the ISC analysts. These events have only an ISC determination of hypocentre.

At the end of analysis for a data month, a set of final checks is run for quality control, with the results reviewed by an analyst and the defects rectified. These are checks for inconsistencies and errors to ensure the general integrity of the ISC Bulletin.

11.1.6 History of Operational Changes

- From data-month January 2001 onwards, both P and S groups of arrival times are used in location.

- From data-month September 2002 onwards, the printed ISC Bulletins have been generated directly from the ISC Relational Database.

- From data-month October 2002, a new location program ISCloc has been used in operations. Also, the IASPEI standard phase list has now been adopted by the ISC. Please see Section 11.2.1 for details.

- From data-month January 2003 onwards, an updated regionalisation scheme has been adopted (*Young et al.*, 1996).

- From data-month January 2006 the ISC hypocentres are computed using the *ak135* earth velocity model (*Kennett et al.*, 1995) and then reviewed by ISC seismologists. The ISC still produces the hypocentre solutions based on Jeffreys-Bullen travel time tables (agency code ISCJB), yet these solutions are no longer reviewed.

- From data-month January 2009, a new location program (*Bondár and Storchak*, 2011) has been used in operations. The new program uses all predicted *ak135* phases and accounts for correlated model errors. An overview of the location algorithm is provided in this volume (Section 11.1.4).

- In February 2020, the ISC finished the Rebuild Project and re-computed data years 1964 - 2010 of the ISC Bulletin using ak135 and the new location program (Section 5) in order to assure homogeneity and consistency of the data in the entire ISC Bulletin (*Storchak et al.* (2017)).

11.2 IASPEI Standards

11.2.1 Standard Nomenclature of Seismic Phases

The following list of seismic phases was approved by the IASPEI Commission on Seismological Observation and Interpretation (CoSOI) and adopted by IASPEI on 9th July 2003. More details can be found in *Storchak et al.* (2003) and *Storchak et al.* (2011). Ray paths for some of these phases are shown in Figures 11.5–11.10.

Crustal Phases

Pg	At short distances, either an upgoing P wave from a source in the upper crust or a P wave bottoming in the upper crust. At larger distances also, arrivals caused by multiple P-wave reverberations inside the whole crust with a group velocity around 5.8 km/s.
Pb	Either an upgoing P wave from a source in the lower crust or a P wave bottoming in the lower crust (alt: P*)
Pn	Any P wave bottoming in the uppermost mantle or an upgoing P wave from a source in the uppermost mantle
PnPn	Pn free-surface reflection
PgPg	Pg free-surface reflection
PmP	P reflection from the outer side of the Moho
PmPN	PmP multiple free surface reflection; N is a positive integer. For example, PmP2 is PmPPmP.
PmS	P to S reflection/conversion from the outer side of the Moho
Sg	At short distances, either an upgoing S wave from a source in the upper crust or an S wave bottoming in the upper crust. At larger distances also, arrivals caused by superposition of multiple S-wave reverberations and SV to P and/or P to SV conversions inside the whole crust.
Sb	Either an upgoing S wave from a source in the lower crust or an S wave bottoming in the lower crust (alt: S*)
Sn	Any S wave bottoming in the uppermost mantle or an upgoing S wave from a source in the uppermost mantle
SnSn	Sn free-surface reflection
SgSg	Sg free-surface reflection
SmS	S reflection from the outer side of the Moho
SmSN	SmS multiple free-surface reflection; N is a positive integer. For example, SmS2 is SmSSmS.
SmP	S to P reflection/conversion from the outer side of the Moho
Lg	A wave group observed at larger regional distances and caused by superposition of multiple S-wave reverberations and SV to P and/or P to SV conversions inside the whole crust. The maximum energy travels with a group velocity of approximately 3.5 km/s
Rg	Short-period crustal Rayleigh wave

Mantle Phases

P	A longitudinal wave, bottoming below the uppermost mantle; also an upgoing longitudinal wave from a source below the uppermost mantle
PP	Free-surface reflection of P wave leaving a source downward
PS	P, leaving a source downward, reflected as an S at the free surface. At shorter distances the first leg is represented by a crustal P wave.
PPP	Analogous to PP
PPS	PP which is converted to S at the second reflection point on the free surface; travel time matches that of PSP
PSS	PS reflected at the free surface
PcP	P reflection from the core-mantle boundary (CMB)
PcS	P converted to S when reflected from the CMB
PcPN	PcP reflected from the free surface N - 1 times; N is a positive integer. For example PcP2 is PcPPcP.
Pz+P	(alt: PzP) P reflection from outer side of a discontinuity at depth z; z may be a positive numerical value in km. For example, P660+P is a P reflection from the top of the 660 km discontinuity.
Pz-P	P reflection from inner side of a discontinuity at depth z. For example, P660-P is a P reflection from below the 660 km discontinuity, which means it is precursory to PP.
Pz+S	(alt:PzS) P converted to S when reflected from outer side of discontinuity at depth z
Pz-S	P converted to S when reflected from inner side of discontinuity at depth z
PScS	P (leaving a source downward) to ScS reflection at the free surface
Pdif	P diffracted along the CMB in the mantle (old: Pdiff)
S	Shear wave, bottoming below the uppermost mantle; also an upgoing shear wave from a source below the uppermost mantle
SS	Free-surface reflection of an S wave leaving a source downward
SP	S, leaving a source downward, reflected as P at the free surface. At shorter distances the second leg is represented by a crustal P wave.
SSS	Analogous to SS
SSP	SS converted to P when reflected from the free surface; travel time matches that of SPS
SPP	SP reflected at the free surface
ScS	S reflection from the CMB
ScP	S converted to P when reflected from the CMB
ScSN	ScS multiple free-surface reflection; N is a positive integer. For example ScS2 is ScSScS.
Sz+S	S reflection from outer side of a discontinuity at depth z; z may be a positive numerical value in km. For example S660+S is an S reflection from the top of the 660 km discontinuity. (alt: SzS)
Sz-S	S reflection from inner side of discontinuity at depth z. For example, S660-S is an S reflection from below the 660 km discontinuity, which means it is precursory to SS.
Sz+P	(alt: SzP) S converted to P when reflected from outer side of discontinuity at depth z
Sz-P	S converted to P when reflected from inner side of discontinuity at depth z
ScSP	ScS to P reflection at the free surface
Sdif	S diffracted along the CMB in the mantle (old: Sdiff)

Core Phases

PKP	Unspecified P wave bottoming in the core (alt: P')
PKPab	P wave bottoming in the upper outer core; ab indicates the retrograde branch of the PKP caustic (old: PKP2)
PKPbc	P wave bottoming in the lower outer core; bc indicates the prograde branch of the PKP caustic (old: PKP1)
PKPdf	P wave bottoming in the inner core (alt: PKIKP)

PKPpre	A precursor to PKPdf due to scattering near or at the CMB (old: PKhKP)
PKPdif	P wave diffracted at the inner core boundary (ICB) in the outer core
PKS	Unspecified P wave bottoming in the core and converting to S at the CMB
PKSab	PKS bottoming in the upper outer core
PKSbc	PKS bottoming in the lower outer core
PKSdf	PKS bottoming in the inner core
P'P'	Free-surface reflection of PKP (alt: PKPPKP)
P'N	PKP reflected at the free surface N - 1 times; N is a positive integer. For example, P'3 is P'P'P'. (alt: PKPN)
P'z-P'	PKP reflected from inner side of a discontinuity at depth z outside the core, which means it is precursory to P'P'; z may be a positive numerical value in km
P'S'	(alt: PKPSKS) PKP converted to SKS when reflected from the free surface; other examples are P'PKS, P'SKP
PS'	P (leaving a source downward) to SKS reflection at the free surface (alt: PSKS)
PKKP	Unspecified P wave reflected once from the inner side of the CMB
PKKPab	PKKP bottoming in the upper outer core
PKKPbc	PKKP bottoming in the lower outer core
PKKPdf	PKKP bottoming in the inner core
PNKP	P wave reflected N - 1 times from inner side of the CMB; N is a positive integer.
PKKPpre	A precursor to PKKP due to scattering near the CMB
PKiKP	P wave reflected from the inner core boundary (ICB)
PKNIKP	P wave reflected N - 1 times from the inner side of the ICB
PKJKP	P wave traversing the outer core as P and the inner core as S
PKKS	P wave reflected once from inner side of the CMB and converted to S at the CMB
PKKSab	PKKS bottoming in the upper outer core
PKKSbc	PKKS bottoming in the lower outer core
PKKSdf	PKKS bottoming in the inner core
PcPP'	PcP to PKP reflection at the free surface; other examples are PcPS', PcSP', PcSS', PcPSKP, PcSSKP. (alt: PcPPKP)
SKS	unspecified S wave traversing the core as P (alt: S')
SKSac	SKS bottoming in the outer core
SKSdf	SKS bottoming in the inner core (alt: SKIKS)
SPdifKS	SKS wave with a segment of mantleside Pdif at the source and/or the receiver side of the ray path (alt: SKPdifS)
SKP	Unspecified S wave traversing the core and then the mantle as P
SKPab	SKP bottoming in the upper outer core
SKPbc	SKP bottoming in the lower outer core
SKPdf	SKP bottoming in the inner core
S'S'	Free-surface reflection of SKS (alt: SKSSKS)
S'N	SKS reflected at the free surface N - 1 times; N is a positive integer
S'z-S'	SKS reflected from inner side of discontinuity at depth z outside the core, which means it is precursory to S'S'; z may be a positive numerical value in km.
S'P'	(alt: SKSPKP) SKS converted to PKP when reflected from the free surface; other examples are S'SKP, S'PKS.
S'P	(alt: SKSP) SKS to P reflection at the free surface
SKKS	Unspecified S wave reflected once from inner side of the CMB
SKKSac	SKKS bottoming in the outer core
SKKSdf	SKKS bottoming in the inner core
SNKS	S wave reflected N - 1 times from inner side of the CMB; N is a positive integer.
SKiKS	S wave traversing the outer core as P and reflected from the ICB
SKJKS	S wave traversing the outer core as P and the inner core as S
SKKP	S wave traversing the core as P with one reflection from the inner side of the CMB and then continuing as P in the mantle

SKKPab	SKKP bottoming in the upper outer core
SKKPbc	SKKP bottoming in the lower outer core
SKKPdf	SKKP bottoming in the inner core
ScSS'	ScS to SKS reflection at the free surface; other examples are ScPS', ScSP', ScPP', ScSSKP, ScPSKP. (alt: ScSSKS)

Near-source Surface reflections (Depth Phases)

pP*y*	All P-type onsets (P*y*), as defined above, which resulted from reflection of an upgoing P wave at the free surface or an ocean bottom. WARNING: The character *y* is only a wild card for any seismic phase, which could be generated at the free surface. Examples are pP, pPKP, pPP, pPcP, etc.
sP*y*	All P*y* resulting from reflection of an upgoing S wave at the free surface or an ocean bottom; for example, sP, sPKP, sPP, sPcP, etc.
pS*y*	All S-type onsets (S*y*), as defined above, which resulted from reflection of an upgoing P wave at the free surface or an ocean bottom; for example, pS, pSKS, pSS, pScP, etc.
sS*y*	All S*y* resulting from reflection of an upgoing S wave at the free surface or an ocean bottom; for example, sSn, sSS, sScS, sSdif, etc.
pwP*y*	All P*y* resulting from reflection of an upgoing P wave at the ocean's free surface
pmP*y*	All P*y* resulting from reflection of an upgoing P wave from the inner side of the Moho

Surface Waves

L	Unspecified long-period surface wave
LQ	Love wave
LR	Rayleigh wave
G	Mantle wave of Love type
G*N*	Mantle wave of Love type; *N* is integer and indicates wave packets traveling along the minor arcs (odd numbers) or major arc (even numbers) of the great circle
R	Mantle wave of Rayleigh type
R*N*	Mantle wave of Rayleigh type; *N* is integer and indicates wave packets traveling along the minor arcs (odd numbers) or major arc (even numbers) of the great circle
PL	Fundamental leaking mode following P onsets generated by coupling of P energy into the waveguide formed by the crust and upper mantle SPL S wave coupling into the PL waveguide; other examples are SSPL, SSSPL.

Acoustic Phases

H	A hydroacoustic wave from a source in the water, which couples in the ground
HPg	H phase converted to Pg at the receiver side
HSg	H phase converted to Sg at the receiver side
HRg	H phase converted to Rg at the receiver side
I	An atmospheric sound arrival which couples in the ground
IPg	I phase converted to Pg at the receiver side
ISg	I phase converted to Sg at the receiver side
IRg	I phase converted to Rg at the receiver side
T	A tertiary wave. This is an acoustic wave from a source in the solid earth, usually trapped in a low-velocity oceanic water layer called the SOFAR channel (SOund Fixing And Ranging).
TPg	T phase converted to Pg at the receiver side
TSg	T phase converted to Sg at the receiver side
TRg	T phase converted to Rg at the receiver side

Amplitude Measurement Phases

The following set of amplitude measurement names refers to the IASPEI Magnitude Standard
(see www.iaspei.org/commissions/CSOI/Summary_of_WG_recommendations.pdf)

compliance to which is indicated by the presence of leading letter I. The absence of leading letter I indicates that a measurement is non-standard. Letter A indicates a measurement in nm made on a displacement seismogram, whereas letter V indicates a measurement in nm/s made on a velocity seismogram.

IAML	Displacement amplitude measured according to the IASPEI standard for local magnitude ML
IAMs_20	Displacement amplitude measured according to IASPEI standard for surface-wave magnitude $MS(20)$
IVMs_BB	Velocity amplitude measured according to IASPEI standard for broadband surface-wave magnitude $MS(BB)$
IAmb	Displacement amplitude measured according to IASPEI standard for short-period teleseismic body-wave magnitude mb
IVmB_BB	Velocity amplitude measured according to IASPEI standard for broadband teleseismic body-wave magnitude $mB(BB)$
AX_IN	Displacement amplitude of phase of type X (e.g., PP, S, etc), measured on an instrument of type IN (e.g., SP - short-period, LP - long-period, BB - broadband)
VX_IN	Velocity amplitude of phase of type X and instrument of type IN (as above)
A	Unspecified displacement amplitude measurement
V	Unspecified velocity amplitude measurement
AML	Displacement amplitude measurement for nonstandard local magnitude
AMs	Displacement amplitude measurement for nonstandard surface-wave magnitude
Amb	Displacement amplitude measurement for nonstandard short-period body-wave magnitude
AmB	Displacement amplitude measurement for nonstandard medium to long-period body-wave magnitude
END	Time of visible end of record for duration magnitude

Unidentified Arrivals

x	unidentified arrival (old: i, e, NULL)
rx	unidentified regional arrival (old: i, e, NULL)
tx	unidentified teleseismic arrival (old: i, e, NULL)
Px	unidentified arrival of P type (old: i, e, NULL, (P), P?)
Sx	unidentified arrival of S type (old: i, e, NULL, (S), S?)
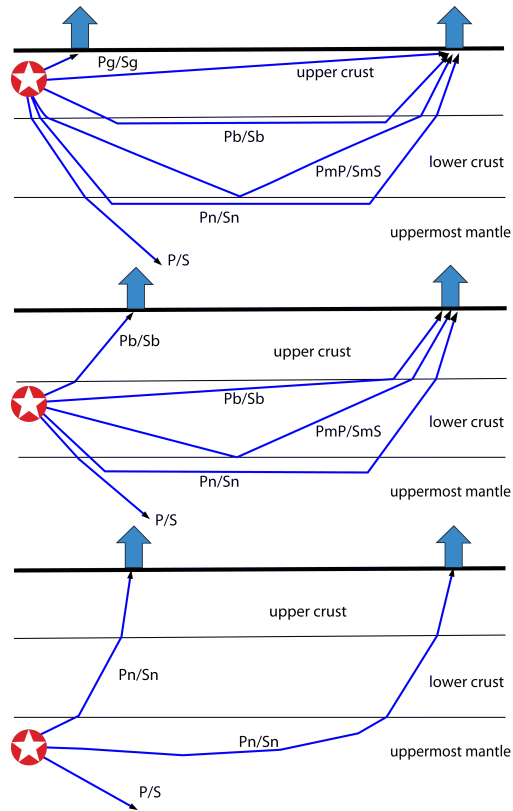
Figure 11.5: *Seismic 'crustal phases' observed in the case of a two-layer crust in local and regional distance ranges (0°<D< about 20°) from the seismic source in the: upper crust (top); lower crust (middle); and uppermost mantle (bottom).*
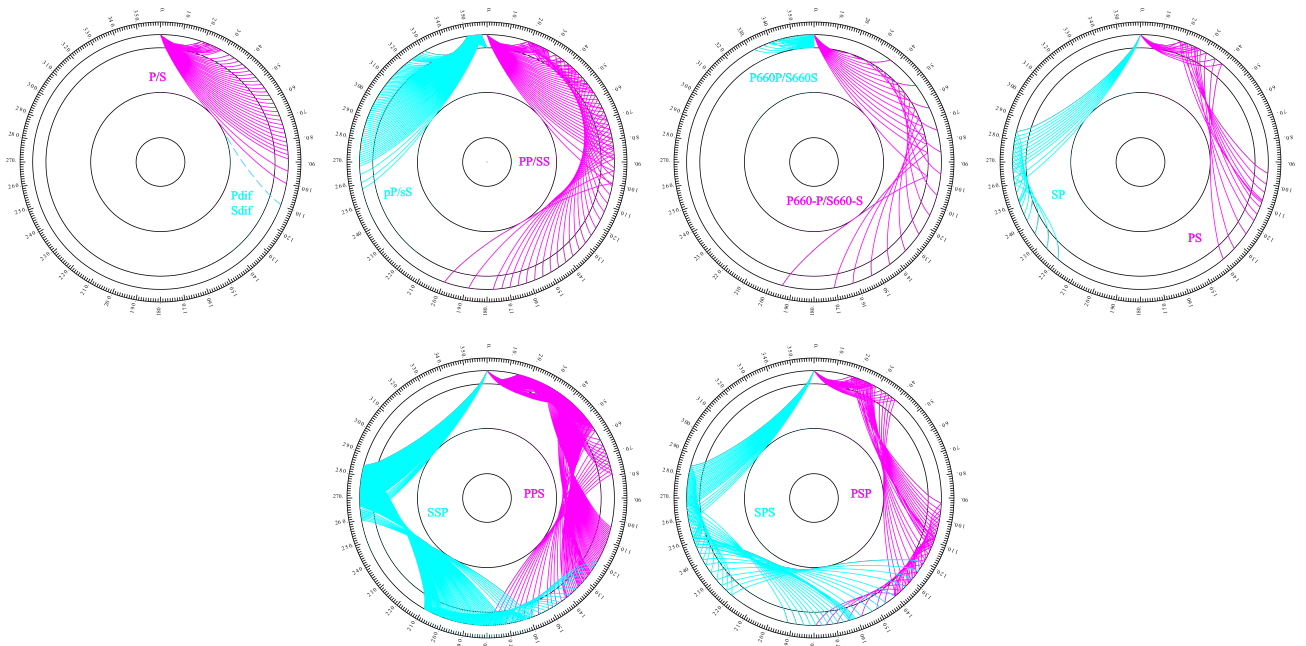
Figure 11.6: *Mantle phases observed at the teleseismic distance range D > about 20°.*
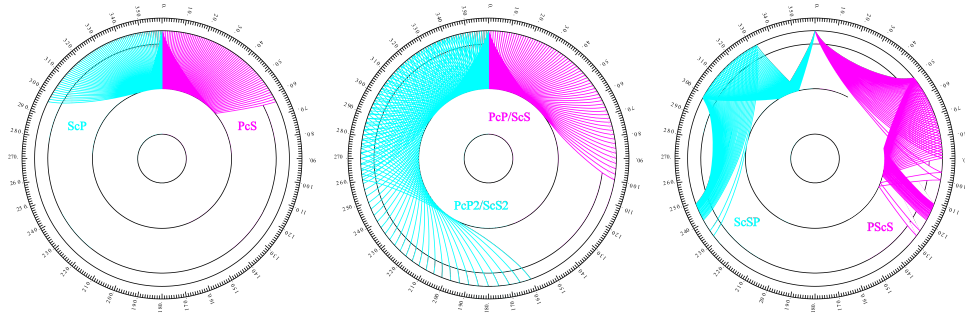
Figure 11.7: *Reflections from the Earth's core.*
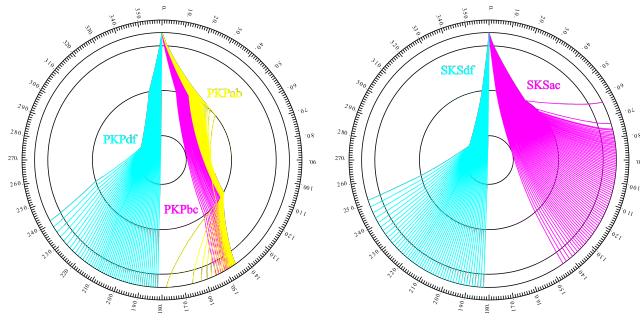
Figure 11.8: *Seismic rays of direct core phases.*
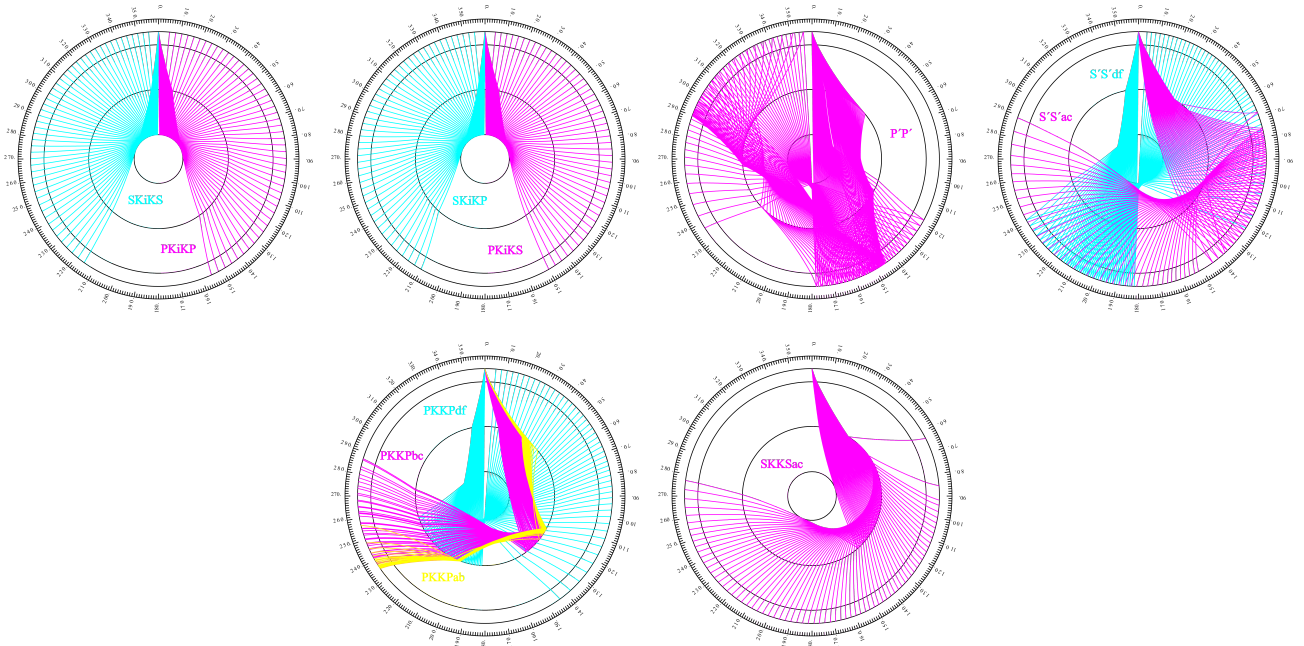
Figure 11.9: *Seismic rays of single-reflected core phases.*
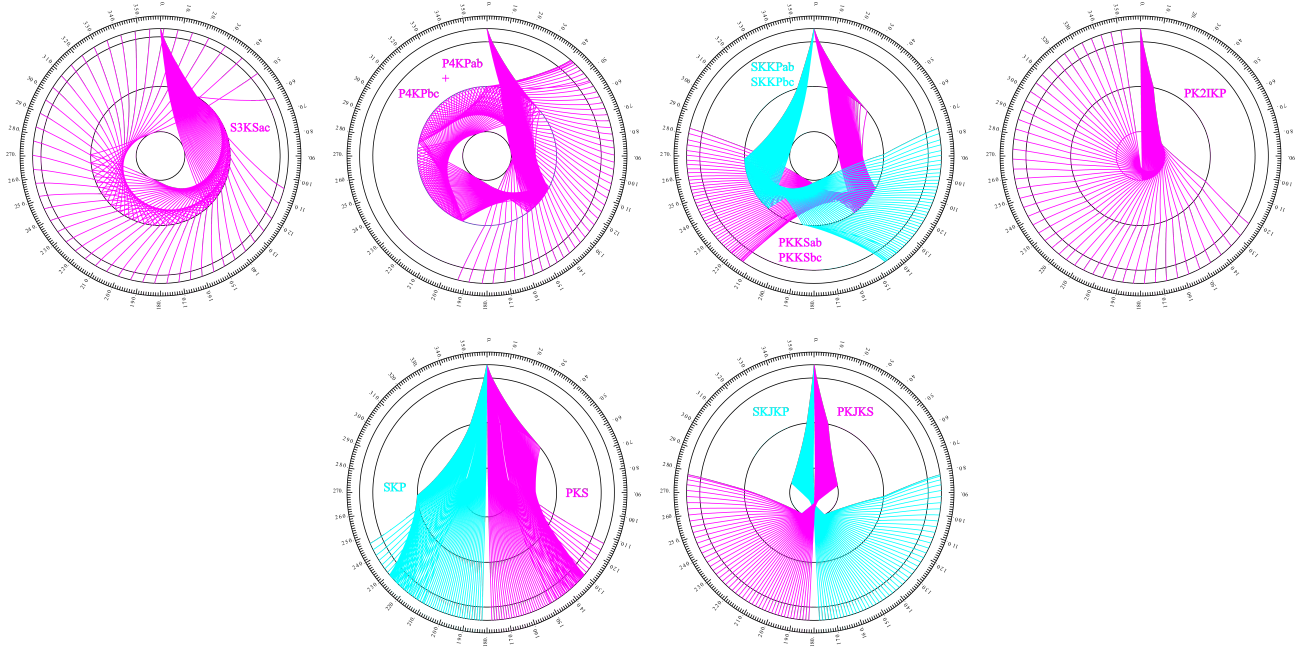
Figure 11.10: Seismic rays of multiple-reflected and converted core phases.

11.2.2 Flinn-Engdahl Regions

The Flinn-Engdahl regions were first proposed by *Flinn and Engdahl* (1965), with the standard defined by *Flinn et al.* (1974). The latest version of the schema, published by *Young et al.* (1996), divides the Earth into 50 seismic regions (Figure 11.11), which are further subdivided producing a total of 754 geographical regions (listed below). The geographic regions are numbered 1 to 757 with regions 172, 299 and 550 no longer in use. The boundaries of these regions are defined at one-degree intervals.
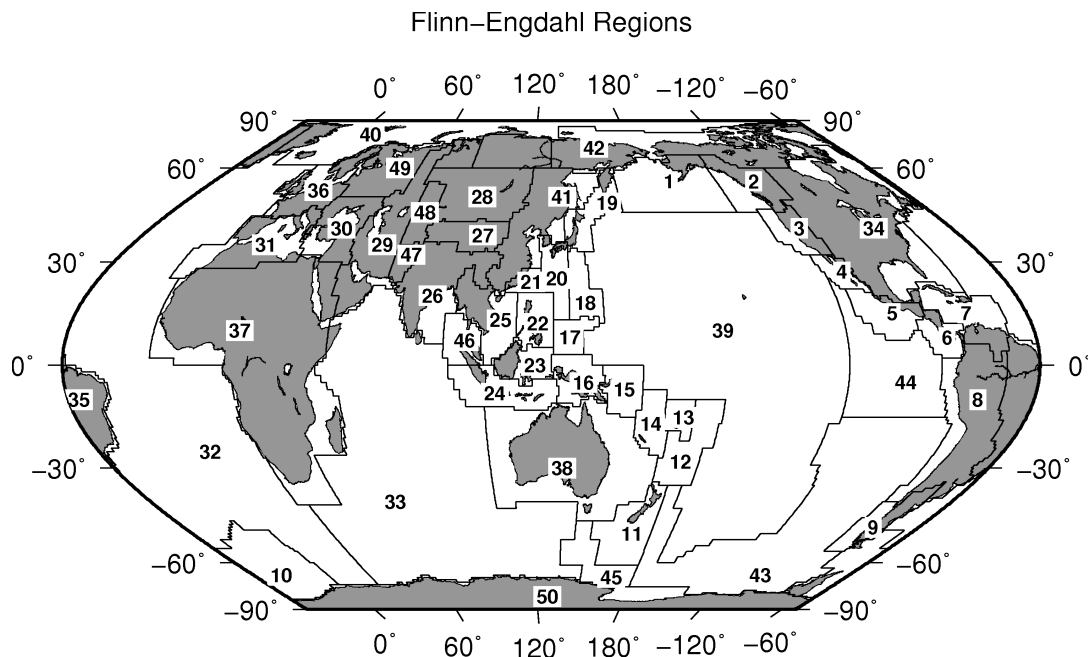
Figure 11.11: Map of all Flinn-Engdahl seismic regions.

Seismic Region 1
Alaska-Aleutian Arc
1. Central Alaska
2. Southern Alaska
3. Bering Sea
4. Komandorsky Islands region
5. Near Islands
6. Rat Islands
7. Andreanof Islands
8. Pribilof Islands
9. Fox Islands
10. Unimak Island region
11. Bristol Bay
12. Alaska Peninsula
13. Kodiak Island region
14. Kenai Peninsula
15. Gulf of Alaska
16. South of Aleutian Islands
17. South of Alaska

Seismic Region 2
Eastern Alaska to Vancouver Island
18. Southern Yukon Territory
19. Southeastern Alaska
20. Off coast of southeastern Alaska
21. West of Vancouver Island
22. Queen Charlotte Islands region
23. British Columbia
24. Alberta
25. Vancouver Island region
26. Off coast of Washington
27. Near coast of Washington
28. Washington-Oregon border region
29. Washington

Seismic Region 3
California-Nevada Region
30. Off coast of Oregon
31. Near coast of Oregon
32. Oregon
33. Western Idaho
34. Off coast of northern California
35. Near coast of northern California
36. Northern California
37. Nevada
38. Off coast of California
39. Central California
40. California-Nevada border region
41. Southern Nevada
42. Western Arizona
43. Southern California
44. California-Arizona border region
45. California-Baja California border region
46. Western Arizona-Sonora border

region

Seismic Region 4
Lower California and Gulf of California
47. Off west coast of Baja California
48. Baja California
49. Gulf of California
50. Sonora
51. Off coast of central Mexico
52. Near coast of central Mexico

Seismic Region 5
Mexico-Guatemala Area
53. Revilla Gigedo Islands region
54. Off coast of Jalisco
55. Near coast of Jalisco
56. Near coast of Michoacan
57. Michoacan
58. Near coast of Guerrero
59. Guerrero
60. Oaxaca
61. Chiapas
62. Mexico-Guatemala border region
63. Off coast of Mexico
64. Off coast of Michoacan
65. Off coast of Guerrero
66. Near coast of Oaxaca
67. Off coast of Oaxaca
68. Off coast of Chiapas
69. Near coast of Chiapas
70. Guatemala
71. Near coast of Guatemala
730. Northern East Pacific Rise

Seismic Region 6
Central America
72. Honduras
73. El Salvador
74. Near coast of Nicaragua
75. Nicaragua
76. Off coast of central America
77. Off coast of Costa Rica
78. Costa Rica
79. North of Panama
80. Panama-Costa Rica border region
81. Panama
82. Panama-Colombia border region
83. South of Panama

Seismic Region 7
Caribbean Loop
84. Yucatan Peninsula
85. Cuba region
86. Jamaica region

87. Haiti region
88. Dominican Republic region
89. Mona Passage
90. Puerto Rico region
91. Virgin Islands
92. Leeward Islands
93. Belize
94. Caribbean Sea
95. Windward Islands
96. Near north coast of Colombia
97. Near coast of Venezuela
98. Trinidad
99. Northern Colombia
100. Lake Maracaibo
101. Venezuela
731. North of Honduras

Seismic Region 8
Andean South America
102. Near west coast of Colombia
103. Colombia
104. Off coast of Ecuador
105. Near coast of Ecuador
106. Colombia-Ecuador border region
107. Ecuador
108. Off coast of northern Peru
109. Near coast of northern Peru
110. Peru-Ecuador border region
111. Northern Peru
112. Peru-Brazil border region
113. Western Brazil
114. Off coast of Peru
115. Near coast of Peru
116. Central Peru
117. Southern Peru
118. Peru-Bolivia border region
119. Northern Bolivia
120. Central Bolivia
121. Off coast of northern Chile
122. Near coast of northern Chile
123. Northern Chile
124. Chile-Bolivia border region
125. Southern Bolivia
126. Paraguay
127. Chile-Argentina border region
128. Jujuy Province
129. Salta Province
130. Catamarca Province
131. Tucuman Province
132. Santiago del Estero Province
133. Northeastern Argentina
134. Off coast of central Chile
135. Near coast of central Chile
136. Central Chile
137. San Juan Province
138. La Rioja Province
139. Mendoza Province

140. San Luis Province
141. Cordoba Province
142. Uruguay

Seismic Region 9
Extreme South America
143. Off coast of southern Chile
144. Southern Chile
145. Southern Chile-Argentina border region
146. Southern Argentina

Seismic Region 10
Southern Antilles
147. Tierra del Fuego
148. Falkland Islands region
149. Drake Passage
150. Scotia Sea
151. South Georgia Island region
152. South Georgia Rise
153. South Sandwich Islands region
154. South Shetland Islands
155. Antarctic Peninsula
156. Southwestern Atlantic Ocean
157. Weddell Sea
732. East of South Sandwich Islands

Seismic Region 11
New Zealand Region
158. Off west coast of North Island
159. North Island
160. Off east coast of North Island
161. Off west coast of South Island
162. South Island
163. Cook Strait
164. Off east coast of South Island
165. North of Macquarie Island
166. Auckland Islands region
167. Macquarie Island region
168. South of New Zealand

Seismic Region 12
Kermadec-Tonga-Samoa Area
169. Samoa Islands region
170. Samoa Islands
171. South of Fiji Islands
172. West of Tonga Islands (REGION NOT IN USE)
173. Tonga Islands
174. Tonga Islands region
175. South of Tonga Islands
176. North of New Zealand
177. Kermadec Islands region
178. Kermadec Islands
179. South of Kermadec Islands

Seismic Region 13
Fiji Area
180. North of Fiji Islands
181. Fiji Islands region
182. Fiji Islands

Seismic Region 14
Vanuatu (New Hebrides)
183. Santa Cruz Islands region
184. Santa Cruz Islands
185. Vanuatu Islands region
186. Vanuatu Islands
187. New Caledonia
188. Loyalty Islands
189. Southeast of Loyalty Islands

Seismic Region 15
Bismarck and Solomon Islands
190. New Ireland region
191. North of Solomon Islands
192. New Britain region
193. Bougainville-Solomon Islands region
194. D'Entrecasteaux Islands region
195. South of Solomon Islands

Seismic Region 16
New Guinea
196. Irian Jaya region
197. Near north coast of Irian Jaya
198. Ninigo Islands region
199. Admiralty Islands region
200. Near north coast of New Guinea
201. Irian Jaya
202. New Guinea
203. Bismarck Sea
204. Aru Islands region
205. Near south coast of Irian Jaya
206. Near south coast of New Guinea
207. Eastern New Guinea region
208. Arafura Sea

Seismic Region 17
Caroline Islands to Guam
209. Western Caroline Islands
210. South of Mariana Islands

Seismic Region 18
Guam to Japan
211. Southeast of Honshu
212. Bonin Islands region
213. Volcano Islands region
214. West of Mariana Islands
215. Mariana Islands region
216. Mariana Islands

Seismic Region 19
Japan-Kurils-Kamchatka
217. Kamchatka Peninsula
218. Near east coast of Kamchatka Peninsula
219. Off east coast of Kamchatka Peninsula
220. Northwest of Kuril Islands
221. Kuril Islands
222. East of Kuril Islands
223. Eastern Sea of Japan
224. Hokkaido region
225. Off southeast coast of Hokkaido
226. Near west coast of eastern Honshu
227. Eastern Honshu
228. Near east coast of eastern Honshu
229. Off east coast of Honshu
230. Near south coast of eastern Honshu

Seismic Region 20
Southwestern Japan and Ryukyu Islands
231. South Korea
232. Western Honshu
233. Near south coast of western Honshu
234. Northwest of Ryukyu Islands
235. Kyushu
236. Shikoku
237. Southeast of Shikoku
238. Ryukyu Islands
239. Southeast of Ryukyu Islands
240. West of Bonin Islands
241. Philippine Sea

Seismic Region 21
Taiwan
242. Near coast of southeastern China
243. Taiwan region
244. Taiwan
245. Northeast of Taiwan
246. Southwestern Ryukyu Islands
247. Southeast of Taiwan

Seismic Region 22
Philippines
248. Philippine Islands region
249. Luzon
250. Mindoro
251. Samar
252. Palawan
253. Sulu Sea
254. Panay

255. Cebu
256. Leyte
257. Negros
258. Sulu Archipelago
259. Mindanao
260. East of Philippine Islands

Seismic Region 23
Borneo-Sulawesi
261. Borneo
262. Celebes Sea
263. Talaud Islands
264. North of Halmahera
265. Minahassa Peninsula, Sulawesi
266. Northern Molucca Sea
267. Halmahera
268. Sulawesi
269. Southern Molucca Sea
270. Ceram Sea
271. Buru
272. Seram

Seismic Region 24
Sunda Arc
273. Southwest of Sumatera
274. Southern Sumatera
275. Java Sea
276. Sunda Strait
277. Jawa
278. Bali Sea
279. Flores Sea
280. Banda Sea
281. Tanimbar Islands region
282. South of Jawa
283. Bali region
284. South of Bali
285. Sumbawa region
286. Flores region
287. Sumba region
288. Savu Sea
289. Timor region
290. Timor Sea
291. South of Sumbawa
292. South of Sumba
293. South of Timor

Seismic Region 25
Myanmar and Southeast Asia
294. Myanmar-India border region
295. Myanmar-Bangladesh border region
296. Myanmar
297. Myanmar-China border region
298. Near south coast of Myanmar
299. Southeast Asia (REGION NOT IN USE)
300. Hainan Island

301. South China Sea
733. Thailand
734. Laos
735. Kampuchea
736. Vietnam
737. Gulf of Tongking

Seismic Region 26
India-Xizang-Szechwan-Yunnan
302. Eastern Kashmir
303. Kashmir-India border region
304. Kashmir-Xizang border region
305. Western Xizang-India border region
306. Xizang
307. Sichuan
308. Northern India
309. Nepal-India border region
310. Nepal
311. Sikkim
312. Bhutan
313. Eastern Xizang-India border region
314. Southern India
315. India-Bangladesh border region
316. Bangladesh
317. Northeastern India
318. Yunnan
319. Bay of Bengal

Seismic Region 27
Southern Xinjiang to Gansu
320. Kyrgyzstan-Xinjiang border region
321. Southern Xinjiang
322. Gansu
323. Western Nei Mongol
324. Kashmir-Xinjiang border region
325. Qinghai

Seismic Region 28
Alma-Ata to Lake Baikal
326. Southwestern Siberia
327. Lake Baykal region
328. East of Lake Baykal
329. Eastern Kazakhstan
330. Lake Issyk-Kul region
331. Kazakhstan-Xinjiang border region
332. Northern Xinjiang
333. Tuva-Buryatia-Mongolia border region
334. Mongolia

Seismic Region 29
Western Asia
335. Ural Mountains region
336. Western Kazakhstan
337. Eastern Caucasus
338. Caspian Sea
339. Northwestern Uzbekistan
340. Turkmenistan
341. Iran-Turkmenistan border region
342. Turkmenistan-Afghanistan border region
343. Turkey-Iran border region
344. Iran-Armenia-Azerbaijan border region
345. Northwestern Iran
346. Iran-Iraq border region
347. Western Iran
348. Northern and central Iran
349. Northwestern Afghanistan
350. Southwestern Afghanistan
351. Eastern Arabian Peninsula
352. Persian Gulf
353. Southern Iran
354. Southwestern Pakistan
355. Gulf of Oman
356. Off coast of Pakistan

Seismic Region 30
Middle East-Crimea-Eastern Balkans
357. Ukraine-Moldova-Southwestern Russia region
358. Romania
359. Bulgaria
360. Black Sea
361. Crimea region
362. Western Caucasus
363. Greece-Bulgaria border region
364. Greece
365. Aegean Sea
366. Turkey
367. Turkey-Georgia-Armenia border region
368. Southern Greece
369. Dodecanese Islands
370. Crete
371. Eastern Mediterranean Sea
372. Cyprus region
373. Dead Sea region
374. Jordan-Syria region
375. Iraq

Seismic Region 31
Western Mediterranean Area
376. Portugal
377. Spain

378. Pyrenees
379. Near south coast of France
380. Corsica
381. Central Italy
382. Adriatic Sea
383. Northwestern Balkan Peninsula
384. West of Gibraltar
385. Strait of Gibraltar
386. Balearic Islands
387. Western Mediterranean Sea
388. Sardinia
389. Tyrrhenian Sea
390. Southern Italy
391. Albania
392. Greece-Albania border region
393. Madeira Islands region
394. Canary Islands region
395. Morocco
396. Northern Algeria
397. Tunisia
398. Sicily
399. Ionian Sea
400. Central Mediterranean Sea
401. Near coast of Libya

Seismic Region 32
Atlantic Ocean
402. North Atlantic Ocean
403. Northern Mid-Atlantic Ridge
404. Azores Islands region
405. Azores Islands
406. Central Mid-Atlantic Ridge
407. North of Ascension Island
408. Ascension Island region
409. South Atlantic Ocean
410. Southern Mid-Atlantic Ridge
411. Tristan da Cunha region
412. Bouvet Island region
413. Southwest of Africa
414. Southeastern Atlantic Ocean
738. Reykjanes Ridge
739. Azores-Cape St. Vincent Ridge

Seismic Region 33
Indian Ocean
415. Eastern Gulf of Aden
416. Socotra region
417. Arabian Sea
418. Lakshadweep region
419. Northeastern Somalia
420. North Indian Ocean
421. Carlsberg Ridge
422. Maldive Islands region
423. Laccadive Sea
424. Sri Lanka
425. South Indian Ocean
426. Chagos Archipelago region

427. Mauritius-Reunion region
428. Southwest Indian Ridge
429. Mid-Indian Ridge
430. South of Africa
431. Prince Edward Islands region
432. Crozet Islands region
433. Kerguelen Islands region
434. Broken Ridge
435. Southeast Indian Ridge
436. Southern Kerguelen Plateau
437. South of Australia
740. Owen Fracture Zone region
741. Indian Ocean Triple Junction
742. Western Indian-Antarctic Ridge

Seismic Region 34
Eastern North America
438. Saskatchewan
439. Manitoba
440. Hudson Bay
441. Ontario
442. Hudson Strait region
443. Northern Quebec
444. Davis Strait
445. Labrador
446. Labrador Sea
447. Southern Quebec
448. Gaspe Peninsula
449. Eastern Quebec
450. Anticosti Island
451. New Brunswick
452. Nova Scotia
453. Prince Edward Island
454. Gulf of St. Lawrence
455. Newfoundland
456. Montana
457. Eastern Idaho
458. Hebgen Lake region, Montana
459. Yellowstone region
460. Wyoming
461. North Dakota
462. South Dakota
463. Nebraska
464. Minnesota
465. Iowa
466. Wisconsin
467. Illinois
468. Michigan
469. Indiana
470. Southern Ontario
471. Ohio
472. New York
473. Pennsylvania
474. Vermont-New Hampshire region
475. Maine
476. Southern New England

477. Gulf of Maine
478. Utah
479. Colorado
480. Kansas
481. Iowa-Missouri border region
482. Missouri-Kansas border region
483. Missouri
484. Missouri-Arkansas border region
485. Missouri-Illinois border region
486. New Madrid region, Missouri
487. Cape Girardeau region, Missouri
488. Southern Illinois
489. Southern Indiana
490. Kentucky
491. West Virginia
492. Virginia
493. Chesapeake Bay region
494. New Jersey
495. Eastern Arizona
496. New Mexico
497. Northwestern Texas-Oklahoma border region
498. Western Texas
499. Oklahoma
500. Central Texas
501. Arkansas-Oklahoma border region
502. Arkansas
503. Louisiana-Texas border region
504. Louisiana
505. Mississippi
506. Tennessee
507. Alabama
508. Western Florida
509. Georgia
510. Florida-Georgia border region
511. South Carolina
512. North Carolina
513. Off east coast of United States
514. Florida Peninsula
515. Bahama Islands
516. Eastern Arizona-Sonora border region
517. New Mexico-Chihuahua border region
518. Texas-Mexico border region
519. Southern Texas
520. Near coast of Texas
521. Chihuahua
522. Northern Mexico
523. Central Mexico
524. Jalisco
525. Veracruz
526. Gulf of Mexico
527. Bay of Campeche

Seismic Region 35
Eastern South America
528. Brazil
529. Guyana
530. Suriname
531. French Guiana

Seismic Region 36
Northwestern Europe
532. Eire
533. United Kingdom
534. North Sea
535. Southern Norway
536. Sweden
537. Baltic Sea
538. France
539. Bay of Biscay
540. The Netherlands
541. Belgium
542. Denmark
543. Germany
544. Switzerland
545. Northern Italy
546. Austria
547. Czech and Slovak Republics
548. Poland
549. Hungary

Seismic Region 37
Africa
550. Northwest Africa (REGION NOT IN USE)
551. Southern Algeria
552. Libya
553. Egypt
554. Red Sea
555. Western Arabian Peninsula
556. Chad region
557. Sudan
558. Ethiopia
559. Western Gulf of Aden
560. Northwestern Somalia
561. Off south coast of northwest Africa
562. Cameroon
563. Equatorial Guinea
564. Central African Republic
565. Gabon
566. Congo
567. Zaire
568. Uganda
569. Lake Victoria region
570. Kenya
571. Southern Somalia
572. Lake Tanganyika region
573. Tanzania
574. Northwest of Madagascar

575. Angola
576. Zambia
577. Malawi
578. Namibia
579. Botswana
580. Zimbabwe
581. Mozambique
582. Mozambique Channel
583. Madagascar
584. South Africa
585. Lesotho
586. Swaziland
587. Off coast of South Africa
743. Western Sahara
744. Mauritania
745. Mali
746. Senegal-Gambia region
747. Guinea region
748. Sierra Leone
749. Liberia region
750. Cote d'Ivoire
751. Burkina Faso
752. Ghana
753. Benin-Togo region
754. Niger
755. Nigeria

Seismic Region 38
Australia
588. Northwest of Australia
589. West of Australia
590. Western Australia
591. Northern Territory
592. South Australia
593. Gulf of Carpentaria
594. Queensland
595. Coral Sea
596. Northwest of New Caledonia
597. New Caledonia region
598. Southwest of Australia
599. Off south coast of Australia
600. Near coast of South Australia
601. New South Wales
602. Victoria
603. Near southeast coast of Australia
604. Near east coast of Australia
605. East of Australia
606. Norfolk Island region
607. Northwest of New Zealand
608. Bass Strait
609. Tasmania region
610. Southeast of Australia

Seismic Region 39
Pacific Basin
611. North Pacific Ocean

612. Hawaiian Islands region
613. Hawaiian Islands
614. Eastern Caroline Islands region
615. Marshall Islands region
616. Enewetak Atoll region
617. Bikini Atoll region
618. Gilbert Islands region
619. Johnston Island region
620. Line Islands region
621. Palmyra Island region
622. Kiritimati region
623. Tuvalu region
624. Phoenix Islands region
625. Tokelau Islands region
626. Northern Cook Islands
627. Cook Islands region
628. Society Islands region
629. Tubuai Islands region
630. Marquesas Islands region
631. Tuamotu Archipelago region
632. South Pacific Ocean

Seismic Region 40
Arctic Zone
633. Lomonosov Ridge
634. Arctic Ocean
635. Near north coast of Kalaallit Nunaat
636. Eastern Kalaallit Nunaat
637. Iceland region
638. Iceland
639. Jan Mayen Island region
640. Greenland Sea
641. North of Svalbard
642. Norwegian Sea
643. Svalbard region
644. North of Franz Josef Land
645. Franz Josef Land
646. Northern Norway
647. Barents Sea
648. Novaya Zemlya
649. Kara Sea
650. Near coast of northwestern Siberia
651. North of Severnaya Zemlya
652. Severnaya Zemlya
653. Near coast of northern Siberia
654. East of Severnaya Zemlya
655. Laptev Sea

Seismic Region 41
Eastern Asia
656. Southeastern Siberia
657. Priamurye-Northeastern China border region
658. Northeastern China
659. North Korea

660. Sea of Japan
661. Primorye
662. Sakhalin Island
663. Sea of Okhotsk
664. Southeastern China
665. Yellow Sea
666. Off east coast of southeastern China

Seismic Region 42
Northeastern Asia, Northern Alaska to Greenland
667. North of New Siberian Islands
668. New Siberian Islands
669. Eastern Siberian Sea
670. Near north coast of eastern Siberia
671. Eastern Siberia
672. Chukchi Sea
673. Bering Strait
674. St. Lawrence Island region
675. Beaufort Sea
676. Northern Alaska
677. Northern Yukon Territory
678. Queen Elizabeth Islands
679. Northwest Territories
680. Western Kalaallit Nunaat
681. Baffin Bay
682. Baffin Island region

Seismic Region 43
Southeastern and Antarctic Pacific Ocean
683. Southeastcentral Pacific Ocean
684. Southern East Pacific Rise
685. Easter Island region
686. West Chile Rise

687. Juan Fernandez Islands region
688. East of North Island
689. Chatham Islands region
690. South of Chatham Islands
691. Pacific-Antarctic Ridge
692. Southern Pacific Ocean
756. Southeast of Easter Island

Seismic Region 44
Galapagos Area
693. Eastcentral Pacific Ocean
694. Central East Pacific Rise
695. West of Galapagos Islands
696. Galapagos Islands region
697. Galapagos Islands
698. Southwest of Galapagos Islands
699. Southeast of Galapagos Islands
757. Galapagos Triple Junction region

Seismic Region 45
Macquarie Loop
700. South of Tasmania
701. West of Macquarie Island
702. Balleny Islands region

Seismic Region 46
Andaman Islands to Sumatera
703. Andaman Islands region
704. Nicobar Islands region
705. Off west coast of northern Sumatera
706. Northern Sumatera
707. Malay Peninsula
708. Gulf of Thailand

Seismic Region 47
Baluchistan
709. Southeastern Afghanistan
710. Pakistan
711. Southwestern Kashmir
712. India-Pakistan border region

Seismic Region 48
Hindu Kush and Pamir
713. Central Kazakhstan
714. Southeastern Uzbekistan
715. Tajikistan
716. Kyrgyzstan
717. Afghanistan-Tajikistan border region
718. Hindu Kush region
719. Tajikistan-Xinjiang border region
720. Northwestern Kashmir

Seismic Region 49
Northern Eurasia
721. Finland
722. Norway-Murmansk border region
723. Finland-Karelia border region
724. Baltic States-Belarus-Northwestern Russia
725. Northwestern Siberia
726. Northern and central Siberia

Seismic Region 50
Antarctica
727. Victoria Land
728. Ross Sea
729. Antarctica

11.2.3 IASPEI Magnitudes

The ISC publishes a diversity of magnitude data. Although trying to be as complete and specific as possible, preference is now given to magnitudes determined according to standard procedures recommended by the Working Group on Magnitude Measurements of the IASPEI Commission on Seismological Observation and Interpretation (CoSOI). So far, such standards have been agreed upon for the local magnitude ML, the local-regional mb_Lg, and for two types each of body-wave (mb and mB_BB) and surface-wave magnitudes (Ms_20 and Ms_BB). With the exception of ML, all other standard magnitudes are measured on vertical-component records only. BB stands for direct measurement on unfiltered velocity broadband records in a wide range of periods, provided that their passband covers at least the period range within which mB_BB and Ms_BB are supposed to be measured. Otherwise, a deconvolution has to be applied prior to the amplitude and period measurement so as to assure that this specification is met. In contrast, mb_Lg, mb and Ms_20 are based on narrowband amplitude measurements around periods of 1 s and 20 s, respectively.

ML is consistent with the original definition of the local magnitude by *Richter* (1935) and mB_BB in close agreement with the original definition of medium-period body-wave magnitude mB measured in a wide range of periods between some 2 to 20 s and calibrated with the *Gutenberg and Richter* (1956) Q-function for vertical-component P waves. Similarly, Ms_BB is best tuned to the unbiased use of the IASPEI (1967) recommended standard magnitude formula for surface-wave amplitudes in a wide range of periods and distances, as proposed by its authors *Vaněk et al.* (1962). In contrast, mb and Ms_20 are chiefly based on measurement standards defined by US agencies in the 1960s in conjunction with the global deployment of the World-Wide Standard Seismograph Network (WWSSN), which did not include medium or broadband recordings. Some modifications were made in the 1970s to account for IASPEI recommendations on extended measurement time windows for mb. Although not optimal for calibrating narrow-band spectral amplitudes measured around 1 s and 20 s only, mb and Ms_20 use the same original calibrations functions as mB_BB and Ms_BB. But mb and Ms_20 data constitute by far the largest available magnitude data sets. Therefore they continue to be used, with appreciation for their advantages (e.g., mb is by far the most frequently measured teleseismic magnitude and often the only available and reasonably good magnitude estimator for small earthquakes) and their shortcomings (see section 3.2.5.2 of Chapter 3 in NMSOP-2).

Abbreviated descriptions of the standard procedures for ML, mb_Lg, mb, mB_BB and Ms_BB are summarised below. For more details, including also the transfer functions of the simulation filters to be used, see www.iaspei.org/commissions/CSOI/Summary_WG-Recommendations_20130327.pdf.

All amplitudes used in the magnitude formulas below are in most circumstances to be measured as one-half the maximum deflection of the seismogram trace, peak-to-adjacent-trough or trough-to-adjacent-peak, where the peak and trough are separated by one crossing of the zero-line: this measurement is sometimes described as "one-half peak-to-peak amplitude." The periods are to be measured as twice the time-intervals separating the peak and adjacent-trough from which the amplitudes are measured. The amplitude-phase arrival-times are to be measured and reported too as the time of the zero-crossing between the peak and adjacent-trough from which the amplitudes are measured. The issue of amplitude and period measuring procedures, and circumstances under which alternative procedures are acceptable or preferable, is discussed further in Section 5 of IS 3.3 and in section 3.2.3.3 of Chapter 3 of NMSOP-2.

Amplitudes measured according to recommended IASPEI standard procedures should be reported with the following ISF amplitude "phase names": IAML, IAmb_Lg, IAmb, IAMs_20, IVmB_BB and IVMs_BB. "I" stands for "International" or "IASPEI", "A" for displacement amplitude, measured in nm, and "V" for velocity amplitude, measured in nm/s. Although the ISC will calculate standard surface-wave magnitudes only for earthquakes shallower than 60 km, contributing agencies or stations are encouraged to report standard amplitude measurements of IAMs_20 and IVMs_BB for deeper earthquakes as well.

Note that the commonly known classical calibration relationships have been modified in the following to be consistent with displacements measured in nm, and velocities in nm/s, which is now common with high-resolution digital data and analysis tools. With these general definitions of the measurement parameters, where R is hypocentral distance in km (typically less than 1000 km), Δ is epicentral distance in degrees and h is hypocentre depth in km, the standard formulas and procedures read as follows:

ML:

$$ML = \log_{10}(A) + 1.11 \log_{10} R + 0.00189 R - 2.09 \qquad (11.14)$$

for crustal earthquakes in regions with attenuative properties similar to those of southern California, and with A being the maximum trace amplitude in nm that is measured on output from a horizontal-component instrument that is filtered so that the response of the seismograph/filter system replicates that of a Wood-Anderson standard seismograph (but with a static magnification of 1). For the normalised simulated response curve and related poles and zeros see Figure 1 and Table 1 in IS 3.3 of NMSOP-2.

Equation (11.14) is an expansion of that of *Hutton and Boore* (1987). The constant term in equation (11.14), -2.09, is based on an experimentally determined static magnification of the Wood-Anderson of 2080 (see *Uhrhammer and Collins* (1990)), rather than the theoretical magnification of 2800 that was specified by the seismograph´s manufacturer. The formulation of equation (11.14) assures that reported ML amplitude data are not affected by uncertainty in the static magnification of the Wood-Anderson seismograph.

For seismographic stations containing two horizontal components, amplitudes are measured independently from each horizontal component and each amplitude is treated as a single datum. There is no effort to measure the two observations at the same time, and there is no attempt to compute a vector average. For crustal earthquakes in regions with attenuative properties that are different from those of coastal California and for measuring magnitudes with vertical-component seismographs the constants in the above equation have to be re-determined to adjust for the different regional attenuation and travel paths as well as for systematic differences between amplitudes measured on horizontal and vertical seismographs.

mb_Lg:

$$mb\_Lg = \log_{10}(A) + 0.833 \log_{10} R + 0.434 \gamma (R - 10) - 0.87 \qquad (11.15)$$

where A = "sustained ground-motion amplitude" in nm, defined as the third largest amplitude in the time window corresponding to group velocities of 3.6 to 3.2 km/s, in the period (T) range 0.7 s to 1.3

s; R = epicentral distance in km, γ = coefficient of attenuation in km^{-1}. γ is related to the quality factor Q through the equation $\gamma = \pi/(QUT)$, where U is group velocity and T is the wave period of the L_g wave. γ is a strong function of crustal structure and should be determined specifically for the region in which the mb_Lg is to be used. A and T are measured on output from a vertical-component instrument that is filtered so that the frequency response of the seismograph/filter system replicates that of a WWSSN short-period seismograph (see Figure 1 and Table 1 in IS 3.3 of NMSOP-2). Arrival times with respect to the origin of the seismic disturbance are used, along with epicentral distance, to compute group velocity U.

mb:

$$mb = \log_{10}(A/T) + Q(\Delta, h) - 3.0 \tag{11.16}$$

where A = vertical component P-wave ground amplitude in nm measured at distances $20° \leq \Delta \leq 100°$ and calculated from the maximum trace-amplitude with $T < 3$ s in the entire P-phase train (time spanned by P, pP, sP, and possibly PcP and their codas, and ending preferably before PP). A and T are measured on output from an instrument that is filtered so that the frequency response of the seismograph/filter system replicates that of a WWSSN short-period seismograph (see Figure 1 and Table 1 in IS 3.3 of NMSOP-2). A is determined by dividing the maximum trace amplitude by the magnification of the simulated WWSSN-SP response at period T.

$Q(\Delta, h)$ = attenuation function for PZ (P-waves recorded on vertical component seismographs) established by *Gutenberg and Richter* (1956) in the tabulated or algorithmic form as used by the U.S. Geological Survey/National Earthquake Information Center (USGS/NEIC) (see Table 2 in IS 3.3 and program description PD 3.1 in NMSOP-2);

mB_BB:

$$mB\_BB = \log_{10}(Vmax/2\pi) + Q(\Delta, h) - 3.0 \tag{11.17}$$

where $Vmax$ = vertical component ground velocity in nm/s at periods between 0.2 s $< T <$ 30 s, measured in the range $20° \leq \Delta \leq 100°$. $Vmax$ is calculated from the maximum trace-amplitude in the entire P-phase train (see mb), as recorded on a seismogram that is proportional to velocity at least in the period range of measurements. $Q(\Delta, h)$ = attenuation function for PZ established by *Gutenberg and Richter* (1956) (see 11.16). Equation (11.16) differs from the equation for mB of *Gutenberg and Richter* (1956) by virtue of the $log_{10}(Vmax/2\pi)$ term, which replaces the classical $\log_{10}(A/T)_{max}$ term. Contributors should continue to send observations of A and T to ISC.

Ms_20:

$$Ms\_20 = \log_{10}(A/T) + 1.66 \log_{10} \Delta + 0.3 \tag{11.18}$$

where A = vertical-component ground displacement in nm at $20° \leq \Delta \leq 160°$ epicentral distance measured from the maximum trace amplitude of a surface-wave phase having a period T between 18 s and 22 s on a waveform that has been filtered so that the frequency response of the seismograph/filter

replicates that of a WWSSN long-period seismograph (see Figure 1 and Table 1 in IS 3.3 of NMSOP-2). A is determined by dividing the maximum trace amplitude by the magnification of the simulated WWSSN-LP response at period T. Equation (11.18) is formally equivalent to the Ms equation proposed by *Vaněk et al.* (1962) but is here applied to vertical motion measurements in a narrow range of periods.

Ms_BB:

$$Ms\_BB = \log_{10}\left(Vmax/2\pi\right) + 1.66\log_{10}\Delta + 0.3 \tag{11.19}$$

where $Vmax$ = vertical-component ground velocity in nm/s associated with the maximum trace-amplitude in the surface-wave train at periods between 3 s $< T <$ 60 s as recorded at distances $2° \leq \Delta \leq 160°$ on a seismogram that is proportional to velocity in that range of considered periods. Equation (11.19) is based on the Ms equation proposed by *Vaněk et al.* (1962), but is here applied to vertical motion measurements and is used with the $\log_{10}\left(Vmax/2\pi\right)$ term replacing the $\log_{10}\left(A/T\right)_{max}$ term of the original. As for mB_BB, observations of A and T should be reported to ISC.

Mw:

$$Mw = \left(\log_{10}M_0 - 9.1\right)/1.5 \tag{11.20}$$

Moment magnitude Mw is calculated from data of the scalar seismic moment M_0 (when given in Nm), or

$$Mw = \left(\log_{10}M_0 - 16.1\right)/1.5 \tag{11.21}$$

its CGS equivalent when M_0 is in dyne·cm.

Please note that the magnitude nomenclature used in this Section uses the IASPEI standards as the reference. However, the magnitude type is typically written in plain text in most typical data reports and so it is in this document. Moreover, writing magnitude types in plain text allows us to reproduce the magnitude type as stored in the database and provides a more direct identification of the magnitude type reported by different agencies. A short description of the common magnitude types available in this Summary is given in table 8.6.

11.2.4   The IASPEI Seismic Format (ISF)

The ISF is the IASPEI approved standard format for the exchange of parametric seismological data (hypocentres, magnitudes, phase arrivals, moment tensors etc.) and is one of the formats used by the ISC. It was adopted as standard in August 2001 and is an extension of the International Monitoring System 1.0 (IMS1.0) standard, which was developed for exchanging data used to monitor the Comprehensive Nuclear-Test-Ban Treaty. An example of the ISF is shown in Listing 11.1.

Bulletins which use the ISF are comprised of origin and arrival information, provided in a series of data blocks. These include: a bulletin title block; an event title block; an origin block; a magnitude sub-block; an effect block; a reference block; and a phase block.

Within these blocks an important extension of the IMS1.0 standard is the ability to add additional comments and thus provide further parametric information. The ISF comments are distinguishable within the open parentheses required for IMS1.0 comments by beginning with a hash mark (#) followed by a keyword identifying the type of formatted comment. Each additional line required in the ISF comment begins with the hash (within the comment parentheses) followed by blank spaces at least as long as the keyword. Optional lines within the comment are signified with a plus sign (+) instead of a hash mark. The keywords include PRIME (to designate a prime origin of a hypocentre); CENTROID (to indicate the centroid origin); MOMTENS (moment tensor solution); FAULT_PLANE (fault plane solution); PRINAX (principal axes); PARAM (an origin parameter e.g. hypocentre depth given by a depth phase).

The full documentation for the ISF is maintained at the ISC and can be downloaded from:
www.isc.ac.uk/doc/code/isf/isf.pdf

The documentation for the IMS1.0 standard can be downloaded from:
www.isc.ac.uk/doc/code/isf/ims1_0.pdf

Listing 11.1: *Example of an ISF formatted event*

```
Event 15146084 Near east coast of eastern Honshu
   Date       Time        Err   RMS Latitude Longitude  Smaj  Smin  Az Depth   Err Ndef Nsta Gap  mdist  Mdist Qual     Author      OrigID
2010/09/01 07:32:00                  37.9000  141.9000f         44.0                                             NIED       17047453
 (#MOMTENS sc    M0 fCLVD   MRR    MTT    MPP    MRT    MTP    MPR NST1 NST2 Author   )
 (#              eM0 eCLVD  eRR    eTT    ePP    eRT    eTP    ePR NCO1 NCO2 Duration )
 (#       16 5.760                                              NIED           )
 (#                                                                            )
 (#FAULT_PLANE Typ Strike   Dip    Rake  NP  NS Plane Author   )
 (#            BDC 199.00  19.00   86.00            NIED        )
 (+             23.00  71.00   91.00                 )
 (Epicenter information from JMA Focal Mechanism Solution Determined Manually Variance reduction = 96.98%)
2010/09/01 07:32:47.50      1.470  37.8300  142.2400            37.0          71       281  11.00  51.10    uk BJI       15275482
2010/09/01 07:32:52.20      0.92   38.0320  141.8090  6.7  4.5 110 44.0       114                          MOS         16741494
2010/09/01 07:32:52.53 0.35 0.889  37.9202  141.8229 4.090 2.740 145  49.7  2.76  490  478 122   0.65  92.01 m i fe ISCJB    01631732
 (#PARAM pP_DEPTH=41.11021)
2010/09/01 07:32:52.60      0.10   37.9100  141.8700  1.1  0.9  -1 43.0  1.0                              fe JMA       16271222
 (Felt I=III-III J1)
2010/09/01 07:32:53.66 0.42 0.770  37.9250  141.7880  5.1  3.4 140  44.4  3.9  102       127   3.17 127.67    fe NEIC     01134459
 (#MOMTENS sc    M0 fCLVD   MRR    MTT    MPP    MRT    MTP    MPR NST1 NST2 Author   )
 (#              eM0 eCLVD  eRR    eTT    ePP    eRT    eTP    ePR NCO1 NCO2 Duration )
 (#       16 5.800         3.600 -0.550 -3.040  1.850 -1.140 4.150        NIED      )
 (#                                                                            )
 (#FAULT_PLANE Typ Strike   Dip    Rake  NP  NS Plane Author   )
 (#            BDC 199.00  19.00   86.00            NIED        )
 (+             23.00  71.00   91.00                 )
 (Recorded [3 JMA] in Miyagi; [2 JMA] in Fukushima and Iwate; [1 JMA] in Akita, Aomori, Ibaraki, Tochigi and Yamagata.)
2010/09/01 07:32:53.70      0.20   37.9300  142.0600 2.224 1.112  -1  50.3  1.0  262   89                            GCMT        00124877
 (#CENTROID)
 (#MOMTENS sc    M0 fCLVD   MRR    MTT    MPP    MRT    MTP    MPR NST1 NST2 Author   )
 (#              eM0 eCLVD  eRR    eTT    ePP    eRT    eTP    ePR NCO1 NCO2 Duration )
 (#       16 6.891         5.430 -0.440 -4.990  1.500 -2.070 3.710  64   89 GCMT     )
 (#               0.173  0.118  0.120  0.100  0.094  0.110 102  160      0.90 )
 (#FAULT_PLANE Typ Strike   Dip    Rake  NP  NS Plane Author   )
 (#            BDC  22.00  63.00   91.00            GCMT        )
 (+            201.00  27.00   89.00                 )
 (#PRINAX sc  T_val T_azim  T_pl  B_val B_azim  B_pl  P_val P_azim  P_pl Author   )
 (#       16  6.711 293.00  72.00  0.360 201.00  0.00 -7.072 111.00 18.00 GCMT     )
 (nsta1 refers to body waves, cutoff=40s. nsta2 refers to surface waves, cutoff=50s.)
2010/09/01 07:32:55.05      1.77 1.070  37.8692  141.9450  12.9 10.4 100  63.6  16.8   36       127   3.24 117.04    uk IDC      16680924
2010/09/01 07:32:52.23 0.30 1.333  37.8836  141.9148 5.558 4.001 142  38.9  2.33  542  478  61   0.72 141.68 m i se ISC      01237353
 (#PRIME)
 (#PARAM pP_DEPTH=39.00000)

Magnitude  Err Nsta Author      OrigID
Mw    5.1           NIED       17047453
Ms    4.8      61   BJI        15275482
Ms7   4.6      58   BJI        15275482
mB    5.1      48   BJI        15275482
mb    5.0      63   BJI        15275482
MS    4.7      19   MOS        16741494
mb    5.2      49   MOS        16741494
MS    4.6      43   ISCJB      01631732
mb    4.9     138   ISCJB      01631732
      5.0           JMA        16271222
mb    5.0      55   NEIC       01134459
MW    5.1           NIED       01134459
MW    5.2      89   GCMT       00124877
MS    4.4 0.1  28   IDC        16680924
Ms1   4.4 0.1  28   IDC        16680924
mb    4.4 0.1  27   IDC        16680924
mb1   4.5 0.0  33   IDC        16680924
mb1mx 4.4 0.0  37   IDC        16680924
mbtmp 4.7 0.1  33   IDC        16680924
ms1mx 4.3 0.1  31   IDC        16680924
MS    4.7 0.2  43   ISC        01237353
mb    4.9 0.2 145   ISC        01237353

Sta    Dist  EvAz Phase      Time      TRes  Azim AzRes  Slow   SRes Def  SNR      Amp   Per Qual Magnitude   ArrID
JIO    0.72 322.1 Pn      07:33:05.9  -0.06                    T__                d_           49540510
JIO    0.72 322.1 Sn      07:33:15.0  -0.82                    T__                d_           49540511
JMM    0.89 269.2 Pn      07:33:08.4   0.2                     T__                d_           49540512
JMM    0.89 269.2 Sn      07:33:19.2  -0.68                    T__                d_           49540513
JFK    0.97 238.3 Pn      07:33:09.5   0.1                     T__                d_           49540514
JFK    0.97 238.3 Sn      07:33:21.5  -0.54                    T__                __           49540515
JOU    1.10 296.4 Pn      07:33:11.5   0.4                     T__                d_           49540516
JOU    1.10 296.4 Sn      07:33:25.4   0.3                     T__                _e           49540517
ONAJ   1.18 229.0 Pn      07:33:12.4   0.1                     T__                d_           49540530
JMK    1.20 333.1 Pn      07:33:12.5   0.0                     T__                d_           49540518
JMK    1.20 333.1 Sn      07:33:27.1  -0.39                    T__                _e           49540519
OFUJ   1.21 350.9 Pn      07:33:12.3  -0.34                    T__                d_           49540531
.
.
.
532A   91.05  49.8 P      07:45:52.799 -0.00  90.9             T__                --           05504129
334A   91.18  47.9 P      07:45:54.012  0.7   91.0             T__                --           05504128
HO6N1  91.36  64.9 T      09:27:33.559                         ___   6.0          --           58438458
MIAR   91.43  42.9 P      07:45:54.85   0.5   91.2             T__                --           05504179
Y39A   91.60  43.6 P      07:45:55.543  0.4   91.4             T__                --           05504214
534A   91.98  49.0 P      07:45:57.308  0.2   91.8             T__                --           05504130
KEST   94.59 323.1 LR     08:33:52.432       320.5    38.70    ___       466.5 18.65 --         58438480
ESDC   96.70 334.2 LR     08:34:40.011       345.0    38.30    ___       375.8 20.18 --         58438449
TORD  117.01 315.6 PKPdf  07:51:32.55  -0.82  17.7     2.30    T__   5.1   0.4  0.70 --         58438504
TORD  117.01 315.6 PP     07:52:39.3   -2.90  31.2     6.30    T__   6.5   1.3  0.68 --         58438505
QSPA  127.62 180.0 PKPdf  07:51:52.02  -0.16                   T__                _e           23535420
SNAA  141.68 197.1 PKPdf  07:52:13.751 -4.52                   T__                --           20375340
VNA2  143.24 196.3 PKPbc  07:52:18.562  0.4  122.0     2.31    ___                --           20375338
VNA1  143.64 196.2 PKPbc  07:52:19.77   0.6                    ___                --           20375339
```

11.2.5 Ground Truth (GT) Events

Accurate locations are crucial in testing Earth models derived from body and surface wave tomography as well as in location calibration studies. 'Ground Truth' (GT) events are well-established source locations and origin times. A database of IASPEI reference events (GT earthquakes and explosions) is hosted at the ISC (www.isc.ac.uk). A full description of GT selection criteria can be found in *Bondár and McLaughlin* (2009a).

The events are coded by category GT0, GT1, GT2 or GT5, where the epicentre of a GT X event is known to within X km to a 95% confidence level. A map of all IASPEI reference events is shown in Figure 11.12 and the types of event are categorised in Figure 11.13. GT0 are explosions with announced locations and origin times. GT1 and GT2 are typically explosions, mine blasts or rock bursts either associated to explosion phenomenology located upon overhead imagery with seismically determined origin times, or precisely located by in-mine seismic networks. GT1-2 events are assumed to be shallow, but depth is unknown.

The database consists of nuclear explosions of GT0–5 quality, adopted from the Nuclear Explosion Database (*Bennett et al.*, 2010); GT0–5 chemical explosions, rock bursts, mine-induced events, as well as a few earthquakes, inherited from the reference event set by *Bondár et al.* (2004); GT5 events (typically earthquakes with crustal depths) which have been identified using either the method of *Bondár et al.* (2008) (2,275 events) or *Bondár and McLaughlin* (2009a) (updated regularly from the EHB catalogue (*Engdahl et al.*, 1998)), which uses the following criteria:

- 10 or more stations within 150 km from the epicentre

- one or more stations within 10 km

- $\Delta U \leq 0.35$

- a secondary azimuthal gap $\leq 160°$

where ΔU is the network quality metric defined as the mean absolute deviation between the best-fitting uniformly distributed network of stations and the actual network:

$$\Delta U = \frac{4 \sum |esaz_i - (unif_i + b)|}{360N}, 0 \leq \Delta U \leq 1 \tag{11.22}$$

where N is the number of stations, $esaz_i$ is the ith event-to-station azimuth, $unif_i = 360i/N$ for $i = 0$, ..., $N - 1$, and $b = avg(esaz_i) - avg(unif_i)$. ΔU is normalised so that it is 0 when the stations are uniformly distributed in azimuth and 1 when all the stations are at the same azimuth.

The seismological community is invited to participate in this project by nominating seismic events for the reference event database. Submitters may be contacted for further confirmation and for arrival time data. The IASPEI Reference Event List will be periodically published both in written and electronic form with proper acknowledgement of all submitters.
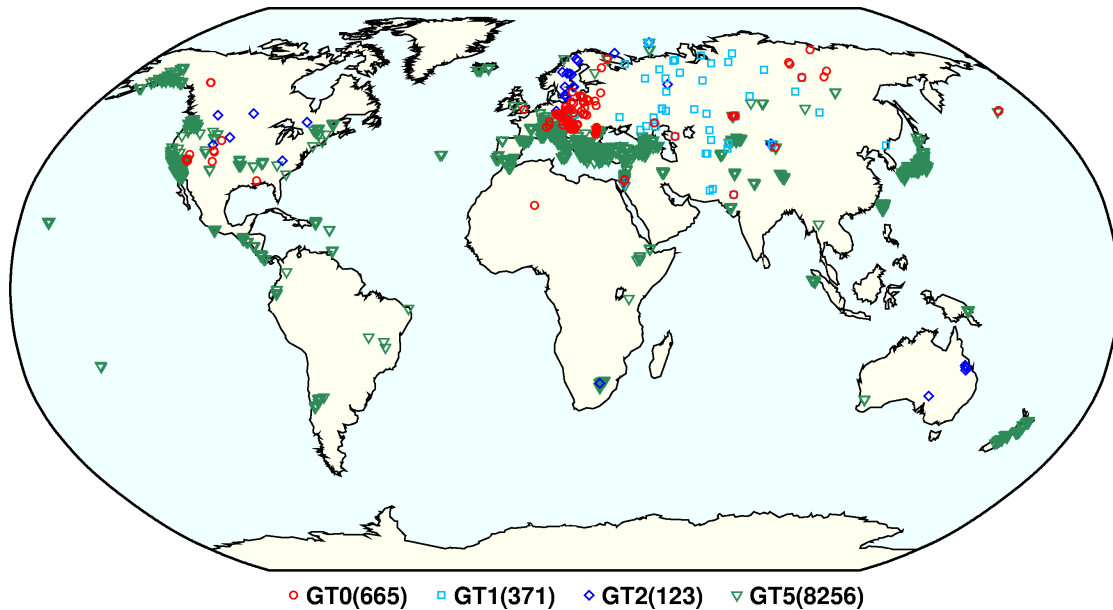
Figure 11.12: *Map of all IASPEI Reference Events as of April 2020.*

Figure 11.13: *Histogram showing the event types within the IASPEI Reference Event list as of April 2020.*
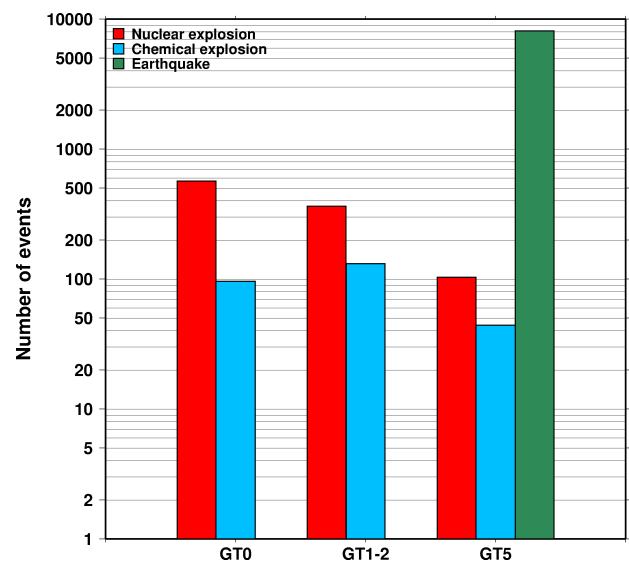
11.2.6   Nomenclature of Event Types

The nomenclature of event types currently used in the ISC Bulletin takes its origin from the IASPEI International Seismic Format (ISF).

Event type codes are composed of a leading character that generally indicates the confidence with which the type of the event is asserted and a trailing character that generally gives the type of the event. The leading and trailing characters may be used in any combination.

The **leading** characters are:

- s = suspected
- k = known
- f = felt (implies known)
- d = damaging (implies felt and known)

The **trailing** characters are:

- c = meteoritic event
- e = earthquake
- h = chemical explosion
- i = induced event
- l = landslide
- m = mining explosion
- n = nuclear explosion
- r = rock burst
- x = experimental explosion

A chemical explosion might be for mining or experimental purposes, and it is conceivable that other types of event might be assigned two or more different event type codes. This is deliberate, and matches the ambiguous identification of events in existing databases.

In addition, the code `uk` is used for events of unknown type and `ls` is used for known landslides.

The frequency of the different event types designated in the ISC Bulletin since 1964 is indicated in Figure 11.14.
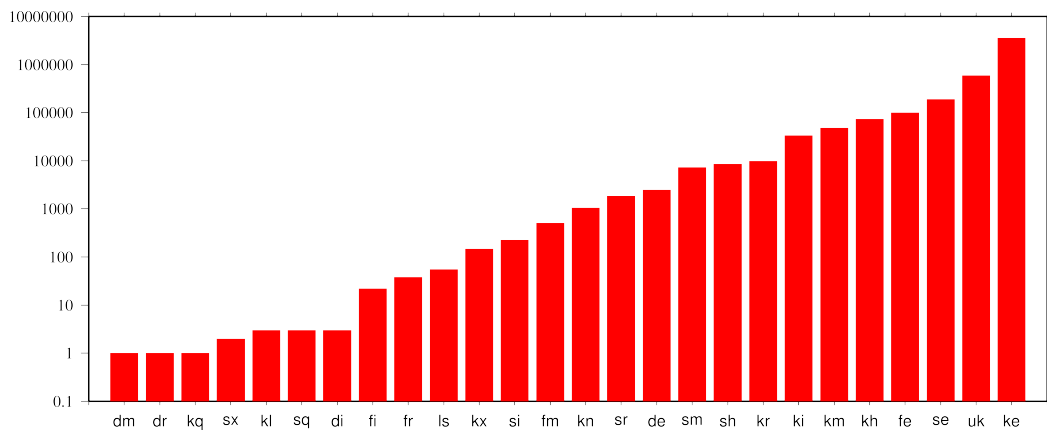
Figure 11.14: *Event types in the ISC Bulletin*

There are currently plans to revise this nomenclature as part of the coordination process between the National Earthquake Information Center (NEIC/USGS), European-Mediterranean Seismological Centre (CSEM) and the ISC.

11.3   Tables

Table 11.2: *Listing of all 381 agencies that have directly reported to the ISC. The 147 agencies highlighted in bold have reported data to the ISC Bulletin for the period of this Bulletin Summary.*

Agency Code	Agency Name
AAA	Alma-ata, Kazakhstan
AAE	**University of Addis Ababa**, **Ethiopia**
AAM	University of Michigan, USA
ADE	**Primary Industries and Resources SA**, **Australia**
ADH	Observatorio Afonso Chaves, Portugal
AEIC	Alaska Earthquake Information Center, USA
AFAR	The Afar Depression: Interpretation of the 1960-2000 Earthquakes, Israel
AFUA	University of Alabama, USA
ALG	Algiers University, Algeria
ANDRE	, USSR
ANF	USArray Array Network Facility, USA
ANT	Antofagasta, Chile
ARE	Instituto Geofisico del Peru, Peru
ARO	Observatoire Géophysique d'Arta, Djibouti
ASIES	**Institute of Earth Sciences, Academia Sinica**, **Chinese Taipei**
ASL	Albuquerque Seismological Laboratory, USA
ASM	University of Asmara, Eritrea
ASRS	**Altai-Sayan Seismological Centre, GS SB RAS**, **Russia**
ATA	The Earthquake Research Center Ataturk University, Turkey
ATH	**National Observatory of Athens**, **Greece**
AUST	**Geoscience Australia**, **Australia**
AVETI	, USSR
AWI	**Alfred Wegener Institute for Polar and Marine Research**, **Germany**
AZER	**Republican Seismic Survey Center of Azerbaijan National Academy of Sciences**, **Azerbaijan**
BCIS	Bureau Central International de Sismologie, France
BDF	Observatório Sismológico da Universidade de Brasília, Brazil
BELR	**Centre of Geophysical Monitoring of the National Academy of Sciences of Belarus**, **Republic of Belarus**
BEO	**Seismological Survey of Serbia**, **Serbia**
BER	**University of Bergen**, **Norway**
BERK	Berkheimer H, Germany
BGR	**Bundesanstalt für Geowissenschaften und Rohstoffe**, **Germany**
BGS	**British Geological Survey**, **United Kingdom**
BGSI	Botswana Geoscience Institute, Botswana
BHUJ2	Study of Aftershocks of the Bhuj Earthquake by Japanese Research Team, Japan
BIAK	Biak earthquake aftershocks (17-Feb-1996), USA
BJI	**China Earthquake Networks Center**, **China**
BKK	Thai Meteorological Department, Thailand
BNS	Erdbebenstation, Geologisches Institut der Universität, Köl, Germany
BOG	Universidad Javeriana, Colombia
BRA	**Geophysical Institute, Slovak Academy of Sciences**, **Slovakia**

Table 11.2: *Continued.*

Agency Code	Agency Name
BRG	**Seismological Observatory Berggießhübel, TU Bergakademie Freiberg**, **Germany**
BRK	Berkeley Seismological Laboratory, USA
BRS	Brisbane Seismograph Station, Australia
BUC	**National Institute for Earth Physics**, **Romania**
BUD	Geodetic and Geophysical Research Institute, Hungary
BUEE	Earth & Environment, USA
BUG	Institute of Geology, Mineralogy & Geophysics, Germany
BUL	**Goetz Observatory**, **Zimbabwe**
BUT	Montana Bureau of Mines and Geology, USA
BYKL	**Baykal Regional Seismological Centre, GS SB RAS**, **Russia**
CADCG	Central America Data Centre, Costa Rica
CAN	Australian National University, Australia
CANSK	Canadian and Scandinavian Networks, Sweden
CAR	Instituto Sismologico de Caracas, Venezuela
CASC	Central American Seismic Center, Costa Rica
CENT	Centennial Earthquake Catalog, USA
CERI	Center for Earthquake Research and Information, USA
CFUSG	**Inst. of Seismology and Geodynamics, V.I. Vernadsky Crimean Federal University**, **Republic of Crimea**
CLL	**Geophysikalisches Observatorium Collm**, **Germany**
CMWS	Laboratory of Seismic Monitoring of Caucasus Mineral Water Region, GSRAS, Russia
CNG	Seismographic Station Changalane, Mozambique
CNRM	**Centre National de Recherche**, **Morocco**
COSMOS	Consortium of Organizations for Strong Motion Observations, USA
CRAAG	**Centre de Recherche en Astronomie, Astrophysique et Géophysique**, **Algeria**
CSC	University of South Carolina, USA
CSEM	Centre Sismologique Euro-Méditerranéen (CSEM/EMSC), France
CUPWA	**Curtin University**, **Australia**
DASA	Defense Atomic Support Agency, USA
DBN	Koninklijk Nederlands Meteorologisch Instituut, Netherlands
DDA	**Disaster and Emergency Management Presidency**, **Turkey**
DHMR	Yemen National Seismological Center, Yemen
DIAS	Dublin Institute for Advanced Studies, Ireland
DJA	**Badan Meteorologi, Klimatologi dan Geofisika**, **Indonesia**
DMN	**National Seismological Centre, Nepal**, **Nepal**
DNAG	, USA
DNK	**Geological Survey of Denmark and Greenland**, **Denmark**
DRS	Dagestan Branch, Geophysical Survey, Russian Academy of Sciences, Russia
DSN	**Dubai Seismic Network**, **United Arab Emirates**
DUSS	Damascus University, Syria, Syria
EAF	East African Network, Unknown
EAGLE	Ethiopia-Afar Geoscientific Lithospheric Experiment, Unknown
EBR	Observatori de l'Ebre, Spain

Table 11.2: *Continued.*

Agency Code	Agency Name
EBSE	Ethiopian Broadband Seismic Experiment, Unknown
ECGS	European Center for Geodynamics and Seismology, Luxembourg
ECX	**Centro de Investigación Científica y de Educación Superior de Ensenada**, **Mexico**
EFATE	OBS Experiment near Efate, Vanuatu, USA
EHB	Engdahl, van der Hilst and Buland, USA
EIDC	Experimental (GSETT3) International Data Center, USA
EKA	Eskdalemuir Array Station, United Kingdom
ENT	Geological Survey and Mines Department, Uganda
EPSI	Reference events computed by the ISC for EPSI project, United Kingdom
ERDA	Energy Research and Development Administration, USA
EST	Geological Survey of Estonia, Estonia
EUROP	, Unknown
EVBIB	Data from publications listed in the ISC Event Bibliography, Unknown
FBR	Fabra Observatory, Spain
FCIAR	Federal Center for Integrated Arctic Research, Russia
FDF	Fort de France, Martinique
FIA0	Finessa Array, Finland
FOR	Unknown Historical Agency, Unknown - historical agency
FUBES	Earth Science Dept., Geophysics Section, Germany
FUNV	**Fundación Venezolana de Investigaciones Sismológicas**, **Venezuela**
FUR	Geophysikalisches Observatorium der Universität München, Germany
GBZT	Marmara Research Center, Turkey
GCG	**INSIVUMEH, Guatemala**
GCMT	**The Global CMT Project**, **USA**
GDNRW	Geologischer Dienst Nordrhein-Westfalen, Germany
GEN	**Dipartimento per lo Studio del Territorio e delle sue Risorse (RSNI)**, **Italy**
GEOAZ	UMR Géoazur, France
GEOMR	GEOMAR, Germany
GFZ	Helmholtz Centre Potsdam GFZ German Research Centre For Geosciences, Germany
GII	**The Geophysical Institute of Israel**, **Israel**
GOM	Observatoire Volcanologique de Goma, Democratic Republic of the Congo
GRAL	**National Council for Scientific Research**, **Lebanon**
GSDM	**Geological Survey Department Malawi**, **Malawi**
GSET2	Group of Scientific Experts Second Technical Test 1991, April 22 - June 2, Unknown
GTFE	German Task Force for Earthquakes, Germany
GUC	**Centro Sismológico Nacional, Universidad de Chile**, **Chile**
HAN	Hannover, Germany
HDC	Observatorio Vulcanológico y Sismológico de Costa Rica, Costa Rica
HEL	**Institute of Seismology, University of Helsinki**, **Finland**
HFS	Hagfors Observatory, Sweden
HFS1	Hagfors Observatory, Sweden

Table 11.2: *Continued.*

Agency Code	Agency Name
HFS2	Hagfors Observatory, Sweden
HIMNT	Himalayan Nepal Tibet Experiment, USA
HKC	**Hong Kong Observatory**, **Hong Kong**
HLUG	Hessisches Landesamt für Umwelt und Geologie, Germany
HLW	**National Research Institute of Astronomy and Geophysics**, **Egypt**
HNR	Ministry of Mines, Energy and Rural Electrification, Solomon Islands
HON	Pacific Tsunami Warning Center - NOAA, USA
HRVD	Harvard University, USA
HRVD_LR	Department of Geological Sciences, Harvard University, USA
HVO	Hawaiian Volcano Observatory, USA
HYB	**National Geophysical Research Institute**, **India**
HYD	National Geophysical Research Institute, India
IAG	Instituto Andaluz de Geofisica, Spain
IASBS	Institute for Advanced Studies in Basic Sciences, Iran
IASPEI	IASPEI Working Group on Reference Events, USA
ICE	Instituto Costarricense de Electricidad, Costa Rica
IDC	**International Data Centre, CTBTO**, **Austria**
IDG	Institute of Dynamics of Geosphere, Russian Academy of Sciences, Russia
IEC	Institute of the Earth Crust, SB RAS, Russia
IEPN	**Institute of Environmental Problems of the North, Russian Academy of Sciences**, **Russia**
IGGSL	Seismology Lab, Institute of Geology & Geophysics, Chinese Academy of Sciences, China
IGIL	**Instituto Dom Luiz, University of Lisbon**, **Portugal**
IGQ	**Servicio Nacional de Sismología y Vulcanología**, **Ecuador**
IGS	Institute of Geological Sciences, United Kingdom
INAM	Instituto Nacional de Meteorologia e Geofisica - INAMET, Angola
INDEPTH3	International Deep Profiling of Tibet and the Himalayas, USA
INET	**Instituto Nicaraguense de Estudios Territoriales - INETER**, **Nicaragua**
INMG	**Instituto Português do Mar e da Atmosfera, I.P.**, **Portugal**
INMGC	Instituto Nacional de Meteorologia e Geofísica, Cape Verde
IPEC	**The Institute of Physics of the Earth (IPEC)**, **Czech Republic**
IPER	Institute of Physics of the Earth, Academy of Sciences, Moscow, Russia
IPGP	Institut de Physique du Globe de Paris, France
IPRG	Institute for Petroleum Research and Geophysics, Israel
IRIS	**IRIS Data Management Center**, **USA**
IRSM	Institute of Rock Structure and Mechanics, Czech Republic
ISK	**Kandilli Observatory and Research Institute**, **Turkey**
ISN	**Iraqi Meteorological and Seismology Organisation**, **Iraq**
ISS	International Seismological Summary, United Kingdom
IST	Institute of Physics of the Earth, Technical University of Istanbul, Turkey
ISU	**Institute of Seismology, Academy of Sciences, Republic of Uzbekistan**, **Uzbekistan**
ITU	Faculty of Mines, Department of Geophysical Engineering, Turkey

Table 11.2: *Continued.*

Agency Code	Agency Name
JEN	Geodynamisches Observatorium Moxa, Germany
JMA	**Japan Meteorological Agency**, **Japan**
JOH	Bernard Price Institute of Geophysics, South Africa
JSN	**Jamaica Seismic Network**, **Jamaica**
JSO	**Jordan Seismological Observatory**, **Jordan**
KBC	Institut de Recherches Géologiques et Minières, Cameroon
KEA	**Korea Earthquake Administration**, **Democratic People's Republic of Korea**
KEW	Kew Observatory, United Kingdom
KHC	Geofysikalni Ustav, Ceske Akademie Ved, Czech Republic
KISR	Kuwait Institute for Scientific Research, Kuwait
KLM	**Malaysian Meteorological Service**, **Malaysia**
KMA	**Korea Meteorological Administration**, **Republic of Korea**
KNET	**Kyrgyz Seismic Network**, **Kyrgyzstan**
KOLA	**Kola Regional Seismic Centre, GS RAS**, **Russia**
KRAR	Krasnoyarsk Scientific Research Inst. of Geology and Mineral Resources, Russia, Russia
KRL	Geodätisches Institut der Universität Karlsruhe, Germany
KRNET	**Institute of Seismology, Academy of Sciences of Kyrgyz Republic**, **Kyrgyzstan**
KRSC	**Kamchatkan Experimental and Methodical Seismological Department, GS RAS**, **Russia**
KRSZO	**Geodetic and Geophysical Reasearch Institute, Hungarian Academy of Sciences**, **Hungary**
KSA	Observatoire de Ksara, Lebanon
KUK	Geological Survey Department of Ghana, Ghana
LAO	Large Aperture Seismic Array, USA
LDG	**Laboratoire de Détection et de Géophysique/CEA**, **France**
LDN	University of Western Ontario, Canada
LDO	Lamont-Doherty Earth Observatory, USA
LED	Landeserdbebendienst Baden-Württemberg, Germany
LEDBW	Landeserdbebendienst Baden-Württemberg, Germany
LER	Besucherbergwerk Binweide Station, Germany
LIB	Tripoli, Libya
LIC	**Station Géophysique de Lamto**, **Ivory Coast**
LIM	Lima, Peru
LIS	Instituto de Meteorologia, Portugal
LIT	**Geological Survey of Lithuania**, **Lithuania**
LJU	**Slovenian Environment Agency**, **Slovenia**
LPA	**Universidad Nacional de La Plata**, **Argentina**
LPZ	Observatorio San Calixto, Bolivia
LRSM	Long Range Seismic Measurements Project, Unknown
LSZ	**Geological Survey Department of Zambia**, **Zambia**
LVSN	**Latvian Seismic Network**, **Latvia**
MAN	**Philippine Institute of Volcanology and Seismology**, **Philippines**
MAT	The Matsushiro Seismological Observatory, Japan
MATSS	, USSR

Table 11.2: *Continued.*

Agency Code	Agency Name
MCO	**Macao Meteorological and Geophysical Bureau, Macao, China**
MCSM	**Main Centre for Special Monitoring, Ukraine**
MDD	**Instituto Geográfico Nacional, Spain**
MED_RCMT	**MedNet Regional Centroid - Moment Tensors, Italy**
MERI	Maharashta Engineering Research Institute, India
MES	Messina Seismological Observatory, Italy
MEX	**Instituto de Geofísica de la UNAM, Mexico**
MIRAS	**Mining Institute of the Ural Branch of the Russian Academy of Sciences, Russia**
MNH	Institut für Angewandte Geophysik der Universitat Munchen, Germany
MOLD	**Institute of Geophysics and Geology, Moldova**
MOS	**Geophysical Survey of Russian Academy of Sciences, Russia**
MOZ	Direccao Nacional de Geologia, Mozambique
MOZAR	, Mozambique
MRB	**Institut Cartogràfic i Geològic de Catalunya, Spain**
MSI	Messina Seismological Observatory, Italy
MSSP	**Micro Seismic Studies Programme, PINSTECH, Pakistan**
MSUGS	Michigan State University, Department of Geological Sciences, USA
MUN	Mundaring Observatory, Australia
NAI	University of Nairobi, Kenya
NAM	**The Geological Survey of Namibia, Namibia**
NAO	**Stiftelsen NORSAR, Norway**
NCEDC	Northern California Earthquake Data Center, USA
NDI	**National Centre for Seismology of the Ministry of Earth Sciences of India, India**
NEIC	**National Earthquake Information Center, USA**
NEIS	National Earthquake Information Service, USA
NERS	**North Eastern Regional Seismological Centre, GS RAS, Russia**
NIC	**Cyprus Geological Survey Department, Cyprus**
NIED	**National Research Institute for Earth Science and Disaster Prevention, Japan**
NKSZ	, USSR
NNC	**National Nuclear Center, Kazakhstan**
NORS	North Ossetia (Alania) Branch, Geophysical Survey, Russian Academy of Sciences, Russia
NOU	**IRD Centre de Nouméa, New Caledonia**
NSSC	National Syrian Seismological Center, Syria
NSSP	**National Survey of Seismic Protection, Armenia**
OBM	Research Centre of Astronomy and Geophysics, Mongolia
OGAUC	Centro de Investigação da Terra e do Espaço da Universidade de Coimbra, Portugal
OGSO	Ohio Geological Survey, USA
OMAN	**Sultan Qaboos University, Oman**
ORF	Orfeus Data Center, Netherlands
OSPL	**Observatorio Sismologico Politecnico Loyola, Dominican Republic**
OSUB	Osservatorio Sismologico Universita di Bari, Italy

Table 11.2: Continued.

Agency Code	Agency Name
OTT	**Canadian Hazards Information Service, Natural Resources Canada, Canada**
PAL	Palisades, USA
PAS	California Institute of Technology, USA
PDA	Universidade dos Açores, Portugal
PDG	**Seismological Institute of Montenegro, Montenegro**
PEK	Peking, China
PGC	Pacific Geoscience Centre, Canada
PLV	**Institute of Geophysics, Viet Nam Academy of Science and Technology, Viet Nam**
PMEL	Pacific seismicity from hydrophones, USA
PMR	Alaska Tsunami Warning Center,, USA
PNNL	Pacific Northwest National Laboratory, USA
PNSN	**Pacific Northwest Seismic Network, USA**
PPT	**Laboratoire de Géophysique/CEA, French Polynesia**
PRE	**Council for Geoscience, South Africa**
PRU	**Geophysical Institute, Academy of Sciences of the Czech Republic, Czech Republic**
PTO	Instituto Geofísico da Universidade do Porto, Portugal
PTWC	Pacific Tsunami Warning Center, USA
QCP	Manila Observatory, Philippines
QUE	Pakistan Meteorological Department, Pakistan
QUI	Escuela Politécnica Nacional, Ecuador
RAB	Rabaul Volcanological Observatory, Papua New Guinea
RBA	Université Mohammed V, Morocco
REN	MacKay School of Mines, USA
REY	**Icelandic Meteorological Office, Iceland**
RHSSO	**Republic Hydrometeorological Service, Seismological Observatory, Banja Luka, Bosnia and Herzegovina**
RISSC	**Laboratory of Research on Experimental and Computational Seimology, Italy**
RMIT	Royal Melbourne Institute of Technology, Australia
ROC	Odenbach Seismic Observatory, USA
ROM	**Istituto Nazionale di Geofisica e Vulcanologia, Italy**
RRLJ	Regional Research Laboratory Jorhat, India
RSMAC	Red Sísmica Mexicana de Apertura Continental, Mexico
RSNC	**Red Sismológica Nacional de Colombia, Colombia**
RSPR	**Red Sísmica de Puerto Rico, USA**
RYD	King Saud University, Saudi Arabia
SAPSE	Southern Alps Passive Seismic Experiment, New Zealand
SAR	Sarajevo Seismological Station, Bosnia and Herzegovina
SBDV	, USSR
SCB	**Observatorio San Calixto, Bolivia**
SCEDC	Southern California Earthquake Data Center, USA
SCSIO	Key Laboratory of Ocean and Marginal Sea Geology, South China Sea, China

Table 11.2: *Continued.*

Agency Code	Agency Name
SDD	**Universidad Autonoma de Santo Domingo, Dominican Republic**
SEA	Geophysics Program AK-50, USA
SET	Setif Observatory, Algeria
SFS	**Real Instituto y Observatorio de la Armada, Spain**
SGS	**Saudi Geological Survey, Saudi Arabia**
SHL	Central Seismological Observatory, India
SIGU	**Subbotin Institute of Geophysics, National Academy of Sciences, Ukraine**
SIK	Seismic Institute of Kosovo, Unknown
SIO	Scripps Institution of Oceanography, USA
SJA	**Instituto Nacional de Prevención Sísmica, Argentina**
SJS	Instituto Costarricense de Electricidad, Costa Rica
SKHL	**Sakhalin Experimental and Methodological Seismological Expedition, GS RAS, Russia**
SKL	Sakhalin Complex Scientific Research Institute, Russia
SKO	**Seismological Observatory Skopje, FYR Macedonia**
SLC	Salt Lake City, USA
SLM	Saint Louis University, USA
SNET	**Servicio Nacional de Estudios Territoriales, El Salvador**
SNM	New Mexico Institute of Mining and Technology, USA
SNSN	Saudi National Seismic Network, Saudi Arabia
SOF	**Geophysical Institute, Bulgarian Academy of Sciences, Bulgaria**
SOMC	**Seismological Observatory of Mount Cameroon, Cameroon**
SOME	**Seismological Experimental Methodological Expedition, Kazakhstan**
SPA	USGS - South Pole, Antarctica
SPGM	Service de Physique du Globe, Morocco
SPITAK	, Armenia
SRI	Stanford Research Institute, USA
SSN	**Sudan Seismic Network, Sudan**
SSNC	**Servicio Sismológico Nacional Cubano, Cuba**
SSS	Centro de Estudios y Investigaciones Geotecnicas del San Salvador, El Salvador
STK	Stockholm Seismological Station, Sweden
STR	**EOST / RéNaSS, France**
STU	Stuttgart Seismological Station, Germany
SVSA	**Sistema de Vigilância Sismológica dos Açores, Portugal**
SYO	**National Institute of Polar Research, Japan**
SZGRF	Seismologisches Zentralobservatorium Gräfenberg, Germany
TAC	Estación Central de Tacubaya, Mexico
TAN	**Antananarivo, Madagascar**
TANZANIA	Tanzania Broadband Seismic Experiment, USA
TAP	**Central Weather Bureau (CWB), Chinese Taipei**
TAU	University of Tasmania, Australia
TEH	**Tehran University, Iran**
TEIC	Center for Earthquake Research and Information, USA

Table 11.2: *Continued.*

Agency Code	Agency Name
THE	**Department of Geophysics, Aristotle University of Thessaloniki**, **Greece**
THR	**International Institute of Earthquake Engineering and Seismology (IIEES)**, **Iran**
TIF	**Institute of Earth Sciences/ National Seismic Monitoring Center**, **Georgia**
TIR	**The Institute of Seismology, Academy of Sciences of Albania**, **Albania**
TRI	**Istituto Nazionale di Oceanografia e di Geofisica Sperimentale (OGS)**, **Italy**
TRN	**The Seismic Research Centre**, **Trinidad and Tobago**
TTG	Titograd Seismological Station, Montenegro
TUL	Oklahoma Geological Survey, USA
TUN	**Institut National de la Météorologie**, **Tunisia**
TVA	Tennessee Valley Authority, USA
TZN	University of Dar Es Salaam, Tanzania
UAF	Department of Geosciences, USA
UATDG	The University of Arizona, Department of Geosciences, USA
UAV	Red Sismológica de Los Andes Venezolanos, Venezuela
UCB	University of Colorado, Boulder, USA
UCC	**Royal Observatory of Belgium**, **Belgium**
UCDES	Department of Earth Sciences, United Kingdom
UCR	**Sección de Sismología, Vulcanología y Exploración Geofísica**, **Costa Rica**
UCSC	Earth & Planetary Sciences, USA
UESG	School of Geosciences, United Kingdom
UGN	Institute of Geonics AS CR, Czech Republic
ULE	University of Leeds, United Kingdom
UNAH	Universidad Nacional Autonoma de Honduras, Honduras
UPA	**Universidad de Panama**, **Panama**
UPIES	Institute of Earth- and Environmental Science, Germany
UPP	**University of Uppsala**, **Sweden**
UPSL	**University of Patras, Department of Geology**, **Greece**
UREES	Department of Earth and Environmental Science, USA
USAEC	United States Atomic Energy Commission, USA
USCGS	United States Coast and Geodetic Survey, USA
USGS	United States Geological Survey, USA
UTEP	Department of Geological Sciences, USA
UUSS	The University of Utah Seismograph Stations, USA
UVC	Universidad del Valle, Colombia
UWMDG	University of Wisconsin-Madison, Department of Geoscience, USA
VAO	**Instituto Astronomico e Geofísico**, **Brazil**
VIE	**Zentralanstalt für Meteorologie und Geodynamik (ZAMG)**, **Austria**
VKMS	Lab. of Seismic Monitoring, Voronezh region, GSRAS & Voronezh State University, Russia
VLA	Vladivostok Seismological Station, Russia

Table 11.2: *Continued.*

Agency Code	Agency Name
VSI	University of Athens, Greece
VUW	Victoria University of Wellington, New Zealand
WAR	**Institute of Geophysics, Polish Academy of Sciences**, **Poland**
WASN	, USA
WBNET	**Institute of Geophysics, Czech Academy of Sciences**, **Czech Republic**
WEL	**Institute of Geological and Nuclear Sciences**, **New Zealand**
WES	Weston Observatory, USA
WUSTL	Washington University Earth and Planentary Sciences, USA
YARS	**Yakutiya Regional Seismological Center, GS SB RAS**, **Russia**
ZAG	**Seismological Survey of the Republic of Croatia**, **Croatia**
ZEMSU	, USSR
ZUR	**Swiss Seismological Service (SED)**, **Switzerland**
ZUR_RMT	Zurich Moment Tensors, Switzerland

Table 11.3: *Phases reported to the ISC. These include phases that could not be matched to an appropriate* ak135 *phases. Those agencies that reported at least 10% of a particular phase are also shown.*

Reported Phase	Total	Agencies reporting
P	4761392	ROM (26%)
AML	2545289	ROM (91%)
S	2193625	ROM (27%), JMA (17%), TAP (14%)
NULL	441901	IDC (35%), NEIC (27%), RSNC (12%)
IAmb	396015	NEIC (97%)
Pn	347085	NEIC (30%), ISK (28%)
Pg	326978	ISK (31%)
IAML	258869	NEIC (59%), GUC (17%)
Sg	222369	ISK (26%)
LR	140000	IDC (68%), BJI (26%)
pmax	123405	MOS (68%), BJI (32%)
Sn	87111	IDC (12%), LDG (11%), ISK (11%)
SG	75886	HEL (59%), PRU (22%)
PG	70130	HEL (62%), PRU (17%), IPEC (11%)
Lg	67738	NNC (46%), SOME (35%), IDC (11%)
IAMs_20	41386	NEIC (98%)
MSG	34746	HEL (100%)
PN	33416	HEL (41%), MOS (33%)
PKP	30252	IDC (45%), VIE (15%)
A	29469	INMG (35%), SKHL (23%), JMA (23%), SVSA (20%)
SN	27663	HEL (81%)
IAmb_Lg	26626	NEIC (100%)
T	26039	IDC (96%)
pP	21341	BJI (41%), ISC1 (18%), IDC (14%)
PKPbc	15994	IDC (56%), NEIC (17%), BGR (13%)
MLR	14680	MOS (100%)
PKIKP	14175	MOS (98%)
Vmb_Lg	13308	MDD (100%)
PcP	13173	IDC (62%), BJI (13%)
SB	12608	HEL (100%)
PKPdf	11574	NEIC (65%)
PP	11066	BJI (30%), IDC (21%), BELR (17%)
PB	10113	HEL (100%)
sP	9138	BJI (72%), ISC1 (18%)
SS	8458	MOS (31%), BJI (27%), BELR (23%)
smax	7410	MOS (80%), BJI (20%)
PKPab	6412	IDC (41%), NEIC (22%), INMG (13%)
Sb	6244	IRIS (99%)
SPECP	5393	DDA (100%)
PKiKP	4790	IDC (30%), IRIS (26%), VIE (25%)
AMB	4516	SKHL (83%), BJI (17%)
ScP	4375	IDC (70%), BJI (13%), ISC1 (11%)
AMS	4367	PRU (71%), CLL (16%)
LRM	4241	BELR (90%)
Amp	4138	BRG (100%)
x	3730	CLL (35%), PRU (27%), NDI (26%)
Trac	3679	OTT (100%)
PPP	3395	BELR (50%), MOS (44%)
END	3263	ROM (100%)
LG	2880	BRA (80%), OTT (19%)
SSS	2839	BELR (60%), MOS (30%)
sS	2742	BJI (80%), BELR (16%)

Table 11.3: *(continued)*

Reported Phase	Total	Agencies reporting
Pb	2733	IRIS (94%)
*PP	2702	MOS (100%)
PKP2	2676	MOS (98%)
LQ	2448	BELR (57%), INMG (23%), IEPN (16%)
I	2242	IDC (100%)
PKKPbc	2112	IDC (97%)
AMP	2056	IEPN (53%), TIR (42%)
Pdiff	1854	IRIS (42%), IDC (24%), VIE (19%)
Vmb_V	1723	MDD (100%)
pPKP	1655	VIE (29%), IDC (26%), BJI (21%)
SKS	1501	BJI (42%), BELR (31%), PRU (12%)
L	1395	BGR (52%), MOLD (22%), WAR (22%)
PKhKP	1374	IDC (100%)
Smax	1320	BYKL (100%)
ScS	1142	BJI (72%), IDC (13%), BELR (11%)
SKPbc	1086	IDC (95%)
Sm	1075	CFUSG (86%), SIGU (14%)
PS	1062	BELR (36%), MOS (35%), CLL (13%)
X	900	JMA (94%)
Pmax	877	BYKL (92%)
PKHKP	700	MOS (100%)
Pdif	619	NEIC (35%), BER (16%), BJI (12%)
Pm	585	CFUSG (74%), SIGU (26%)
SKP	583	IDC (41%), VIE (19%), BELR (17%)
PKKP	580	IDC (49%), VIE (31%)
IVMs_BB	577	BER (83%), HYB (14%)
pPKPdf	574	NEIC (54%), BGR (13%)
SKKS	573	BELR (51%), BJI (45%)
PKPPKP	552	IDC (94%)
sPKP	534	BJI (75%), BELR (15%)
pPKPbc	492	IDC (68%), BGR (24%)
max	485	BYKL (100%)
*SP	470	MOS (100%)
PcS	448	BJI (95%)
PDIFF	448	PRU (47%), BRA (28%), IPEC (25%)
*SS	435	MOS (100%)
SKSac	384	BER (46%), CLL (21%)
PKPDF	376	PRU (100%)
IVmB_BB	376	BER (65%), HYB (27%)
SP	340	MOS (31%), BER (19%), BELR (12%)
Sgmax	337	NERS (99%)
PKPAB	335	PRU (100%)
AmB	294	KEA (100%)
SKKPbc	225	IDC (99%)
PKP1	216	LIC (82%), PPT (14%)
PKP2bc	215	IDC (100%)
PKKPab	211	IDC (96%)
PKS	210	BJI (47%), BELR (47%)
PPS	202	CLL (60%), MOS (21%)
pPKiKP	199	VIE (65%), UCC (14%)
IVmBBB	166	BER (94%)
Snm	155	SIGU (61%), CFUSG (39%)
PKPpre	152	NEIC (68%), PRU (20%), CLL (12%)

Table 11.3: *(continued)*

Reported Phase	Total	Agencies reporting
SSSS	146	CLL (100%)
P3KPbc	140	IDC (100%)
Rg	140	IDC (46%), NNC (31%), DNK (16%)
SmS	127	BGR (91%)
pPKPab	127	CLL (41%), IDC (40%)
Pgmax	115	NERS (100%)
SKPdf	115	CLL (54%), BER (30%)
r	111	BRG (100%)
PCP	110	PRU (45%), LPA (34%)
PmP	100	BGR (71%), ZUR (28%)
m	92	SIGU (100%)
Sgm	91	SIGU (69%), CFUSG (31%)
LQM	78	MOLD (100%)
SKKSac	73	CLL (66%), HYB (23%)
E	73	ZAG (90%)
SKKP	71	VIE (31%), IDC (31%), PRU (21%)
pPP	67	LPA (49%), CLL (46%)
P'P'	66	VIE (91%)
pPdiff	66	VIE (41%), BGR (39%), SYO (12%)
P4KPbc	61	IDC (100%)
Sdif	58	CLL (74%), BELR (21%)
MSN	57	HEL (72%), BER (28%)
Pnm	55	SIGU (58%), CFUSG (42%)
SKPab	50	IDC (86%)
Lm	50	CLL (100%)
SKIKS	47	LPA (100%)
p	47	ROM (98%)
SKIKP	45	LPA (100%)
pPcP	44	IDC (89%), CLL (11%)
Pgm	44	SIGU (70%), CFUSG (30%)
LmV	44	CLL (100%)
Px	43	CLL (100%)
PKIKS	43	LPA (100%)
PKiKp	41	IRIS (100%)
PPPP	39	CLL (100%)
PKP2ab	38	IDC (100%)
sSKS	38	BELR (97%)
SCS	37	LPA (100%)
sPP	37	CLL (97%)
MPN	36	HEL (64%), BER (31%)
PSKS	36	CLL (100%)
pwP	33	ISC1 (97%)
SKPa	33	NAO (100%)
PKSdf	32	CLL (75%), BER (22%)
M	29	MOLD (83%), LJU (17%)
PgPg	29	BYKL (93%)
LmH	28	CLL (100%)
SKSdf	25	HYB (44%), BER (40%), CLL (12%)
SPP	25	CLL (48%), BELR (40%), MOS (12%)
SKiKP	25	IDC (60%), LJU (20%), IEPN (16%)
(sP)	25	CLL (100%)
Lq	24	MOLD (96%)
PKPf	24	BRG (100%)

Table 11.3: *(continued)*

Reported Phase	Total	Agencies reporting
PnPn	22	SOME (100%)
pPdif	21	BELR (52%), CLL (29%), IEPN (14%)
Plp	20	CLL (100%)
AMd	20	NIC (100%)
Pif	20	BRG (100%)
sSS	20	CLL (100%)
del	20	AUST (85%), KNET (15%)
P*	19	MOS (53%), BGR (32%), BJI (16%)
sPdif	18	BELR (67%), CLL (28%)
PKKPdf	18	CLL (50%), AWI (28%), NEIC (22%)
P3KP	18	IDC (94%)
(PP)	17	CLL (100%)
H	17	IDC (100%)
(SSSS)	17	CLL (100%)
(SS)	17	CLL (100%)
(PKiKP)	16	CLL (100%)
Lmax	15	CLL (100%)
SgSg	15	BYKL (87%), UCC (13%)
(Sg)	15	CLL (67%), SIGU (33%)
sPKiKP	14	HYB (50%), UCC (36%)
(SSS)	14	CLL (100%)
R2	14	CLL (100%)
SKSP	14	CLL (93%)
(pP)	14	CLL (100%)
SDIFF	13	LPA (69%), BRA (31%)
sPdiff	13	VIE (85%)
SKKSdf	12	CLL (83%), HYB (17%)
PPPrev	12	CLL (100%)
SMZ	12	BJI (100%)
Sx	12	CLL (100%)
(Sn)	12	CLL (67%), SIGU (33%)
ASSG	11	OSPL (64%), BER (36%)
(Pn)	11	CLL (55%), SIGU (45%)
ATSG	11	OSPL (64%), BER (36%)
PKPPKPdf	11	CLL (100%)
PKPdif	11	CLL (64%), NEIC (36%)
PSPS	10	CLL (100%)
rx	10	SKHL (100%)
sSdif	10	CLL (50%), BELR (50%)
ATPG	10	OSPL (70%), BER (30%)
sPKPdf	10	CLL (100%)
ASPG	10	OSPL (70%), BER (30%)
AMSG	10	PRE (80%), LSZ (20%)
tx	10	IEPN (100%)
LqM	10	MOLD (100%)
Sif	10	BRG (100%)
mb	10	KMA (100%)
(PKPdf)	10	CLL (100%)
pPiKP	10	AWI (100%)
SDIF	9	PRU (100%)
P'P'df	9	AWI (56%), LJU (44%)
SKKPdf	9	CLL (100%)
PSS	9	CLL (100%)

Table 11.3: *(continued)*

Reported Phase	Total	Agencies reporting
(PKP)	9	CLL (100%)
(Pg)	8	CLL (62%), SIGU (38%)
AP	8	MOS (100%)
IVMsBB	8	BER (50%), HYB (38%), DNK (12%)
PPlp	8	CLL (100%)
Sdiff	8	LJU (88%), IDC (12%)
RG	8	IPEC (100%)
PSSrev	7	CLL (100%)
PPmax	7	CLL (100%)
S*	7	BGR (57%), BJI (43%)
(PcP)	7	CLL (100%)
sSSS	7	CLL (100%)
SKSSKSac	7	CLL (100%)
(PKPab)	7	CLL (100%)
sPKPab	7	CLL (100%)
PM	6	MOLD (100%)
Amb	6	MDD (100%)
sPKPbc	6	CLL (67%), IDC (17%), HYB (17%)
sPS	6	CLL (100%)
LV	6	CLL (100%)
PKKS	6	IDC (67%), BRG (17%), IEPN (17%)
PKPmax	5	CLL (100%)
LMZ	5	WAR (100%)
sPPS	5	CLL (100%)
PKPlp	5	CLL (100%)
(Sb)	5	CLL (100%)
(PPS)	5	CLL (100%)
pPPS	5	CLL (100%)
SCP	4	PRU (100%)
sSSSS	4	CLL (100%)
P5KPbc	4	IDC (100%)
AMPG	4	PRE (100%)
pPS	4	CLL (100%)
P(2)	4	CLL (100%)
(SP)	4	CLL (100%)
pPDIFF	4	IPEC (100%)
SKSp	4	BRA (75%), WAR (25%)
PKSbc	4	CLL (75%), LJU (25%)
AMb	4	LVSN (100%)
SN4	4	AAE (100%)
(sPP)	4	CLL (100%)
PSP	4	LPA (100%)
Sgd	3	WAR (100%)
SKKSa	3	BRG (100%)
sSKKSac	3	CLL (100%)
(SKSP)	3	CLL (100%)
(PPP)	3	CLL (100%)
pPSKS	3	CLL (100%)
PKSab	3	CLL (67%), UCC (33%)
LgM	3	MOLD (100%)
Li	3	MOLD (100%)
pPKKPdf	3	CLL (100%)
(PKPdif)	3	CLL (100%)

Table 11.3: *(continued)*

Reported Phase	Total	Agencies reporting
DIFF	3	BRA (100%)
PsP	3	MOLD (100%)
pPPP	3	CLL (100%)
pS	3	CLL (67%), LJU (33%)
sSKSac	3	CLL (33%), LJU (33%), HYB (33%)
SKPPKPdf	3	CLL (100%)
PKKSbc	3	CLL (67%), IEPN (33%)
PKPc	3	WAR (100%)
Sd0	2	ATH (100%)
PKPPKPbc	2	CLL (100%)
PSPSrev	2	CLL (100%)
PN2	2	LVSN (100%)
(SKPbc)	2	CLL (100%)
pSKKSac	2	CLL (100%)
N	2	SOME (50%), IRIS (50%)
Slp	2	CLL (100%)
Pd2	2	ATH (100%)
sPcP	2	CLL (100%)
(PKSdf)	2	CLL (100%)
PKKPb	2	BRG (100%)
3PKPbc	2	CLL (100%)
Sglp	2	CLL (100%)
(SKKSac)	2	CLL (100%)
PKKPf	2	BRG (100%)
(PS)	2	CLL (100%)
pPKKPbc	2	CLL (100%)
sPSPS	2	CLL (100%)
pPif	2	BRG (100%)
PKPbc(2)	2	CLL (100%)
ESg	2	ZAG (100%)
sPKKSbc	2	CLL (100%)
SKSf	2	BRG (100%)
(PKPbc)	2	CLL (100%)
P5KP	2	NAO (50%), CLL (50%)
sPKKPbc	2	CLL (100%)
pSKPdf	2	CLL (100%)
PN3	2	LVSN (100%)
PKKSdf	2	CLL (100%)
sPSKS	2	CLL (100%)
pScP	2	IDC (100%)
Sc	2	WAR (100%)
SN2	2	LVSN (100%)
(PPPP)	2	CLL (100%)
(SKPdf)	2	CLL (100%)
sPPP	2	CLL (100%)
(pPKPab)	2	CLL (100%)
sPKSdf	2	CLL (100%)
(pPdif)	2	CLL (100%)
sPKKPab	2	CLL (100%)
(sSS)	1	CLL (100%)
PC	1	ECX (100%)
pPKPab2	1	CLL (100%)
sPKKPdf	1	CLL (100%)

Table 11.3: *(continued)*

Reported Phase	Total	Agencies reporting
pPKSdf	1	CLL (100%)
pSdiff	1	CLL (100%)
(pPPPP)	1	CLL (100%)
sPn	1	HYB (100%)
sPPPrev	1	CLL (100%)
rg	1	BRG (100%)
(pPSKS)	1	CLL (100%)
(SKKPbc)	1	CLL (100%)
SPn	1	HYB (100%)
pZP	1	SYO (100%)
SKPdf(2)	1	CLL (100%)
s	1	DNK (100%)
PKPg	1	NAO (100%)
(SKSac)	1	CLL (100%)
(PKPm)	1	CLL (100%)
Pnmax	1	CLL (100%)
pSKPab	1	CLL (100%)
S'S'df	1	HYB (100%)
(Sdif)	1	CLL (100%)
KIKS	1	LPA (100%)
P9	1	RSNC (100%)
PKPPKP'	1	BRG (100%)
(PSS)	1	CLL (100%)
PSPN	1	MOS (100%)
PKKSab	1	HYB (100%)
SKKPab	1	IDC (100%)
(sPKPbc)	1	CLL (100%)
SN5	1	AAE (100%)
AMSN	1	LSZ (100%)
PKPadiff	1	CLL (100%)
(pPKPdf)	1	CLL (100%)
SKSacmax	1	CLL (100%)
PKPab2	1	CLL (100%)
pPKKPab	1	CLL (100%)
SSSrev	1	CLL (100%)
SN3	1	LVSN (100%)
OEPG	1	IPEC (100%)
PSKSrev	1	CLL (100%)
PPME	1	BJI (100%)
pSP	1	CLL (100%)
SKKSf	1	BRG (100%)
Pd0	1	ATH (100%)
(sPSPS)	1	CLL (100%)
(pPKPbc)	1	CLL (100%)
(pPP)	1	CLL (100%)
(PKSab)	1	CLL (100%)
Pnd	1	WAR (100%)
(sSSS)	1	CLL (100%)
sSKKSdf	1	CLL (100%)
(sPKPdf)	1	CLL (100%)
SSmax	1	CLL (100%)
Pdifmax	1	CLL (100%)
PPPPrev	1	CLL (100%)

Table 11.3: *(continued)*

Reported Phase	Total	Agencies reporting
sPPPPrev	1	CLL (100%)
(pPKSdf)	1	CLL (100%)
SKKSacr	1	CLL (100%)
(sPKPab)	1	CLL (100%)
SSP	1	CLL (100%)
SSrev	1	CLL (100%)
Sgc	1	WAR (100%)
(PKKSbc)	1	CLL (100%)
(sPS)	1	CLL (100%)
pSPP	1	CLL (100%)
(PSKS)	1	CLL (100%)
(SKKPdf)	1	CLL (100%)
PKiPK	1	BRG (100%)
pSKSP	1	CLL (100%)
Sd2	1	ATH (100%)
P4KP	1	IDC (100%)
PN5	1	AAE (100%)
S9	1	SVSA (100%)
Pd1	1	ATH (100%)
SKPSKP	1	BRG (100%)
sSb	1	VIE (100%)

Table 11.4: *Reporters of amplitude data*

Agency	Number of reported amplitudes	Number of amplitudes in ISC located events	Number used for ISC mb	Number used for ISC MS
ROM	2319695	55379	0	0
NEIC	605456	243896	172640	19531
IDC	501173	469656	118888	67045
WEL	337356	49162	4	0
ISK	157988	30513	0	0
DDA	135912	16403	0	0
MOS	109798	105494	52805	9926
NNC	105135	36095	88	0
DJA	86187	52533	10226	0
ATH	82606	17213	0	0
SOME	80677	21828	1854	0
BJI	77961	75201	20999	23130
RSNC	54066	4385	0	0
GUC	42897	9880	0	0
VIE	42469	22488	7402	0
HEL	34691	1183	0	0
THE	32807	9129	0	0
LDG	21830	4975	0	0
MRB	16420	582	0	0
MAN	16407	3491	0	0
MDD	15037	4203	0	0
INMG	13996	7900	3079	0
BER	13473	3816	1651	56
JMA	13357	13331	0	0
PRU	11216	4285	0	1792
SJA	11191	9732	0	0
SKHL	10908	5039	0	0
PPT	9750	8589	660	3808
DMN	9535	8692	0	0
PRE	9273	2697	1396	0
DNK	8808	5254	4285	30
NIC	7853	2516	0	0
BELR	7799	5943	1051	1424
ZUR	6779	548	0	0
BGR	6301	6066	4073	0
SVSA	6292	607	386	0
WBNET	6067	0	0	0
NOU	5945	5723	3930	0
BUC	5766	1614	0	0
SDD	5532	1220	0	0
LJU	4795	115	0	6
YARS	4294	93	0	0
BRG	4138	2162	0	0
KNET	4057	1831	0	0

Table 11.4: *Continued.*

Agency	Number of reported amplitudes	Number of amplitudes in ISC located events	Number used for ISC mb	Number used for ISC MS
PDG	3984	2573	0	0
SSNC	3716	556	1	0
OTT	3679	312	0	0
NDI	3392	2890	767	32
BGS	3357	1989	1196	451
ECX	3333	230	0	0
SNET	3217	760	0	0
SKO	3027	341	0	0
CLL	2780	2549	436	463
BYKL	2640	1265	0	0
AWI	2505	1610	705	0
KRSZO	2298	125	0	0
LVSN	2147	198	0	0
UCC	1889	1668	1438	0
NAO	1872	1847	1343	0
SCB	1820	262	0	0
IEPN	1771	1328	42	1
CFUSG	1745	1433	0	0
IPEC	1658	280	0	0
MIRAS	1413	91	0	0
OSPL	1394	565	0	0
KEA	1367	637	0	124
ASRS	1081	625	0	0
LIC	1066	979	591	0
IGIL	1021	543	90	165
MOLD	1008	701	124	0
TIR	869	499	0	0
ISN	755	423	0	0
SIGU	529	336	0	0
NERS	471	130	0	0
WAR	315	303	0	252
HYB	201	197	1	0
AAE	186	71	0	25
MCSM	178	157	0	0
THR	138	138	0	0
INET	131	88	0	0
LIT	112	72	5	0
UPA	67	23	0	0
PLV	50	4	0	0
LSZ	24	3	0	0
BEO	6	6	0	0
SSN	4	2	0	0
ISC	4	4	0	0

12

Glossary of ISC Terminology

- Agency/ISC data contributor

  An academic or government institute, seismological organisation or company, geological/meteorological survey, station operator or author that reports or contributed data in the past to the ISC or one of its predecessors. Agencies may contribute data to the ISC directly, or indirectly through other ISC data contributors.

- Agency code

  A unique, maximum eight-character code for a data reporting agency (e.g. NEIC, GFZ, BUD) or author (e.g. ISC, ISC-EHB, IASPEI). Often the agency code is the commonly used acronym of the reporting institute.

- Arrival

  A phase pick at a station is characterised by a phase name and an arrival time.

- Associated phase

  Associated phase arrival or amplitude measurements represent a collection of observations belonging to (i.e. generated by) an event. The complete set of observations are associated to the prime hypocentre.

- Azimuthal gap/Secondary azimuthal gap

  The azimuthal gap for an event is defined as the largest angle between two stations with defining phases when the stations are ordered by their event-to-station azimuths. The secondary azimuthal gap is the largest azimuthal gap a single station closes.

- BAAS

  Seismological bulletins published by the British Association for the Advancement of Science (1913-1917) under the leadership of H.H. Turner. These bulletins are the predecessors of the ISS Bulletins and include reports from stations distributed worldwide.

- Bulletin

  An ordered list of event hypocentres, uncertainties, focal mechanisms, network magnitudes, as well as phase arrival and amplitude observations associated to each event. An event bulletin may list all the reported hypocentres for an event. The convention in the ISC Bulletin is that the preferred (prime) hypocentre appears last in the list of reported hypocentres for an event.

- Catalogue

  An ordered list of event hypocentres, uncertainties and magnitudes. An event catalogue typically lists only the preferred (prime) hypocentres and network magnitudes.

- CoSOI/IASPEI

  Commission on Seismological Observation and Interpretation, a commission of IASPEI that prepares and discusses international standards and procedures in seismological observation and interpretation.

- Defining/Non-defining phase

  A defining phase is used in the location of the event (time-defining) or in the calculation of the network magnitude (magnitude-defining). Non-defining phases are not used in the calculations because they suffer from large residuals or could not be identified.

- Direct/Indirect report

  A data report sent (e-mailed) directly to the ISC, or indirectly through another ISC data contributor.

- Duplicates

  Nearly identical phase arrival time data reported by one or more agencies for the same station. Duplicates may be created by agencies reporting observations from other agencies, or several agencies independently analysing the waveforms from the same station.

- Event

  A natural (e.g. earthquake, landslide, asteroid impact) or anthropogenic (e.g. explosion) phenomenon that generates seismic waves and its source can be identified by an event location algorithm.

- Grouping

  The ISC algorithm that organises reported hypocentres into groups of events. Phases associated to any of the reported hypocentres will also be associated to the preferred (prime) hypocentre. The grouping algorithm also attempts to associate phases that were reported without an accompanying hypocentre to events.

- Ground Truth

  An event with a hypocentre known to certain accuracy at a high confidence level. For instance, GT0 stands for events with exactly known location, depth and origin time (typically explosions); GT5 stands for events with their epicentre known to 5 km accuracy at the 95% confidence level, while their depth and origin time may be known with less accuracy.

- Ground Truth database

  On behalf of IASPEI, the ISC hosts and maintains the IASPEI Reference Event List, a bulletin of ground truth events.

- IASPEI

  International Association of Seismology and Physics of the Earth Interior, www.iaspei.org.

- International Registry of Seismograph Stations (IR)

  Registry of seismographic stations, jointly run by the ISC and the World Data Center for Seismology, Denver (NEIC). The registry provides and maintains unique five-letter codes for stations participating in the international parametric and waveform data exchange.

- ISC Bulletin

  The comprehensive bulletin of the seismicity of the Earth stored in the ISC database and accessible through the ISC website. The bulletin contains both natural and anthropogenic events. Currently the ISC Bulletin spans more than 50 years (1960-to date) and it is constantly extended by adding both recent and past data. Eventually the ISC Bulletin will contain all instrumentally recorded events since 1900.

- ISC Governing Council

  According to the ISC Working Statutes the Governing Council is the governing body of the ISC, comprising one representative for each ISC Member.

- ISC-located events

  A subset of the events selected for ISC review are located by the ISC. The rules for selecting an event for location are described in Section 11.1.3; ISC-located events are denoted by the author ISC.

- ISC Member

  An academic or government institute, seismological organisation or company, geological/meteorological survey, station operator, national/international scientific organisation that contribute to the ISC budget by paying membership fees. ISC members have voting rights in the ISC Governing Council.

- ISC-reviewed events

  A subset of the events reported to the ISC are selected for ISC analyst review. These events may or may not be located by the ISC. The rules for selecting an event for review are described in Section 11.1.3. Non-reviewed events are explicitly marked in the ISC Bulletin by the comment following the prime hypocentre "Event not reviewed by the ISC".

- ISF

  International Seismic Format (www.isc.ac.uk/standards/isf). A standard bulletin format approved by IASPEI. The ISC Bulletin is presented in this format at the ISC website.

- ISS

  International Seismological Summary (1918-1963). These bulletins are the predecessors of the ISC Bulletin and represent the major source of instrumental seismological data before the digital era. The ISS contains regionally and teleseismically recorded events from several hundreds of globally distributed stations.

- Network magnitude

The event magnitude reported by an agency or computed by the ISC locator. An agency can report several network magnitudes for the same event and also several values for the same magnitude type. The network magnitude obtained with the ISC locator is defined as the median of station magnitudes of the same magnitude type.

- Phase

A maximum eight-character code for a seismic, infrasonic, or hydroacoustic phase. During the ISC processing, reported phases are mapped to standard IASPEI phase names. Amplitude measurements are identified by specific phase names to facilitate the computation of body-wave and surface-wave magnitudes.

- Prime hypocentre

The preferred hypocentre solution for an event from a list of hypocentres reported by various agencies or calculated by the ISC.

- Reading

Parametric data that are associated to a single event and reported by a single agency from a single station. A reading typically includes one or more phase names, arrival time and/or amplitude/period measurements.

- Report/Data report

All data that are reported to the ISC are parsed and stored in the ISC database. These may include event bulletins, focal mechanisms, moment tensor solutions, macroseismic descriptions and other event comments, as well as phase arrival data that are not associated to events. Every single report sent to the ISC can be traced back in the ISC database via its unique report identifier.

- Shide Circulars

Collections of station reports for large earthquakes occurring in the period 1899-1912. These reports were compiled through the efforts of J. Milne. The reports are mainly for stations of the British Empire equipped with Milne seismographs. After Milne's death, the Shide Circulars were replaced by the Seismological Bulletins of the BAAS.

- Station code

A unique, maximum six-character code for a station. The ISC Bulletin contains data exclusively from stations registered in the International Registry of Seismograph Stations.

13

Acknowledgements

We thank our colleagues at the Department of Geophysics of the Aristotle University of Thessaloniki and Latvian Environment, Geology and Meteorology Center for kindly accepting our invitation and submitting the articles on their seismic network's history, current status and operational procedures for this issue of the Summary.

We are also grateful to the developers of the Generic Mapping Tools (GMT) suite of software (Wessel and Smith, 1998) that was used extensively for producing the graphical figures.

References

Adamaki, A. (2017), Seismicity analysis using dense network data : Catalogue statistics and possible foreshocks investigated using empirical and synthetic data, Ph.D. thesis, Uppsala University, `urn: nbn:se:uu:diva-328057`.

Adams, R. D., A. A. Hughes, and D. M. McGregor (1982), Analysis procedures at the International Seismological Centre, *Physics of the Earth and Planetary Interiors*, *30*, 85–93.

Amante, C., and B. W. Eakins (2009), ETOPO1 1 arc-minute global relief model: procedures, data sources and analysis, *NOAA Technical Memorandum NESDIS NGDC-24*, NOAA.

Balfour, N., R. Baldwin, and A. Bird (2008), Magnitude calculations in Antelope 4.10, *Analysis Group Note of Geological Survey of Canada*, pp. 1–13.

Bennett, T. J., V. Oancea, B. W. Barker, Y.-L. Kung, M. Bahavar, B. C. Kohl, J. . Murphy, and I. K. Bondár (2010), The nuclear explosion database NEDB: a new database and web site for accessing nuclear explosion source information and waveforms, *Seismological Research Letters*, *81*, doi:10.1785/gssrl.81.1.12.

Bisztricsany, E. A. (1958), A new method for the determination of the magnitude of earthquakes, *Geofiz. Kozl*, pp. 69–76.

Bolt, B. A. (1960), The revision of earthquake epicentres, focal depths and origin time using a high-speed computer, *Geophysical Journal of the Royal Astronomical Society*, *3*, 434–440.

Bondár, I., and K. McLaughlin (2009a), A new ground truth data set for seismic studies, *Seismological Research Letters*, *80*, 465–472.

Bondár, I., and K. McLaughlin (2009b), Seismic location bias and uncertainty in the presence of correlated and non-Gaussian travel-time errors, *Bulletin of the Seismological Society of America*, *99*, 172–193.

Bondár, I., and D. Storchak (2011), Improved location procedures at the International Seismological Centre, *Geophysical Journal International*, *186*, 1220–1244.

Bondár, I., E. R. Engdahl, X. Yang, H. A. A. Ghalib, A. Hofstetter, V. Kirchenko, R. Wagner, I. Gupta, G. Ekström, E. Bergman, H. Israelsson, and K. McLaughlin (2004), Collection of a reference event set for regional and teleseismic location calibration, *Bulletin of the Seismological Society of America*, *94*, 1528–1545.

Bondár, I., E. Bergman, E. R. Engdahl, B. Kohl, Y.-L. Kung, and K. McLaughlin (2008), A hybrid multiple event location technique to obtain ground truth event locations, *Geophysical Journal International*, *175*, doi:10.1111/j.1365,246X.2008.03,867x.

Bormann, P., and J. W. Dewey (2012), The new iaspei standards for determining magnitudes from digital data and their relation to classical magnitudes, is 3.3, *New Manual of Seismological Observatory Practice 2 (NMSOP-2), P. Bormann (Ed.)*, pp. 1–44, doi:10.2312/GFZ.NMSOP-2_IS_3.3,10.2312/ GFZ.NMSOP-2, `http://nmsop.gfz-postsdam.de`.

Bormann, P., and J. Saul (2008), The new IASPEI standard broadband magnitude mB, *Seism. Res. Lett*, *79*(5), 698–705.

Bormann, P., R. Liu, X. Ren, R. Gutdeutsch, D. Kaiser, and S. Castellaro (2007), Chinese national network magnitudes, their relation to NEIC magnitudes and recommendations for new IASPEI magnitude standards, *Bulletin of the Seismological Society of America*, *97*(1B), 114–127, doi:10.1785/012006007835.

Bormann, P., R. Liu, Z. Xu, R. Ren, and S. Wendt (2009), First application of the new IASPEI tele-seismic magnitude standards to data of the China National Seismographic Network, *Bulletin of the Seismological Society of America*, *99*, 1868–1891, doi:10.1785/0120080010.

Chang, A. C., R. H. Shumway, R. R. Blandford, and B. W. Barker (1983), Two methods to improve location estimates - preliminary results, *Bulletin of the Seismological Society of America*, *73*, 281–295.

Choy, G. L., and J. L. Boatwright (1995), Global patterns of readiated seismic energy and apparent stress, *J. Geophys. Res.*, *100*(B9), 18,205–18,228.

Dziewonski, A. M., and F. Gilbert (1976), The effect of small, aspherical perturbations on travel times and a re-examination of the correction for ellipticity, *Geophysical Journal of the Royal Astronomical Society*, *44*, 7–17.

Dziewonski, A. M., T.-A. Chou, and J. H. Woodhouse (1981), Determination of earthquake source parameters from waveform data for studies of global and regional seismicity, *J. Geophys. Res.*, *86*, 2825–2852.

Engdahl, E. R., and R. H. Gunst (1966), Use of a high speed computer for the preliminary determination of earthquake hypocentres, *Bulletin of the Seismological Society of America*, *56*, 325–336.

Engdahl, E. R., and A. Villaseñor (2002), Global seismicity: 1900-1999, *International Handbook of Earthquake Engineering and Seismology, International Geophysics series*, *81A*, 665–690.

Engdahl, E. R., R. van der Hilst, and R. Buland (1998), Global teleseismic earthquake relocation with improved travel times and procedures for depth determination, *Bulletin of the Seismological Society of America*, *88*, 722–743.

Flinn, E. A., and E. R. Engdahl (1965), Proposed basis for geographical and seismic regionalization, *Reviews of Geophysics*, *3*(1), 123–149.

Flinn, E. A., E. R. Engdahl, and A. R. Hill (1974), Seismic and geographical regionalization, *Bulletin of the Seismological Society of America*, *64*, 771–993.

Gutenberg, B. (1945a), Amplitudes of P, PP and S and magnitude of shallow earthquakes, *Bulletin of the Seismological Society of America*, *35*, 57–69.

Gutenberg, B. (1945b), Magnitude determination of deep-focus earthquakes, *Bulletin of the Seismological Society of America*, *35*, 117–130.

Gutenberg, B. (1945c), Amplitudes of surface waves and magnitudes of shallow earthquakes, *Bulletin of the Seismological Society of America*, *35*, 3–12.

Gutenberg, B., and C. F. Richter (1956), Magnitude and Energy of earthquakes, *Ann. Geof.*, *9*, 1–5.

Hutton, L. K., and D. M. Boore (1987), The ML scale in southern California, *Bulletin of the Seismological Society of America*, *77*, 2074–2094.

IASPEI (2005), Summary of magnitude working group recommendations on standard procedures for determining earthquake magnitudes from digital data, `http://www.iaspei.org/commissions/CSOI.html#wgmm,http://www.iaspei.org/commissions/CSOI/summary_of_WG_recommendations_2005.pdf`.

IASPEI (2013), Summary of magnitude working group recommendations on standard procedures for determining earthquake magnitudes from digital data, `http://www.iaspei.org/commissions/CSOI/Summary_of_WG_recommendations_20130327.pdf`.

IDC (1999), IDC processing of seismic, hydroacoustic and infrasonic data, *IDC Documentation*.

Jeffreys, H., and K. E. Bullen (1940), *Seismological Tables*, British Association for the Advancement of Science.

Kanamori, H. (1977), The energy release in great earthquakes, *J. Geophys. Res.*, *82*, 2981–2987.

Kennett, B. L. N. (2006), Non-linear methods for event location in a global context, *Physics of the Earth and Planetary Interiors*, *158*, 45–64.

Kennett, B. L. N., E. R. Engdahl, and R. Buland (1995), Constraints on seismic velocities in the Earth from traveltimes, *Geophysical Journal International*, *122*, 108–124.

Kennett, B. L. N., E. R. Engdahl, and R. Buland (1996), Ellipticity corrections for seismic phases, *Geophysical Journal International*, *127*, 40–48.

Lee, W. H. K., R. Bennet, and K. Meagher (1972), A method of estimating magnitude of local earthquakes from signal duration, *U.S. Geol. Surv.*, Open-File Rep.

Leptokaropoulos, K. M., A. K. Adamaki, R. G. Roberts, C. G. Gkarlaouni, and P. M. Paradisopoulou (2018), Impact of magnitude uncertainties on seismic catalogue properties, *Geophysical Journal International*, *213*(2), 940–951, `https://doi.org/10.1093/gji/ggy023`.

Murphy, J. R., and B. W. Barker (2006), Improved focal-depth determination through automated identication of the seismic depth phases pP and sP, *Bulletin of the Seismological Society of America*, *96*, 1213–1229.

NMSOP-2 (2012), *New Manual of Seismological Observatory Practice (NMSOP-2)*, IASPEI, GFZ, German Research Centre for Geosciences, Potsdam, doi:10.2312/GFZ.NMSOP-2, `http://nmsop.gfz-potsdam.de`, urn:nbn:de:kobv:b103-NMSOP-2.

Nuttli, O. W. (1973), Seismic wave attenuation and magnitude relations for eastern North America, *J. Geophys. Res.*, *78*, 876–885.

Richter, C. F. (1935), An instrumental earthquake magnitude scale, *Bulletin of the Seismological Society of America*, *25*, 1–32.

Ringdal, F. (1976), Maximum-likelihood estimation of seismic magnitude, *Bulletin of the Seismological Society of America*, *66*(3), 789–802.

Sambridge, M. (1999), Geophysical inversion with a neighbourhood algorithm, *Geophysical Journal International*, *138*, 479–494.

Sambridge, M., and B. L. N. Kennett (2001), Seismic event location: non-linear inversion using a neighbourhood algorithm, *Pure and Applied Geophysics*, *158*, 241–257.

Storchak, D., J. Harris, L. Brown, K. Lieser, B. Shumba, R. Verney, D. Di Giacomo, and E. I. M. Korger (2017), Rebuild of the bulletin of the international seismological centre (isc), part 1: 1964–1979, *Seismological Research Letters*, *4*(32), doi:10.1186/s40,562–017–0098–z.

Storchak, D. A., J. Schweitzer, and P. Bormann (2003), The IASPEI standard seismic phases list, *Seismological Research Letters*, *74*(6), 761–772.

Storchak, D. A., J. Schweitzer, and P. Bormann (2011), Seismic phase names: IASPEI standard, in *Encyclopedia of Solid Earth Geophysics*, edited by H. Gupta, pp. 1162–1173, Springer.

Tsuboi, C. (1954), Determination of the Gutenberg-Richter's magnitude of earthquakes occurring in and near Japan, *Zisin (J. Seism. Soc. Japan)*, *Ser. II*(7), 185–193.

Tsuboi, S., K. Abe, K. Takano, and Y. Yamanaka (1995), Rapid determination of Mw from broadband P waveforms, *Bulletin of the Seismological Society of America*, *85*(2), 606–613.

Uhrhammer, R. A., and E. R. Collins (1990), Synthesis of Wood-Anderson Seismograms from Broadband Digital Records, *Bulletin of the Seismological Society of America*, *80*(3), 702–716.

Vaněk, J., A. Zapotek, V. Karnik, N. V. Kondorskaya, Y. V. Riznichenko, E. F. Savarensky, S. L. Solov'yov, and N. V. Shebalin (1962), Standardization of magnitude scales, *Izvestiya Akad. SSSR.*, *Ser. Geofiz.*(2), 153–158, pages 108–111 in the English translation.

Villaseñor, A., and E. R. Engdahl (2005), A digital hypocenter catalog for the International Seismological Summary, *Seismological Research Letters*, *76*, 554–559.

Villaseñor, A., and E. R. Engdahl (2007), Systematic relocation of early instrumental seismicity: Earthquakes in the International Seismological Summary for 1960–1963, *Bulletin of the Seismological Society of America*, *97*, 1820–1832.

Woessner, J., and S. Wiemer (2005), Assessing the quality of earthquake catalogues: estimating the magnitude of completeness and its uncertainty, *Bulletin of the Seismological Society of America*, *95*(2), doi:10/1785/012040,007.

Young, J. B., B. W. Presgrave, H. Aichele, D. A. Wiens, and E. A. Flinn (1996), The Flinn-Engdahl regionalisation scheme: the 1995 revision, *Physics of the Earth and Planetary Interiors*, *96*, 223–297.

Smart buildings with GeoSMART
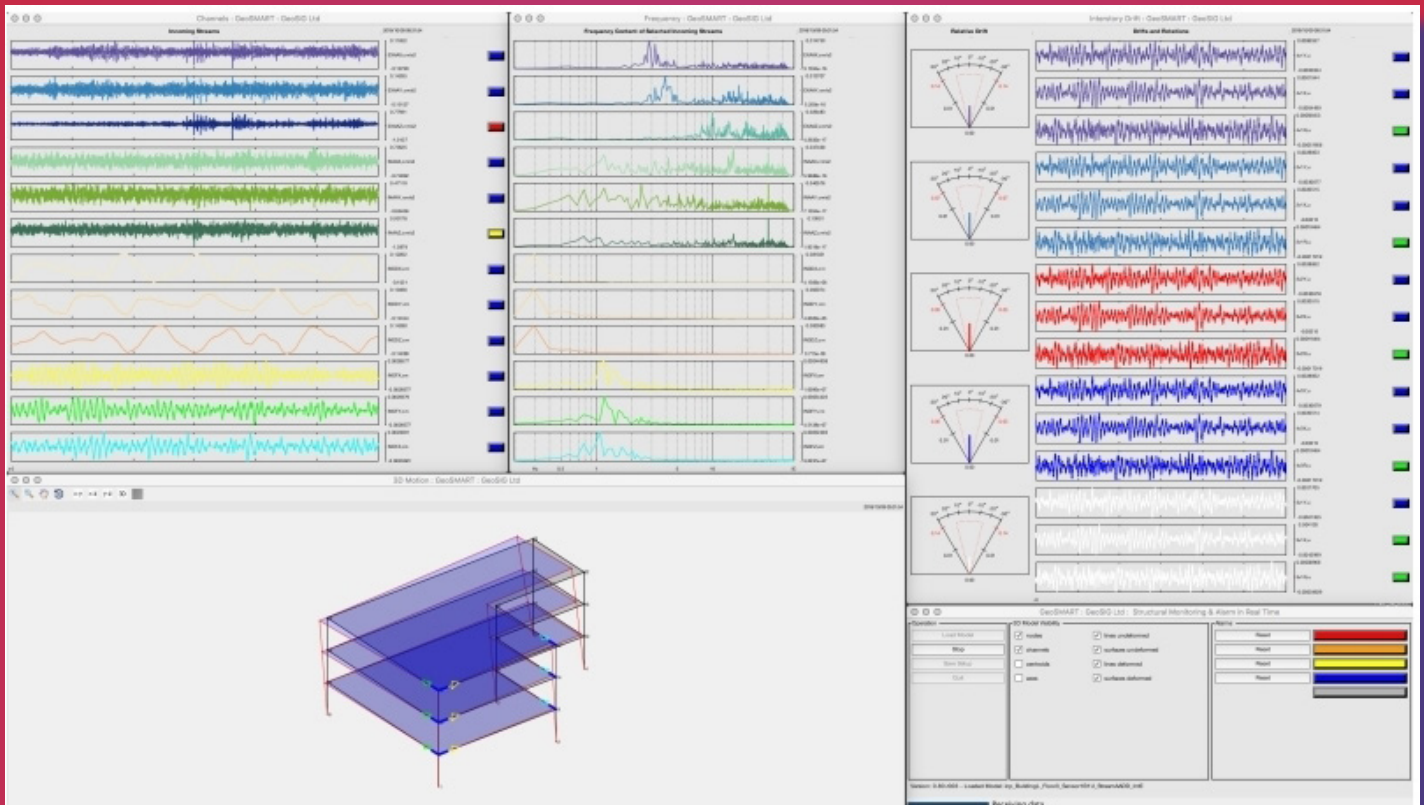
GeoSMART is an innovative graphical Java-based application that provides tools for realtime structural health monitoring for civil engineering structures. With its "smart" features, GeoSMART can monitor and display the status of a structure that is equipped with GeoSIG measuring instruments. It has been designed to meet fundamental engineering requirements with respect to structural health monitoring applications.

Visit www.geosig.com to download the data sheet or to see some sample models.

KEY FEATURES

- Real-time structural health monitoring software for civil engineering structures like buildings, dams, bridges and so on.
- Animated 3D model of the structure with various viewing options.
- Real-time data viewer, analyser and recorder for instrument(s) providing data streams as well as replay of pre-recorded data.
- Calculation and evaluation of rigid body motions and interstory drifts as well as interpolations for non-instrumented parts of a structure.
- Real-time frequency content and response spectrum calculations
- Exceedance levels with four colour-coded alarm levels to assist decision making for occupancy resumption or re-use after a potentially damaging event.
- Email notifications to users, operators or owners, as well as alarm relay options to to enable automated shutdown or emergency management processes.

GeoSIG
swiss made to measure

If It Moves, You'll Know It. Immediately.
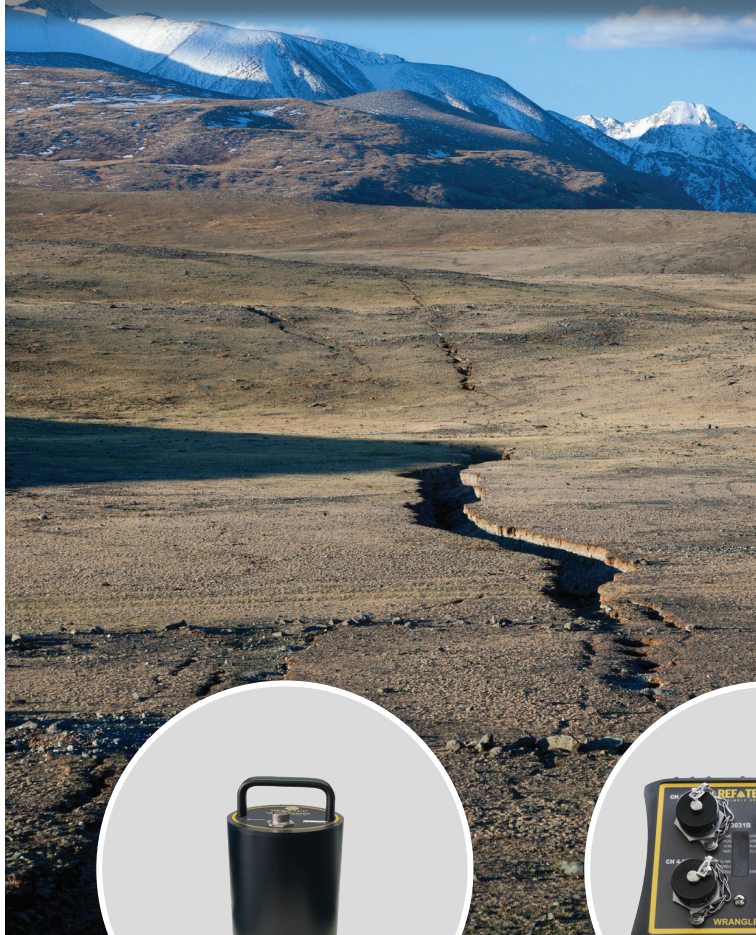
For over 40 years REF TEK®, a Trimble brand, has been the trusted partner for seismologists around the globe. **If it shakes, sinks or shifts our reliable sensors and recorders will know about it instantaneously.** And you will too, anytime, as sophisticated application software informs you immediately. Always on the job, offering some peace of mind in an unstable world.

REF TEK COLT
High Performance Broadband Seismometer

Setting a new industry standard for low self-noise performance in a compact form factor, REF TEK's new Colt broadband seismometer features a large dynamic range, so it can observe and measure high-quality ground motion data. Scientists requiring portable or small vault style seismometers now have a high-performance instrument available for quick, easy deployment.

REF TEK WRANGLER
High Resolution Seismic Recorder

The latest compact and lightweight seismic recorder introduces **a 32-bit analog-to-digital converter providing high quality data** and an increased dynamic range. The simple setup and flexible communication delivers reliable, robust data from geophysical sensors when and where you need it.

REF TEK 147A
Strong Motion Accelerometer

With high sensitivity, large linear range, high resolution and dynamic range the 147A is suitable for free field applications such as microzonation, site response, earthquake monitoring and more.

For more information visit **www.reftek.com**
Follow @REFTEK_Trimble

**REF TEK®**
A TRIMBLE BRAND

# TDE-324CI/FI Digitizer

Key Features：

- o True 26-bit, exceptionally low noise, up to 1000sps, high dynamic range > 145dB@100sps

- o High precision time Service：better than 0.05ppm

- o Records in MiniSEED, standard storages 32GB, max 256GB supports Liss, Seedlink, JOPENS data streaming protocols

- o Compatible with any seismometers & accelerometers

- o Humanized Interface, include pushbuttons and large LCD, setup & display real-time wave and running status

- o Built-in seismic station performance and data quality analysis, include PSD/PDF, sine/pulse calibration, sensor response, waveform, run rate, environmental status monitoring etc.

- o Installation checking & setup available for both android and IOS devices

- o Remote control multiple seismometers calibration, mass center, mass lock/unlock
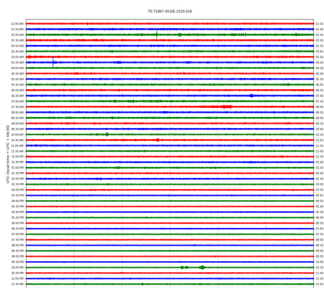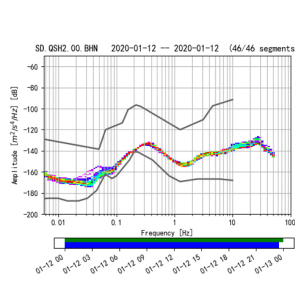
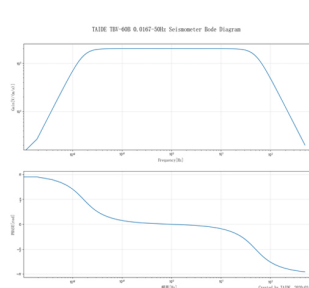TDE-324CI Digitizer
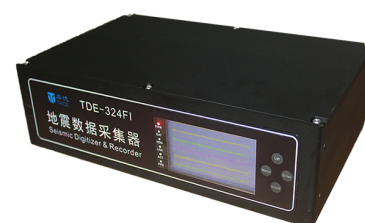
TDE-324FI Digitizer
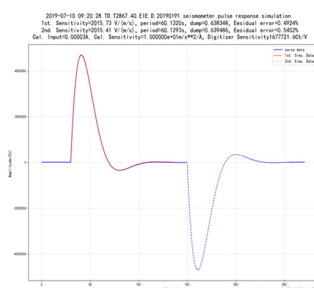
Built in auto pulse cal. signal analysis   Built-in 1 day's seismic wave display   Built-in 1 day's PDF analysis   Built-in seismometer response analysis

Technical Specifications：

Channels	TDE-324CI: 3 channels TDE-324FI: 6 channels	Main channel resolution	True 26 bits, ≥145dB@100sps Support 24 bits output
Input noise	＜1.0μVrms(input ±20Vpp)	Interface	Standard 10/100M RJ45/LAN
Time Service	Support Beidou,GPS Satellites Support NTP Time Service Time error: better than 0.01ms Timing accuracy:better than 0.05ppm	Signal input	Differential Input, ±20Vpp Full Scale, Program Gain 1/2/4
Sample rate	1sps、10sps、20sps、50sps、100sps、200sps、500sps、1000sps	Environment	Temperature：-40℃～70℃, Humidity：0～100%(RH),IP67